

8-21-2023 2:00 PM

Towards Smart and Cost-effective Bridge Infrastructure Monitoring Systems

Premjeet Singh, *Western University*

Supervisor: Sadhu, Ayan, *The University of Western Ontario*

A thesis submitted in partial fulfillment of the requirements for the Doctor of Philosophy degree in Civil and Environmental Engineering

© Premjeet Singh 2023

Follow this and additional works at: <https://ir.lib.uwo.ca/etd>



Part of the [Civil Engineering Commons](#), [Structural Engineering Commons](#), and the [Transportation Engineering Commons](#)

Recommended Citation

Singh, Premjeet, "Towards Smart and Cost-effective Bridge Infrastructure Monitoring Systems" (2023). *Electronic Thesis and Dissertation Repository*. 9566.
<https://ir.lib.uwo.ca/etd/9566>

This Dissertation/Thesis is brought to you for free and open access by Scholarship@Western. It has been accepted for inclusion in Electronic Thesis and Dissertation Repository by an authorized administrator of Scholarship@Western. For more information, please contact wlsadmin@uwo.ca.

Abstract

Bridge health monitoring (BHM) has recently gained significant interest worldwide in the inspection and maintenance of aging bridge infrastructure in the era of climate change and adverse weather conditions. However, extensive datasets resulting from these monitoring systems require appropriate tools to diagnose the data systematically under various operating conditions of bridges, leading to expensive and time intensive BHM strategies. To mitigate this challenge, a smart and cost-effective bridge infrastructure management system is of paramount need in today's world. This thesis aims to develop a suite of cost-effective bridge management strategies by employing limited and mobile sensing technology and addressing their inherent challenges in real-world situations. First, a limited sensor-based cost-effective approach is developed to analyze the traffic-induced nonstationary vibration response of the bridge. The proposed technique can deal with practical challenges of direct BHM, such as traffic interruptions, bridge closures, limited space, and the limited number of sensors, thereby eliminating the need for high labor and equipment costs. Secondly, the visualization of BHM data is explored for systematic diagnosis of the bridge data. A visualization tool based on Bridge Information Modeling (BrIM) is proposed which is suitable for real-time system identification of bridges. The objective of the proposed tool is to take one step forward from static to dynamic BrIM by representing and visualizing real-time BHM data.

Contact-based BHM usually involves direct instrumentation with sensors to extract the modal parameters from the ambient or forced vibrations. As an alternative to direct BHM, indirect BHM (iBHM) has emerged as a promising avenue for effective and inexpensive monitoring of bridge infrastructure. However, the existing iBHM methods face challenges associated with the accurate identification of bridge properties under various driving and vehicle conditions. In this thesis, a hybrid time-frequency method is proposed for decoupling vehicle bridge interactions and performing robust bridge modal identification under various operational challenges. The method is capable of bridge condition assessment using vehicle response from a passing vehicle traveling over a bridge, resulting in a smart drive-by BHM technology. The vehicle response in iBHM is often criticized as the presence of vehicle frequency can make vehicle scanning ineffective. Therefore, this thesis also explores the

robust contact point (CP)-based BHM method, which is free from vehicle conditions and provides more accurate estimates of bridge frequencies.

Summary for Lay Audience

Modern bridge infrastructure plays a significant role in stimulating economic development. Bridge health monitoring (BHM) is essential for ensuring the safety, performance, and longevity of bridges, especially as climate change and extreme weather conditions impact aging bridge infrastructure. Monitoring a large inventory of bridges can result in a sizable amount of data which can be costly and time-consuming to analyze. To address this challenge, there is a need for a smart and affordable system bridge monitoring system. The proposed research of this doctoral thesis is focused on exploring cost-effective BHM strategies to identify structural defects in bridges using remote, noncontact, and fewer sensors. Firstly, a limited sensor-based approach is developed to analyze bridge vibrations caused by the traffic. This method can overcome the practical challenges associated with direct BHM. A visualization tool based on Bridge Information Modeling (BrIM) is developed to visualize the dynamic behavior of the bridge using real-time BHM data.

Indirect BHM (iBHM) has shown promise as a cost-effective alternative to direct BHM. However, it faces challenges in accurately determining bridge properties under different driving and vehicle conditions. This thesis introduces an innovative method to accurately identify characteristics of bridge structure, even when faced with different operational challenges. This method can assess the condition of a bridge by analyzing the response of a vehicle passing over it. However, it is often argued that analyzing vehicle responses may not be reliable due to the interference of vehicle and driving conditions. Hence, a contact point-based BHM method is developed, which is independent of vehicle conditions and provides a more precise estimation of bridge parameters.

Co-Authorship Statement

This thesis has been prepared in accordance with the regulations for an integrated-article format thesis as stipulated by the School of Graduate and Postdoctoral Studies at the University of Western Ontario. The co-authorship statements for the research chapters in this thesis are given below.

Chapter 2: Literature Review

Literature review presented in this chapter was summarized by P. Singh. He contributed to the conceptualization, organization, and writing of this chapter. S. Mittal was responsible for the organization and review of contact point response literature. M. Barbosh contributed to the review of variants of time-frequency methods. The initial and final versions of chapter 2 were written by P. Singh. Prof. A. Sadhu provided comments and reviewed the final version of this chapter. The research from this chapter was published as review papers in the peer-reviewed journals *Practice Periodical on Structural Design and Construction* and *Smart Materials and Structures*.

Singh, P., Mittal, S., and Sadhu, A. (2023). Recent advancements and future trends in indirect bridge health monitoring. *Practice Periodical on Structural Design and Construction*, ASCE, 28(1).

Barbosh, M., **Singh, P.**, and Sadhu, A. (2020). Empirical Mode Decomposition and its variants: A review with applications in structural health monitoring. *Smart Materials and Structures*, 29(9), 093001.

Chapter 3: Bridge Condition Assessment with Limited Sensors using an Improved Time-Varying Empirical Mode Decomposition

The proposed method and numerical study presented in this chapter were developed by P. Singh. He contributed to the experimental design, interpretation, and writing of the manuscript as the primary author. M. Keyvanlou was responsible for data analysis and manuscript writing for the full-scale study. The initial and final versions of chapter 3 were written by P. Singh. The role of Prof. A. Sadhu included review and supervision of initial and

final versions of the chapter. This chapter was published in the peer reviewed journal *Engineering Structures*.

Singh, P., Keyvanlou, M., and Sadhu, A. (2021). An improved time-varying Empirical Mode Decomposition for structural condition assessment using limited sensors. *Engineering Structures*, Elsevier, 232, 111882.

Chapter 4: An Integrated Time-Frequency Damage Detection Method using Vehicle-induced Nonstationary Response.

The proposed method and validation studies presented in this chapter were developed by P. Singh. He contributed to the experimental design, interpretation, and writing of the manuscript. Prof. A. Sadhu supervised the research and provided feedback on the manuscript of this chapter which is also published as a journal paper in the peer-reviewed journal *Structures*.

Singh, P., and Sadhu, A. (2021). Limited sensor-based bridge condition assessment using vehicle-induced nonstationary measurements. *Structures*, Elsevier, 32, 1207-1220.

Chapter 5: Drive-by Modal Identification of Bridges utilizing Wavelet Decomposition

Conceptualization of proposed methodology, numerical simulation, laboratory experiment, and full-scale study was performed by P. Singh. He was also responsible for data analysis, results interpretation, and writing of the manuscript of this chapter. Prof. A. Sadhu supervised and provided comments on the initial and final versions of the manuscript. This chapter was published in the peer-reviewed journal *Engineering Structures*.

Singh, P., and Sadhu, A. (2022). A hybrid time-frequency method for robust drive-by modal identification of bridges. *Engineering Structures*, Elsevier, 264, 114624.

Chapter 6: Vehicle Scanning Method based on Contact Point Response

P. Singh presented a novel condition assessment method for bridges using passing vehicles independent of vehicle dynamics. He developed numerical simulation and full-scale validation study. This chapter was written by P. Singh with supervision and feedback from Prof. A. Sadhu.

A journal paper co-authored by P. Singh, and A. Sadhu entitled “Contact point response-based indirect bridge health monitoring using Robust Empirical Mode Decomposition” is currently under review in a peer-reviewed journal.

Chapter 7: Visualization Tool for Bridge Infrastructure Monitoring and Maintenance

P. Singh developed a tool for visualization of long-term bridge monitoring data. The framework was conceptualized, developed, and validated by him. The manuscript in its initial and final versions were prepared by P. Singh. The role of Prof. A. Sadhu included supervision and providing comments on the manuscript. This chapter was published in the peer-reviewed journal *Frontier in Built-up Environment*.

Singh, P., and Sadhu, A. (2020). System identification enhanced automated visualization tool for infrastructure monitoring and maintenance. *Structural Sensing*, Froniter in Built Environments, 6(76).

Acknowledgments

I would like to take this chance to extend my special gratitude to Dr. Ayan Sadhu, my doctoral supervisor, for his generous support, excellent guidance, valuable suggestions, and continuous engagement throughout this research. Without his support and guidance, the completion of this dissertation would not have been possible. It was a great pleasure and honor to work with him. Aside from my supervisor, I wish to express my gratitude towards my thesis supervisory committee members Dr. Girma Bitsuamlak, and Dr. Maged A. Youssef. I would like to thank Dr. Aiham Adawi for his continued support throughout my research at the University of Western Ontario. I would also like to thank Dr. Mohamed Zaki and Dr. Samuel Asokanthan for agreeing to serve on my thesis examination committee. I am grateful to Dr. Babak Moaveni from Tufts University for agreeing to serve on my thesis committee as an external examiner.

I am also grateful for my colleagues Kyle Dunphy, Mohamed Barbosh, Sandeep Sony, Ali Abasi, Shivank Mittal, Mengchen Zhao, Zuyi Ba, Michael Sakr, and Rashinda Wijethunga without whom the task of data collection would have been impossible. I must acknowledge the engineers, Jane Fullick and Karl Grabowski from the City of London for their valuable assistance during the data collection on city bridges.

The presented research is supported by Post Graduate Scholarship – Doctoral (PGS-D) from the Natural Sciences and Engineering Research Council of Canada (NSERC). I also want to thank MITACS Canada for providing additional financial support for this research.

Finally, I am particularly indebted to my parents, my wife Priya, and my parents-in-law for their understanding, encouragement, patience, and sacrifice throughout this endeavor.

Table of Contents

Abstract	ii
Summary for Lay Audience	iv
Co-Authorship Statement.....	v
Acknowledgments.....	viii
Table of Contents	ix
List of Tables	xiv
List of Figures	xvi
List of Acronyms	xxiii
List of Symbols	xxv
Chapter 1	1
1 Introduction	1
1.1 Research Motivation	1
1.2 Research Scope	2
1.3 Research Objectives.....	4
1.4 Outline of the Thesis.....	4
Chapter 2.....	5
2 Literature Review	5
2.1 Direct Bridge Health Monitoring.....	5
2.1.1 Challenges of direct bridge health monitoring.....	8
2.2 Indirect Bridge Health Monitoring	9
2.2.1 Contact point-based bridge health monitoring.....	13
2.2.2 Challenges of indirect bridge health monitoring	16
2.3 Advanced Time-Frequency Methods in Bridge Health Monitoring.....	17
2.3.1 Empirical Mode Decomposition	17

2.3.2	Wavelet Transform	18
2.3.3	Synchro-Squeezing Transform	20
2.4	Visualization Techniques of Bridge Health Monitoring.....	21
2.4.1	Challenges of bridge health monitoring visualization techniques	23
2.5	Thesis Objectives	24
2.6	Summary	24
Chapter 3.....		26
3	Bridge Condition Assessment with Limited Sensors using an Improved Time-Varying Empirical Mode Decomposition	26
3.1	Introduction.....	26
3.2	Background	28
3.2.1	Multi-Synchro Squeezing Transform	29
3.2.2	Time-Varying Filter Empirical Mode Decomposition	30
3.3	Proposed Method	31
3.4	Numerical Validation.....	33
3.4.1	4-DOF model	34
3.4.2	10-DOF model	36
3.5	Full-Scale Validation	41
3.5.1	Details of full-scale validation.....	42
3.5.2	Identification results.....	43
3.6	Summary	48
Chapter 4.....		49
4	An Integrated Time-Frequency Damage Detection Method using Vehicle-induced Nonstationary Response.....	49
4.1	Introduction.....	49
4.2	Background	52
4.2.1	Synchro-Extracting Transform	52

4.3	Proposed Method	54
4.4	Numerical Study	56
4.5	Finite Element Study.....	61
4.5.1	Effect of sensor location	62
4.5.2	Effect of vehicle speed.....	66
4.5.3	Effect of vehicle class	68
4.5.4	Effect of structural damage.....	69
4.6	Full-Scale Study.....	70
4.6.1	Details of full-scale study	70
4.6.2	Identification results.....	72
4.7	Summary	73
Chapter 5	75
5	Drive-by Modal Identification of Bridges utilizing Wavelet Decomposition	75
5.1	Introduction.....	75
5.2	Background.....	81
5.2.1	Vehicle bridge interaction.....	81
5.2.2	Wavelet Packet Transform.....	84
5.3	Proposed Framework	85
5.4	Numerical Investigation.....	86
5.4.1	Model description	86
5.4.2	Effect of vehicle speed.....	87
5.4.3	Effect of structural damage.....	91
5.4.4	Effect of measurement noise.....	98
5.5	Experimental Validation	101
5.6	Full-Scale Validation	104
5.6.1	Details of full-scale study	104

5.6.2	Identification results.....	106
5.7	Summary	110
Chapter 6	112
6	Vehicle Scanning Method Based on Contact Point Response	112
6.1	Introduction.....	112
6.2	Background	114
6.2.1	Contact point response	114
6.2.2	Robust Empirical Mode Decomposition.....	116
6.3	Proposed Methodology	118
6.4	Numerical Validation.....	119
6.4.1	Effect of vehicle speed.....	120
6.4.2	Effect of measurement noise.....	123
6.4.3	Effect of structural damage	126
6.5	Full-Scale Validation	128
6.5.1	Direct bridge health monitoring.....	129
6.5.2	Indirect bridge health monitoring	131
6.6	Summary	135
Chapter 7	136
7	Visualization Tool for Bridge Infrastructure Monitoring and Maintenance	136
7.1	Introduction.....	136
7.2	Proposed Visualization Framework	139
7.3	Full-Scale Validation	143
7.3.1	Details of instrumentation.....	144
7.3.2	Bridge Information Modeling-based model.....	145
7.3.3	Implementation of the proposed framework.....	147
7.4	Summary	152

Chapter 8.....	153
8 Conclusion and Discussion	153
8.1 Key Conclusions	153
8.2 Thesis Contributions	154
8.2.1 Journal papers	155
8.2.2 Conference papers.....	156
8.3 Limitations of the Proposed Thesis.....	156
8.4 Potential Future Research	158
Bibliography	160
Curriculum Vitae	182

List of Tables

Table 3.1: Comparison of the analytical and estimated modal parameters of the 4-DOF model.....	36
Table 3.2: Frequency values identified with different levels of measurement noise.....	40
Table 3.3: Modal identification results for the 10-DOF model with 10% measurement noise.	41
Table 3.4: Comparison of identification results from two stages.	47
Table 4.1: Comparison of the analytical and identified frequencies of the beam subjected to vehicle-induced load.	61
Table 4.2: Frequency values identified from span 1 and span 2.....	65
Table 4.3: Frequency values identified from the mid-span length of span 1 and span 2.....	67
Table 4.4: Frequency values identified from bridge acceleration response.....	73
Table 5.1: Frequency values identified with different values of vehicle speed.....	90
Table 5.2: Frequency values identified for vehicle speed of 80 km/h with different levels of structural damage.	94
Table 5.3: Frequency values identified for vehicle speed of 40 km/h with different levels of structural damage.	97
Table 5.4: Frequency values identified for vehicle speed of 80 km/h with different levels of measurement noise.....	100
Table 5.5: Frequency values identified for vehicle speed of 40 km/h with different levels of measurement noise.....	100
Table 5.6: Properties of the scaled bridge model.....	102
Table 5.7: Frequency values identified from the scaled VBI model.	103

Table 5.8: Frequency values identified from direct and indirect BHM results.	109
Table 6.1: Properties of test vehicle and bridge.....	120
Table 6.2: Frequency and damping ratio values identified with different levels of measurement noise.....	126
Table 6.3: Frequency values identified with different levels of structural damage.....	128
Table 6.4: Frequency and damping ratio values identified from direct and indirect BHM results.	134
Table 7.1: Description of test data.	145
Table 7.2: Frequency values identified from free vibration response of bridge.....	151
Table 7.3: Frequency values identified from bridge response originating from various sensors.....	152

List of Figures

Figure 1.1: A schematic showing the scope of the proposed research.	3
Figure 1.2: A schematic showing the proposed validation studies.	3
Figure 2.1: Setup of a Direct BHM strategy.	6
Figure 2.2: Direct and indirect BHM.	9
Figure 3.1: Flowchart of the proposed methodology.	33
Figure 3.2: Fourier spectra of the fourth-floor vibration response.	34
Figure 3.3: Identification results from the fourth-floor vibration response.	35
Figure 3.4: Identification results from the first-floor vibration response.	35
Figure 3.5: Damping ratio estimation for (a) first, and (b) second mode of the fourth-floor vibration response.	36
Figure 3.6: (a) Time history, and (b) MSST results of the first-floor vibration response.	37
Figure 3.7: Identification results for the first-floor vibration response.	38
Figure 3.8: Identification results for the fifth-floor vibration response.	39
Figure 3.9: MSST results of the first-floor vibration response with (a) 5%, and (b) 10% measurement noise.	40
Figure 3.10: Damping ratio estimation for (a) first, and (b) second mode of the first-floor vibration response.	41
Figure 3.11: Elevation and plan view of the Z24 bridge.	42
Figure 3.12: Schematic of the sensor locations and various setup configurations.	44

Figure 3.13: (a) Time history, (b) Fourier spectra, (c) SST, and (d) MSST results for vibration response of sensor #229 (Stage 1).	45
Figure 3.14: Identification results for vibration response of sensor #229 (Stage 1).	46
Figure 3.15: Identification results for vibration response of sensor #229 (Stage 7).	46
Figure 3.16: Identification results for vibration response of sensor #221 (Stage 1).	47
Figure 3.17: Identification results for vibration response of sensor #221 (Stage 7).	47
Figure 4.1: (a) Time history, and (b) SET result of the frequency modulated signal.	54
Figure 4.2: Framework of the proposed BHM method.	56
Figure 4.3: Schematic of the vehicle traveling along a simply supported beam.	57
Figure 4.4: Fourier spectra of the acceleration response of the beam for vehicle speed of (a) 60 km/h, (b) 80 km/h, and (c) 100 km/h.	59
Figure 4.5: (a-d) Fourier spectra, and (e-h) SET results of the first four IMFs of the acceleration response of the beam for vehicle speed of 80 km/h.	61
Figure 4.6: (a) Schematics of the FEM bridge, and (b) cross-section A-A of span 2.	62
Figure 4.7: Typical time history of the bridge acceleration response.	62
Figure 4.8: Fourier spectra of bridge response at (a) quarter-span length, and (b) mid-span length for vehicle speed of 80 km/h.	63
Figure 4.9: (a-b) TVF-EMD results, and (c-d) SET results for the bridge response at quarter-span length of span 2.	64
Figure 4.10: (a-b) TVF-EMD results, and (c-d) SET results for the bridge response at the mid-span length of span 2.	65
Figure 4.11: Fourier spectra of bridge response at mid-span length for vehicle speed of (a) 40 km/h, and (b) 100 km/h.	66

Figure 4.12: Frequency profile of (a) 1.44 Hz and (b) 8.2 Hz identified from the mid-span length of span 2 for vehicle speed of 40 km/h.	67
Figure 4.13: Frequency profile of (a) 1.44 Hz and (b) 8.2 Hz identified from the mid-span length of span 2 for vehicle speed of 100 km/h.	67
Figure 4.14: Fourier spectra of bridge response due to (a) different vehicle weights, (b) different number of vehicle axles, and (c) different number of vehicles.	68
Figure 4.15: Frequency profile of (a) 1.44 Hz, and (b) 8.2 Hz identified from the mid-span length of span 2 subjected to two trucks.	69
Figure 4.16: Fourier spectra of undamaged and damaged bridge response for vehicle speed of 100 km/h.	70
Figure 4.17: Frequency profile of 1.24 Hz identified from the mid-span length of damaged span 2 for vehicle speed of 100 km/h.	70
Figure 4.18: (a) Steel truss bridge, and (b) sensor instrumentation.	71
Figure 4.19: Time history of bridge acceleration response at mid-span length.	71
Figure 4.20: Fourier spectra of bridge acceleration response subjected to (a) a bus, and (b) multiple vehicles.	72
Figure 4.21: SET results for (a-c) the first three natural bridge frequencies.	73
Figure 4.22: (a) First, and (b) second mode shape of the bridge.	73
Figure 5.1: Schematic of the vehicle traveling along a simply supported beam.	82
Figure 5.2: Framework of the proposed drive-by BHM method.	86
Figure 5.3: (a) Time history, and (b) Fourier spectra of vehicle acceleration response for vehicle speed of 40 km/h.	88
Figure 5.4: WPT coefficients of vehicle acceleration response for vehicle speed of 40 km/h.	88

Figure 5.5: SET results of vehicle acceleration response for vehicle speed of 40 km/h.	89
Figure 5.6: (a) Time history, and (b) Fourier spectra of vehicle acceleration response for vehicle speed of 80 km/h.	90
Figure 5.7: WPT coefficients of vehicle acceleration response for vehicle speed of 80 km/h.	90
Figure 5.8: SET results of vehicle acceleration response for vehicle speed of 80 km/h.	91
Figure 5.9: Fourier spectra of vehicle acceleration response for vehicle speed of 80 km/h with (a) 20%, and (b) 50% structural damage.	92
Figure 5.10: WPT coefficients of vehicle acceleration response for vehicle speed of 80 km/h with 20% structural damage.....	93
Figure 5.11: SET results of vehicle acceleration response for vehicle speed of 80 km/h with 20% structural damage.....	93
Figure 5.12: SET results of vehicle acceleration response for vehicle speed of 80 km/h with 50% structural damage.....	94
Figure 5.13: Fourier spectra of vehicle acceleration response for vehicle speed of 40 km/h with (a) 20%, and (b) 50% structural damage.	95
Figure 5.14: WPT coefficients of vehicle acceleration response for vehicle speed of 40 km/h with 20% structural damage.....	96
Figure 5.15: SET results of vehicle acceleration response for vehicle speed of 40 km/h with 20% structural damage.....	97
Figure 5.16: SET results of vehicle acceleration response for vehicle speed of 40 km/h with 50% structural damage.....	98
Figure 5.17: SET results of vehicle acceleration response with 10% measurement noise.	99
Figure 5.18: SET results of vehicle acceleration response with 20% measurement noise. ...	100

Figure 5.19: (a) Simply supported wooden beam, and (b) two-axle vehicle model.	102
Figure 5.20: Simply supported wooden beam subjected to measurement noise excitation..	102
Figure 5.21: (a) Time history, and (b) Fourier spectra of vehicle acceleration response.	103
Figure 5.22: WPT coefficients of vehicle acceleration response.....	103
Figure 5.23: SET results of vehicle acceleration response.	103
Figure 5.24: Five-span continuous box-girder bridge.....	104
Figure 5.25: (a) Data acquisition system, and (b) contact sensor instrumented on the bridge.	105
Figure 5.26: (a) Test vehicle, (b) plan view of sensor arrangement, sensor instrumentation in the (c) front, and (d) back of the test vehicle.	106
Figure 5.27: (a) Time history, and (b) Fourier spectra of bridge acceleration response.....	107
Figure 5.28: WPT coefficients of bridge acceleration response.	107
Figure 5.29: Fourier spectra of test vehicle acceleration response from (a) front sensor, and (b) back sensor.	108
Figure 5.30: SET results of test vehicle acceleration response from the front sensor.	109
Figure 5.31: SET results of test vehicle acceleration response from the back sensor.	110
Figure 6.1: Schematic of the vehicle traveling along a simply supported beam.	115
Figure 6.2: Framework of the proposed CP-based BHM method.	119
Figure 6.3: (a) Time history, and (b) Fourier spectra of CP response for vehicle speed of 18 km/h.	121
Figure 6.4: Fourier spectra of CP response for vehicle speed of 30 km/h.....	121

Figure 6.5: REMD results of (a-c) the first, second, and third modes of bridge model obtained from CP response for vehicle speed of 18 km/h.	122
Figure 6.6: REMD results of (a-c) the first, second, and third modes of bridge model obtained from CP response for vehicle speed of 30 km/h.	123
Figure 6.7: Fourier spectra of CP response with 20% measurement noise.	124
Figure 6.8: (a) Time history, and (b) Fourier spectra of CP response with 50% measurement noise.	124
Figure 6.9: REMD results of (a-c) the first, second, and third modes of bridge model obtained from CP response with 20% measurement noise.	125
Figure 6.10: REMD results of (a-c) the first, second, and third modes of bridge model obtained from CP response with 50% measurement noise.	125
Figure 6.11: Fourier spectra of CP response with 20% structural damage.	127
Figure 6.12: Fourier spectra of CP response with 50% structural damage.	127
Figure 6.13: REMD results of (a-c) the first, second, and third mode of bridge model obtained from CP response with 20% structural damage.	127
Figure 6.14: REMD results of (a-c) the first, second, and third mode of bridge model obtained from CP response with 50% structural damage.	128
Figure 6.15: Five-span continuous box-girder bridge.	129
Figure 6.16: Schematics of the five-span test bridge.	129
Figure 6.17: Fourier spectra of bridge acceleration response.	130
Figure 6.18: REMD results of (a-c) the first, second, and third modes of test bridge obtained from bridge acceleration response.	130
Figure 6.19: (a) Test vehicle, sensor instrumentation in the (b) front, and (c) back of the test vehicle.	132

Figure 6.20: Fourier spectra of vehicle acceleration response.....	133
Figure 6.21: Fourier spectra of CP response generated using vehicle acceleration response.	133
Figure 6.22: REMD results of (a-c) the first, second, and third modes of test bridge obtained from CP response generated using vehicle acceleration response.....	134
Figure 6.23: Distribution of (a) bridge natural frequencies, and (b) bridge damping ratio values.	135
Figure 7.1: Virtual sensor modeled in Autodesk REVIT.	139
Figure 7.2: IFC sensor data.	140
Figure 7.3: Proposed framework for the BrIM-based BHM method.....	142
Figure 7.4: (a) Direct sensor instrumentation of steel bridge, (b) DAQ system, and (c) sensor instrumented on bridge sidewalk.	144
Figure 7.5: Virtual 3D model of bridge and sensor.	146
Figure 7.6: Sensor metadata defined in Autodesk REVIT.	147
Figure 7.7: DAQ file containing raw and unprocessed data.	148
Figure 7.8: Execution of SID in Autodesk REVIT using MATLAB online portal.....	149
Figure 7.9: Time history of measured bridge response.....	149
Figure 7.10: Fourier spectra of the measured (a) free vibration response, and (b) vehicle traffic-induced response of the bridge.	150
Figure 7.11: TVF-EMD results of vehicle traffic-induced response of the bridge.....	151

List of Acronyms

Abbreviation	Explanation
ANN	Artificial Neural Network
API	Application Programming Interface
AR	Augmented Reality
BHM	Bridge Health Monitoring
BIM	Building Information Modeling
BrIM	Bridge Information Modeling
BSS	Blind Source Separation
CP	Contact Point
CS	Crowdsourcing
CWT	Continuous Wavelet Transform
DAQ	Data Acquisition
DOF	Degree of Freedom
DT	Digital Twin
DWT	Discrete Wavelet Transform
HHT	Hilbert-Huang Transform
HT	Hilbert Transform
EEMD	Ensemble Empirical Mode Decomposition
EMD	Empirical Mode Decomposition
EWT	Empirical Wavelet Transform
FE	Finite Element
FEM	Finite Element Modeling
FT	Fourier Transform
iBHM	Indirect Bridge Health Monitoring
IF	Instantaneous Frequency
IFC	Industry Foundation Classes
IMF	Intrinsic Mode Function
IOT	Internet of Things
LiDAR	Light Detection and Ranging
MDOF	Multi Degree of Freedom
MEMD	Multivariate Empirical Mode Decomposition
MR	Mixed Reality
MSST	Multi Synchro Squeezing Transform
NDT	Non-Destructive Testing
RDT	Random Decrement Technique
REMD	Robust Empirical Mode Decomposition
RMS	Root Mean Square
SDOF	Single Degree of Freedom
SET	Synchro Extracting Transform
SHM	Structural Health Monitoring
SID	System Identification

SSSC	Soft Sifting Stopping Criterion
SST	Synchro Squeezing Transform
STFT	Short-Time Fourier Transform
TF	Time Frequency
TVF-EMD	Time-Varying Filter Empirical Mode Decomposition
VBI	Vehicle Bridge Interaction
VMD	Variation Mode Decomposition
VR	Virtual Reality
WIM	Weigh-in-Motion
WPT	Wavelet Packet Transform
WT	Wavelet Transform
WVD	Wigner-Ville Distribution

List of Symbols

Symbol	Explanation
A	State Matrix
A_k	Time-Varying Amplitude
$A(t)$	Instantaneous Amplitude
B	Input Matrix
C	Damping Matrix
\hat{C}	Output Matrix
D	Transmission/Feedback Matrix
E	Modulus of Elasticity for Bridge
$F_s(t, \eta)$	Frequency-Reassignment Operator
$F_s^{[N]}$	Synchro Squeezing Transform at N -th Iteration
$H_{bl,n}$	Bridge Frequency Amplitude-Left
$\tilde{H}_{bl,n}$	Bridge Frequency Coefficient-Left
$H_{br,n}$	Bridge Frequency Amplitude-Right
$\tilde{H}_{br,n}$	Bridge Frequency Coefficient-Right
$H_{dl,n}$	Driving Frequency Amplitude -Left
$\tilde{H}_{dl,n}$	Bridge Frequency Coefficient-Left
$H_{dr,n}$	Driving Frequency Amplitude -Right
$\tilde{H}_{dl,n}$	Bridge Frequency Coefficient-Right
$H(t, \omega)$	Short-Time Fourier Transform
$H_{v,n}$	Vehicle Frequency Amplitude
$\tilde{H}_{v,n}$	Vehicle Frequency Coefficient
I	Moment of Inertia for Bridge
$IMF_j(t)$	Intrinsic Mode Function
K	Stiffness Matrix
L	Bridge Length
$L_j(n)$	Lower Envelope REMD
M	Mass Matrix
S_e	Short-Time Fourier Transform
S_n	Non-Dimensional Speed Parameter
S_x	Non-linear Operator for Synchro Squeezing Transform
$SET_i(t, \omega)$	Synchro Extracting Transform
$U_j(n)$	Upper Envelope REMD
W_f	Continuous Wavelet Transform
$c_k^{j,s}(t)$	Wavelet Packet Coefficient
d	Scale of Mother Wavelet
f_{bn}	Bridge Frequency (Hz)
\hat{f}_b	Estimated Bridge Frequency (Hz)
\hat{f}_{bn}	Estimated Bridge Frequency (Hz)
f_d	Estimated Driving Frequency (Hz)

f_{jk}	Stopping Criterion REMD
$f^{j,s}$	Wavelet Packet Component Signal
$f_{kj}(t)$	Intrinsic Mode Function
$h_j(n)$	Proto-Intrinsic Mode Function
$h(u)$	Window Function
\hat{h}	Fourier Transform of Window Function
$i_j(t)$	Intrinsic Mode Function
$i_{kj}(t)$	Multicomponent Signal
k_v	Vehicle Stiffness
\bar{m}	Mass Per Unit Length
$m_j(n)$	Mean of Envelope REMD
m_v	Vehicle Mass
$q(j)$	B-Spline Coefficient
$q(t)$	Vehicle Displacement Response
$\ddot{q}(t)$	Vehicle Acceleration Response
$r_n(t)$	Residue Signal of $x(t)$
$r_j(n)$	Updated Residual REMD
$r_o(t)$	Residual REMD
$u_c(t)$	Contact Point Displacement Response
$\ddot{u}_c(t)$	Contact Point Acceleration Response
$u(t)$	Excitation Vector
$u(x, t)$	Bridge displacement Response
$\ddot{u}(x, t)$	Bridge Acceleration Response
v	Vehicle Speed
w_v^p	Pre- and Post-Filter
$x(t)$	Time-Frequency Signal
\ddot{y}_v	Vehicle Acceleration Response
$y(t)$	Time-Frequency Signal
z	Displacement Response Vector
δ	Dirac Delta Function
δ_2	Synchro Extracting Operator
δ_v^2	Approximation Error
φ_k	Phase Function
$\hat{\varphi}_{kn}$	Normalized Modeshape Matrix
φ_{mxn}	Mode Transformation Matrix
$\varphi(t)$	Instantaneous Phase
$\varphi'(t)$	Derivative of Instantaneous Phase
η	Modal Response Vector
τ	Translation of Mother Wavelet
ζ	Damping Ratio
ω	Angular Frequency
$\omega(a, t)$	Instantaneous Frequency

$\hat{\omega}(t, \omega)$	Instantaneous Frequency
$\hat{\omega}^{[N]}$	Estimate of instantaneous Frequency at N -th iteration
ω_{bn}	Bridge Frequency
$\omega_{bn,avg}$	Average Bridge Frequency
ω_d	Driving Frequency
ω_v	Vehicle Frequency
ω_x	Phase Transform
$\psi_k^{j,s}(t)$	Linear Combination of Wavelet Basis Functions
$\psi(t)$	Mother Wavelet
Δ_{stn}	Static Deflection Caused by the Vehicle
Δt	Sampling Interval
$\{-\}_{\uparrow \nu}$	Up-sampling Operation
$\{-\}_{\downarrow \nu}$	Down-Sampling Operation

Chapter 1

1 Introduction

1.1 Research Motivation

Civil infrastructure systems are being significantly threatened by age-related degradation, neglected maintenance, natural disasters, and anthropogenic hazards such as earthquakes, floods, hurricanes, fires, explosions, and toxic releases. The primary factor that leads to the failure of civil infrastructure systems is degradation. According to the ASCE Report Card, 42% of the bridges in the United States are at least 50 years old, and 7.5% of them are considered structurally deficient (ASCE, 2021). In Canada, the number of bridges rated fair or worse has reached 40%, according to the Canadian Infrastructure Report Card (CIRC 2019). Deteriorating bridge infrastructure is a major public safety concern that requires a multi-pronged solution that can be economical and efficient. Most of the bridges are assessed periodically using visual inspections, which can be subjective, expensive, and susceptible to errors. The drawbacks of a conventional bridge inspection approach restrict its widespread use in urban and highway bridges. Rapid detection methods and approaches are urgently required to satisfy the growing maintenance requirements for these bridges and have drawn increased attention recently.

Bridge health monitoring (BHM) can provide an effective solution to address these challenges of assessing the severity of the degrading state of bridge infrastructure. Recently developed vibration-based BHM techniques (An *et al.* 2019, Sun *et al.* 2020, Sony *et al.* 2022, Singh *et al.* 2022) utilize the vibration data, which can expedite the accuracy of damage detection compared to visual inspection. Bridge modal parameters such as modal frequencies, damping, and mode shapes, measured from collected vibration data, can be effective indicators of structural degradation and damage. The visual representation and efficient management of real-time monitoring data is a challenge for BHM approaches. There is a need to standardize, integrate, and visualize the collected BHM data through a visualization framework for systematic monitoring of bridges based on their current condition.

Conventional BHM requires a dense array of sensors directly instrumented on the bridge structure to get the dynamic responses from different locations of the bridge, which demand significant time and expense, and often suffer from limited access to critical locations. It is imperative to develop robust and cost-effective direct BHM methods based on limited sensors capable of keeping the same information as a large network of sensors while providing high accuracy in damage detection and localization. As an alternative to direct BHM, indirect BHM (iBHM) or drive-by BHM (Yang *et al.* 2004a) has been put forth as a convenient, efficient, and low-cost monitoring technique. The dynamic parameters of the bridge are extracted from the response of an instrumented passing vehicle. Besides frequency identification, iBHM can be extended to estimate bridge damping and mode shapes. A passing vehicle acts as an exciter and a data collection device simultaneously in this method. However, to delineate bridge dynamic response from vehicle dynamic response, vehicle-bridge interaction (VBI) needs to be accurately analyzed to prevent inaccuracies in BHM. Powerful signal processing methods are required for analyzing nonstationary and nonlinear signals originating from direct BHM and iBHM networks. In this thesis, output-only system identification (SID) using limited sensors is explored to enhance the condition assessment and damage detection capabilities of direct BHM as well as iBHM to provide autonomous monitoring of bridge infrastructure. The visualization of long-term BHM data is also investigated in this thesis using Bridge Information Modeling (BrIM).

1.2 Research Scope

The scope of this thesis is bounded in the search for smart and cost-effective BHM schemes by implementing output-only SID to supplement the practical application of direct BHM and propose iBHM methods for autonomous and real-time damage detection using limited sensors. This thesis also intends to provide a framework for a visual representation of long-term BHM data. This thesis aims to develop the theory as well as to validate the formulations and presumptions utilizing a variety of numerical, experimental, and full-scale studies. The proposed research and validation studies of this thesis are summarized in Figs. 1.1 and 1.2, respectively.

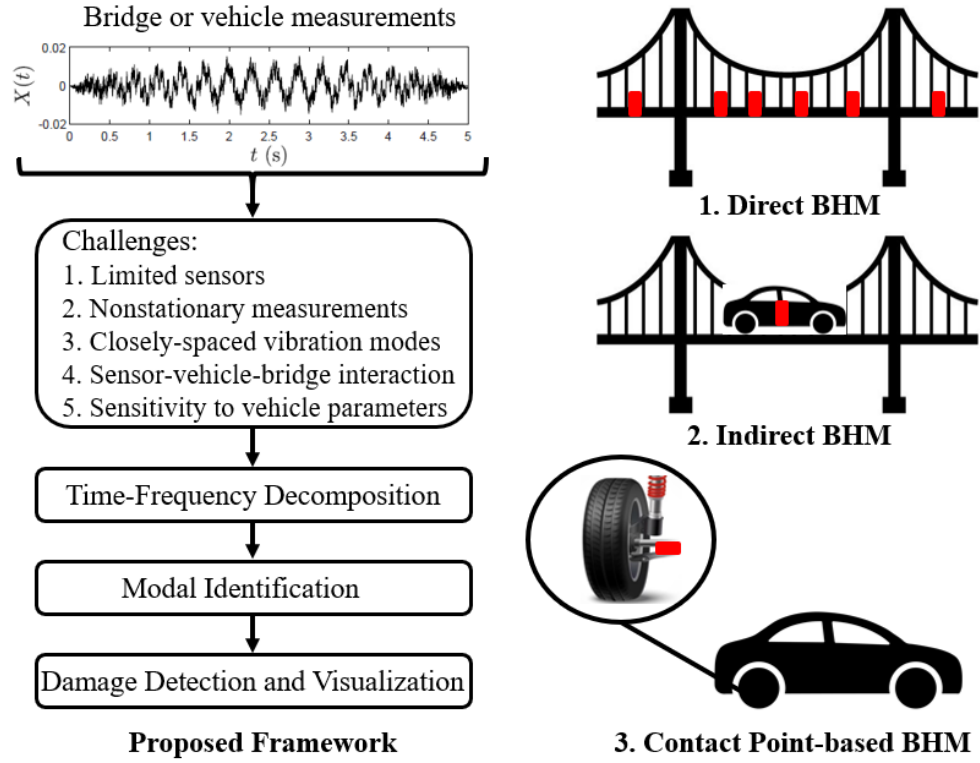


Figure 1.1: A schematic showing the scope of the proposed research.

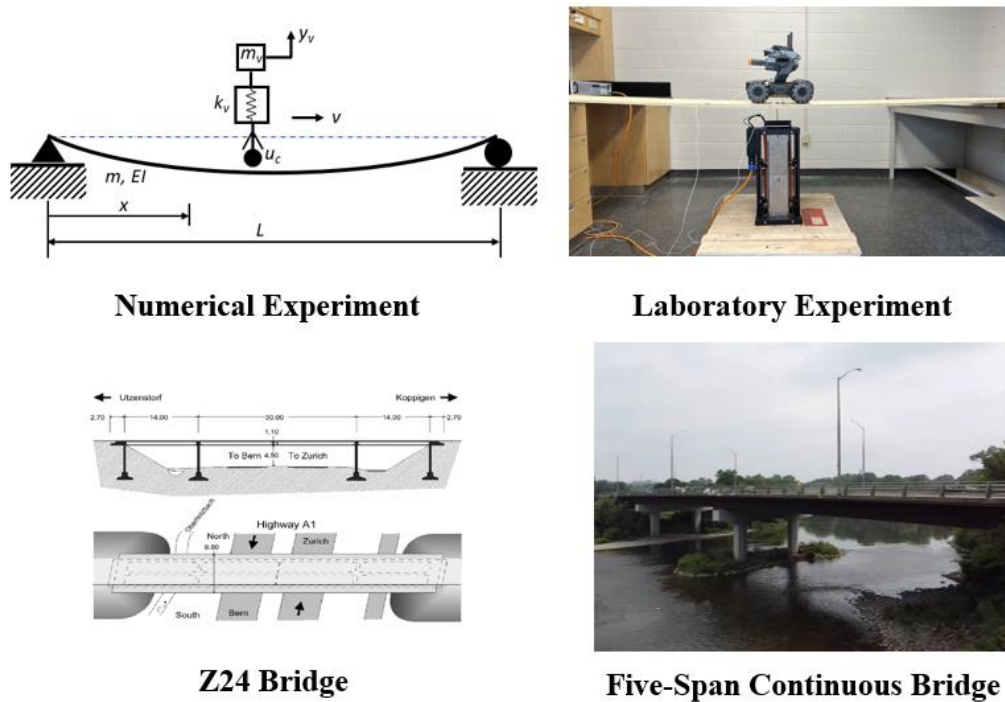


Figure 1.2: A schematic showing the proposed validation studies.

1.3 Research Objectives

The general objective of the current research is to accomplish the following broad tasks:

- To develop a limited sensor-based SID method for cost-effective condition assessment of bridges subjected to ambient and traffic-induced vibrations.
- To explore smart drive-by modal identification of bridges using a moving instrumented vehicle and its contact point (CP) response.
- To investigate the visualization and big data management capabilities of BrIM.

1.4 Outline of the Thesis

The thesis is organized as follows:

A general introduction and thesis objectives, along with the organization of the thesis, are provided in Chapter 1. Chapter 2 provides a brief introduction and literature review of conventional and modern bridge infrastructure management along with the associated limitations and challenges.

An improved time-varying Empirical Mode Decomposition method is proposed in Chapter 3, which utilizes limited sensors to process the bridge data containing ambient vibrations. In Chapter 4, Synchro-Extracting Transform is proposed for condition assessment using vehicle-induced nonstationary response.

A hybrid time-frequency method is proposed for drive-by modal identification of bridges in Chapter 5. In Chapter 6, a novel vehicle scanning method independent of vehicle dynamics is proposed based on CP response. BrIM-based visualization tool for long-term bridge monitoring is presented in Chapter 7.

Chapter 8 summarizes the key conclusions, research contributions, and provides some future directions from this thesis.

Chapter 2

2 Literature Review

A brief introduction to conventional and modern bridge health monitoring (BHM) is provided in this chapter. Direct BHM has utilized contact-based techniques and time-frequency methods for structural condition assessment of bridges. With the advancement of noncontact sensing technologies, indirect BHM (iBHM) and visualization techniques have been explored in the literature. However, these techniques have several limitations that hinder their direct implementation in providing cost-effective and smart bridge infrastructure management. In this context, literature on conventional and modern BHM has been reviewed and their existing challenges are identified. Based on these challenges and gap areas, the key objectives of this thesis are identified at the end of this chapter.

2.1 Direct Bridge Health Monitoring

The ability to continuously maintain the desired functionality of bridge infrastructure demands robust damage assessment techniques that are reliable, cost-effective, and autonomous. Traditional bridge monitoring has relied on visual inspection, which is highly variable, lacks resolution, and can only detect visible damage. With the advancements in signal acquisition and data transmission techniques, contact-based BHM (An *et al.* 2019) has emerged as a popular alternative to bridge monitoring and maintenance. Contact-based BHM relies on the detection of anomalies in bridge dynamics using the dynamic responses of the bridge. The underlying principle is that if damage occurs in a structure, it results in a change in physical properties such as stiffness loss, and subsequently causes discernible variations in dynamic properties. BHM offers robust diagnostic and prognostic tools to detect any unusual symptoms, serviceability, and safety concerns (Wu and Jahanshahi 2018). In a typical BHM setup, sensors are directly installed on a bridge and are connected to a data acquisition system that feeds raw data to a central unit. Fig. 2.1 shows a typical representation of a direct BHM system where the sensors are connected to a data acquisition (DAQ) system and send the acquired raw data to a central unit or a computer.

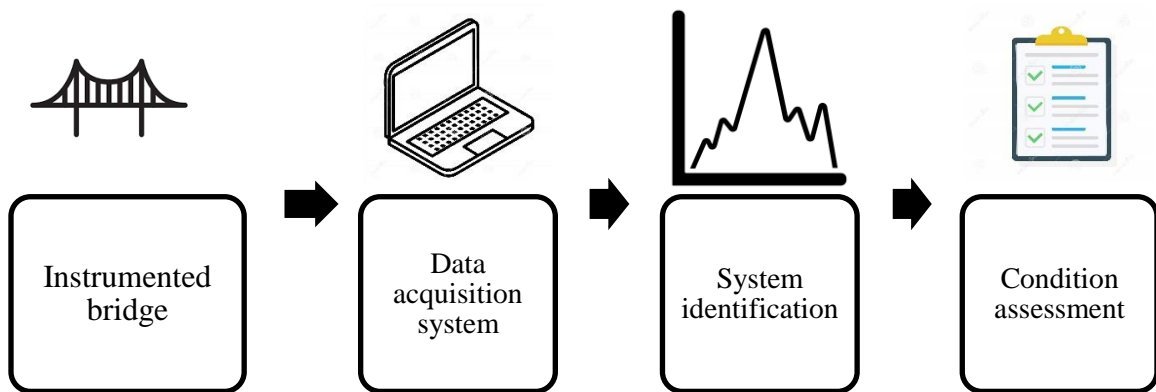


Figure 2.1: Setup of a Direct BHM strategy.

Chang and Kim (2011) used Empirical Mode Decomposition (EMD) and proper orthogonal decomposition to extract structural displacement responses and mode shapes under impact and moving load. The results were compared with directly measured displacement, modal assurance criteria, and energy difference tracking method using the data collected from a three-story experimental model and a full-scale bridge. He *et al.* (2011) integrated EMD with Random Decrement Technique (RDT) to obtain the natural frequency and damping ratio of a steel truss bridge under ambient vibration. The results were compared with the peak-picking method using vibration data collected from the Nanjing Yangtze River bridge. The results showed that EMD-based RDT could be a suitable modal identification technique for large-scale civil structures. Reddy *et al.* (2014) used EMD to conduct damage detection in beams and bridge models using strain data. The results presented that EMD can detect even a 0.01% reduction in stiffness for a beam and up to 0.5% for a real bridge. In another study, Qin *et al.* (2015) utilized improved EMD to extract natural frequencies and damping ratios under ambient vibration. The results were compared with Finite Element Modeling (FEM), peak-picking, and stochastic subspace identification using vibration responses collected from the Songtoujiang railway bridge. The results proved the significant efficiency of the proposed method compared to the other methods.

Aied *et al.* (2016) applied the ensemble EMD (EEMD) method to the mid-span acceleration response of a bridge to capture the sudden stiffness changes. Minor stiffness changes were successfully identified in cases of relatively high vehicle speeds and even significant noise since EEMD can separate high-frequency components related to stiffness changes from other frequency components associated with the vehicle-bridge interaction system. In another research, Wu *et al.* (2016) applied EMD to undertake damage detection and assess the bearing capacity using a numerical beam model and a real bridge subjected to moving loads. The results showed that the EMD method could accurately identify the location and intensity of the damage. Song *et al.* (2017) used EMD and the natural excitation technique to identify the natural frequency and damping ratio of the Tingkau bridge. The results showed that the proposed method could accurately extract the structural modal parameters, which makes it a suitable candidate tool for system identification (SID) of large civil structures.

Recently, Barbosh *et al.* (2018) explored multivariate EMD (MEMD) to extract the modal parameters of various civil engineering structures using multichannel signals under different practical situations. The MEMD method was validated utilizing multichannel vibration data that was collected from a suite of numerical, experimental, and two full-scale structures such as the Canton Tower in China and a highway bridge in Canada. Due to the mode-mixing issue in some modal responses, a powerful blind source separation (BSS) technique, namely, Independent Component Analysis, was used, which involved less computational effort and time. It was concluded that the proposed method was able to extract the closely spaced with 2% separation and low-energy modes, which makes it a suitable candidate as a modal identification tool using multiple vibration responses collected from various types of structures. On the other hand, Ni *et al.* (2018) utilized variational mode decomposition and EMD to identify the instantaneous frequency of the four degrees of freedom (DOF) numerical model and a bridge subjected to free vibration and moving load. The results showed that the proposed method was more accurate than EMD-based methods. Trung (2018) utilized the Hilbert Huang Transform (HHT) to identify instantaneous variations in the dynamic characteristics of bridge caisson foundations under liquefaction.

A novel data analysis method that combined permutation entropy and spectral substitution with EEMD (Huang *et al.* (2019)) showed that the technique could extract multiple frequencies from the data with significant noise. Data collected from the full-scale bridge was analyzed using the proposed method, where the results indicated the capability of the proposed method to extract multi-frequencies. Shao *et al.* (2019) used a combination of EMD and fractal conservation law to de-noise and filter the vibration data collected from a full-scale long-span bridge. The results of the proposed filter were compared with the other methods and showed the high performance of the proposed filter over the other techniques. Lastly, Celik *et al.* (2020) used a noise-assisted version of the MEMD to extract the modal parameters of civil structures under the operational load using multichannel data from various experimental and full-scale studies. The authors applied complete EEMD with adaptive noise to alleviate the mode-mixing issue in the resulting intrinsic mode functions (IMFs) obtained from MEMD. It was concluded that the proposed method was successfully able to extract the modal parameters even in the case of vibration data with a short duration.

2.1.1 Challenges of direct bridge health monitoring

- To reap the benefits of contact-based sensing for direct BHM, a dense array of direct contact sensors is required, which can transmit the data to a central computer. However, direct instrumentation requires too many sensors, which subsequently results in high labor costs, lane closures, and traffic congestion. As a result, this approach cannot be implemented in a large inventory of bridges for continuous monitoring.
- The vibration response of a bridge due to ambient and traffic-induced vibrations is primarily processed using various time-domain, frequency-domain, and time-frequency domain methods. Most of these methods rely on multi-channel measurements and are not suitable for SID using a limited number of sensors.
- Finer time-frequency representation of a nonstationary multi-component signal is significant for the successful identification of structural systems such as bridges. The vibration signal originating from bridges needs a powerful time-frequency (TF)

method that can effectively deal with the nonstationary signal in the presence of measurement noise, closely spaced, and low energy modes.

2.2 Indirect Bridge Health Monitoring

In recent years, BHM techniques have evolved from contact to non-contact sensors (Na and Baek 2017, Sony *et al.* 2019, Bodupalli *et al.* 2019, Sun *et al.* 2020, Dertimanis and Chatzi 2020, Sony *et al.* 2021) due to next-generation inexpensive sensors such as camera, robots, and drones. iBHM leverages the vehicle traveling over the bridge as a data-collecting device and a source of excitation. While traversing over the bridge, an instrumented vehicle can excite the bridge and collect the vibration response of the bridge. A conceptual difference between direct BHM and iBHM is shown in Fig. 2.2. It is expected that the moving sensor will have better damage localization capability than the direct BHM due to its thorough scanning of the bridge. The majority of iBHM studies have focused on moving mass, moving load, and moving the sprung mass model to capture the dynamic effects of bridges. Out of these studies, the moving sprung mass model best represents the moving vehicle over the bridge by considering the inertia effects of the vehicle. The measured vehicle response includes the contribution of bridge dynamics, vehicle dynamics, and surface-induced roughness (Yang *et al.* 2012). Therefore, it is always a challenge to delineate the effects of the latter two parameters from the measured data. Moreover, many other factors, such as road profile, test vehicle systems, and vehicle-bridge interactions, affect the performance of iBHM (Yang *et al.* 2020a).

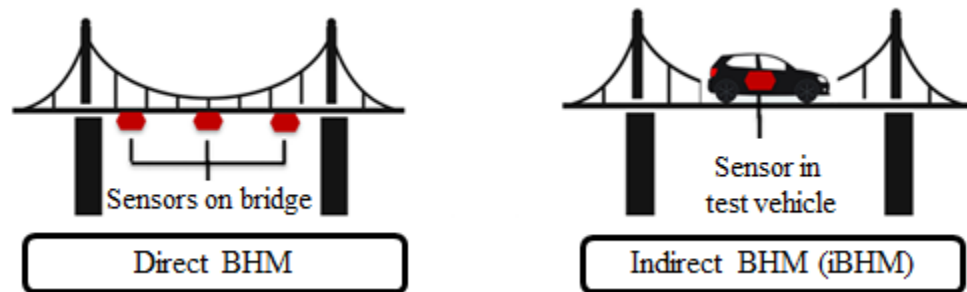


Figure 2.2: Direct and indirect BHM.

The idea of using a test vehicle to extract the bridge frequencies was initially proposed by Yang *et al.* (2004) and was validated numerically by Yang and Lin (2005a) using a simply supported beam. It was concluded that vehicle response was largely dominated by driving frequency, vehicle frequency, and the associated pairs of shifted frequencies of bridges. It was observed that the displacement response of the vehicle was influenced by the vehicle speed, while the vehicle acceleration response was affected by the bridge frequencies. In this study, it was assumed the mass of the vehicle was small compared to the bridge. Later, EMD was used by Yang and Chang (2009) to extract the higher modes of the bridge using experimental studies. The importance of the selection of the most appropriate test vehicle properties was discussed. The idea of estimating bridge frequency from a common vibration component among multiple vehicle responses was put forth by Nagamaya *et al.* (2017). The frequency estimation strategy was based on the cross-spectral density function estimated through a novel signal processing method. In the drive-by bridge inspection, the vehicle's speed significantly affects the success of the method as high speed induces sufficient kinetic energy to excite the bridge mode, whereas low speed helps in collecting more data with less effect of road roughness on vehicle vibration.

Elhatab *et al.* (2018) introduced the new Frequency Independent Underdamped Pinning Stochastic Resonance technique, which could extract the bridge dynamics properties from the vehicle response moving at high speed over the bridge. The vehicle at high speed had more noise components over the bridge vibration, so using Stochastic resonance, the feeble information, such as bridge vibration, could be amplified by the background noise. Passing vehicle across a bridge is excited by two sources which are pavement roughness and bridge vibration. Wang *et al.* (2018) based their work on this idea and proposed a frequency extraction method from the response of a vehicle with its parameters calibrated. Vehicle excitation sources, such as displacement inputs at the front and rear tires, were estimated from vehicle response using a particle filter method. The roughness influence was eliminated by shifting and subtracting the displacement inputs. The method was verified using numerical simulations and field tests. Wang *et al.* (2019) contributed to the field of vehicle bridge interaction (VBI) by estimating the vertical tire forces resulting from a vehicle-induced load. The estimation method was based on

vertical acceleration and angular velocity of the vehicle body. The measured data was analyzed using an augmented Kalman filter, and good accuracy was achieved against noise and error in numerical and experimental conditions.

FE model updating was attempted by Kong *et al.* (2017) using the measured accelerations and strains of the bridge obtained from a passing vehicle. A tractor-trailer system was used to determine the bridge dynamic parameters. The test vehicle response was used to calculate the bending stiffness of the bridge by Yang *et al.* (2018b) using the frequency-domain method and time-domain method. While the frequency-domain method was economical as it could estimate the initial bridge stiffness, the time-domain method was computationally demanding in nature. The field test results indicated that both methods were useful for assessing the bending stiffness of a full-scale bridge. In another study, Matsuoka *et al.* (2021) proposed the drive-by system to track down resonant bridges by high-speed trains using track irregularities. In this study, devices were mounted on the first and last train vehicles to measure the difference between two-track irregularities at the same position. The last vehicle response was attributed to abnormal bridge displacement due to resonance mechanisms and track irregularities. However, the first vehicle response was generated primarily due to the track irregularities, a resonance phenomenon yet to be completely excited. This difference between the track irregularities measured by the first and last mounted devices was used to compute the resonance detection index. This index would be used to detect the resonant bridge component excited by the vehicle length. Micu *et al.* (2022) investigated the static and dynamic effects of the railway bridge by repeated dynamic responses collected from an instrumented passing train to assess the condition of a bridge. This study proved that instrumented trains could potentially be used for ongoing monitoring and identification for repair or rehabilitation.

A comprehensive monitoring method responsible for detecting the frequency, damping, mode shape, and local stiffness of a girder bridge was put forth by Yang *et al.* (2022a). In numerical and field investigations, a tractor was used in conjunction with two identical trailers whose residual acceleration was used to eliminate the effect of road roughness. The bridge frequency component was obtained using bandpass filtering and damping

ratio and mode shapes were reconstructed using Short-Time Fourier Transform (STFT). Bridge stiffness was determined using the reconstructed mode shape. The vehicle frequency and road roughness were two trouble-causing factors that hindered the vehicle scanning method in identifying bridge frequencies. Yang *et al.* (2022b) proposed a simple yet physically robust technique to detect adverse factors by recording the vehicle response in the parked state. The test vehicle in a parked condition would be free of pavement roughness and self-frequency if vehicle frequency were made far higher than the bridge frequency. This proposed methodology presented a trade-off between fixed sensors on the bridge deck to moving test vehicles with good data quality and less measurement time.

With the recent developments in sensing technologies, there has been a paradigm shift in the sensing techniques that outperform traditional sensors, including wired or wireless sensors. Such emergent iBHM technologies that have been developed in the past few years and the use of next-generation sensing techniques such as smartphone monitoring or crowdsourcing (CS), and contact point (CP) response monitoring are reviewed. Modern smartphones are equipped with accelerometers, gyroscopes, and global positioning system (GPS) that can efficiently detect the structural health of bridges (Sony *et al.* 2019). Monitoring data collected through smartphones, even though it may be imperfect, can contribute valuable BHM information when aggregated using the crowdsourcing framework.

Shirzad *et al.* (2020) investigated various vehicle features to enhance the implication of CS for bridge monitoring. The fundamental frequency of the bridge was captured using a large set of passing vehicles with different features. The proposed method was validated using different combinations of vehicle suspension and vehicle speed on two bridges with different support systems. Sitton *et al.* (2020) examined the applicability of CS for bridge monitoring using the analytical FEM simulation and a scaled laboratory experiment. Analytical and experimental results showed that the bridge frequency could be identified using the multi-vehicle approach. The CS framework established that iBHM could be accomplished without the information related to the mass and stiffness of the vehicle or bridge. For large-scale road network monitoring, test vehicles need to be calibrated, and

road condition needs to be evaluated. Xue *et al.* (2020) proposed an algorithm capable of estimating the road profile while simultaneously identifying the vehicle parameters. The responses from the vehicle were collected using a smartphone, and optimization of estimated profiles was conducted using an objective function and constraint conditions.

Shirzad and Gul (2021) proposed the drive-by frequency identification technique with enhanced inverse filtering-based methodology using smartphones as a vehicle's vibration recorder. The study aimed to suppress the effect of vehicle features and road features by inverse filtering as vehicle response was dominated by the effect of the suspension system, road roughness, and vehicle speed. In this novel approach to inverse filtration, a dataset of vehicle response at different speeds was constructed to account for the effects of vehicle speed on the performance of the proposed method. At the same time, the impact of surface roughness on the performance was examined by the proposed energy-based surface roughness criterion. In a recent study, Matarrazo *et al.* (2022, Preprint) attempted to achieve high-precision bridge monitoring and maintenance using CS smartphone data. Various datasets were collected from both short and long-span bridges using a variety of smartphone and vehicle models. The extraction of the most probable modal frequencies was conducted using a synchro-squeezed wavelet transform. The results from three broad classes of CS data: controlled, uncontrolled, and partially controlled, provided accurate modal properties. This study also suggested that data collection features such as vehicle speed and smartphone orientation do not necessarily need to be designed or influenced. It was also found that the service life of existing and new bridges could be significantly enhanced using CS monitoring data.

2.2.1 Contact point-based bridge health monitoring

While using a test vehicle to scan the bridge's dynamic properties, vibration sensors fixed on the car body are used to obtain the vehicle response. The presence of vehicle frequency in the vehicle response may render the extraction of bridge frequency difficult in spectral analysis, especially in the presence of road roughness. To overcome this challenge, the vehicle's CP response was proposed as a better method for scanning bridge properties (Yang *et al.* 2018a). The advantage of CP response is that it is independent of vehicle frequency and therefore allows more detection of bridge frequencies with

minimal inference of vehicle parameters. Hashlamon *et al.* (2021) investigated the effectiveness of the CP response of the stationary vehicle under various conditions, including damped and undamped conditions, road roughness, vehicle speeds, and masses, vehicle frequencies, and span length of the bridge to conduct iBHM. In this study, the bridge was excited by another moving vehicle while a stationary parked vehicle recorded the response, and a numerical model was developed. In previous studies, the damping effect of the test vehicle was ignored since the test vehicle was designed with high transmissibility/less damping to receive high bridge vibration. However previous studies suggested that vehicle damping could affect vehicle frequency, bridge response, and measured pavement roughness.

The vehicle scanning method using CP response was not just restricted to highway bridges. Yang *et al.* (2021a) implemented it to assess the condition of the rail tracks and rail bridges. This study presented the theory of extracting the track/bridge frequencies and track modulus over a dual-beam model using an instrumented vehicle. This dual-beam system simulated the track-bridge system and replicated the effect of sleepers and ballast. The recorded vehicle response was further translated into vehicle-track CPs using closed-form equations, and the solution provided the track and bridge frequencies. Rarely had any publication discussed the effect of torsional-flexural vibration on bridge health as that could not be represented well in 2D beams. Yang *et al.* (2022c) proposed a procedure to eliminate the vehicle frequencies and road roughness by skillful use of a two-axle moving test vehicle. This study presented that the vehicle-bridge CP would eliminate the vehicle frequencies, and the front and rear CP response residue would remove road roughness. Using vertical and rotational equations of motion, the CP response was derived, which would be processed by the Variational Mode Decomposition (VMD) to bring out the component response, followed by the mode shapes using Hilbert Transform (HT).

Yang and Wang (2022a) proposed an improved vehicle scanning method to identify modal properties while considering the damping and road roughness of the bridge. Since the damping effect produced a weak signal by degrading it over time and road roughness corrupted the signal; thus appropriately tuned elliptic filter was employed over a

conventional bandpass filter, such as the Butterworth filter. Firstly, the dynamic response was computed by the moving internal node element method, and then the Fourier transform of the CP response would extract the bridge frequencies. Once the targeted natural frequencies are known, an appropriately tuned elliptic filter would be used to decompose the CP response time series. Finally, the instantaneous amplitude function would construct the mode shape from an analytic signal. The improved vehicle scanning method was further used to locate the bridge damage from the extracted mode shapes with minimal postprocessing effort in Yang and Wang (2022b). The narrowband signals from the CP response, when processed through the elliptical filter, revealed visible kinks that indicated the locations of bridge damage. Yang *et al.* (2021c) to decompose the vibration data under the desired frequency range. Then the CP response was calculated from the backward procedure by using vehicle response. The combined approach provided a more elegant response decomposition and removed the mode-coupling problem and undesired roughness frequencies. The double-pass mass-addition technique was formularized by Zhan *et al.* (2021) to obtain the CP response difference from vehicle response in the presence of bridge surface roughness. The study determined the bridge mode shapes from signal filtering and HT, and the possible damage locations could be identified by applying Wavelet Transform (WT) on CP displacement difference. Significant effects could be seen due to the presence of surface roughness in the simulated results. Other factors that may affect the high fidelity were also investigated, including vehicle speed, traffic, measured noise, and distribution of added mass.

The dual Kalman filter and Singular Spectrum Analysis were employed by Li *et al.* (2022) in the drive-by bridge health monitoring to explore the bridge condition by identifying the dynamic response of the CP between the bridge and vehicle using two successive instrumental vehicles. It was a three-step formulation in which a dual Kalman filter identifies the input forces of two successive vehicles, and by using input forces and vehicle parameters, the responses of two CPs were extracted. After that, the subtraction technique assisted in the reduction of the road surface roughness effect from the identified CP responses. Finally, auto-singular spectrum analysis decomposed the response residue and brought out the mono-component modes of bridge response. Yang *et al.* (2022d) proposed a technique where a single-axle test vehicle was modeled as a 2-

DOF system by installing the sensor near the test vehicle's wheels to catch the rocking motion. Since both wheels of the test vehicle might experience different surface roughness due to the uneven profile of the road and induce rocking motion, thus CP response was determined for both wheels separately. On the flat road surface, the vertical bridge frequencies can be extracted by averaging the CP responses and rocking frequencies by calculating the angular response. Factors such as vehicle frequencies and road roughness affected the vehicle scanning methods in extracting the bridge modal properties.

2.2.2 Challenges of indirect bridge health monitoring

- In the iBHM field of studies, most researchers used the responses recorded by the vehicle-mounted sensor to detect the bridge modal properties and damage extent. However, it had been observed that the recorded vehicle responses were contaminated with the vehicle and driving frequencies, which may mask the bridge frequencies. Therefore, it requires a high-resolution iBHM that can suppress the effects of vehicle and pavement conditions and extract the bridge frequencies.
- The majority of iBHM studies have focused on moving mass, moving load, and moving sprung-mass models to capture the dynamic effects of bridges in the collected responses. Out of these studies, the moving sprung mass model best represents the moving vehicle over the bridge by considering the inertia effects of the vehicle. However, the vehicle response passing over a bridge always contains bridge frequencies along with driving frequency and vehicle frequency. Therefore, it is always a challenge to delineate the effects of the latter two parameters from the measured data and accurately extract bridge parameters. Moreover, many factors, such as road profile, vehicle systems, and vehicle-bridge interactions, affect the performance of iBHM. Therefore, a thorough investigation is required to explore the vehicle-bridge interaction in iBHM under these conditions.

2.3 Advanced Time-Frequency Methods in Bridge Health Monitoring

The main goal after data collection is to analyze observed vibration data and extract damage-sensitive features using reliable SID techniques (Amezquita-Sanchez and Adeli 2014). Traditional signal processing methods, whether used in the time or frequency domains, assume that the signal is linear and stationary (Ibrahim and Mikulcik 1973, Juang and Pappa 1985, Zhang *et al.* 1985, Allemang and Brown 1998, Perry and Koh 2000, Brincker *et al.* 2001a, Ma *et al.* 2005). For non-stationary vibration signals of aging structures exposed to complex excitations, such as traffic loads, strong wind gusts, and earthquakes, this assumption does not hold (Entezami and Shariatmadar 2019). To extract damage-sensitive features from these non-stationary signals of time-varying systems, adaptive TF analysis is needed.

TF methods offer a better depiction of the energy variation of a signal in the TF domain (Perez-Ramirez *et al.* 2016, Sadhu 2013). The use of TF techniques for structural health monitoring (SHM) of civil infrastructure has grown over the past two decades. WT (Wang and Deng 1999, Hong *et al.* 2002, Douka *et al.* 2003, Loutridis *et al.* 2004, Sadhu *et al.* 2019), Empirical Wavelet Transform (EWT) (Yuan *et al.* 2017), Wigner-Ville Distributions (WVD) (Tang *et al.* 2010, Goyal and Pabla 2015, Zoubi *et al.* 2019), BSS (Sadhu *et al.* 2017), HHT (Huang *et al.* 1998, Xu *et al.* 2003, Bahar and Ramezani 2012), EMD (Yang and Chang 2009, Tang *et al.* 2011), RDT (Zhang *et al.* 2015, Zhang and Song 2016, Kodestani *et al.* 2018) and Short-Time Fourier Transform (STFT) (Nagarajaiah 2009, Nagarajaiah and Basu 2009, Ditommaso *et al.* 2012, Mata *et al.* 2013) are the most popular TF methods that have been used in modal identification for large-scale civil infrastructure.

2.3.1 Empirical Mode Decomposition

HHT is specifically developed to examine nonlinear and nonstationary data and to describe its TF energy variations. It combines Hilbert Spectral Analysis (Huang *et al.* 1998) and EMD. Any complex multicomponent data can be broken down using the EMD approach into a limited number of IMFs. EMD is adaptive (i.e. free of any basis function)

and performs decomposition based on a local characteristic of the data (Huang *et al.* 1998) from a single-channel measurement, in contrast to many other TF approaches. This characteristic has led to the widespread usage of EMD as an SHM approach to extract complex dynamic behavior from structures. EMD generally divides the measured vibration signal into multiple mono-component signals (i.e., modal responses), which are then analyzed for structural condition assessment. This TF domain method has seen a substantial increase in popularity in output-only modal identification.

An IMF is a function that satisfies the following two conditions (Huang *et al.* 1998): (a) the number of extrema and the number of zero-crossings must be either equal or differ at most by one in the whole data set, and (b) at any point, the mean value of the envelope denoted by the local maxima and the local minima is zero. The procedure of extracting an IMF is called *sifting*. The signal after the sifting process can be represented as:

$$x(t) = \sum_{j=1}^n i_j(t) + r_n(t) , \quad (2.1)$$

where $i_j(t)$ ($j = 1, 2, 3, \dots, n$) represents the IMFs of the original signal $x(t)$ and $r_n(t)$ is residue signal of $x(t)$. Theoretically, every IMF must have only one frequency component. However, sometimes, a single IMF contains multiple frequency components, which is known as mode mixing. EMD has been extended to include its variations, EEMD and Time-Varying Filter-based EMD (TVF-EMD), Robust EMD (REMD) to combat mode-mixing in the IMFs, particularly when analyzing signals with closely-spaced frequencies and measurement noise. A detailed review of variants of EMD and their application to vibration-based monitoring is provided in (Barbosh *et al.* 2020).

2.3.2 Wavelet Transform

WT can be viewed as an extension of conventional Fourier Transform (FT) with adjustable window location and size (Hou *et al.* 2000). FT can only be used to identify ambient systems since the sinusoidal basis it uses prevents a meaningful depiction of the nonstationary response of a system. STFT was created as an alternative to accommodate the time domain information because the Fourier basis functions are exclusively confined

to the frequency domain. However, because STFT uses fixed windows, the resulting temporal and frequency resolutions are severely constrained. It is impossible to obtain good time and frequency resolutions, simultaneously analogous to Heisenberg's uncertainty principle. This motivated the development of a different transform, called WT, which offers a superior time-frequency representation of the signals in a multi-resolution framework. The advantage of WT lies in its capability to examine the local data in an adaptive manner that can provide multiple levels of details of the original signal. As a result, this method can preserve the transient behavior of data.

WT is essentially divided into two classes: Continuous Wavelet Transform (CWT) and Discrete Wavelet Transform (DWT). WT provides flexibility to achieve greater time and frequency resolutions with a suitable basis function. Many condition assessment applications, such as signal noise filtering, data compression, and pattern recognition, use the CWT as a signal processing method. It separates mixed signals into their components and filters out noise, and is given by:

$$W_f(d, \tau) = \int_{-\infty}^{\infty} x(t) \frac{1}{\sqrt{d}} \psi^* \left(\frac{t - \tau}{d} \right) dt , \quad (2.2)$$

where d and τ represent the scale and translation of the mother wavelet, respectively. d relates to frequency scale, where a higher value of d corresponds to a low-frequency signal, and a lower value of d corresponds to a high-frequency signal. At a point in time, when the spectral component of the signal is similar to the value of d , the product between the wavelet and signal will be higher. The wavelet shifts along with the signal to locate the frequencies in the time domain. The basis function is called mother wavelet $\psi(t)$, where superscript (*) denotes its complex conjugate. With the right selection of d and τ , the CWT uses the shifted and scaled versions of φ and subsequently forms its inner product with $f(t)$. However, the selected basis function (e.g., basis such as *Morlet*, *Daubechies*, etc.) has a significant impact on its performance.

2.3.3 Synchro-Squeezing Transform

A signal having time-varying oscillatory features can be identified using the TF approach known as Synchro-Squeezing Transform (SST). It is designed to examine and separate signals into the following components:

$$x(t) = \sum_{k=1}^K A_k(t) e^{2i\pi\varphi_k(t)} \quad , \quad (2.3)$$

where A_k and φ_k are time-varying amplitude and phase functions, respectively. SST is a variant of reassignment, a set of approaches that apply a non-linear postprocessing mapping of CWT. In the instance of synchro-squeezing, the coefficients resulting from a CWT are reallocated to generate a concentrated TF representation, from which instantaneous frequency (IF) can be retrieved. The fundamental steps of extracting the IFs utilizing SST begin with the CWT, $W_\psi x(a, t)$ at a scale a and time shift t and is given by:

$$W_\psi x(a, t) = a^{-1/2} \int_{-\infty}^{\infty} x(u) \psi\left(\frac{u-t}{a}\right) du \quad . \quad (2.4)$$

The phase transform $\omega_{x(a,t)}$, is defined as the derivative of the complex phase of $W_\psi f$:

$$\omega_{f(a,t)} = \frac{\frac{d}{dt} W_\psi x(a, t)}{2\pi i W_\psi x(a, t)} \quad . \quad (2.5)$$

This nonlinear operator can be conceptualized as eliminating the impact of ψ from the CWT and "encoding" the necessary localized frequency information using:

$$S_{x(t,\eta)} = \int_{\{(a,t):\eta=\omega_{x(a,t)}\}} a^{-\frac{3}{2}} W_\psi x(a, t) da \quad . \quad (2.6)$$

The IFs are then extracted using:

$$\omega(a, t) = \frac{-i}{W_s(a, b)} \frac{d}{dt} W_s(a, b) \quad . \quad (2.7)$$

2.4 Visualization Techniques of Bridge Health Monitoring

Vibration-based BHM can produce a large amount of condition data over the design life of the bridge asset. Metadata relevant to BHM should be visualized, such as location, types of sensors and data sheets, status of BHM components, etc. Poor visualization of BHM data and metadata can lead to miscommunication about the condition of the structure and BHM system functionality. In conventional bridge inspection practices, there is a lack of data management and visualization tools. The challenge of accurately analyzing and interpreting the resulting big data can be solved by sensor-driven BHM through various visualization techniques. Tools such as Building Information Modeling (BIM), digital twins (DT), augmented reality (AR), virtual reality (VR), and mixed reality (MR) have been recently developed for data management and visualization.

Kim *et al.* (2012) developed new software that made use of the ARToolKit toolkit and the OpenGL application programming interface (API) to allow multiple users to collaborate on the same 3D virtual object. Finally, a case study employing the software to simulate a cable-stayed bridge was carried out. To preserve and record damage data from a bridge inspection, McGuire *et al.* (2016) created a software add-in using Autodesk REVIT. Leap Bridge, Tekla Structures, and Autodesk Revit were the three BIM software environments assessed in the study, and it was determined that Revit had the best capability for documenting bridge SHM data. In another study, Jeong *et al.* (2017) provided a framework for exchanging BIM and SHM data based on existing Open Bridge Information Modeling (BrIM) standards. The study used SensorML to assign sensor descriptions to the BIM model and a NoSQL database to store massive amounts of SHM data. After that, a case study on the Telegraph Road bridge in Michigan was conducted using the established framework. The development of the database schema was supported by the CSiBridge software, which further enhanced BIM's capacity to contain a variety of useful metadata.

Moreu *et al.* (2017) presented a framework for creating a conceptual design for AR-based structural inspection tools. Microsoft HoloLens device was used to simulate a dynamic response in the AR environment for the hologram of a railroad bridge. Napolitano *et al.* (2017) demonstrated a digital approach for classifying and incorporating pre-existing

documentation and SHM data through a customized interface into a VR environment. In this study, the virtual environment combined VR software (Kolor Panotour Pro) and 360° spherical imagery (Ricoh Theta) to provide a highly educational virtual experience for the end-user. The structure was viewed and examined using a combination of virtual tour (VT) and informational modeling (IM) technologies. A 350-foot pedestrian bridge was used for the full-scale demonstration, and fiber-optic strain, temperature, and displacement sensors were used for monitoring.

Delgado *et al.* (2018) suggested gathering, standardizing, integrating, and visualizing monitoring data in a BIM setting. These procedures were utilized to circumvent the restrictions placed on the interpretation, analysis, and sharing of monitoring data by contemporary BIM software. A railway bridge was equipped with a widespread network of fiber-optic monitoring sensors to track changes in strain data and verify the suggested structure. Using the established BIM framework, the most important structural performance parameters were dynamically displayed. To address existing shortcomings in available methods for accessing and displaying topologically complex SHM data, VT and IM technologies were investigated by Napolitano *et al.* (2018). The effectiveness of the suggested visualization approach for both SHM data and metadata for a pedestrian bridge was evaluated based on two criteria: ease of access to sensor network data and method effectiveness as a 3D visualization tool.

To ensure efficiency both on- and off-site, Napolitano *et al.* (2019) created a framework for recording and displaying data about the built environment using a combination of image-based documentation and AR. For a pedestrian bridge at Princeton University, a cross-platform, client-server system was created and put into place for making, saving, and displaying annotations. Alignment testing was used to assess the performance of GPS and AR location tracking. Dang and Shim (2020) suggested an approach to monitor bridges based on the nexus of BIM and AR. Over a year, BIM data from a cable-stayed bridge was collected and visualized using Microsoft HoloLens. To examine cracks and track bridge movement, Kilic and Caner (2020) used several advanced non-destructive testing (NDT) techniques, including ground-penetrating radar, light detection and ranging (LiDAR) distance sensors, infrared thermography, and a telescopic camera. The study

showed how to locate rebar and potential defects using AR technology by scanning the internal structure of a bridge.

A bridge monitoring system capable of visual safety and early warning was presented by Deng *et al.* (2021) which featured a BIM-based integrated management framework linked with a SQL database. The technique incorporated visual warning and monitoring information management plug-ins using the Revit API and employed Revit as the primary development platform. The framework enhanced the visualization of monitoring data for a bridge in China and could record early warning signals and transmit them to the relevant personnel.

2.4.1 Challenges of bridge health monitoring visualization techniques

Long-term BHM, equipped with next-generation sensors, yields a significant amount of data. To undertake risk and hazard reduction promptly, high-quality data gathering from sensors and SID is essential. The processing, transmission, and analysis of huge amounts of data have been a significant barrier to the long-term monitoring of large-scale structures. It is not possible to monitor a significant amount of BHM data and make systematic decisions using only data-driven methodologies. There are few data management and visualization systems used in current structural inspection procedures. Despite the significant development of visualization techniques in BHM, several challenges remain:

- The interoperability of different software pertaining to BIM, AR, and VR technologies and a variety of existing standards need to integrate with a wide range of BHM data and metadata originating from a suite of sensing technologies (e.g., vibration sensing, visual sensing).
- The visualization environments or technologies lack incorporation and linkage of dynamic information related to SID and damage diagnostics to the adequate user interface of these technologies.

- Other practical challenges include the inability to use AR devices in bright conditions, limited analysis capacity, damage due to impact and moisture, mandatory user training, the need for frequent calibration, etc.

2.5 Thesis Objectives

Based on the challenges identified in the BHM literature, the key objectives of the thesis are as follows:

- Develop a sparse SID technique to track the dynamic behavior of a bridge using ambient vibrations and a limited number of sensors (Chapter 3).
- Develop a SID method for condition assessment of bridges subjected to moving vehicle-induced nonstationary vibrations (Chapter 4).
- Develop a drive-by modal identification method using a moving instrumented vehicle (Chapter 5).
- Develop a vehicle scanning method based on the CP response of a moving test vehicle (Chapter 6).
- Develop a BrIM-based visualization framework for bridge infrastructure management (Chapter 7).

2.6 Summary

In this chapter, a brief overview of the traditional and modern BHM is presented, along with their challenges and limitations. Aging transportation infrastructure around the globe requires optimized maintenance programs. This is especially significant for existing structures that were built using antiquated design techniques, knowledge, and technology. Direct BHM has leveraged the advancements in sensing technologies to provide effective damage detection schemes using next-generation sensors. However, it cannot still use limited sensors and limited datasets for condition assessment and damage detection and a decentralized sensor network. The output-only and data-driven approaches are proposed to overcome these shortcomings. The proposed methods can provide an autonomous framework for inspecting bridges using passing vehicles. It is to be noted that chapters 3 and 4 improve upon direct BHM by improving the existing SID methods. To create a

passing vehicle-based framework for bridge inspections, chapters 5 and 6 contribute to the advancement of indirect BHM. Chapter 7 takes one step forward from static to dynamic BrIM, which facilitates the representation and visualization of real-time BHM data.

Chapter 3

3 Bridge Condition Assessment with Limited Sensors using an Improved Time-Varying Empirical Mode Decomposition

In this chapter, a cost-effective structural condition assessment technique is proposed to identify the modal parameters of the bridge using a fewer number of sensors. The proposed method is explored not only for system identification (SID) but also for structural damage detection. Multi Synchro Squeezing Transform (MSST) enables a clear delineation of modal frequencies of the intrinsic mode functions (IMFs) (with improved frequency resolution) under the presence of closely-spaced and low energy frequencies, as well as facilitates tracking the change in frequency resulting from the structural damage. Such MSST-enabled automated visualization of instantaneous frequencies (IFs) yields accurate structural assessment even when there is a limited number of sensors.

3.1 Introduction

Direct bridge health monitoring (BHM) requires extensive instrumentation to collect responses using a large number of sensors from different locations on the bridge (Yi *et al.* 2012). This direct sensing approach poses several practical challenges, such as the need for the closure of the bridge or highway, accidental damage to the equipment, and high initial costs of the sensory system, etc. Moreover, effective deployment of BHM to a wide number of bridges is hampered by the necessity of power, data storage, data transfer, and the complexity of installation (Malekjafarian *et al.* 2015). Blocking one or more lanes of the bridge for sensor instrumentation also affects the roadway capacity and causes traffic interruptions. The objective of this research is to alleviate these challenges and develop a structural condition assessment technique using fewer sensor measurements.

The vibration response of a bridge due to traffic loads provides valuable information about the dynamic parameters such as frequency, damping, and mode shapes of the bridge. The measured data is primarily processed using various time-domain, frequency-

domain, and time-frequency (TF) methods to track the variation of structural parameters over a long period (Perez-Ramirez *et al.* 2016). In the past two decades, TF methods have become increasingly popular, including the techniques such as Wavelet transform (WT) (Kankanamge *et al.* 2020), Wigner-Ville distributions (WVD) (Zoubi *et al.* 2019), Blind Source Separation (BSS) (Sadhu *et al.* 2017), Hilbert Huang Transform (HHT) (Bahar and Ramezani 2012), and Random Decrement Technique (RDT) (Kodestani *et al.* 2018). However, most of these methods rely on a multi-channel measurement and are not suitable for SID using a fewer number of sensors.

To address the above challenge, sparse SID using a fewer number of sensors has been attempted in recent years (Khorram *et al.* 2012, Nguyen 2013, He *et al.* 2017). Sparse SID can be characterized as an underdetermined modal identification problem. Sparsity-based methods (Hazra *et al.* 2012), tensor decomposition (Antoni and Chauhan 2011, Sadhu 2013, Sadhu *et al.* 2014), Hankel matrix-based method (McNeill 2013) and Empirical Mode Decomposition (EMD) (Barbosh *et al.* 2020) have been employed to solve this problem. In this study, a variant of EMD has been explored as a sparse SID technique to track the dynamic behavior of a structure using a fewer number of sensors.

EMD is a TF signal decomposition technique that decomposes a multi-component signal into its simpler components or oscillatory waveforms, known as IMFs. An IMF is a function that satisfies the following two conditions: (a) the number of extrema and the number of zero-crossings has to be either equal or differ at most by one in the whole data set, and (b) at any point, the mean value of the envelope denoted by the local maxima and the local minima is zero. The procedure of extracting an IMF is called *sifting*, which is vulnerable to intermittence and separation problems and gives rise to mode-mixing. Recently, Barbosh *et al.* (2020) provided an extensive review of EMD-based structural health monitoring (SHM) literature, illustrating applications of EMD and its variants in a broad range of SID and damage detection methods. In another recent study (Lofrano *et al.* 2019), orthogonal EMD was explored for mode shape-based damage identification using experimental data. However, EMD frequently results in mode-mixing, which can be resolved using a variant of EMD, namely Time-Varying Filter-based EMD (TVF-EMD) (Li *et al.* 2017). TVF-EMD uses B-spline functions, which are piecewise

polynomials with time-varying cut-off frequencies. With such property, TVF-EMD using a cluster diagram of frequencies (Lazhari and Sadhu 2019) can deal with vibration response to identify the structural frequencies without any mode-mixing issue in the modal responses. In this study, TVF-EMD is further enhanced by integrating with WT to identify the modal parameters and undertake damage detection using a single-channel nonstationary response of bridges with less user intervention.

WT is one of the powerful TF methods that can provide good time and frequency resolutions of the signal. A few variants of WT, such as Continuous Wavelet Transform (CWT), Empirical Wavelet Transform (EWT) (Yuan *et al.* 2017), and Wavelet Packet Transform (WPT) (Sadhu 2013, Plaza and Lopez 2018) have been used to detect anomalies and structural damage in the data. Synchro Squeezing Transform (SST) is another recently developed wavelet-based reallocation method (Daubechies *et al.* 2010) that yields a finer TF representation of a nonstationary multi-component signal. SST has shown significant potential for the identification of structural systems (Kumar *et al.* 2017, Li and Park 2017, Mahato and Chakraborty 2019, Sony and Sadhu 2020). In this study, an improved version of SST, MSST is integrated with TVF-EMD to improve its capability to track the changes in modal parameters of a nonstationary response. MSST consists of an iterative reassignment process that results in a sharper energy concentration of TF representation (Yu *et al.* 2019). It is proposed to integrate MSST with TVF-EMD such that MSST of the resulting IMFs obtained from TVF-EMD can show better energy concentration and suppresses the cross-terms over the TF-plane to effectively deal with the nonstationary signal in the presence of measurement noise, closely-spaced and low energy modes, and structural damage using a fewer number of sensors.

This chapter is organized as follows. A brief background of MSST and TVF-EMD is presented first, followed by the formulation of the proposed method. The proposed method is then illustrated using various analytical and numerical simulations, followed by a case study using a full-scale bridge.

3.2 Background

In this section, a brief background of MSST and TVF-EMD is presented.

3.2.1 Multi-Synchro Squeezing Transform

SST (Thakur 2015) has been recently developed to enhance the TF representation of a signal as an improvised version of CWT. In SST, the sparsity and localization properties of TF representation are combined with the invertibility of conventional TF transform. It can be observed that the error between the estimated and true IF increases with increasing non-stationarity in the signal (Yu *et al.* 2019). By iteratively applying multiple SST operations, the resulting TF energy can be concentrated in a stepwise manner. An improved version of SST, MSST has been recently proposed by (Yu *et al.* 2019), consisting of an iterative reassignment process, which results in sharper energy concentration of TF representation. Sun *et al.* (2019) utilized MSST for fault diagnostics in bearings, whereas it was explored in high-rate systems by Yan *et al.* (2020); however, it has not been yet explored for structural SID. MSST employs a Short-Time Fourier Transform (STFT) as a post-processing tool. STFT of a signal $x(t)$ for a real and even window is shown as:

$$H(t, \omega) = \int_{-\infty}^{+\infty} h(u - t)x(u)e^{-i\omega(u-t)}du \quad , \quad (3.1)$$

where $h(u)$ is the window function, and ω is the angular frequency. The SST employs a frequency-reassignment operator to estimate the spread of TF coefficients, which is expressed as:

$$F_s(t, \eta) = \int_{-\infty}^{+\infty} H(t, \omega)\delta(\eta - \hat{\omega}(t, \omega))d\omega \quad , \quad (3.2)$$

where δ is the Dirac delta function and $\hat{\omega}(t, \omega)$ is the IF. Performing SST iteratively yields:

$$F_s^{[N]}(t, \eta) = \int_{-\infty}^{+\infty} F_s^{[N-1]}(t, \omega)\delta(\eta - \hat{\omega}(t, \omega))d\omega \quad , \quad (3.3)$$

where $F_s^{[N]}(t, \eta)$ is the SST at N -th iteration for $N \geq 2$. Replacing Eq. 3.2 in Eq. 3.3 yields (Yu *et al.* 2019):

$$F_s^{[N]}(t, \eta) = \int_{-\infty}^{+\infty} H(t, \omega)\delta(\eta - \hat{\omega}^{[N]}(t, \omega))d\omega \quad , \quad (3.4)$$

where, $\hat{\omega}^{[N]}(t, \omega)$ represents the estimate of IF at N -th iteration, which is calculated as (Yu *et al.* 2019):

$$\hat{\omega}^{[N]}(t, \omega) = \varphi'(t) + \left(\frac{\varphi''(t)^2}{1 + \varphi''(t)^2} \right)^N (\omega - \varphi'(t)) \quad , \quad (3.5)$$

where $\varphi'(t)$ is the first-order derivative of the instantaneous phase $\varphi(t)$ of $x(t)$. With an appropriate number of iterations, the estimates of IF will be closer to the true estimate (Yu *et al.* 2019). In this study, MSST is employed to track the frequency change of the IMFs resulting from the TVF-EMD.

3.2.2 Time-Varying Filter Empirical Mode Decomposition

EMD decomposes a multi-component signal into a set of oscillatory waveforms known as IMFs (Yang *et al.* 2004b). The mode-mixing problem of EMD can be dealt with using a time-varying filter (TVF) (Li *et al.* 2017). The cut-off frequency of a TVF is time-varying, which makes it suitable for nonstationary vibration signals. In TVF-EMD, each signal can be estimated in B-spline space by (Li *et al.* 2017):

$$b_v^p(t) = \sum_{j=-\infty}^{+\infty} q(j) \beta^p\left(\frac{t}{v} - j\right) \quad , \quad (3.6)$$

where $q(j)$ is the B-spline coefficient, and it is enlarged by a factor of v , which is the step size of the knot sequence. The signal is determined by the order p, v , and $q(j)$. The B-spline coefficients $q(j)$ are determined using the B-spline approximation that minimizes the approximation error. For an original signal $y(t)$, $q(j)$ is determined by minimizing the approximation error δ_v^2 :

$$\delta_v^2 = \sum_{t=-\infty}^{+\infty} (y(t) - \{q\}_{\uparrow v} * w_v^p(t))^2 \quad , \quad (3.7)$$

where $\{-\}_{\uparrow v}$ is the up-sampling operation by v . It is assumed that the filter $w_v^p(t) = \beta^p\left(\frac{t}{v}\right)$ and the asterisk denotes the convolution operator. After introducing the concept of B-spline approximation (i.e., revealing its low-pass filtering property), the solution of $q(j)$ is obtained as:

$$q(j) = \{c_v^p * y\}_{\downarrow v}(j) \quad , \quad (3.8)$$

where $\{-\}_{\downarrow v}$ is the down-sampling operation by v and c_v^p is the pre-filter represented by:

$$c_v^p = \{(\{w_v^p * w_v^p\}_{\downarrow v})^{-1}\}_{\uparrow v} * w_v^p \quad . \quad (3.9)$$

$b_v^p(t)$ can be rewritten as:

$$b_v^p(t) = \{c_v^p * y\}_{\downarrow v} * w_v^p(t) \quad . \quad (3.10)$$

In summary, the signal y is first band-limited through a pre-filter w_v^p . Next, by a factor of v , the band-limited signal is decimated. Finally, the approximation is reconstructed using a post-filter w_v^p . In this chapter, TVF-EMD is used to decompose a single-channel nonstationary response of the bridge into multiple IMFs.

3.3 Proposed Method

This section builds on the background of MSST and TVF-EMD provided in the previous section. The proposed method is formulated for analyzing vibration signals collected from limited sensors. Let us consider the following equation of motion of a linear and discrete lumped mass n degrees of freedom (DOFs) structural system subjected to a wideband random input force, $\mathbf{u}(t)$:

$$\mathbf{M}\ddot{\mathbf{z}}(t) + \mathbf{C}\dot{\mathbf{z}}(t) + \mathbf{K}\mathbf{z}(t) = \mathbf{u}(t) \quad , \quad (3.11)$$

where \mathbf{z} is the displacement response vector at different DOFs. \mathbf{M} , \mathbf{C} , and \mathbf{K} are the mass, damping, and stiffness matrices, respectively. A state-space model with the following form can be used to solve the dynamical system given in Eq. (3.11):

$$\bar{\mathbf{z}} = \begin{bmatrix} \mathbf{z}_1 \\ \mathbf{z}_2 \end{bmatrix} \quad , \quad (3.12)$$

$$\dot{\mathbf{z}} = \mathbf{A}\bar{\mathbf{z}} + \mathbf{B}\mathbf{u} \quad , \quad (3.13)$$

$$\mathbf{p} = \hat{\mathbf{C}}\bar{\mathbf{z}} + \mathbf{D}\mathbf{u} \quad , \quad (3.14)$$

where \mathbf{A} is the state matrix, \mathbf{B} is the input matrix, $\hat{\mathbf{C}}$ is the output matrix, and \mathbf{D} is the transmission matrix. Under the excitation $\mathbf{u}(t)$, the resulting solution can be written in terms of vibration modes:

$$\mathbf{z} = \boldsymbol{\varphi} \boldsymbol{\eta} \quad , \quad (3.15)$$

where \mathbf{z} and $\boldsymbol{\eta}$ are the physical and modal responses, respectively. $\boldsymbol{\varphi}_{m \times n}$ is the mode transformation matrix. m and n are the number of modal responses and measurements, respectively. In Eq. 3.15, the measurement at the k -th DOF ($k=1,2,\dots,m$) can be shown as:

$$z_k(t) = \sum_{j=1}^n \varphi_{kj} \eta_j(t) \quad . \quad (3.16)$$

By performing TVF-EMD of the k -th measurement $z_k(t)$, it can be expressed in terms of IMFs:

$$z_k(t) = \sum_{j=1}^n f_{kj}(t) \quad . \quad (3.17)$$

By comparing Eq. 3.16 and Eq. 3.17, we get:

$$\varphi_{kj} \eta_j(t) = f_{kj}(t) \quad . \quad (3.18)$$

Once the IMFs are obtained, MSST is undertaken on each IMF $f_{kj}(t)$ to provide a precise TF representation of a nonstationary signal. MSST (Yu *et al.* 2019) uses a frequency-reassignment operator to estimate the TF coefficients, which is shown in Eq. 3.2 where $H(t, \omega)$ is the STFT (Eq. 3.1) of a signal $x(t)$. Eq. 3.2 can be written for a number of iterations (say, N), which gives Eq. 3.3 by performing multiple SST operations to achieve improved TF representation. In this way, each of the resulting IMFs obtained from TVF-EMD is analyzed using MSST. For a given IMF $f_{kj}(t)$ of Eq. 3.18, it can be written as:

$$f(t) = A(t) e^{i\varphi(t)} \quad , \quad (3.19)$$

where $A(t)$ is the instantaneous amplitude, and $\varphi(t)$ denotes the instantaneous phase. Eqs. 3.4 and 3.5 can be utilized to track the IF of the IMF, as shown below:

$$I(t, \omega) = \int_{-\infty}^{+\infty} h(u - t)f(u)e^{-i\omega(u-t)}du \quad . \quad (3.20)$$

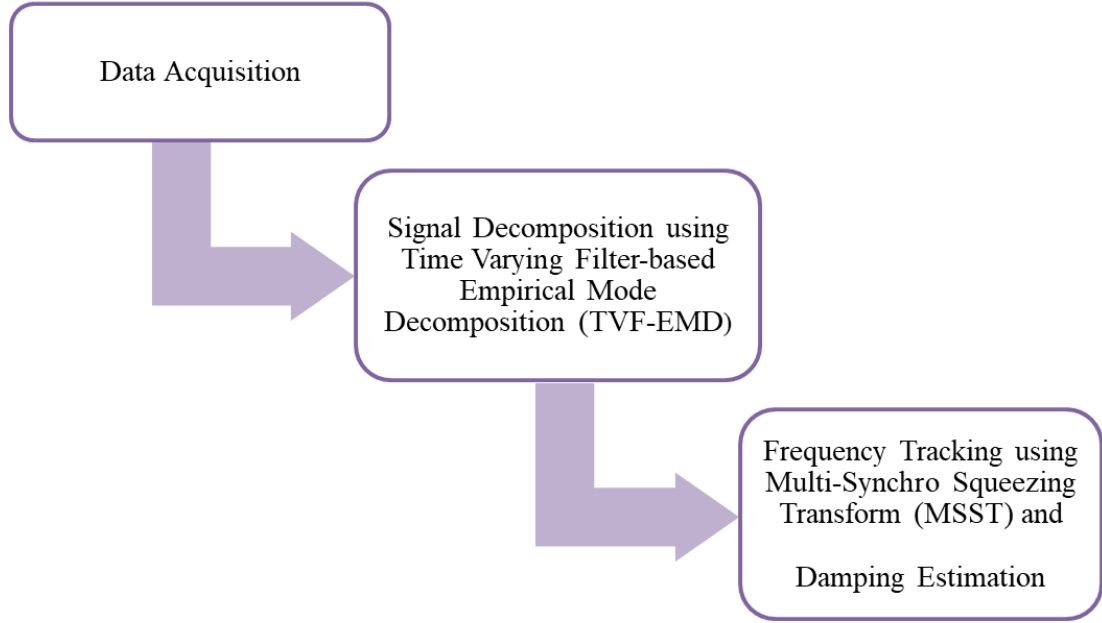


Figure 3.1: Flowchart of the proposed methodology.

The proposed method (Singh *et al.* 2021) is finally illustrated using a flowchart, as shown in Fig. 3.1. Following the sensor instrumentation of a structural system, vibration data is collected using a data acquisition system. The collected data is decomposed into its IMFs using TVF-EMD, and the resulting IMFs are fed into MSST to track the IF. The resulting IMFs are used to estimate the modal damping ratio.

3.4 Numerical Validation

In this section, the proposed method is validated using the data originating from the multi-degrees of freedom (MDOF) systems. The capability of the proposed method is used to delineate and track the structural frequencies in the presence of closely-spaced and low energy frequencies, measurement noise, and structural damage using a fewer number of sensors.

3.4.1 4-DOF model

A dynamic 4-DOF model is considered with the lumped mass values of 20 kg for each floor. The stiffness values for the first to the fourth floor are assumed to be 8, 7, 5, and 3 kN/m, respectively. The natural frequencies of the 4-DOF model are 0.98, 2.4, 3.7, and 5.2 Hz. The model is excited with the Imperial Valley earthquake at its base. Fig. 3.2 shows the resulting Fourier spectra of vibration response of the fourth floor, illustrating the presence of a low energy mode (i.e., fourth mode) in the data. The proposed method is used for the fourth-floor and first-floor vibration responses, and the results are shown in Figs. 3.3 and 3.4, respectively.

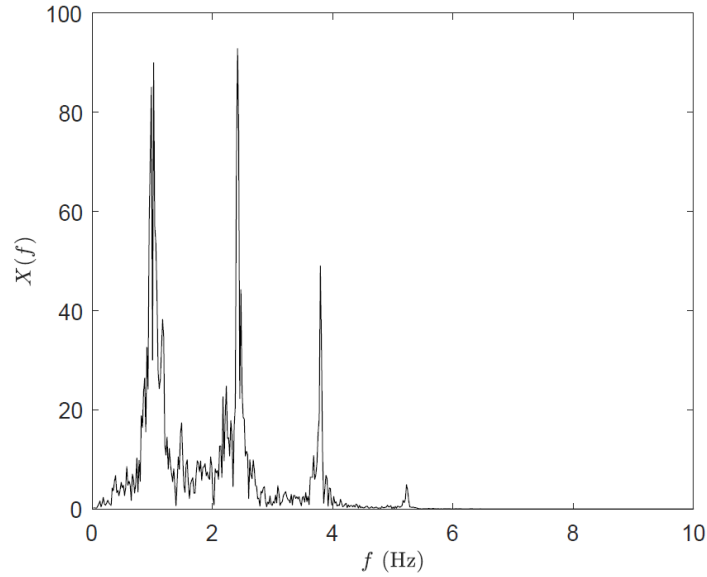


Figure 3.2: Fourier spectra of the fourth-floor vibration response.

The first row of Fig. 3.3 shows the IMFs of each modal response of the fourth-floor vibration response resulting from TVF-EMD, while the second row of Fig. 3.3 shows MSST results for each of the corresponding IMFs. Fig. 3.4 shows the modal responses and their MSST of the first-floor vibration response. It may be observed that the TVF-EMD has been successful in differentiating the natural frequencies using single-channel data obtained from both the first and fourth-floor responses. IMFs generated from TVF-EMD are used to estimate the modal damping ratio. Fig. 3.5 shows the damping ratio estimation for two IMFs from the fourth-floor vibration response. Damping values are

calculated for IMFs from the first and fourth floors. The results are compared with the analytical values and are summarized in Table 3.1.

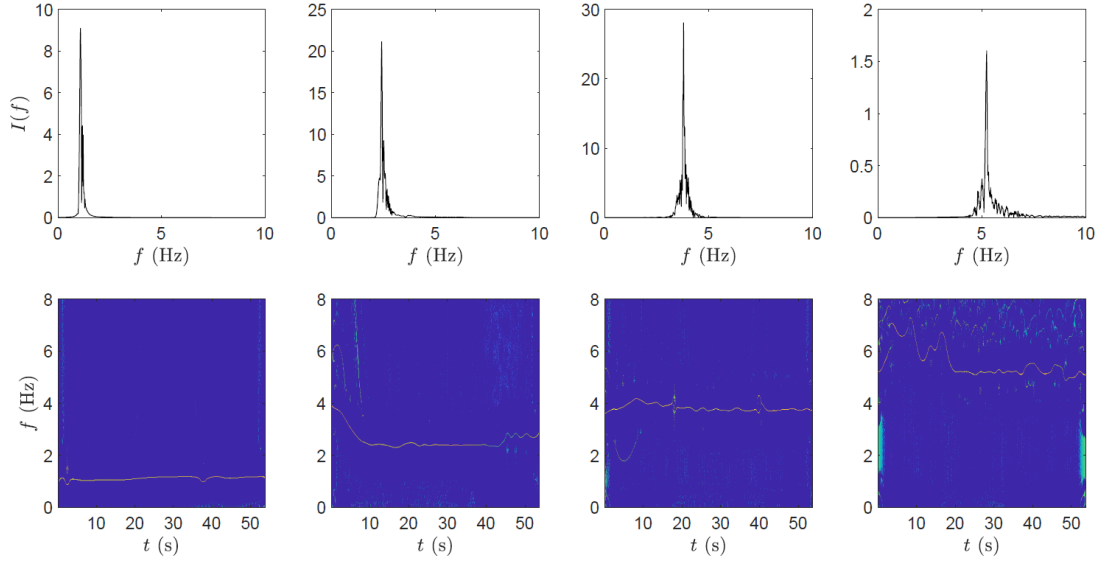


Figure 3.3: Identification results from the fourth-floor vibration response.

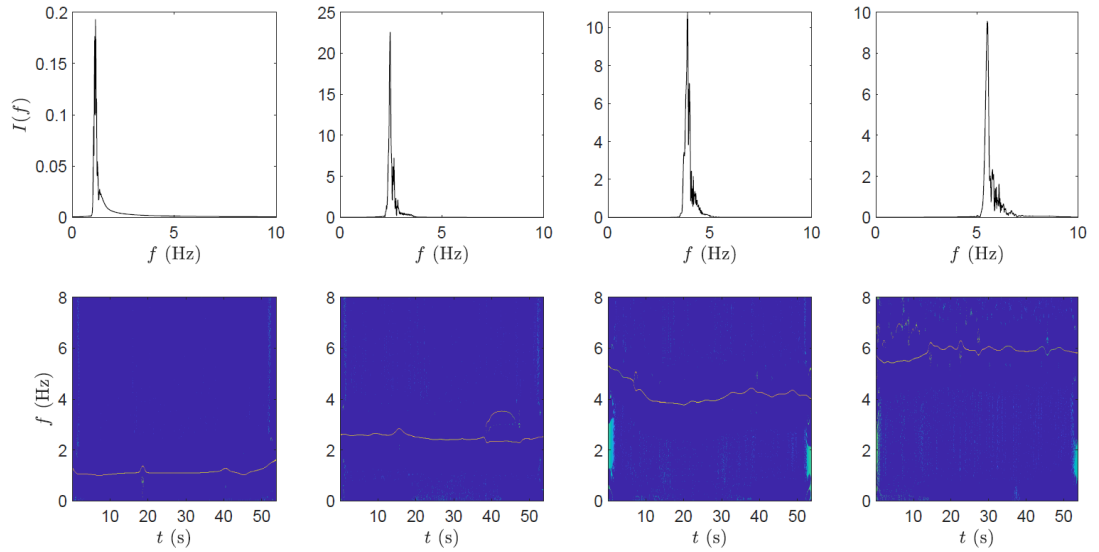


Figure 3.4: Identification results from the first-floor vibration response.

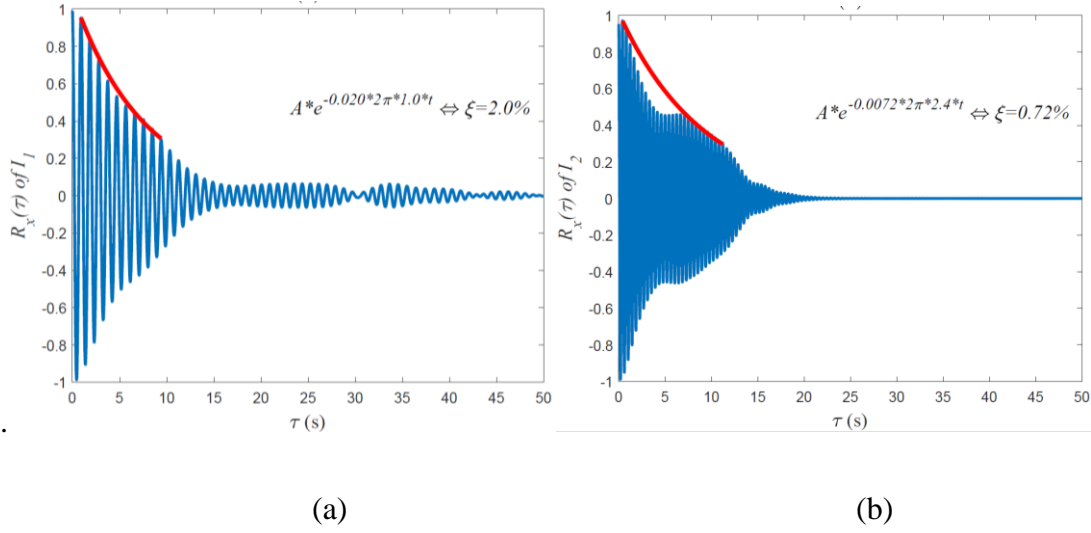


Figure 3.5: Damping ratio estimation for (a) first, and (b) second mode of the fourth-floor vibration response.

Table 3.1: Comparison of the analytical and estimated modal parameters of the 4-DOF model.

Mode #	Analytical f (Hz)/ ζ (%)	Estimated f (Hz)/ ζ (%)	
		First floor	Fourth floor
1	0.98/2.1	1.0/2.1	1.0/2.0
2	2.4/0.82	2.4/1.0	2.4/0.72
3	3.7/0.53	3.9/0.5	4.0/0.45
4	5.2/0.38	5.3/0.39	5.7/0.4

3.4.2 10-DOF model

In this section, the validity of the proposed method is tested using a 10-DOF system. The properties of the model are chosen to cover a wide range of dynamical characteristics of a flexible civil structure, such as closely-spaced and low energy frequencies. The lumped mass of each floor is assumed to be 1 kg, and the stiffness values from the first to the tenth DOF are 1.75, 1.575, 1.4, 1.225, 1.05, 0.875, 0.7, 0.525, 0.35 and 0.175 kN/m, respectively. The model is excited by the Imperial Valley earthquake at its base. Fig. 3.6 shows (a) time-history, and (b) MSST results of the first-floor vibration response. Fig. 3.6 (b) also illustrates the presence of closely-spaced frequencies in the data. MSST results

show how the individual frequencies of the 10-DOF system evolve in the raw data; however, the individual IMFs are now analyzed using the proposed method.

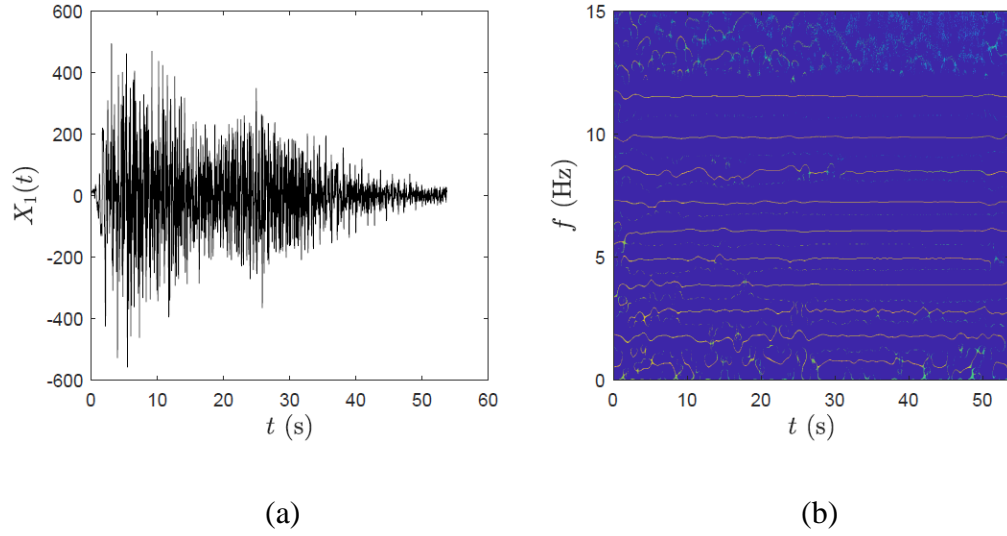


Figure 3.6: (a) Time history, and (b) MSST results of the first-floor vibration response.

Fig. 3.7 is generated by combining TVF-EMD and MSST results for the first-floor vibration response. The first and third rows of Fig. 3.7 show the IMFs containing the modal frequencies that are separated using TVF-EMD. The second and fourth rows contain MSST results that are developed using the IMFs resulting from TVF-EMD.

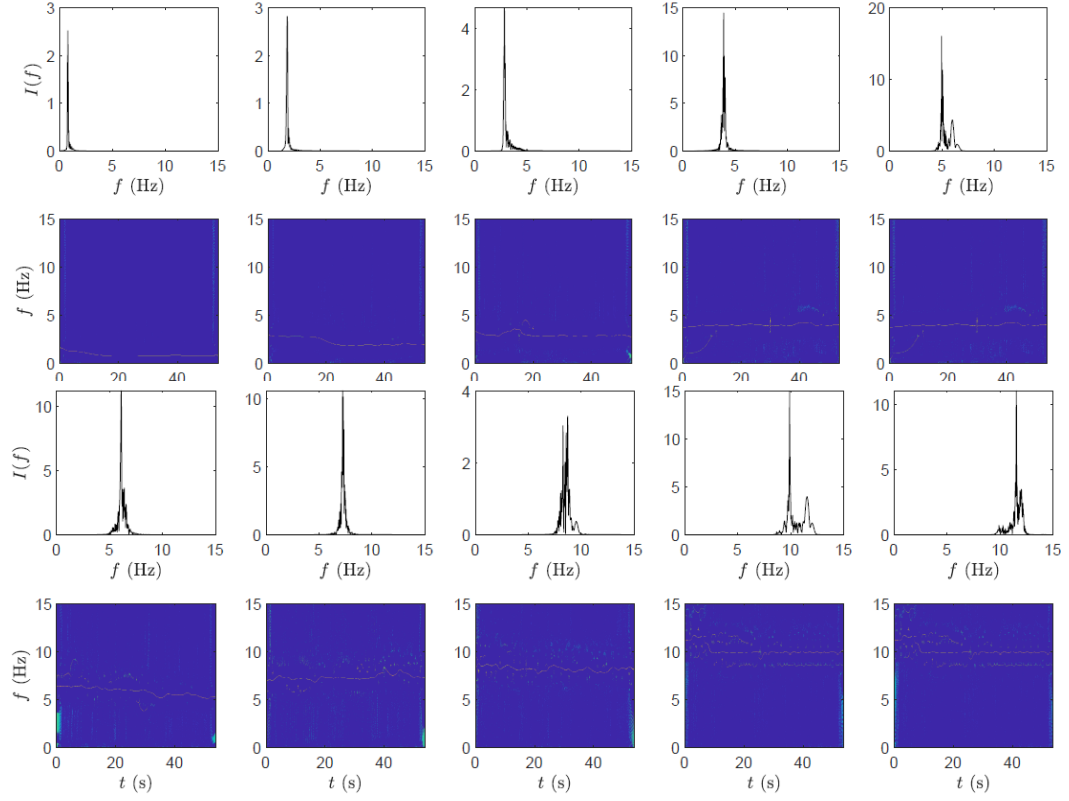


Figure 3.7: Identification results for the first-floor vibration response.

Similarly, Fig. 3.8 shows the TVF-EMD and MSST results for the fifth-floor vibration response. The first and third rows of Fig. 3.8 show the IMFs generated by TVF-EMD for each modal frequency of the 10-DOF model. Those IMFs are utilized in the next step to show the frequency evolution using MSST in the second and fourth rows of Fig. 3.8.

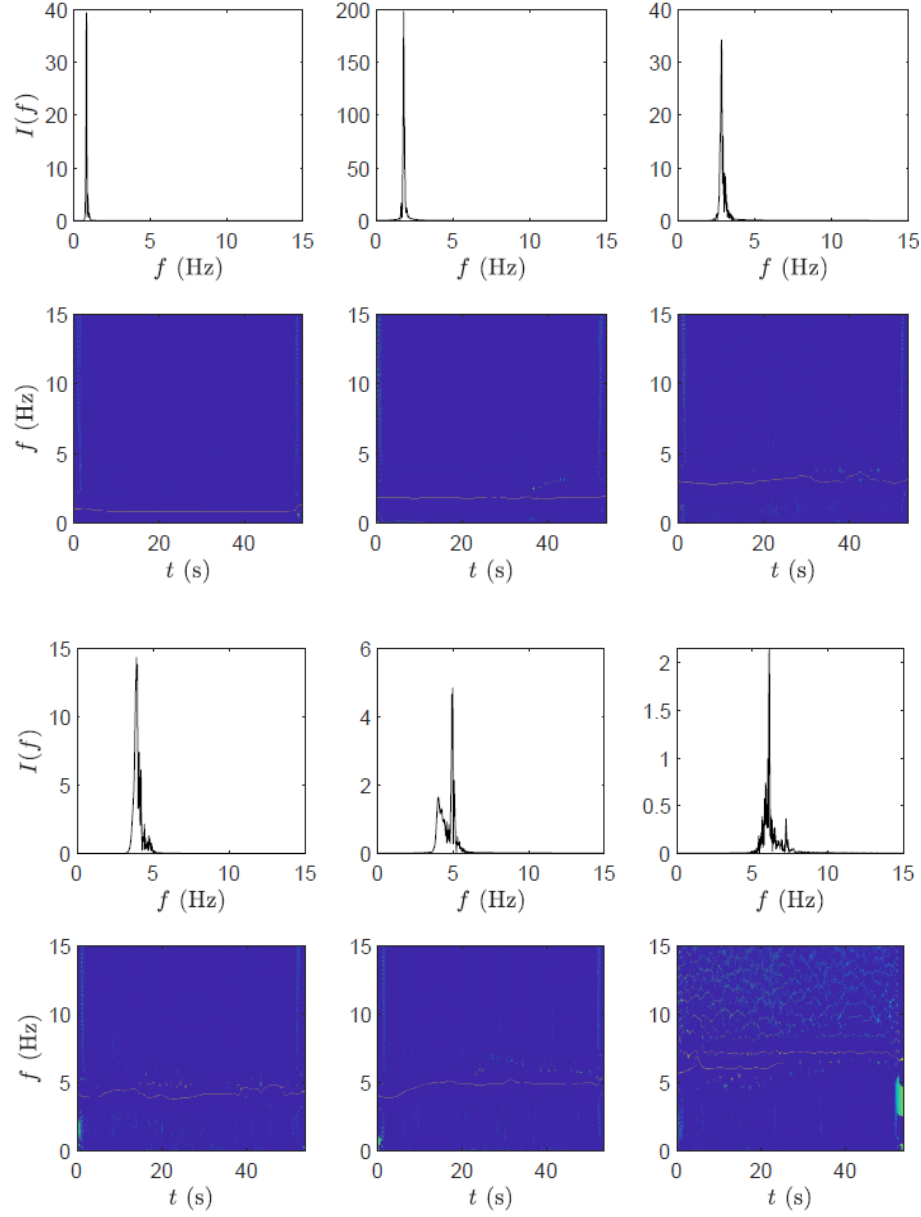


Figure 3.8: Identification results for the fifth-floor vibration response.

To compare the performance of the proposed method against noise contamination, 5%, and 10% measurement noise is added to the first-floor vibration response. Fig. 3.9 shows the MSST results for the first-floor vibration response with (a) 5% measurement noise and (b) 10% measurement noise, showing the insensitivity of MSST to the level of measurement noise. Vibration data collected under various levels of measurement noise is summarized in Table 3.2, in which the natural frequency for each mode of the 10-DOF model is tabulated under different levels of measurement noise.

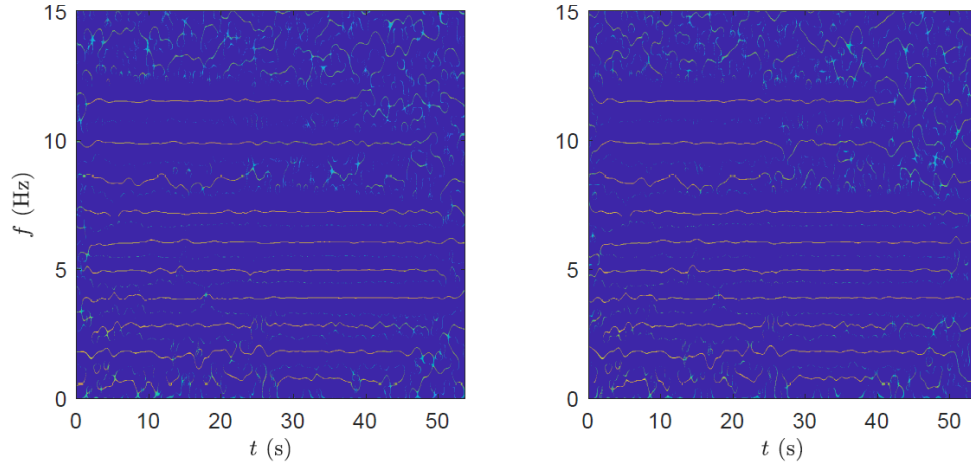


Figure 3.9: MSST results of the first-floor vibration response with (a) 5%, and (b) 10% measurement noise.

Table 3.2: Frequency values identified with different levels of measurement noise.

Mode #	0% Noise f (Hz)	5% Noise f (Hz)	10% Noise f (Hz)
1	0.76	0.76	0.76
2	1.78	1.78	1.78
3	2.83	2.83	2.83
4	3.89	3.89	3.89
5	4.95	4.95	4.95
6	6.09	6.09	6.09
7	7.22	7.22	7.22
8	8.45	8.45	8.43
9	9.89	9.89	9.89
10	11.53	11.53	11.53

Once the modal responses or IMFs are obtained from a single channel measurement using TVF-EMD, the autocorrelation function of modal responses is used to extract the modal damping ratio. Fig. 3.10 shows the estimation of the damping ratio as obtained from the IMFs of vibration response of the first floor. The variation in frequency and damping ratio has been further investigated among the first and fifth-floor vibration responses in the presence of 10% measurement noise. The data relating to frequency and damping ratio has been summarized in Table 3.3. Although the frequency estimates merely change with the change in sensor location, there are variations in modal damping

ratio across different measurements as the damping estimates are often sensitive (Adhikari 2007) to the amplitude of the autocorrelation functions of modal responses of two different sensor locations and the random measurement noise.

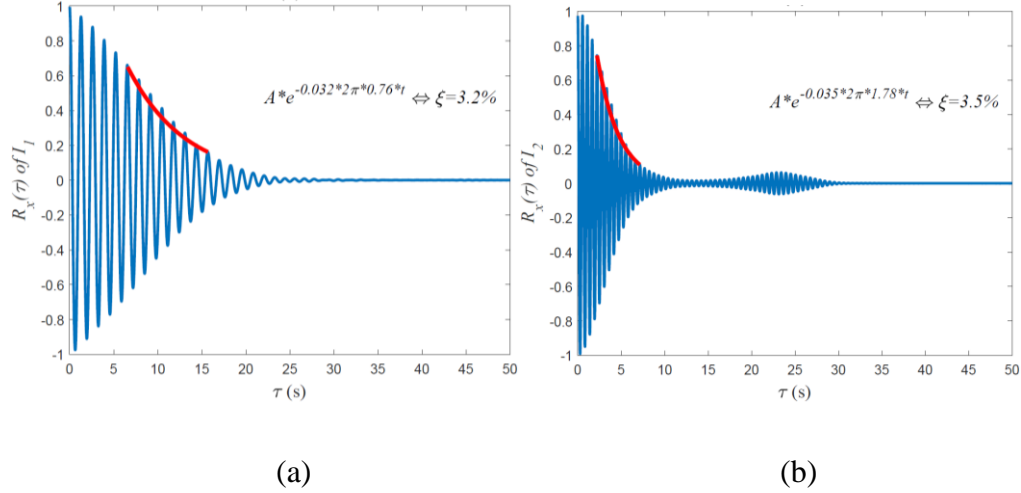


Figure 3.10: Damping ratio estimation for (a) first, and (b) second mode of the first-floor vibration response.

Table 3.3: Modal identification results for the 10-DOF model with 10% measurement noise.

Mode #	1st floor f (Hz)/ ξ (%)	5th floor f (Hz)/ ξ (%)
1	0.76 (3.2)	0.78 (2.3)
2	1.78 (3.5)	1.78 (2.5)
3	2.83 (2.1)	2.83 (1.8)
4	3.89 (0.96)	3.89 (1.1)
5	4.95 (0.62)	4.95 (0.7)
6	6.09 (1.4)	6.09 (1.5)
7	7.22 (0.75)	7.22 (0.6)
8	8.43 (1.4)	8.45 (1.1)
9	9.89 (1.67)	9.89 (1.5)
10	11.53 (0.31)	11.53 (0.4)

3.5 Full-Scale Validation

In this section, a full-scale bridge under different damage conditions is used to evaluate the performance of the proposed method.

3.5.1 Details of full-scale validation

The Z24 ridge (Kramer *et al.* 1999) was a highway overpass connecting Utzenstorf to Koppigen in Switzerland. It was a post-tension concrete bridge consisting of three spans with an overall length of 58 m and two lines. The length of the middle span was 30 m, and the two side spans were 14 m. As shown in Fig. 3.11, both end abutments were made up of triplet columns connected to the girder, while two intermediate concrete piers were rigidly clamped to the main girder. The original bridge was built in 1963 and was eventually destroyed in 1998 to build a new one with a larger side span as a part of a new railway infrastructure project. This bridge has many progressive damage cases, forming a good database for the proposed research. Moreover, this bridge has been used by many researchers (Maeck *et al.* 2001, Kullaa 2003, Masciotta *et al.* 2016) in the past.

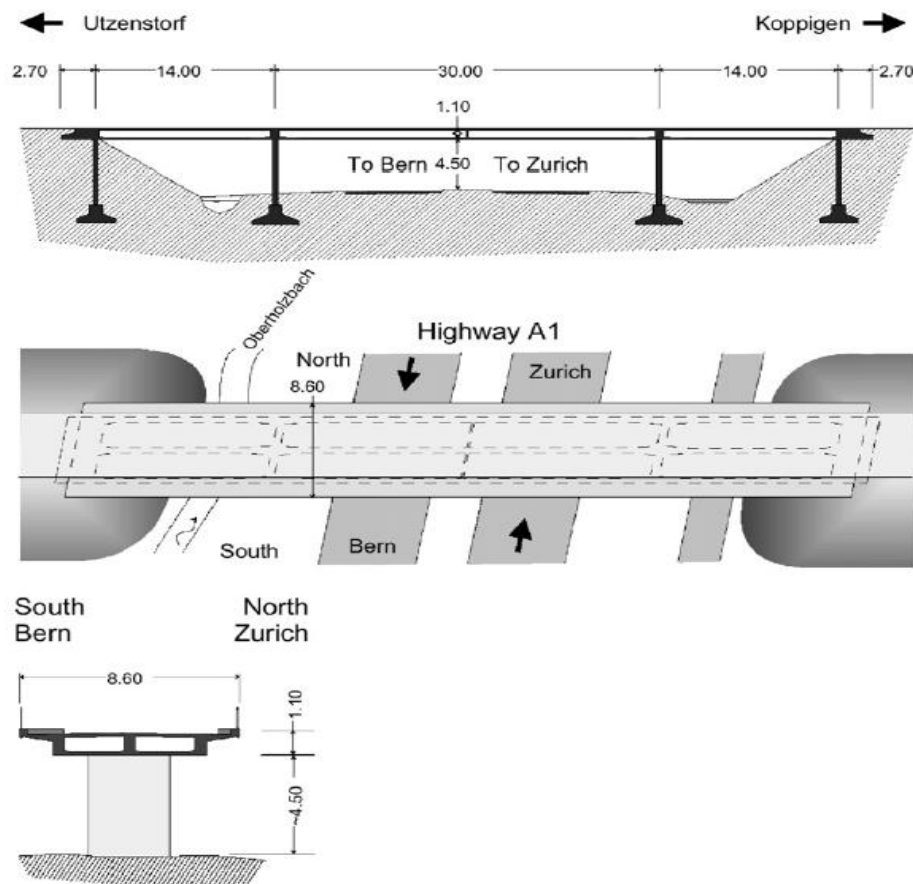


Figure 3.11: Elevation and plan view of the Z24 bridge.

A progressive damage test was conducted to study the effect of different damage scenarios on the dynamic behavior of the Z-24 Bridge. Ambient and forced vibration tests were carried out before and after each damage scenario. A complete description of the damage scenarios can be found in (Kramer *et al.* 1999). Two shakers (1 kN and 0.5 kN) were placed in two locations of the bridge to implement forced vibration tests. The bridge was divided into several grids on the bridge deck and on two supports for installing sensors, which resulted in 291 DOFs being measured. Therefore, the data were collected in nine different setups since the number of available accelerometers was less than the number of degrees of freedom (i.e., an ideal example of limited sensor measurements). The sampling frequency used in the study was 100 Hz. Results obtained using the proposed methods are discussed in the next section.

3.5.2 Identification results

In this study, the forced vibration data of two sensors are selected to assess the dynamic properties of the bridge subjected to two discrete damage cases. The recorded vertical accelerations of sensor 221 (from setup 5) and sensor 229 (from setup 7) are analyzed using the proposed method, which is indicated in Fig. 3.12. To capture the effect of structural damage on the dynamic characteristics of the bridge, the stage #1 and #7 are selected. Stage #1 represents the undamaged condition of the bridge, whereas stage #7 shows the damaged state of the bridge after the tilt of the foundation (Kramer *et al.* 1999).

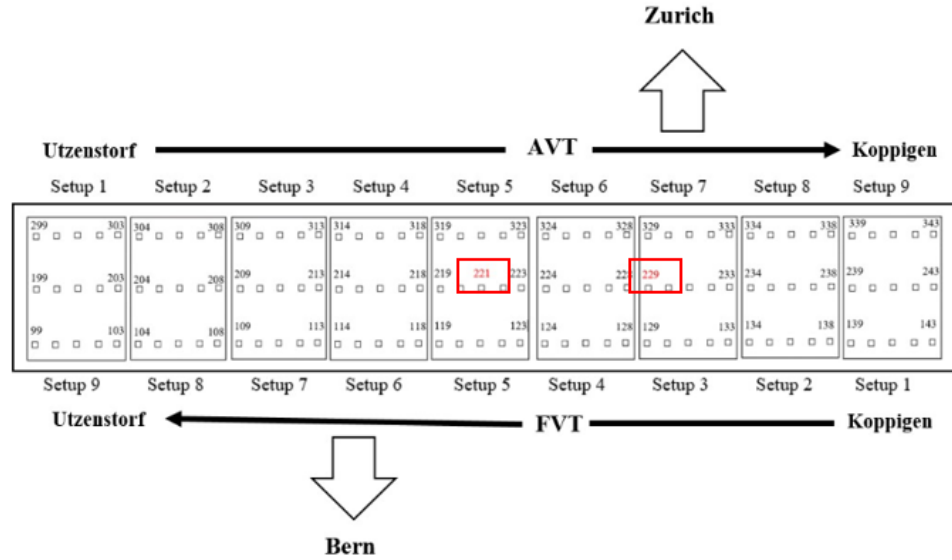
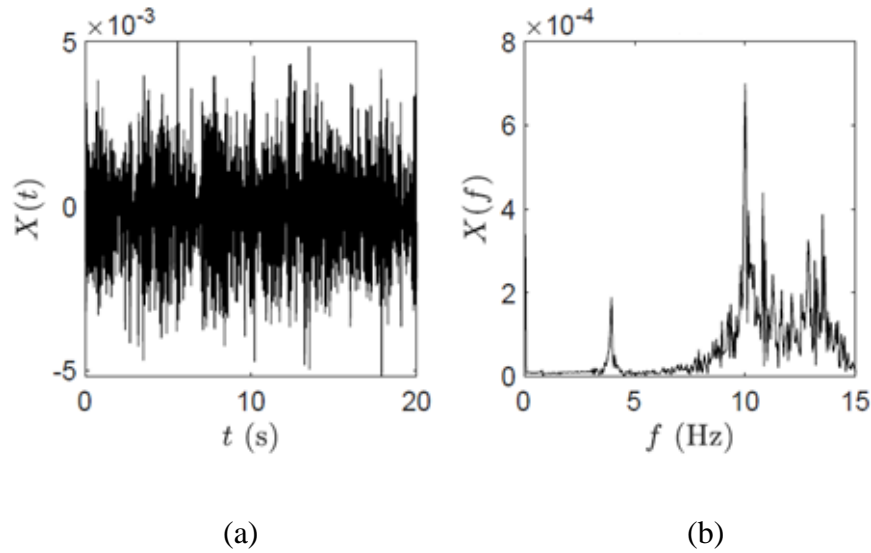


Figure 3.12: Schematic of the sensor locations and various setup configurations.

Fig. 3.13 shows the data related to stage 1 of sensor #229. Fig. 3.13 shows (a) time-history, and (b) Fourier spectra of the vibration response. Furthermore, Fig. 3.13 shows (c) SST, and (d) MSST results of the vibration response from stage #1 of sensor #229, respectively, and demonstrate that MSST outperforms SST in terms of resolution and accurate TF representation.



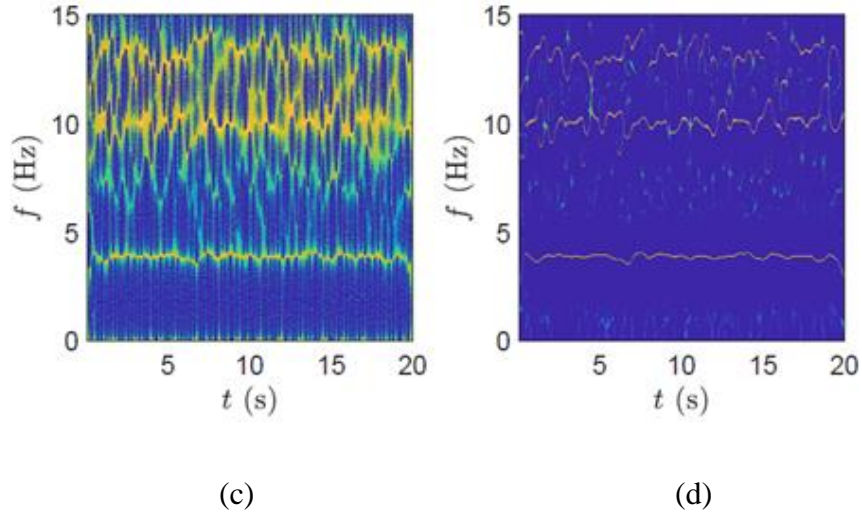


Figure 3.13: (a) Time history, (b) Fourier spectra, (c) SST, and (d) MSST results for vibration response of sensor #229 (Stage 1).

A comparison has been performed between the undamaged and damaged stages for two sensor responses. Fig. 3.14 shows the identification results for the vibration response of sensor #229 of stage #1, showing the undamaged conditions. The first row of Fig. 3.14 shows the IMFs generated by TVF-EMD, and the second row shows the MSST results generated using those IMFs. Fig. 3.15 shows the identification results of vibration response for sensor #229 of stage #7, showcasing damaged conditions. The frequency estimates from Figs. 3.14 and 3.15 are summarized in Table 3.4, in which it is evident that the frequency values are reduced from stage #1 to #7 due to the initiation of structural damage.

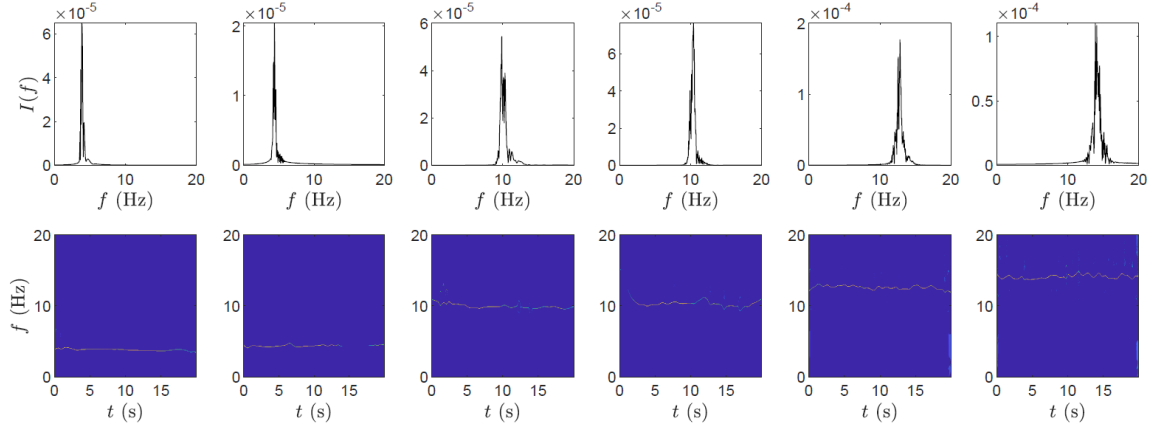


Figure 3.14: Identification results for vibration response of sensor #229 (Stage 1).

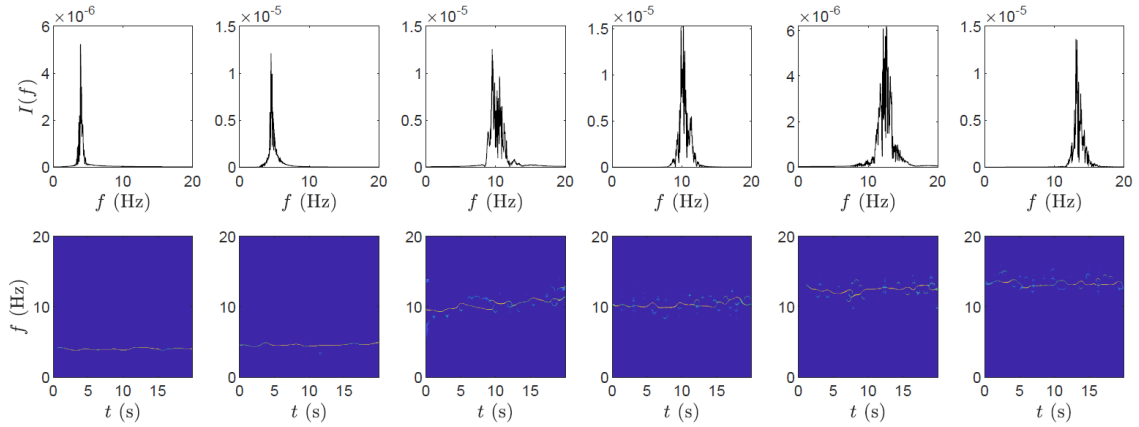


Figure 3.15: Identification results for vibration response of sensor #229 (Stage 7).

Another sensor is chosen from a different setup for comparison of damaged and undamaged states. Fig. 3.16 shows the identification results of measured data from stage #1 of sensor #221 in which the first row shows the TVF-EMD results, and the second row shows the MSST results. Similarly, the results for stage #7 of sensor #221 are shown in Fig. 3.17. The first row of Fig. 3.17 shows the IMFs generated by TVF-EMD, and the second row shows the MSST results for the vibration response of the damaged state. Using the autocorrelation function, IMFs generated from TVF-EMD are utilized to estimate the damping ratios for the sensor data. A detailed comparison is performed using the frequency and damping ratio obtained from the Finite Element Modeling (FEM) method (Brincker *et al.* 2001b) and sensor data. Table 3.4 contains the FEM and identification results obtained from the measured data with undamaged and damaged

conditions, showing the efficiency of the proposed method under both undamaged and damaged states. It may be observed that the proposed method performed well despite the presence of closely-spaced frequencies in the data.

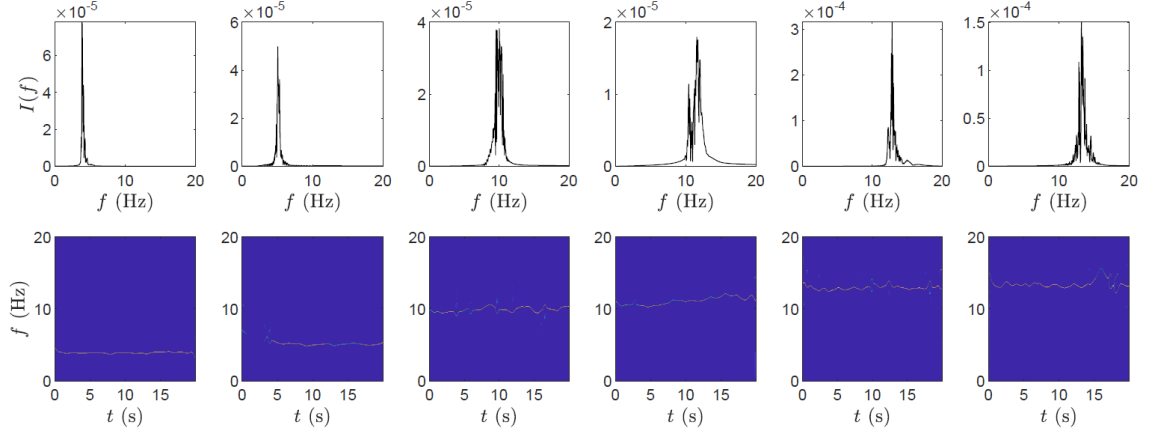


Figure 3.16: Identification results for vibration response of sensor #221 (Stage 1).

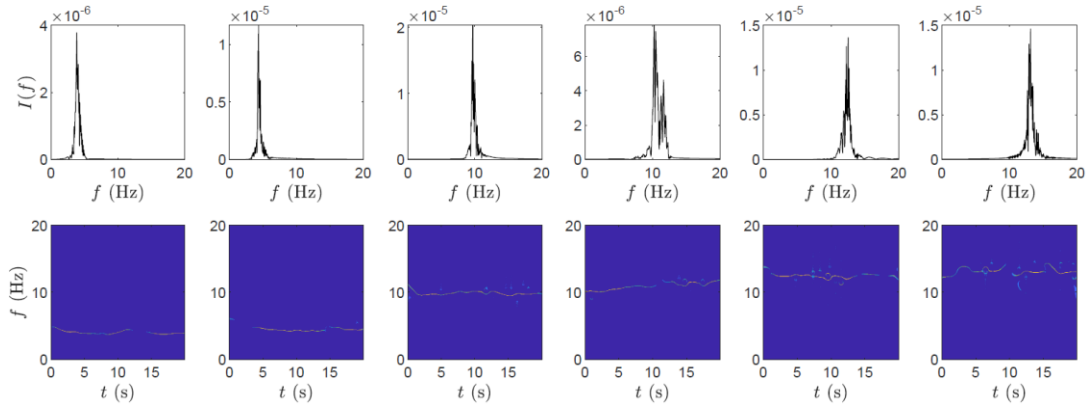


Figure 3.17: Identification results for vibration response of sensor #221 (Stage 7).

Table 3.4: Comparison of identification results from two stages.

Mode #	Stage #1 (undamaged)			Stage #7 (damaged)		
	FEM f (Hz)/ ζ (%)	Sensor #221 f (Hz)/ ζ (%)	Sensor #229 f (Hz)/ ζ (%)	FEM f (Hz)/ ζ (%)	Sensor #221 f (Hz)/ ζ (%)	Sensor #229 f (Hz)/ ζ (%)
1	3.88/0.85	3.95/0.76	3.95/0.7	3.84/0.75	3.90/0.86	3.75/0.77
2	5.02/1.4	4.7/1.42	4.7/1.38	4.65/1.74	4.40/1.76	4.55/1.77
3	9.83/1.21	9.9/1.32	9.9/1.33	9.71/1.23	9.70/1.28	9.55/1.30
4	10.28/1.23	10.45/1.28	10.45/1.2	10.16/1.12	10.25/1.13	10.25/1.25

5	12.70/1.17	12.85/1.3	12.85/1.5	12.11/1.7	12.55/1.78	12.2/1.75
6	13.48/0.86	13.9/0.8	13.9/0.75	13.13/1.73	13.15/1.64	13.7/1.5

3.6 Summary

In this study, a wavelet-based TVF-EMD method is proposed to identify modal parameters of structures using a fewer number of measurements. The proposed method is validated using a suite of numerical and full-scale studies. The results show that the proposed method can identify the modal parameters under the various levels of measurement noise, closely-spaced and low energy frequencies, and damages using a limited number of measurement channels. The full-scale study reflects the capability of the proposed method to identify the modal parameters under the damaged condition with reasonable frequency resolution.

Chapter 4

4 An Integrated Time-Frequency Damage Detection Method using Vehicle-induced Nonstationary Response

In this chapter, a limited sensing-based novel bridge health monitoring (BHM) technique is proposed for bridge condition assessment using vehicle-induced vibration responses. It is shown that the proposed method can successfully identify the time-varying modal frequencies of the bridge in both Finite Element Modeling (FEM) study and full-scale study using a limited number of sensors. In this chapter, the evaluation of the dynamic behavior of a bridge has been attempted only under traffic loading conditions. The effect of environmental conditions on the bridge dynamics and damage identification is not considered in this study.

4.1 Introduction

In the majority of BHM studies, conventional monitoring requires extensive instrumentation and actuation along the bridge. Depending on the length of the bridge or underneath water bodies, this approach has several practical challenges, such as the risk of accidental damage to equipment, extravagant initial equipment cost, accessibility, and obligation for bridge closures. Moreover, in existing techniques, vibration data is collected by exciting the bridge using ambient and forced vibration. However, ambient vibrations are produced using wind loads that may not be able to excite a stiff bridge with adequate participation of all key modes and are often contaminated with measurement noise. Forced vibration is used to excite the bridges to collect vibration data and is conventionally achieved using hydraulic actuators, impact hammers, or human-induced excitation. However, depending on the length of the bridge, more than one actuator may be required, which leads to significant serviceability issues in the bridge and potentially increases the maintenance budget to the bridge owners. Acquiring bridge vibrations using a moving load (i.e., a moving vehicle) is another active research topic of BHM (Yang and Yang 2017, Zhu *et al.* 2019). In these cases, the probability of collecting a noisy signal is significantly reduced since the data is collected only for the duration when the vehicle is traveling over the bridge, causing active motion of the bridge (Arjomandi and Araki

2019). Moreover, the process of bridge excitation becomes inexpensive since it can be achieved through ongoing traffic, and the data can be easily acquired when the vehicles remain on the bridge.

Recently, Cantero and Gonzalez (2015) proposed a damage detection technique for short to medium-span bridges using weigh-in-motion (WIM) technology. The authors compared a pavement-based WIM station with a bridge-based WIM system. The ratio of estimated vehicle weights at different bridge locations allowed the distinguishing between global and local damage making the damage localization possible. In another study, OBrien *et al.* (2015) used a novel approach of moving force identification to estimate the deterioration of the bridge. The authors used the weigh-in-motion data from two axles of a vehicle and detected structural damage using deflection data of the bridge subjected to the traffic. Aied *et al.* (2016) used ensemble Empirical Mode Decomposition (EMD) for damage detection by identifying the stiffness changes due to rough profiles, high vehicle speeds, and noisy signals. For the load rating of reinforced concrete slab bridges, Bagheri *et al.* (2018) proposed a method based on structural monitoring and non-destructive approaches. Li *et al.* (2018) investigated the dynamic performance of a curved continuous truss girder bridge under moving vehicles by combining field testing and numerical simulations. The dynamic characteristics and vehicle ride comfort were tested using moving test vehicles. It was concluded that the dynamic impact factors varied significantly among the bridge components.

In another vein, Meng *et al.* (2018) investigated vehicle-bridge interactions and proposed a new method for assessing bridge conditions based on nonlinear vibration analysis. A five-span bridge was instrumented with accelerometers and was excited by a truck. The nonlinear dynamic characteristics were identified using Lyapunov exponents, which can be utilized to identify damage-sensitive features for BHM. To improve the sensor requirements, Nie *et al.* (2019) proposed a method to detect the structural damage of bridges subjected to moving loads. The cross-correlation was calculated using the windowed pair time-series extracted from the two measured responses and was used as a local damage index. Taking into account the bridge-vehicle interaction, Pagnoncelli and Miguel (2019) determined the dynamic response of a bridge due to the moving load

caused by vehicles traveling over rough pavement. Synchronous identification of structural damage and vehicle loads was attempted by Zhang *et al.* (2020) using long-gauge fiber Bragg grating sensors on a bridge. The effectiveness of the approach was validated using a numerical case study and a laboratory experiment. However, the dynamic behavior of bridges under moving vehicular loads gives rise to a time-varying system. The effect of various parameters such as vehicle speed, vehicle size, sensor location, structural damage, etc., on such a system, remains a challenge. Furthermore, the bridge vibrations due to moving vehicles last for a short duration (Kaloop *et al.* 2020, O'Brien *et al.* 2020, Tian and Zhang 2020). The use of limited sensors to capture such short-duration vehicle-induced excitation and the performance of the modal identification of the bridge has not been fully explored.

The objective of this chapter is to develop a system identification (SID) method that can utilize fewer sensor measurements of a bridge when subjected to moving loads. Traditional SID methods assume the vibration signal to be linear and stationary (Ma *et al.* 2005). This assumption does not hold well for nonstationary signals collected from aging bridges, which are subjected to random excitation ranging from time-varying traffic load, high-intensity wind, and earthquakes (Entezami and Shariatmadar 2019). Time-frequency (TF) decomposition-based SID can provide a picture of the signal both in the time and frequency domain for time-varying systems. Some of the popular TF methods, such as Wavelet Transform (WT) (Douka *et al.* 2003, Loutridis *et al.* 2004, Sadhu *et al.* 2013), Blind Source Separation (BSS) (Sadhu *et al.* 2017), and EMD (Barbosh *et al.* 2020) are explored for structural SID using ambient vibration responses. Lazhari and Sadhu (2019) explored Time-Varying Filter (TVF)-based EMD (another variant of EMD) for modal identification under stationary and ambient loading conditions. This approach was illustrated using a decentralized framework of wireless sensors using a suite of numerical, experimental, and full-scale studies. Although MSST offers better TF resolution than any standard WT, it requires an appropriate selection of the iteration number, which involves significant user intervention (Yan *et al.* 2020). Moreover, the capability of TVF-EMD to undertake damage detection using nonstationary vehicle-induced vibrations has not been explored yet.

To alleviate the above challenges, an integrated TF method is proposed to undertake bridge condition assessment using a fewer number of sensors. The novelty of this chapter lies in the SID of a bridge from moving-vehicle-induced nonstationary data obtained from limited sensors. In addition, the sensitivity study of various vehicular parameters such as vehicle speed, vehicle size, presence of multiple vehicles, the extent of structural damage, etc., on damage identification constitutes the main contribution of this study. First, TVF-EMD is used to analyze the fewer measurements and identify the modal responses of the bridge, and then, a feature extraction tool, Synchro Extracting Transform (SET), is employed to extract the time-varying features of the signal containing vehicle-bridge dynamics. Unlike MSST, SET is free of pre-selection of iteration numbers, which enables the condition assessment autonomous in nature.

This chapter is organized as follows. After introducing the concepts of moving vehicle-based BHM and the associated practical challenges, the proposed idea is briefly explained in this section. In Section 4.2, a brief background of SET is provided. The proposed method is presented next in Section 4.3. In Section 4.4, the analytical study illustrates results for vehicles traveling over a bridge at different speeds. The Finite Element (FE) study in Section 4.5 shows the effect of the sensor location, vehicle speed, vehicle model, presence of multiple vehicles, and the effect of structural damage in a bridge. Lastly, a full-scale bridge is analyzed using the proposed method in Section 4.6, followed by key conclusions in Section 4.7.

4.2 Background

A brief background of SET is provided in this section.

4.2.1 Synchro-Extracting Transform

TVF-EMD, as explained in section 3.2.2, decomposes a signal into its mono-component signals; however, the resulting signals cannot track the time-varying bridge frequency over time as a vehicle travels over the bridge. Therefore, after the signal decomposition using TVF-EMD, a TF method is required that can provide information about the time-varying frequencies of vehicle-bridge dynamics. Synchro Squeezing Transform (SST), a special form of WT (Yan *et al.* 2020), squeezes all TF coefficients of the instantaneous

frequency (IF) trajectories. Unlike the squeezing operation over entire trajectories of IFs, SET retains only the TF information that is most related to time-varying features and eliminates any smeared region of TF representation (Yu *et al.* 2017). Therefore, SST has lesser TF resolution when it is used to reconstruct the key components of a nonstationary signal, while SET results in more energy-concentrated TF results compared to any other TF analysis (Li *et al.* 2020, Yu and Lin 2020).

Short-Time Fourier Transform (STFT) representation $S_e(t, \omega)$ of the signal $x(t)$ can be derived by using the first-order approximation form:

$$S_e(t, \omega) \approx \sum_{i=1}^K A_i(t) * \hat{h}(\omega - \omega_i(t)) e^{j \int \omega_i(t) dt} , \quad (4.1)$$

where ω is the angular frequency and \hat{h} represents the Fourier Transform (FT) of the window function. The IF is represented by:

$$\omega(t) = \sum_{i=1}^K \omega_i(t) = -j * \frac{\partial S_e(t, \omega)}{S_e(t, \omega)} . \quad (4.2)$$

Yu *et al.* (2017) proposed to retain only the TF information that is highly correlated with the IF of the data and eliminate the effect of random noise that may be present in the data. A Dirac delta function is initiated to represent the TF representation of the signal along with the key IF:

$$SET_e(t, \omega) = S_e(t, \omega) * \delta_2(\omega - \omega_i(t)) , \quad (4.3)$$

where $\delta_2(\omega - \omega_i(t))$ is termed as the synchro-extracting operator, and is represented as:

$$\delta_2(\omega - \omega_i(t)) = \begin{cases} 1, & \omega = \omega_i(t) \\ 0, & \text{else} \end{cases} . \quad (4.4)$$

It is shown that SET yields a more energy-concentrated TF representation than SST (Yu *et al.* 2017); thereby, the TF resolution is enhanced while the effect of measurement noise is significantly reduced. Recently, Li *et al.* (2020) compared the performance of SET

with the Fourier-based SST, where the authors concluded that SET is more concentrated with fewer cross-terms, and it is less sensitive to its window parameter. In this method, SET is used to analyze the IMFs resulting from TVF-EMD to track the vehicle and bridge frequencies. The applicability of SET is illustrated using a frequency-modulated signal (similar to a bridge response subjected to moving vehicles), as shown in Fig. 4.1. The data contains a signal with a frequency of 3 Hz and a frequency modulation of 1 Hz. Fig. 4.1 shows (a) the modulated signal, and (b) its SET results, indicating a clear decomposition of the frequency-modulated signal with a mean frequency of 3 Hz and modulation of 1 Hz.

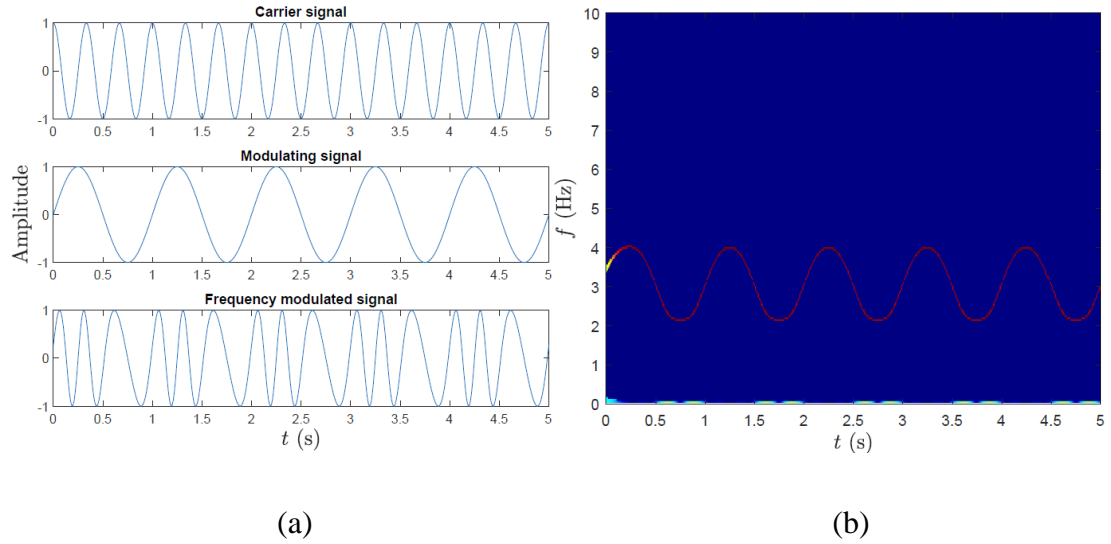


Figure 4.1: (a) Time history, and (b) SET result of the frequency modulated signal.

4.3 Proposed Method

After illustrating a brief background of TVF-EMD and SET, the proposed methodology is presented in this section. Consider a linear with n degrees of freedom (DOFs), damped and discrete lumped-mass structural system, subjected to a random input force, $u(t)$:

$$\mathbf{M}\ddot{\mathbf{y}}(t) + \mathbf{C}\dot{\mathbf{y}}(t) + \mathbf{K}\mathbf{y}(t) = \mathbf{u}(t) \quad , \quad (4.5)$$

where \mathbf{M} , \mathbf{C} , and \mathbf{K} are mass, damping, and stiffness matrix, respectively, and $\mathbf{y}(t)$ is a displacement response vector at various available DOFs. A state-space model can be used to find the solution for a dynamical system given above:

$$\bar{\mathbf{y}} = \begin{bmatrix} y_1 \\ y_2 \end{bmatrix} , \quad (4.6)$$

$$\dot{\mathbf{y}} = \mathbf{A}\bar{\mathbf{y}} + \mathbf{B}\mathbf{u} , \quad (4.7)$$

$$\mathbf{p} = \hat{\mathbf{C}}\bar{\mathbf{y}} + \mathbf{D}\mathbf{u} , \quad (4.8)$$

where \mathbf{A} is the state matrix, \mathbf{B} is the input matrix, $\hat{\mathbf{C}}$ is the output matrix, and \mathbf{D} is the feedback matrix. Under excitation $u(t)$, the resulting solution can be written in terms of expansion of vibration modes:

$$\mathbf{y} = \boldsymbol{\varphi}\boldsymbol{\eta} , \quad (4.9)$$

where \mathbf{y} and $\boldsymbol{\eta}$ are response and mode shape matrix, respectively. $\boldsymbol{\varphi}_{m \times n}$ is the mode transformation matrix. n and m are the number of modal responses and measurements, respectively. The measurement at k -th DOF ($k=1,2,\dots,m$) from the above equation can be expressed as:

$$y_k(t) = \sum_{j=1}^n \varphi_{kj} \eta_j(t) . \quad (4.10)$$

TVF-EMD is capable of eliminating the mode-mixing or end-effects under the presence of closely spaced modes or measurement noise. This method performs local cut-off filtering where a signal is filtered and decomposed into narrowband components called intrinsic mode functions (IMFs). By performing TVF-EMD of the k -th measurement $y_k(t)$ in terms of IMFs (i.e., i_{kj}), one can get:

$$y_k(t) = \sum_{j=1}^n i_{kj}(t) . \quad (4.11)$$

From Eqs. 4.10 and 4.11, we get:

$$i_{kj}(t) = \varphi_{kj} \eta_j(t) . \quad (4.12)$$

Normalized mode shape ordinates for k -th DOF w.r.t. n -th DOF can be calculated using the ratio of Eq. 4.12 for k -th and n -th DOF:

$$\frac{i_{kj}}{i_{nj}} = \frac{\varphi_{kj}\eta_j(t)}{\varphi_{nj}\eta_j(t)} = \frac{\varphi_{kj}}{\varphi_{nj}} = \widehat{\varphi_{kn}} . \quad (4.13)$$

A multicomponent amplitude and frequency-modulated signal $i_{kj}(t)$ can also be written in the following form:

$$i_{kj}(t) = \sum_{k=1}^K A_k(t) e^{2i\pi\phi_k(t)} . \quad (4.14)$$

By applying Eqs. (4.1-4.3) to the IMF from Eq. 4.14, we get:

$$SET_i(t, \omega) = S_i(t, \omega) * \delta_2(\omega - \omega_i(t)) . \quad (4.15)$$

Fig. 4.2 shows the framework for the proposed methodology (Singh and Sadhu 2021). The measured signal is decomposed using TVF-EMD followed by SET to extract the IFs of the structure and track the structural frequencies.

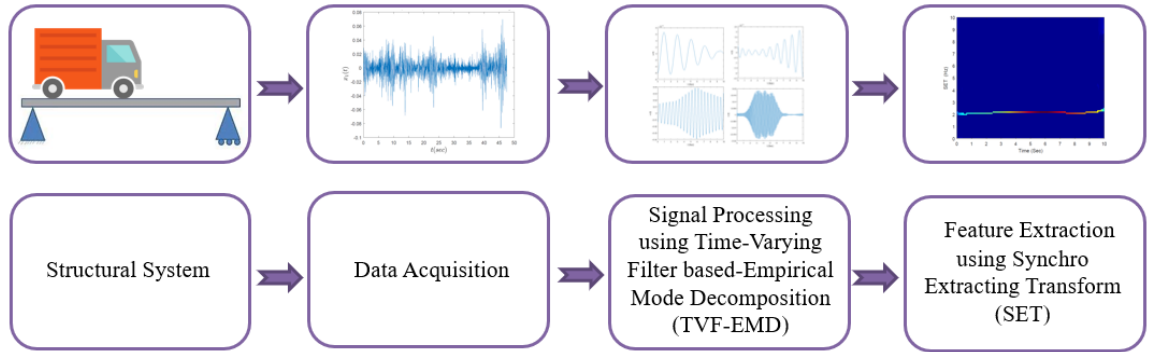


Figure 4.2: Framework of the proposed BHM method.

4.4 Numerical Study

To simulate the dynamic characteristics of the coupled vehicle-bridge system, a mathematical model is adopted, as shown in Fig. 4.3 (Yang and Lin 2005a). Consider a simply supported beam subjected to a vehicle load moving at speed v . The vehicle is modeled as a lumped mass m_v supported by a spring of stiffness k_v and the effective damping of the suspension system is neglected. The beam is assumed to be of the Bernoulli-Euler type with a constant cross-section. Only a single moving vehicle is

considered to travel on the beam, and the mass of the vehicle is assumed to be small compared to the bridge. The inertial effect of the vehicle is neglected. The vehicle traverses over the beam of length L at a constant speed. The beam is assumed to have a constant mass density \bar{m} per unit length and a constant flexural rigidity EI .

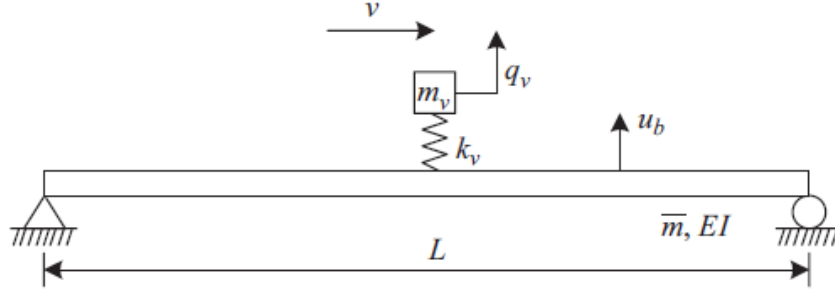


Figure 4.3: Schematic of the vehicle traveling along a simply supported beam.

The mass and stiffness of the vehicle are 1200 kg and 500 kN/m, respectively (Yang and Lin 2005a). The simply supported beam has a length of 25 m and a mass density of 4800 kg/m. Young's modulus of elasticity, E for the beam is 2.75×10^{10} N/m², and the moment of inertia, I for the beam is 0.12 m⁴. The frequency of vibration of the n -th mode of the bridge is given by:

$$\omega_{bn} = \frac{n^2 \pi^2}{L^2} \sqrt{\frac{EI}{\bar{m}}} , \quad (4.16)$$

$$f_{bn} = \frac{\omega_{bn}}{2\pi} . \quad (4.17)$$

The frequency of vibration of the vehicle is as follows:

$$\omega_v = \sqrt{\frac{k_v}{m_v}} . \quad (4.18)$$

The expression for driving frequency ω_d can be given as:

$$\omega_d = \frac{n\pi v}{L} . \quad (4.19)$$

The non-dimensional speed parameter S_n is given by:

$$S_n = \frac{n\pi v}{L\omega_{bn}} . \quad (4.20)$$

The static deflection caused by the vehicle w.r.t the n -th mode, Δ_{stn} is given by:

$$\Delta_{stn} = \frac{-2m_v g L^3}{n^4 \pi^4 EI} . \quad (4.21)$$

The displacement response of the beam to a moving vehicle at speed v is:

$$u(x, t) = \sum_n \frac{\Delta_{stn}}{1 - S_n^2} \left\{ \sin \frac{n\pi x}{L} \left[\sin \frac{n\pi v t}{L} - S_n \sin \omega_{bn} t \right] \right\} . \quad (4.22)$$

By differentiating $u(x, t)$ twice w.r.t time t , the acceleration response of the beam can be obtained as (Yang and Lin 2005a):

$$\ddot{u}(x, t) = \sum_n \frac{\Delta_{stn}}{1 - S_n^2} \left\{ \sin \frac{n\pi x}{L} \left[(\omega_{bn}^2 S_n) \sin \omega_{bn} t - \left(\frac{n\pi v}{L} \right)^2 \sin \omega_{bn} t \right] \right\} . \quad (4.23)$$

When the sensors are installed on the beam, the beam response is dominated by the natural frequencies as compared to vehicle frequencies. The acceleration responses are simulated using Eq. 4.23 at the quarter-span length of the beam, and the Fourier spectra of the simulated acceleration responses for a vehicle traveling at (a) 60, (b) 80, and (c) 100 km/h are shown in Fig. 4.4. The acceleration amplitude, most notably in the first few modes, increases as the speed of the vehicle increases. Also, the relatively smaller peaks at the beginning of all three plots corresponding to driving frequencies provide an idea about vehicle speed. The estimated values of driving frequencies for 60 km/h are 0.3 and 0.7 Hz, and for 100 km/h are 0.6 and 1.1 Hz, respectively. Analytical values for driving frequencies (f_d) are calculated using Eq. 4.19 and are 0.33, and 0.67 Hz for 60 km/h and 0.55 and 1.1 Hz for 100 km/h. Since the estimated values are close to analytical values, therefore, theoretically, it is feasible to detect the speed of the vehicle if the bridge response is recorded and processed in real-time.

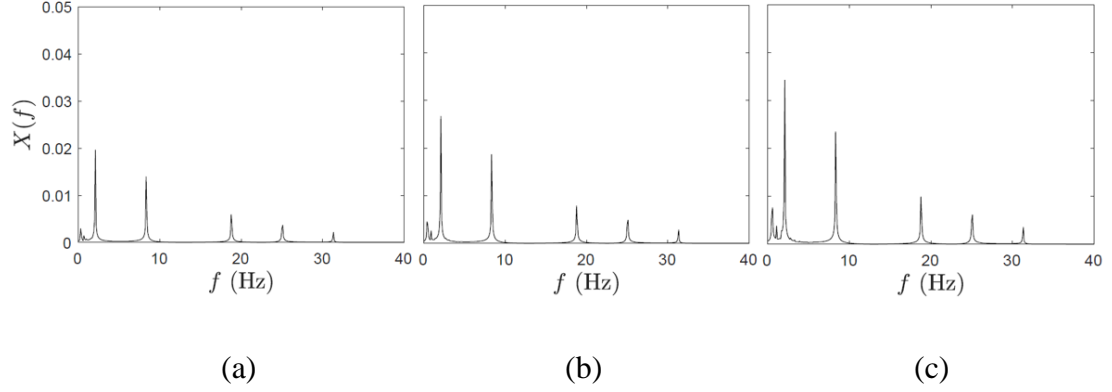
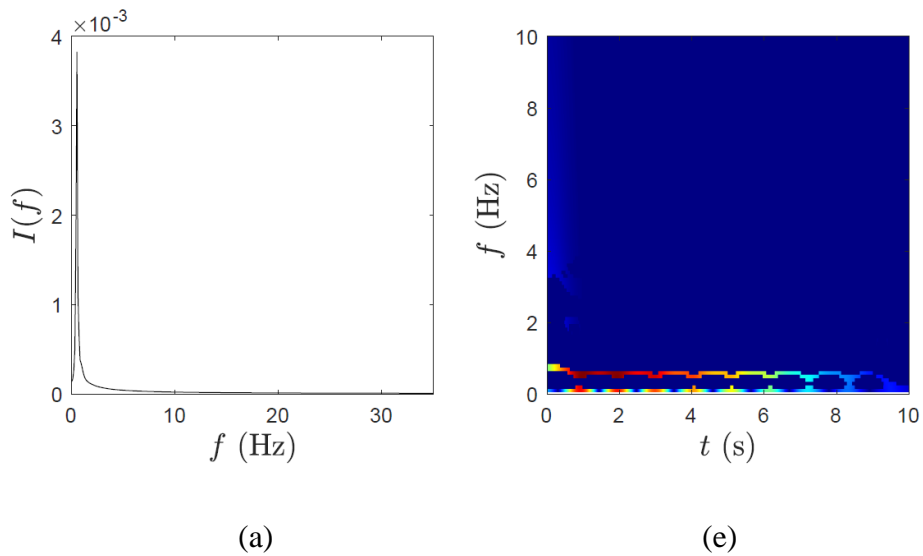
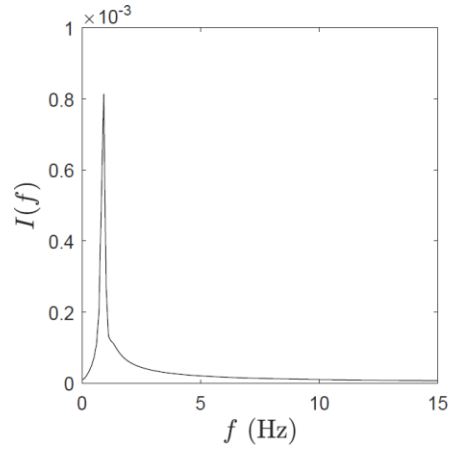


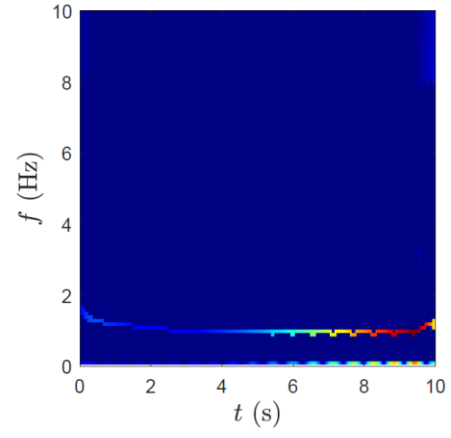
Figure 4.4: Fourier spectra of the acceleration response of the beam for vehicle speed of (a) 60 km/h, (b) 80 km/h, and (c) 100 km/h.

The proposed method is employed to decompose the data, as shown in Fig. 4.5. Fig. 4.5 shows (a-d) the TVF-EMD results, and (e-h) SET results of the beam response for a vehicle traveling at 80 km/h. It can be seen that the combination of TVF-EMD and SET can separate the closely spaced vehicle frequency content of acceleration data (i.e., 0.4 and 0.9 Hz), as shown in Figs. 4.5 (e-f). The analytical value of driving frequency, according to Eq. 4.19, is 0.44 and 0.88 Hz. It is also seen that the vehicle excites the low-frequency modes more compared to higher-frequency modes, which are excited for only a shorter duration, as reflected in Fig. 4.5 (h). As shown in SET, the active period reduces with higher modes, which cannot be observed from the Fourier spectra of the IMFs.

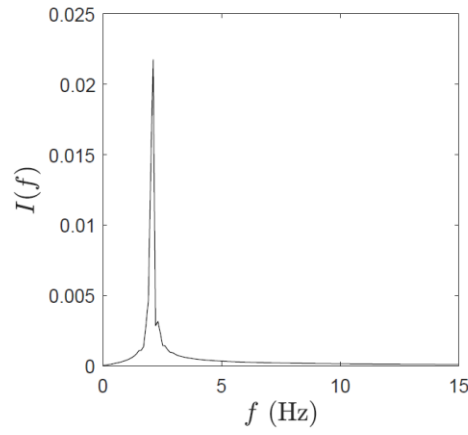




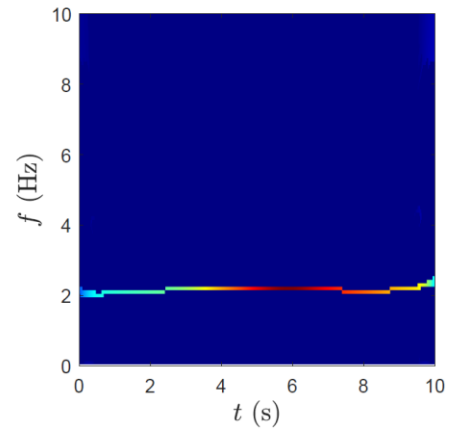
(b)



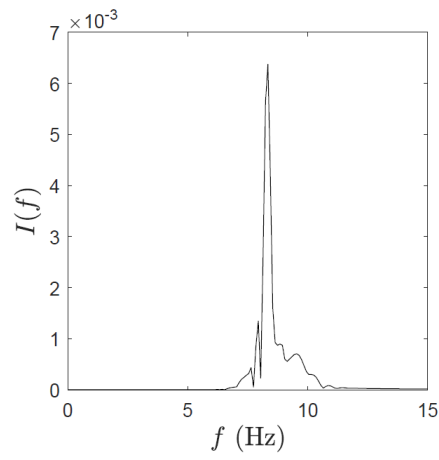
(f)



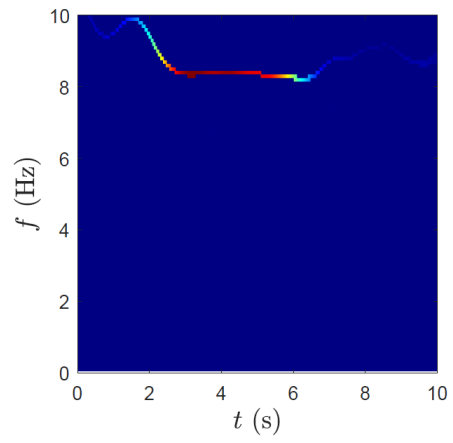
(c)



(g)



(d)



(h)

Figure 4.5: (a-d) Fourier spectra, and (e-h) SET results of the first four IMFs of the acceleration response of the beam for vehicle speed of 80 km/h.

Table 4.1: Comparison of the analytical and identified frequencies of the beam subjected to vehicle-induced load.

Mode #	f_{bn} (Hz)	\hat{f}_{bn} (Hz)		
		$v = 60 \text{ km/h}$	$v = 80 \text{ km/h}$	$v = 100 \text{ km/h}$
1	2.08	2.1	2.1	2.1
2	8.33	8.3	8.3	8.3
3	18.76	18.7	18.7	18.7
4	33.35	31.3	31.3	31.3

The identification results obtained from Fig. 4.5 are reported in Table 4.1. The estimated frequencies (\hat{f}_{bn}) calculated from the SET coincide with the analytical values of the natural frequencies (f_{bn}) calculated using Eq. 4.17.

4.5 Finite Element Study

The FEM model of a bridge is used to study the effect of various parameters of a vehicle traveling over a bridge. A reinforced concrete bridge of 100 m length consisting of three spans is used in this study. Frame elements are used to model the beams and columns. Fixed supports are used at the bottom of the columns, which restrict the translations as well as rotations along with all three directions. The bridge is subjected to dead load, live load, and moving load. No other lateral loads, such as wind and seismic loads, are considered. Fig. 4.6 (a) shows the schematic of the bridge, which is made up of 35 MPa concrete. Each span is 33 m in length, and the height of the pier is 4m. The typical cross-section A-A of the bridge is 500 mm in height and 300 mm in width and is shown in Fig. 4.6 (b). FEM beam contains discretized beam elements of 0.1 m in length. The bridge is excited using moving vehicles of different classes and sizes provided by AASTHO standards. A typical time history of the bridge acceleration response due to the non-overlapping presence of multiple moving vehicles is shown in Fig. 4.7. The first four natural frequencies of the bridges are obtained as 1.43, 3.24, 4.10, and 7.87 Hz, respectively. TVF-EMD and SET are utilized to analyze acceleration responses generated from different configurations of passing vehicles and compare the identified frequencies with the above analytical values.

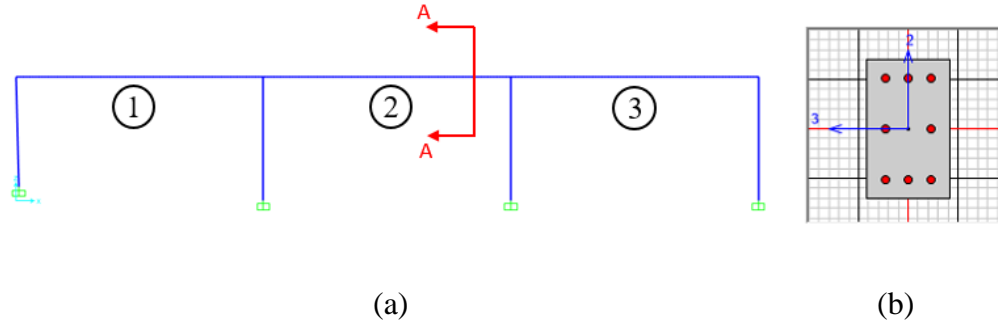


Figure 4.6: (a) Schematics of the FEM bridge, and (b) cross-section A-A of span 2.

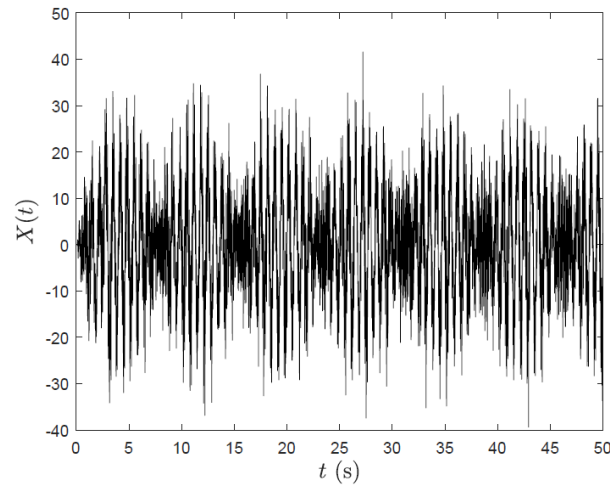


Figure 4.7: Typical time history of the bridge acceleration response.

4.5.1 Effect of sensor location

The effect of sensor location is investigated in this study to gain insight into the optimization of sensor instrumentation. A heavy vehicle (AASHTO HS20) traveling at 80 km/h passes over the bridge, and the corresponding acceleration response is analyzed at quarter-length and mid-length of spans 1 and 2. Fig. 4.8 shows the Fourier spectra of (a) quarter-length, and (b) mid-length responses. By comparing Figs. 4.8 (a) with (b), it is evident that the first mode has higher amplitude (i.e. higher energy) at mid-length as compared to quarter-length, while the second or third modes have higher energy in quarter-length acceleration response. Therefore, sensor location at the mid-span remains important to capture the first mode. In the acceleration response of the mid-span, which is

denoted by the blue line in Figs. 4.8 (a) and (b), more natural frequencies are excited as compared to span 1.

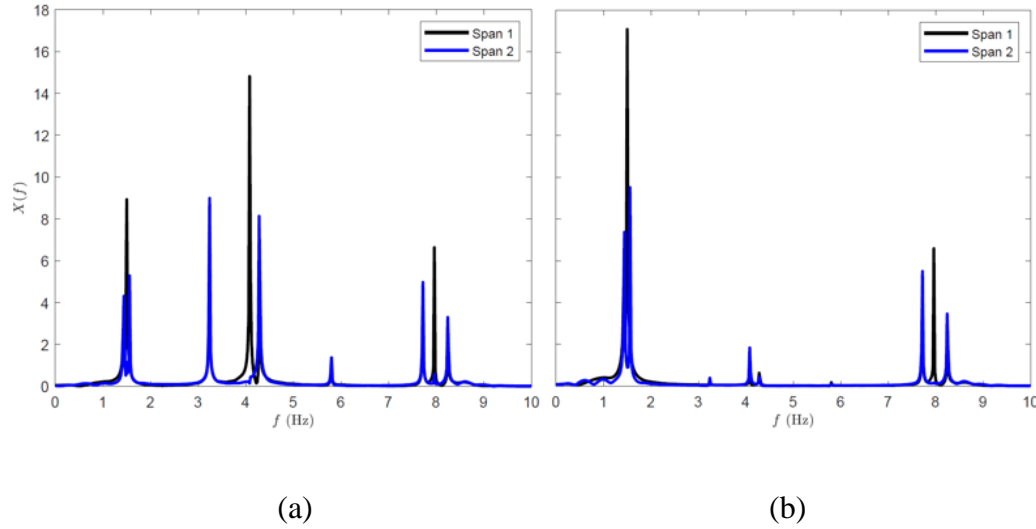


Figure 4.8: Fourier spectra of bridge response at (a) quarter-span length, and (b) mid-span length for vehicle speed of 80 km/h.

Fig. 4.9 shows (a-b) the TVF-EMD results, and (c-d) SET results for the quarter-length response. Mode-mixing with the first two modes can be seen in Fig. 4.9 (a). Fig. 4.10 shows (a-b) the TVF-EMD results, and (c-d) SET results for the mid-length response. Contrary to Fig. 4.9, Fig. 4.10 shows a lower number of modes and a higher and continuous energy profile for the first mode. The identification results from Fig. 4.9 are shown in Table 4.2. Depending on sensor locations, some of the resonant frequencies of the bridge have low (e.g., nearly zero) energy (as shown in Fig. 4.8) in the respective sensors, which are not identified in Table 4.2. More modes of vibration or higher frequencies can be seen in the mid-length of the mid-span response. Therefore, any responses analyzed further will be focused on that specific location.

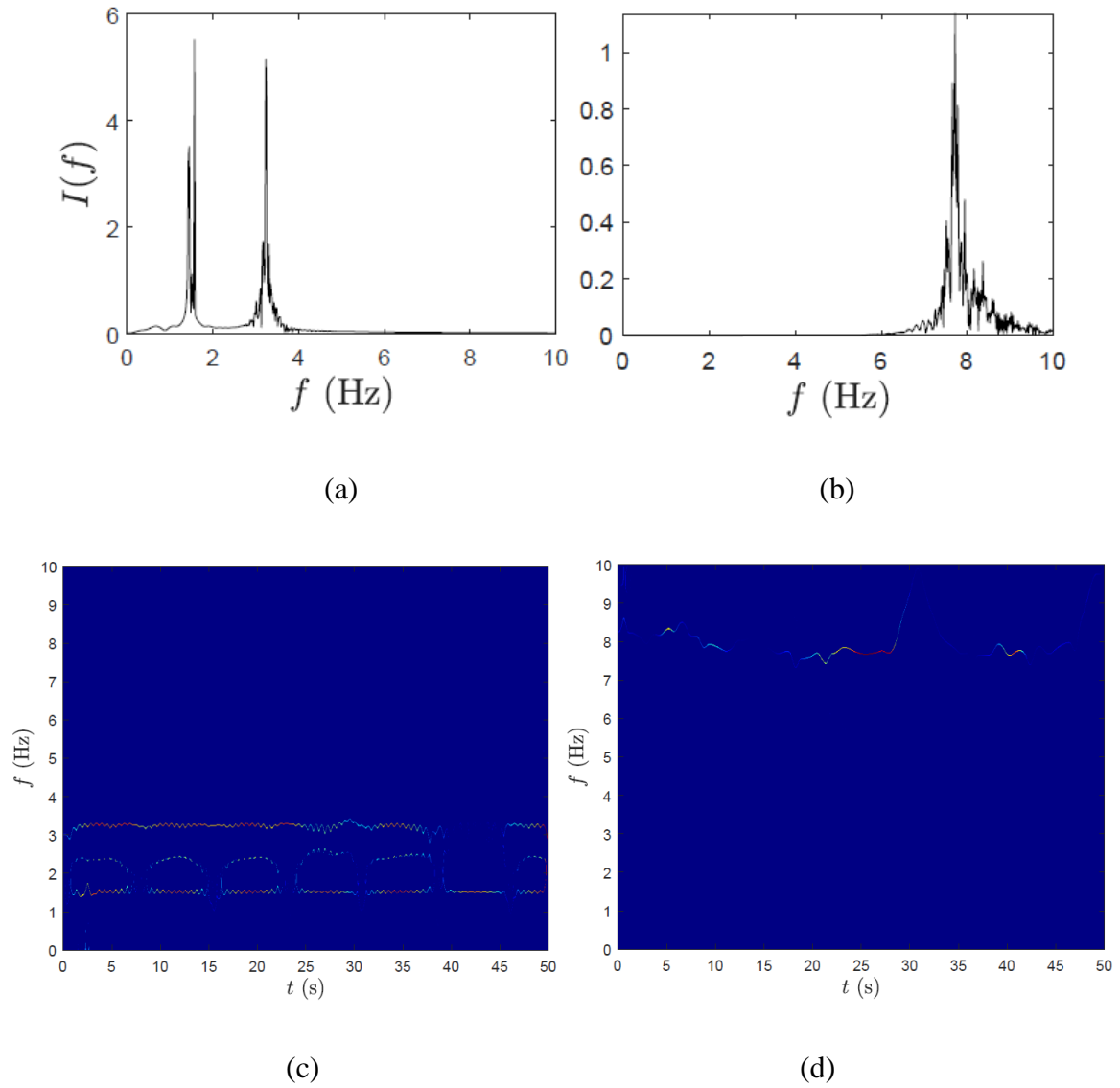


Figure 4.9: (a-b) TVF-EMD results, and (c-d) SET results for the bridge response at quarter-span length of span 2.

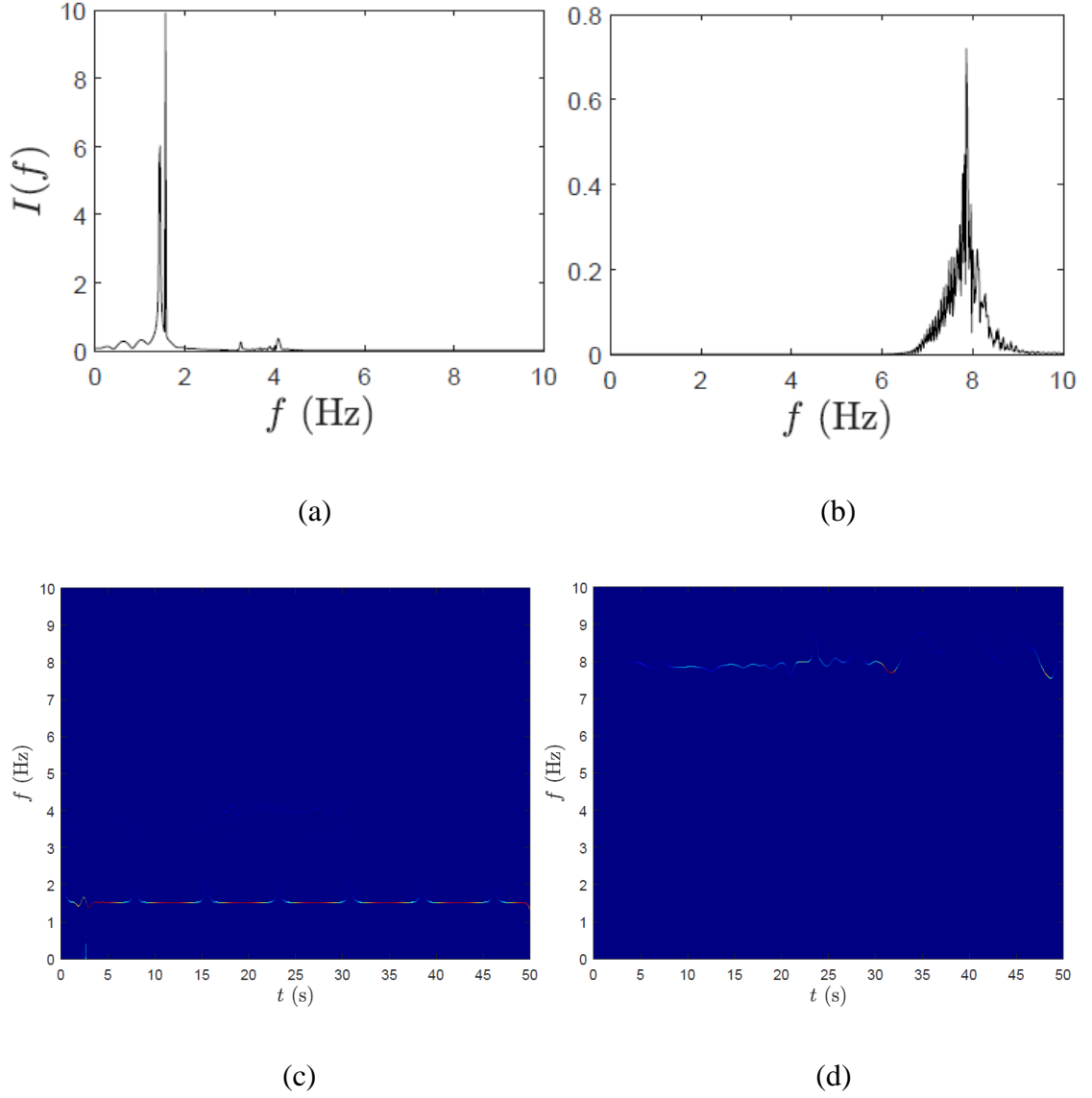


Figure 4.10: (a-b) TVF-EMD results, and (c-d) SET results for the bridge response at the mid-span length of span 2.

Table 4.2: Frequency values identified from span 1 and span 2.

Mode #	f (Hz)	$v = 80$ km/h 0.25L		$v = 80$ km/h 0.5L	
		Span 1	Span 2	Span 1	Span 2
1	1.43	1.42	1.44	1.44	1.44
2	3.24	3.24	3.24	-	3.24
3	4.10	4.08	4.08	4.08	4.08
4	7.87	7.96	7.72	7.96	7.72

4.5.2 Effect of vehicle speed

To simulate the effect of vehicle speed, the same truck (AASHTO HS20) used in section 4.5.1 is used to excite the bridge traveling at 40 and 100 km/h, and acceleration responses from mid-length of spans 1 and 2 are analyzed. Fig. 4.11 shows the Fourier spectra of the acceleration responses of the bridge generated by a vehicle traveling at (a) 40, and (b) 100 km/h. With an increase in speed, the amplitude of each mode of vibration increases. It implies that if some modes of vibration have comparatively lower energy, they may have higher energy due to higher speed. The practical importance of this observation lies in the field-testing of a stiff bridge.

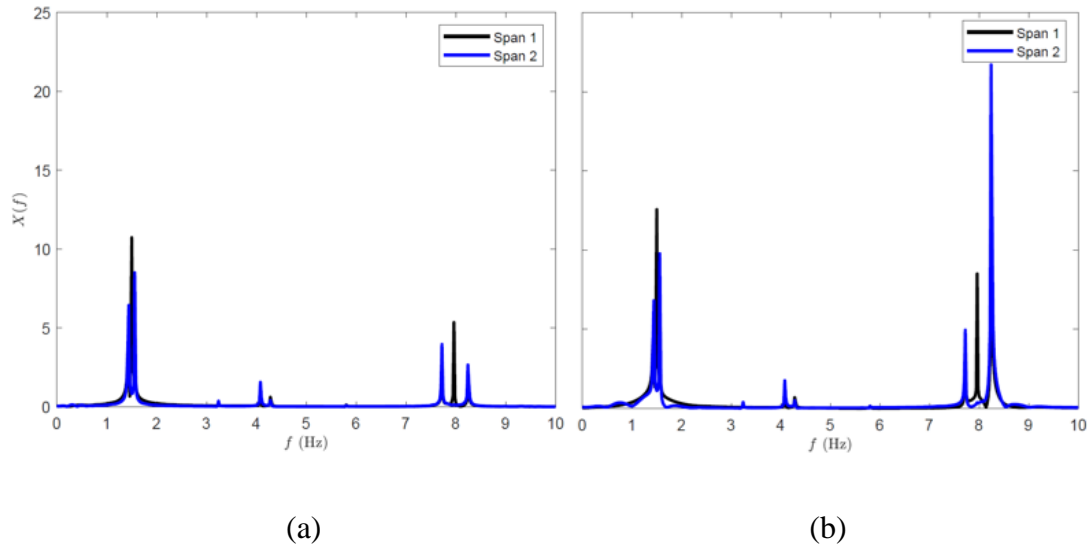


Figure 4.11: Fourier spectra of bridge response at mid-span length for vehicle speed of (a) 40 km/h, and (b) 100 km/h.

SET results from Figs. 4.12 and 4.13 show that the frequency profiles are more stabilized in case of higher speed since higher energy is imparted to the system by the passing vehicle. Table 4.3 shows the detailed identification results.

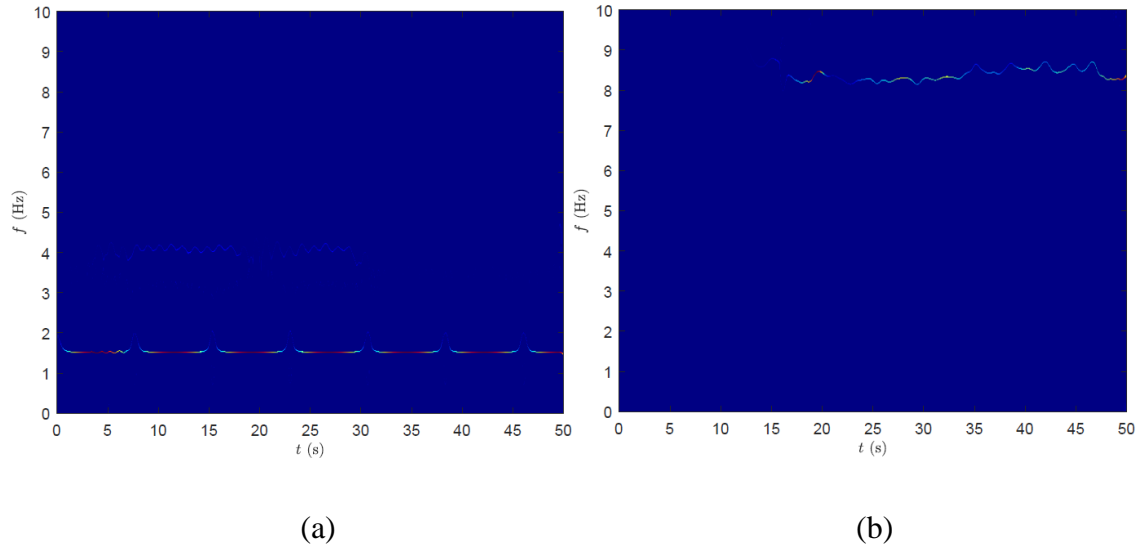


Figure 4.12: Frequency profile of (a) 1.44 Hz and (b) 8.2 Hz identified from the mid-span length of span 2 for vehicle speed of 40 km/h.

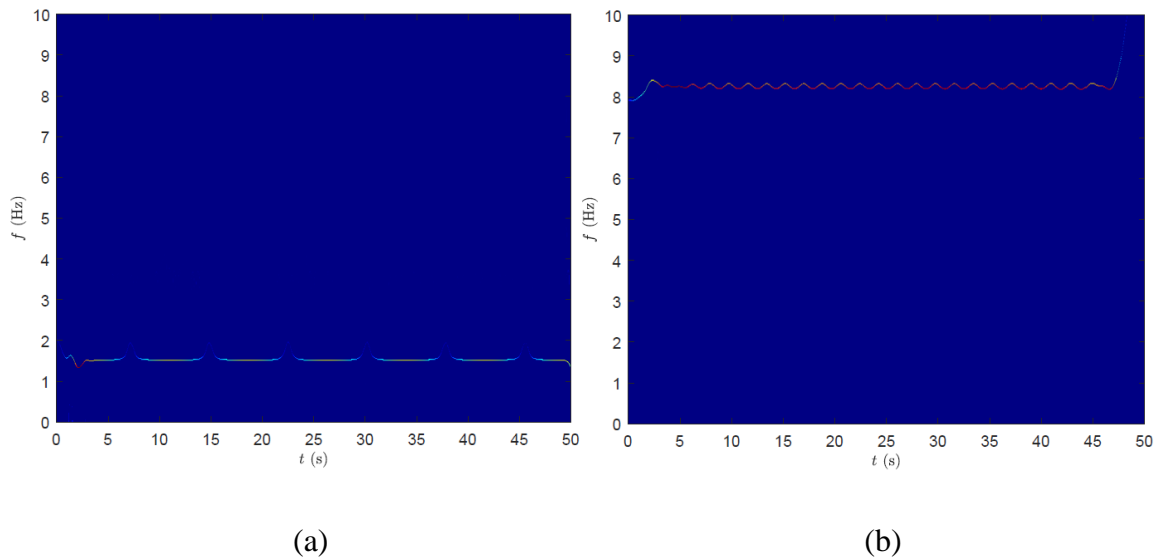


Figure 4.13: Frequency profile of (a) 1.44 Hz and (b) 8.2 Hz identified from the mid-span length of span 2 for vehicle speed of 100 km/h.

Table 4.3: Frequency values identified from the mid-span length of span 1 and span 2.

Mode #	f (Hz)	$v = 40$ km/h		$v = 100$ km/h	
		Span 1	Span 2	Span 1	Span 2
1	1.43	1.42	1.44	1.42	1.44
2	3.24	-	3.24	-	3.24

3	4.10	4.08	4.08	4.08	4.08
4	7.87	7.96	7.72	8.2	8.2

4.5.3 Effect of vehicle class

In this section, the vehicle speed is kept constant at 40 km/h. The effect of vehicle weight is simulated using two vehicles from AASTHO standards (HS15 and HS25) and is shown in Fig. 4.14 (a). By using a heavier vehicle, the vibration modes can be excited with higher amplitudes. A practical limitation of the bridge with permitted low speed can be overcome with this observation of using a heavier vehicle to excite the bridge. Fig. 4.14 (b) shows the acceleration responses due to H20 and HS20 trucks, which differ in terms of the number of axles. H20 is a two-axle truck, and HS20 is a three-axle truck. It is evident from Fig. 4.14 (b) that the three-axle truck enables higher excitation and higher energy for each mode of vibration. The effect of the presence of vehicles is simulated in Fig. 4.14 (c). With an increase in the number of vehicles present on the bridge, the amplitudes of vibration for each mode are increased.

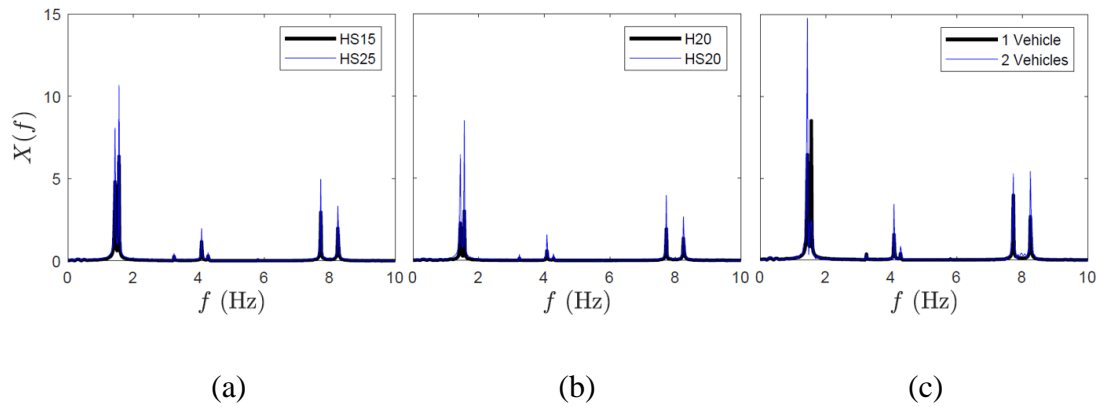


Figure 4.14: Fourier spectra of bridge response due to (a) different vehicle weights, (b) different number of vehicle axles, and (c) different number of vehicles.

Figs. 4.15 (a) and (b) show the SET results for the two natural bridge frequencies when multiple vehicles are traveling over the bridge at a speed of 40 km/h. By comparing Fig. 4.15 with Fig. 4.12, it is evident that the presence of two trucks on the bridge imparts higher energy to the structure and, in turn, the frequency profiles of vibration modes are active for a longer duration and are continuous over-time.

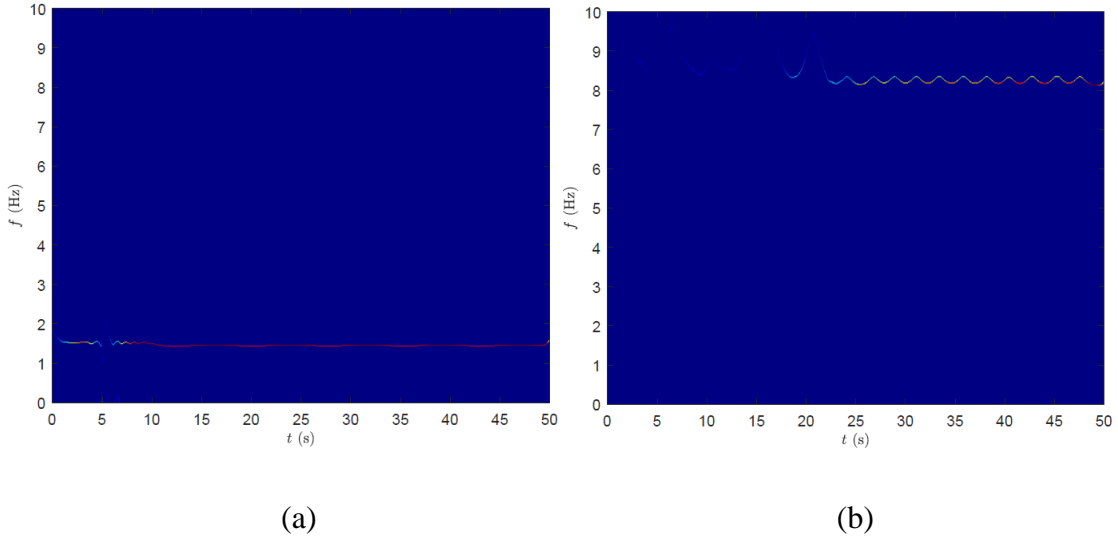


Figure 4.15: Frequency profile of (a) 1.44 Hz, and (b) 8.2 Hz identified from the mid-span length of span 2 subjected to two trucks.

4.5.4 Effect of structural damage

The damage in a bridge causes stiffness discontinuity. In this section, structural damage is introduced into the FEM, and the performance of the proposed method is verified. The structural damage is simulated using a change in cross-section of the middle span (i.e., span 2), and Fig. 4.16 shows the comparison of Fourier spectra of response between undamaged and damaged cross-sections. A reduction of depth of 100 mm in the cross-section is introduced in the damaged case. Fig. 4.16 shows that there is evidence of a reduction in the frequency values of the damaged case. Fig. 4.17 shows the SET results for the first natural frequencies for the damaged case. By comparing the SID results of Fig. 4.15 (a) and with Fig. 4.17, it is evident that the natural frequencies of the bridge are changed and reduced as the structural damage is introduced to the bridge.

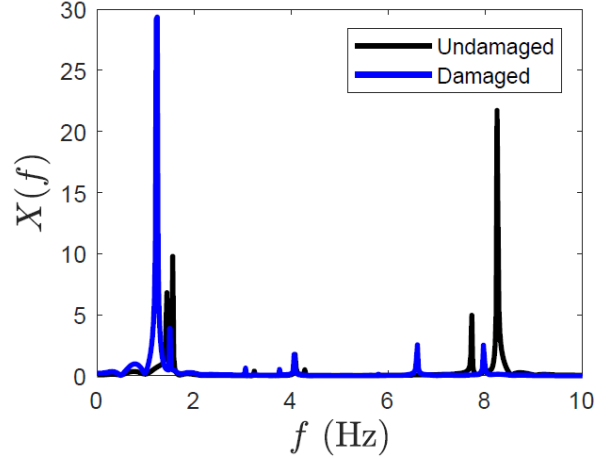


Figure 4.16: Fourier spectra of undamaged and damaged bridge response for vehicle speed of 100 km/h.

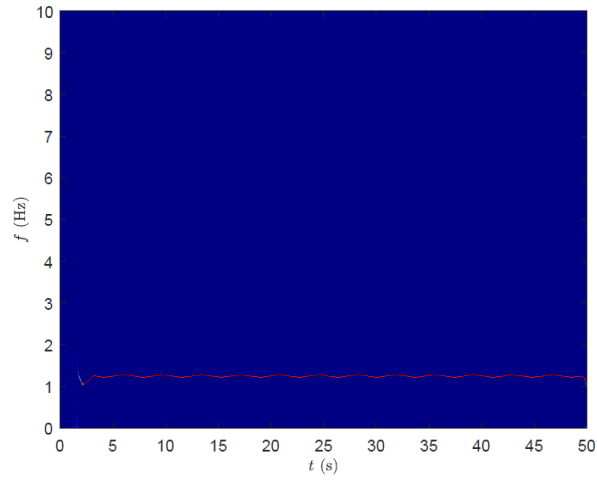


Figure 4.17: Frequency profile of 1.24 Hz identified from the mid-span length of damaged span 2 for vehicle speed of 100 km/h.

4.6 Full-Scale Study

This section demonstrates the in-field application of the proposed framework developed in this chapter.

4.6.1 Details of full-scale study

In this section, the proposed method is illustrated using a 90 m pony truss steel bridge, as shown in Fig. 4.18 (a). Bridge vibrations are monitored while different numbers of

vehicles travel over the bridge. BHM data is collected using accelerometers instrumented throughout the bridge. The temperature during the testing is around 24°C. Nine high-sensitive sensors with a sensitivity of 10 V/g are placed along the walkway on the southside of the bridge, and the sensors are set up to measure uniaxial vertical vibration. A sampling frequency of 200 Hz is used. Sensors are placed at a distance of 3, 6, 15, and 30 m on both sides from the centerline of the bridge shown in Fig. 4.18 (b). The data collection is performed through the data acquisition (DAQ) system by connecting it with sensors using BNC cables and with a laptop using a USB cable. The duration of each test was between 30 seconds to 5 minutes. A typical time history of the acceleration response at the mid-span of the bridge is shown in Fig. 4.19.

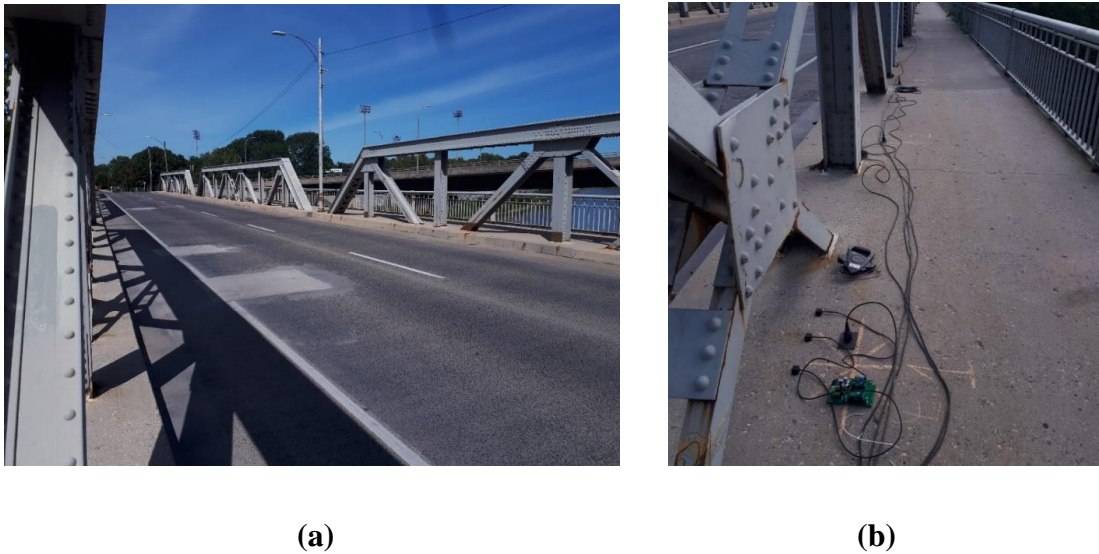


Figure 4.18: (a) Steel truss bridge, and (b) sensor instrumentation.

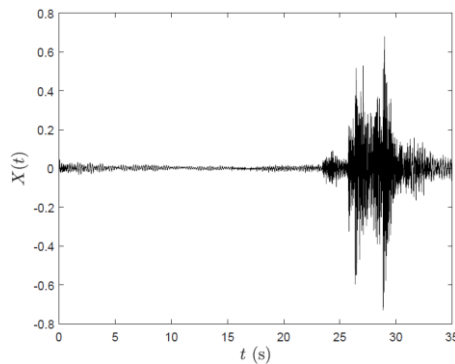


Figure 4.19: Time history of bridge acceleration response at mid-span length.

4.6.2 Identification results

Two tests are selected to be analyzed and compared using the proposed method. The first test contains the vibration data for a bus traveling over the bridge, and the second test entails multiple vehicles (11 vehicles) traveling over the bridge. For both tests, sensor data at the center of the bridge is used to validate the proposed method. Fig. 4.20 shows the comparison of the Fourier spectra of (a) a bus and (b) multiple cars. From Fig. 4.20, it is evident that a single heavy vehicle is sufficient to excite the various modes of the bridge to a greater extent as compared to multiple smaller vehicles.

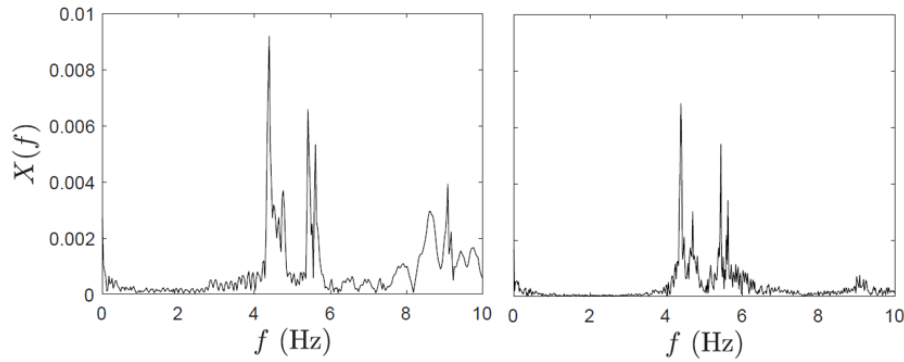


Figure 4.20: Fourier spectra of bridge acceleration response subjected to (a) a bus, and (b) multiple vehicles.

Using TVF-EMD and SET, the modal responses are separated and shown in Fig. 4.21. The identified frequencies for two test data sets in Fig. 4.21 are shown in Table 4.4. The identified mode shapes of the first two modes of the bridge are extracted in Fig. 4.22 using the proposed methodology, as shown in Eq. 4.13. In Fig. 4.22, ‘s’ denotes the supports for the bridge. Since the proposed approach is based on the utilization of limited sensors, responses from only three pairs of sensors are used to generate the mode shapes.

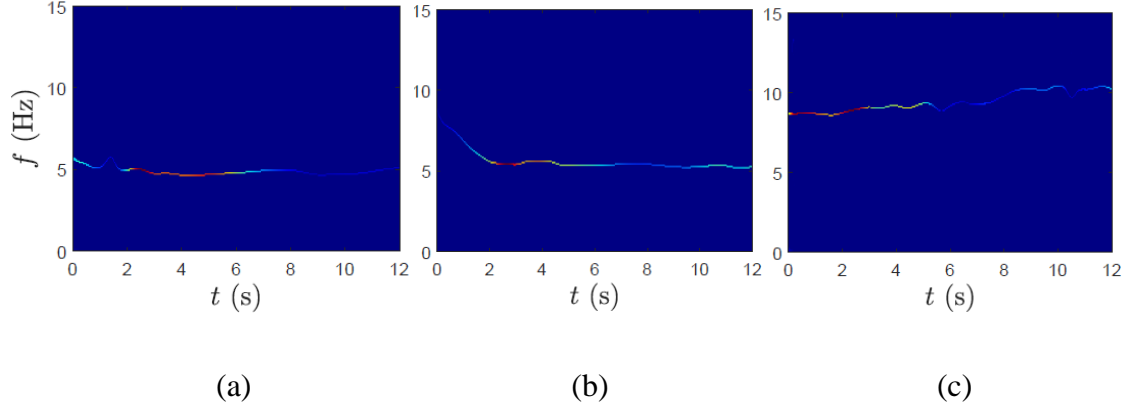


Figure 4.21: SET results for (a-c) the first three natural bridge frequencies.

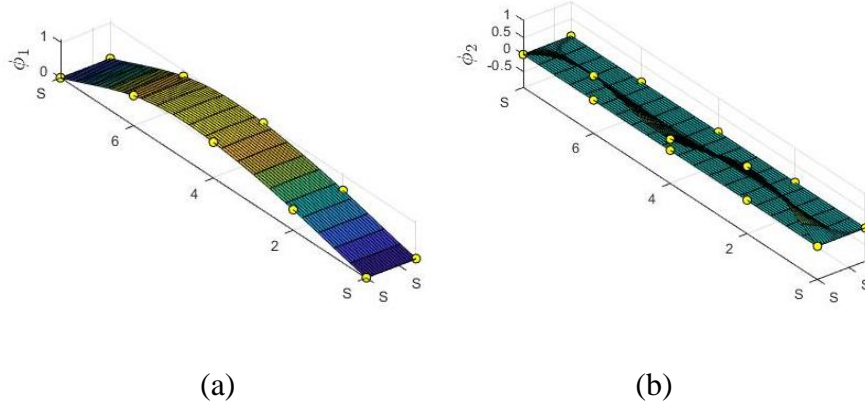


Figure 4.22: (a) First, and (b) second mode shape of the bridge.

Table 4.4: Frequency values identified from bridge acceleration response.

Mode #	Test 1	Test 2
	f (Hz)	f (Hz)
1	4.38	4.38
2	5.40	5.43
3	9.08	9.07

4.7 Summary

In this chapter, an improved TF decomposition-based modal identification method is proposed to address the practical challenges associated with BHM using vehicle-induced responses. In the proposed method, TVF-EMD is first employed to decompose the vibration responses of the bridge, and then, the time-varying modal frequencies of the bridges are tracked using SET. Detailed analytical and FEM simulations are conducted to

investigate the effect of sensor locations, vehicle speeds, vehicle parameters, and damage identification due to the vehicle-induced excitation. A full-scale validation is also conducted to investigate the modal identification of the bridge using limited sensors subjected to a suite of vehicles of different sizes.

Chapter 5

5 Drive-by Modal Identification of Bridges utilizing Wavelet Decomposition

This chapter presents a hybrid time-frequency (TF) method capable of decoupling vehicle-bridge interactions (VBI) of vehicle response and performing robust bridge modal identification under various operational challenges. Results from this chapter demonstrate that the proposed method can be used to decompose the signal collected from the moving vehicle. Modal frequencies, which hold key importance in bridge health monitoring (BHM), can be successfully identified using the proposed hybrid TF method. Numerical results confirmed that the proposed algorithm could be used in varying conditions of vehicle speed, structural damage, and measurement noise. Laboratory experiments and full-scale validation provide further evidence of the potential of the proposed algorithm.

5.1 Introduction

Direct BHM (Elhatab and Uddin 2017, An *et al.* 2019, Sun *et al.* 2020, Singh and Sadhu 2021, Singh *et al.* 2021, Sony *et al.* 2022) usually involves direct instrumentation with sensors such as accelerometers to extract the modal parameters from the ambient or forced vibrations. As an alternative to direct BHM, researchers have recently geared toward indirect BHM (iBHM) (Malekjafarian *et al.* 2015, Yang and Yang 2017, Shokravi *et al.* 2020). iBHM leverages a vehicle traveling over a bridge as a data acquisition device as well as a source of excitation. While traversing over a bridge, an instrumented vehicle can excite the bridge and collect the vibration response of the bridge. The idea of using a test vehicle to extract the bridge frequencies was initially proposed by Yang *et al.* (2004a).

Unlike the identification of bridge frequencies in previous iBHM methods, Gonzalez *et al.* (2012) conducted a study to identify the absolute damping of a bridge from the vehicle response and detect structural damage. Theoretical simulations, including a simplified 2-degrees of freedom (DOF) half-car VBI model, were used to validate the method for a

range of bridge spans and vehicle speeds. The relationship between driving speed, vehicle frequency, and bridge frequency was examined analytically and experimentally by Siringorongo and Fujino (2012). In their study, the effects of surface roughness, vehicle damping, and expansion joints were ignored. From the results, it was clear that higher vehicle velocities (e.g., larger than 30 km/h) created practical difficulties due to vehicle bouncing impact on expansion joints and shorter response duration.

O'Brien *et al.* (2014) used the vehicle response to identify VBI forces. The bridge modal identification was completed using a coupled 4-DOF half-car model in theoretical simulations. Based on moving force identification theory, the proposed method identified the global bending stiffness of a bridge and predicted the pavement roughness, which was insensitive to measurement noise. Malekjafarian and O'Brien (2014) extracted the mode shapes of a bridge by monitoring the accelerations in two connected axles of the passing vehicle. This study proposed a short-time frequency-domain decomposition method that relied on multi-stage measurements. After the segmentation of the bridge, the proposed method was applied to the acceleration responses, and local mode shape elements were estimated. Furthermore, global mode shape vectors for the bridge were constructed from the local mode shape elements using a correction procedure.

Recently, time-frequency methods (Sadhu *et al.* 2017, Yan *et al.* 2020, Barbosh *et al.* 2020) such as Short-Time Fourier Transform (STFT), Wavelet Transform (WT), Hilbert Transform (HT), and Empirical Mode Decomposition (EMD) have shown significant success in analyzing iBHM data. For example, EMD was used by Yang and Chang (2009) to extract the higher modes of the bridge using experimental studies (Yang and Lin 2005b), and the importance of the selection of the most appropriate vehicle properties in a bridge was discussed. EMD was used by O'Brien *et al.* (2017) for bridge damage detection using the response measured in a passing vehicle. EMD was applied to the axle response to decompose it into various component, and the resulting intrinsic mode functions (IMFs) corresponding to the pseudo-frequency component of the vehicle speed was used to extract the damaged location.

In a recent study, the finer frequency resolution capability of WT was leveraged to detect structural damage in bridges using the response from a passing vehicle. Tan *et al.* (2019) used the HT to analyze the acceleration responses and extract bridge modal parameters from a passing vehicle. The proposed algorithm was used to extract the mode shapes and damping ratio of a bridge. Another relevant research was further explored by Tan *et al.* (2020a), where a damage index, based on the extracted mode shape, was proposed to detect structural damage in bridges. Tan *et al.* (2020b) introduced the wavelet entropy theory in which the optimal wavelet scale was selected by minimizing wavelet entropy. This approach was a step forward in enhancing the existing wavelet-based damage detection methods. Fitzgerald *et al.* (2019) detected the presence of bridge scours using acceleration responses from a passing train. The structural damage was identified in terms of pier stiffness reduction by analyzing the acceleration of train passages using continuous wavelet transform. A damage indicator was developed using wavelet coefficients from healthy and damaged bridge states, which performed well in the blind test.

The feasibility and challenges of the implementation of bridge parameter identification were explored by Li *et al.* (2019a). An experimental investigation was performed in the laboratory using a vehicle-bridge system. The numerical simulation of the VBI system was accomplished using a single-DOF (SDOF) quarter-car model and an Euler-Bernoulli beam. Effects of measurement noise, vehicle properties, and bridge surface roughness were numerically studied. In another study, Li *et al.* (2019b) proposed a blind modal identification method to extract bridge modal frequencies from the dynamic vehicle response. Singular spectrum analysis was used to decompose the vehicular response and blind modal identification to extract the bridge frequencies. Bridge frequencies were successfully identified in laboratory experimentation. The effects of vehicle speed and other vehicle parameters on the results were investigated.

In drive-by monitoring, variabilities in vehicle responses can be caused by environmental and operational conditions such as temperature, traffic, vehicle speed, road roughness, etc. Tan *et al.* (2017) investigated the use of a subtracted signal from two consecutive axles to remove the effect of road roughness and showed good agreement between the

extracted and theoretical bridge frequencies, followed by damage identification. The variabilities and numerous levels of structural damage were also examined by Locke *et al.* (2020). Vehicle acceleration data was analyzed using a neural network architecture to study the changes in dynamic response due to noise-inducing variables. The application of machine learning for bridge damage detection was attempted by Malekjafarian *et al.* (2019). An artificial neural network was trained using data from a vehicle traveling over a healthy bridge. Numerical case studies verified the proposed damage indicator, based on a Gaussian process, by successfully detecting the structural damage despite the contribution of road profile roughness and measurement noise.

The study by Shirzad-Ghaleroudkhani and Gul (2020) filtered out the effects of vehicle speed and vehicle suspension using a smartphone-based inverse filtering technique. This study utilized the off-bridge data to design an inverse filter to process the on-bridge data. A scaled lab experiment was used to demonstrate the validity of the proposed method. Although smartphones have relatively low accuracy than accelerometers, the proposed filter was able to successfully extract the bridge frequencies. In another recent study, Sitton *et al.* (2020) examined the applicability of crowdsourcing for bridge monitoring using the analytical Finite Element Modeling (FEM) simulation and a scaled laboratory experiment. Analytical and experimental results showed that the bridge frequency could be identified using the multi-vehicle approach. The crowdsourcing framework established that iBHM could be accomplished without the information related to the mass and stiffness of the vehicle.

Cronin *et al.* (2021) solved the problem of preprocessing data that results from iBHM and contains noise from road profile roughness and vehicle suspension dynamics. This approach focused on tire-level response estimation and deconvolved the signal collected from the cabin of the vehicle containing the input from the suspension system using autoencoders. A network of moving vehicles was used by Eshkevari *et al.* (2020a) for the system identification (SID) of a bridge. The noise due to the vehicle suspension system was removed by deconvolving the vehicle response in the frequency domain. Two approaches, such as vehicle transfer function and Ensemble EMD (EEMD), were utilized, while road profile roughness was delineated using the second-order blind identification

method. Various road surface patterns were considered, and the results indicated that the proposed framework could extract the bridge vibrations for a long-span bridge with various levels of traffic volume. VBI problems related to medium to long-span bridges were examined by Eshkevari *et al.* (2020b). The authors concluded that with an increase in bridge flexibility, the decoupling between the bridge and the vehicle increases considerably. In another recent study, Eshkevari *et al.* (2020c) proposed a crowdsourcing method that was capable of considering vibration data collected by multiple sensors with random motions.

Kildashti *et al.* (2020) developed drive-by monitoring by extending its application to cable-stayed bridges for structural damage detection. The study identified the location and severity of damage incurred by the cables by measuring the vibration response from a passing vehicle over the bridge. The FEM was used for new formulations of dynamic coupling between the vehicle and the bridge. Various damage cases due to changes in structural stiffness were considered, and it was demonstrated that the vehicle vibration response identified the structural damage, its location, and severity. The limitations in Shirzad-Ghaleoudkhani and Gul (2020) related to constant vehicle speed and similar surface roughness throughout the test were addressed in Shirzad-Ghaleoudkhani and Gul (2021). The inverse filtering methodology was enhanced with a new framework along with a full-scale validation. A database of off-bridge acceleration signals to sort out different vehicle speeds was developed. In addition, a surface roughness criterion was defined based on the average energy level of the acceleration signal.

Shi and Uddin (2021) worked on a closed-form solution and decoupling of the VBI system. Effects of bridge damping, vehicle frequency, vehicle speed, vehicle mass, and vehicle damping on extracting the bridge frequencies from the vehicle were studied. This theoretical study provided guidelines for designing a field test vehicle for bridge monitoring. In another study, Alamdari *et al.* (2021) examined the practical viability of drive-by bridge inspection using numerical and experimental investigations. The authors proposed an index based on vehicle and bridge frequencies to quantify the performance of transmission between the bridge and the vehicle. The first few bridge vibration modes were identified using the test vehicle moving at constant and low speed. Zhang *et al.*

(2021) proposed an instantaneous frequency identification technique based on modified S-transform reassignment. The resolution was enhanced by introducing a frequency function in the Gaussian window with two parameters determined by the time-frequency concentration criterion. Numerical studies validated the effect of road profile roughness and vehicle parameters such as weight and speed on the time-varying characteristic identification.

The influence of vehicle parameters such as vehicle-to-bridge mass ratio, vehicle speed, and frequency ratio on the frequency identification accuracy was investigated by Wu *et al.* (2022). Through parametric analysis in laboratory tests, it was found that the vehicle-to-bridge mass ratio and vehicle speed had a great impact on the identified frequency patterns. Additionally, a frequency extraction method was proposed in this study to filter out the bridge frequency from the vehicle response. In another vein, Micu *et al.* (2022) validated the idea of using dynamic responses taken on a passing train to determine the condition of a railway bridge. The full-scale experiment successfully showed that instrumented trains could be used for bridge maintenance and monitoring.

Throughout the literature, limited attention has been undertaken to the investigation of time-varying VBI resulting from noisy vehicle movement due to the combination of various factors, including vehicle speed, vehicle suspension system, road roughness, limited sensor measurement, structural damage, and operational condition. To address these challenges in a unified fashion, the proposed method harnesses the decomposition and denoising capability of a powerful TF method, Wavelet Packet Transform (WPT), and delineates the bridge frequencies found in the noisy vehicle response. Since vehicle response contains significant measurement noise and closely-spaced frequencies, WPT is used to eliminate the vehicle noise and other unwanted noise sources from the bridge and vehicle dynamic component.

In addition, WPT enables robust decomposition of a single channel measurement, facilitating bridge SID using limited measurement. Afterwards, Synchro Extracting Transform (SET) is used as a quantification method to classify the individual bridge and vehicle dynamic components, namely bridge frequencies, vehicle frequencies, and

driving frequencies. The accuracy of the proposed hybrid TF method is then validated using numerical, experimental investigations and a full-scale study. In the numerical investigation, a vehicle travels over a beam model at varying speeds, varying degrees of structural damage, and measurement noise, and the vehicle responses are analyzed using the proposed method. In the laboratory experiment, a moving vehicle model travels over a scaled bridge model, and the resulting vehicle response is used for the validation of the proposed method. The full-scale study shows the field application of the proposed method to a 220m long box-girder bridge. Both direct and indirect monitoring data are compared to validate the efficacy of the proposed research.

This chapter is organized as follows: section 5.2 is used to provide a background about the VBI, WPT, SET, and their respective governing equations. Section 5.3 is used to formulate the proposed methodology from the dynamics of the vehicle response. In sections 5.4 and 5.5, the numerical and experimental investigations are presented. Section 5.6 illustrates the full-scale study using both direct BHM and iBHM. Section 5.7 summarizes the highlights and contributions of this chapter.

5.2 Background

In this section, a brief background of VBI, and WPT is provided. The governing equations are provided for each topic, followed by a detailed description of the proposed methodology.

5.2.1 Vehicle bridge interaction

The concept of iBHM uses a vehicle passing over a bridge as an excitation source as well as a sensor. Fig. 5.1 shows an example of a simplified VBI model that is used for the theoretical formulation. The vehicle is modeled as an SDOF system with a lumped mass m_v and spring of stiffness k_v and the effective damping of the suspension system is neglected. The bridge is modeled as a simply supported Euler Bernoulli beam with length L and a constant cross-section and smooth profile; therefore, it has a constant flexural rigidity EI and a constant mass density \bar{m} throughout the length. The vertical displacements of the vehicle, moving at a speed of v , and the beam are denoted by q_v and u_b , respectively.

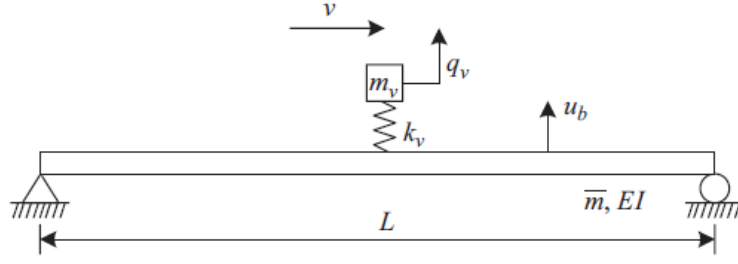


Figure 5.1: Schematic of the vehicle traveling along a simply supported beam.

From the equation of motion of a coupled VBI system, the solution in the form of vertical displacement of the beam can be expressed as (Yang and Lin 2005a):

$$u_b(x, t) = \sum_n \frac{\Delta_{stn}}{1 - S_n^2} \left\{ \sin \frac{n\pi x}{L} \left[\sin \frac{n\pi v t}{L} - S_n \sin \omega_{bn} t \right] \right\}, \quad (5.1)$$

where n represents the number of modes of vibration.

Using Duhamel's integral, the vertical displacement of the vehicle (q) can be obtained as (Yang and Chang 2009):

$$q(t) = \sum_n \left\{ H_{dl,n} \cos \frac{(n-1)\pi v}{L} t - H_{dr,n} \cos \frac{(n+1)\pi v}{L} t + H_{v,n} \cos \omega_v t \right. \\ \left. - H_{bl,n} \cos \left(\omega_{b,n} - \frac{n\pi v}{L} \right) t + H_{br,n} \cos \left(\omega_{b,n} + \frac{n\pi v}{L} \right) t \right\}. \quad (5.2)$$

The coefficients $H_{dl,n}$, $H_{dr,n}$, $H_{v,n}$, $H_{bl,n}$, and $H_{br,n}$ are defined in Eqs. 5.3-5.7:

$$H_{dl,n} = \frac{\Delta_{st,n}}{2(1 - S_n^2)(1 - \mu_{n-1}^2 S_{n-1}^2)}, \quad (5.3)$$

$$H_{dr,n} = \frac{\Delta_{st,n}}{2(1 - S_n^2)(1 - \mu_{n+1}^2 S_{n+1}^2)}, \quad (5.4)$$

$$H_{v,n} = \frac{2\Delta_{st,n}\mu_n^2 S_n^2}{(1 - S_n^2)} * \left[\frac{1}{(1 - \mu_{n-1}^2 S_{n-1}^2)(1 - \mu_{n+1}^2 S_{n+1}^2)} - \frac{1}{\{1 - \mu_n^2(1 - S_n^2)\}\{1 - \mu_n^2(1 + S_n)\}^2} \right]$$

$$, \quad (5.5)$$

$$H_{bl,n} = \frac{\Delta_{st,n} S_n}{2(1 - S_n^2)\{1 - \mu_n^2(1 - S_n)^2\}} , \quad (5.6)$$

$$H_{br,n} = \frac{\Delta_{st,n} S_n}{2(1 - S_n^2)\{1 - \mu_n^2(1 + S_n)^2\}} . \quad (5.7)$$

The vertical acceleration response of a vehicle can be obtained by differentiating Eq. 5.2 (Yang and Chang 2009):

$$\begin{aligned} \ddot{q}(t) = \sum_n \left\{ -\tilde{H}_{dl,n} \cos \frac{(n-1)\pi v}{L} t + \tilde{H}_{dr,n} \cos \frac{(n+1)\pi v}{L} t - \tilde{H}_{v,n} \cos \omega_v t \right. \\ \left. + \tilde{H}_{bl,n} \cos \left(\omega_{b,n} - \frac{n\pi v}{L} \right) t - \tilde{H}_{br,n} \cos \left(\omega_{b,n} + \frac{n\pi v}{L} \right) t \right\} . \end{aligned} \quad (5.8)$$

The coefficients $\tilde{H}_{dl,n}$, $\tilde{H}_{dr,n}$, $\tilde{H}_{v,n}$, $\tilde{H}_{bl,n}$, and $\tilde{H}_{br,n}$ are further explained in Eqs. 5.9-5.13:

$$\tilde{H}_{dl,n} = H_{dl,n} \omega_{b,n-1}^2 S_{n-1}^2 , \quad (5.9)$$

$$\tilde{H}_{dr,n} = H_{dr,n} \omega_{b,n+1}^2 S_{n+1}^2 , \quad (5.10)$$

$$\tilde{H}_{v,n} = H_{v,n} \omega_v^2 , \quad (5.11)$$

$$\tilde{H}_{bl,n} = H_{bl,n} \omega_{b,n}^2 (1 - S_n)^2 , \quad (5.12)$$

$$\tilde{H}_{br,n} = H_{br,n} \omega_{b,n}^2 (1 + S_n)^2 . \quad (5.13)$$

Five terms involved in vehicle response in Eq. 5.8 can be labeled into three groups as driving frequencies (in rad/s), including $(\frac{(n-1)\pi v}{L} \text{ and } \frac{(n+1)\pi v}{L})$; vehicle frequency ω_v ; and bridge frequencies, including $(\omega_{bn} - \frac{n\pi v}{L} \text{ and } \omega_{bn} + \frac{n\pi v}{L})$, where n indicates the index of the vibration mode. It may be observed that bridge frequency ω_{bn} is shifted by an equal amount to the vehicle speed $\pm \frac{n\pi v}{L}$. The importance of bridge frequency terms $(\omega_{bn} - \frac{n\pi v}{L})$

and $\omega_{bn} + \frac{n\pi v}{L}$) is crucial, and most of these terms may be visible in the vehicle response depending on the bridge-vehicle interaction.

5.2.2 Wavelet Packet Transform

WPT is a TF technique that can decompose a signal into consecutive low and high-frequency components. WPT has several advantages over Fourier Transform (FT) (Wu and Liu 2009, Sadhu 2013) and serves as an excellent decomposition tool for analyzing nonstationary and nonlinear signals. As the signal, originating from the passing vehicle, containing coupled dynamic information related to the bridge and the vehicle, is nonstationary, WPT is used to analyze the vehicle response. This method results in both approximation and detailed coefficients to further decompose and provide a wider and more flexible analysis base for the signal (Kankanamge *et al.* 2020).

The decomposition process using WPT is a recursive filter-decimation operation. After j -th level of decomposition, a signal $f(t)$ can be represented as (Mallat 2009):

$$f(t) = \sum_{s=0}^{2^j-1} f^{j,s} . \quad (5.14)$$

A linear combination of wavelet basis functions $\psi_k^{j,s}(t)$ can be used to represent the wavelet packet component signal $f^{j,s}$ at each node (j,s) :

$$f^{j,s}(t) = \sum_{k=-\infty}^{\infty} c_k^{j,s} \psi_k^{j,s}(t) , \quad (5.15)$$

where a wavelet basis is a function with three indices, s , j , and k , which correspond to modulation, scale, and translation, respectively (Mallat 2009). Furthermore, wavelet packet coefficients, $c_k^{j,s}(t)$, can be calculated as:

$$c_k^{j,s}(t) = \frac{1}{2^{\frac{j}{2}}} * \int_{-\infty}^{\infty} f^{j,s}(t) \psi^s\left(\frac{t-k}{2^j}\right) dt \quad . \quad (5.16)$$

The process of WPT starts with decomposing the parent signal into an approximate and detailed component using a pair of low-frequency and high-frequency filters, respectively derived through multi-resolution analysis. Both the approximate and detailed coefficients are further divided into the next level approximate and detailed parts. The operation proceeds until the stopping criterion is met.

5.3 Proposed Framework

The response of the VBI system from Eq. (5.8) can be expressed in terms of WPT coefficients using Eq. 5.14.

$$\ddot{q}(t) = \sum_{s=0}^{2^j-1} \ddot{q}^{j,s} \quad . \quad (5.17)$$

In this chapter, Daubechies (“db5”) is used as the wavelet basis function due to its oscillatory nature to capture vibration time-history. Depending on the selected scale level, which is considered a stopping criterion, WPT generates a suite of low- and high-pass frequency coefficients. The scale level for WPT is determined based on sampling frequency and the lowest frequency of interest (Sadhu 2013). The WPT coefficients include driving frequencies, bridge frequencies, and vehicle frequencies. After j levels of decomposition, the WPT coefficient $\ddot{q}^{j,s}$ can be calculated using Eq. 5.15:

$$\ddot{q}^{j,s} = \sum \ddot{q}_k^{j,s} \psi_k^{j,s}(t) \quad . \quad (5.18)$$

WPT yields well-separated frequency components; however, they do not provide time-varying information related to the individual frequency content of the data. Therefore, SET is used to examine the WPT coefficients. By applying Eqs. 4.2-4.4 to the WPT coefficients, the SET of the WPT coefficients is obtained as:

$$S_e^q(t, \omega) \approx \sum_{i=1}^K \ddot{q}^{j,s} * \hat{h}(\omega - \omega_i(t)) e^{j \int \omega_i(t) dt} , \quad (5.19)$$

$$SET_e(t, \omega) = S_e^q(t, \omega) * \delta_2(\omega - \omega_i(t)) . \quad (5.20)$$

The WPT coefficients are classified as the modal responses of the bridge if they remain stationary in the spectrogram of the SET. The flowchart of the proposed methodology (Singh and Sadhu 2022) is shown in Fig. 5.2.

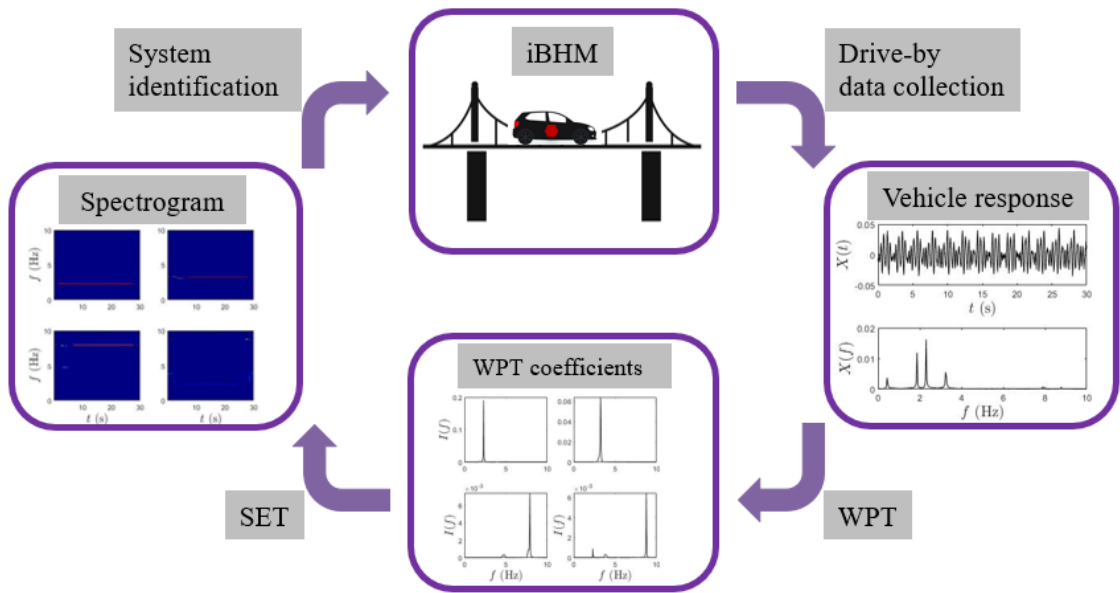


Figure 5.2: Framework of the proposed drive-by BHM method.

5.4 Numerical Investigation

This section begins with a description of the model used for numerical simulation. The effect of vehicle speed, structural damage, and measurement noise on the vehicle response is investigated in the following sub-sections.

5.4.1 Model description

A coupled VBI system is simulated using the model shown in Fig. 5.1. The values of m_v and k_v are 1200 kg and 500 kN/m, respectively. Only a single moving vehicle is considered passing on the beam at one instance of time. The mass of the vehicle is

assumed to be small compared to the beam. The inertial effect of the vehicle is neglected. The vehicle traverses over the beam of length L at a constant speed. The simply supported beam has an L of 25m and \bar{m} of 4800 kg/m. The values of E and I for the beam used in this study are 2.75×10^{10} N/m² and 0.12 m⁴, respectively. The natural frequencies of the beam are f_{b1} and f_{b2} , 2.08 Hz and 8.33 Hz, whereas the vehicle frequency, f_v , is calculated as 3.2 Hz. Finally, the vehicle acceleration response is simulated using Eq. 5.8.

5.4.2 Effect of vehicle speed

Vehicle speed plays a crucial role in the excitation of the bridge. In this section, the vehicle travels over the beam at a speed of 40 and 80 km/h, respectively, while keeping the other vehicle properties the same. Fig. 5.3 shows (a) the time history, and (b) Fourier spectra of the vehicle acceleration response for vehicle speed of 40 km/h. The first resonant peak in Fig. 5.3 (b) shows the primary driving frequency, f_d , of 0.43 Hz, and the next two resonant peaks represent the frequency pair of f_{b1} , 1.86 Hz, and 2.30 Hz. It can be noted that the frequency pair values can be averaged out to compute the first natural frequency of the beam (i.e., 2.08 Hz), which matches the theoretical value (i.e., 2.08 Hz). The fourth resonant peak in Fig. 5.3 (b), 3.2 Hz, represents f_v , whereas the last two resonant peaks, 7.9 Hz and 8.8 Hz, indicate the frequency pair of f_{b2} . The average value of the second frequency pair is 8.35 Hz, and the theoretical value of the second natural frequency is 8.33 Hz. The vehicle response is decomposed using WPT, which results in WPT coefficients, and their Fourier spectra are shown in Fig. 5.4. It can be observed that WPT can efficiently decompose the signal into its components, where f_v , f_d , and f_{bn} are well separated. The WPT coefficients are analyzed using SET to differentiate the beam frequencies from driving and vehicle frequencies. Fig. 5.5 shows SET results of the WPT coefficients of the vehicle response at a speed of 40 km/h.

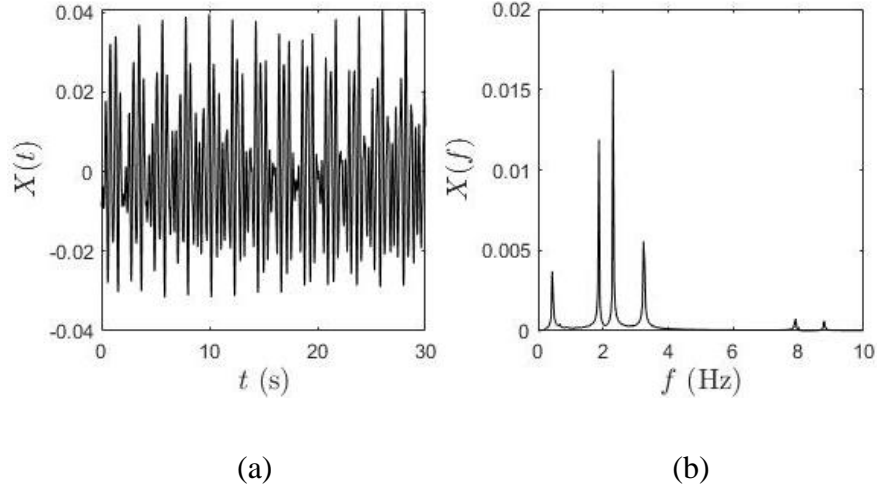


Figure 5.3: (a) Time history, and (b) Fourier spectra of vehicle acceleration response for vehicle speed of 40 km/h.

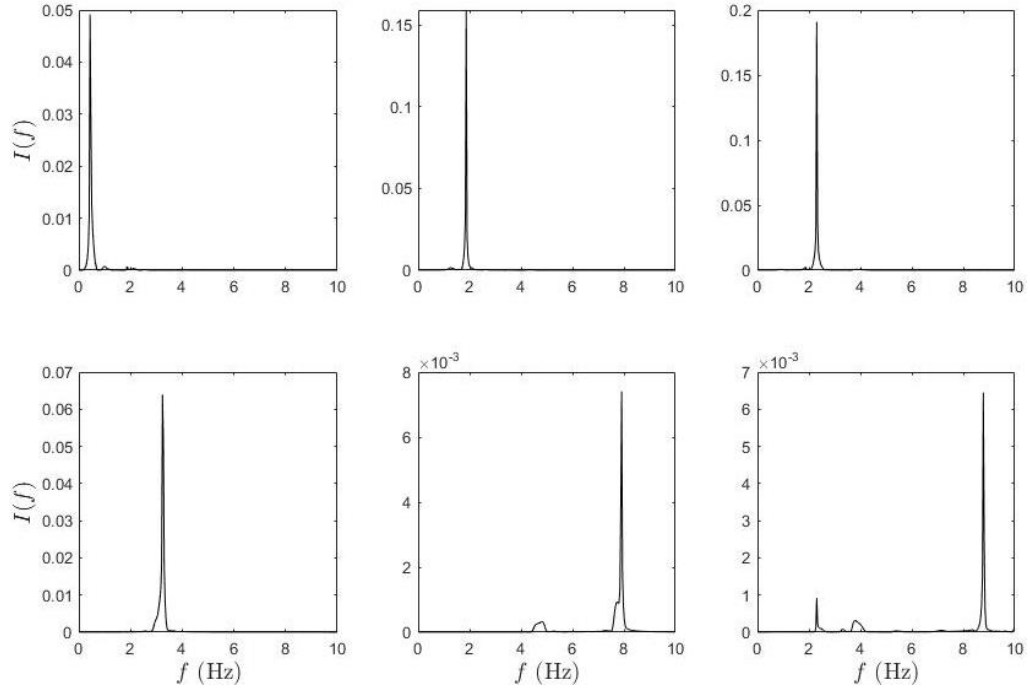


Figure 5.4: WPT coefficients of vehicle acceleration response for vehicle speed of 40 km/h.

To show the effect of speed, another data set is generated using the vehicle speed of 80 km/h. As the vehicle speed increases, the amount of energy imparted by the vehicle to the beam increases, and the value of f_d changes which also affects the f_{bn} pairs. Fig. 5.6 shows

(a) the time history, and (b) Fourier spectra of the vehicle acceleration response while the vehicle travels at 80 km/h. Fourier spectra of vehicle response show that the value of f_d , the first resonant peak in Fig. 5.6 (b), as 0.9 Hz, which is nearly doubled as compared to the f_d value from the last case (i.e., 0.43 Hz) due to the doubling of the vehicle speed. The values of structural frequency pairs are also changed due to the change in vehicle speed. WPT and SET results for vehicle acceleration response at 80 km/h are presented in Figs. 5.7 and 5.8, respectively. The identified frequency values from Figs. 5.5 and 5.8 are summarized in Table 5.1. The theoretical values are also provided for comparison in Table 5.1, which are depicted in brackets. It can be observed that the bridge and vehicle frequencies are identified using the proposed method for both cases of vehicle speed.

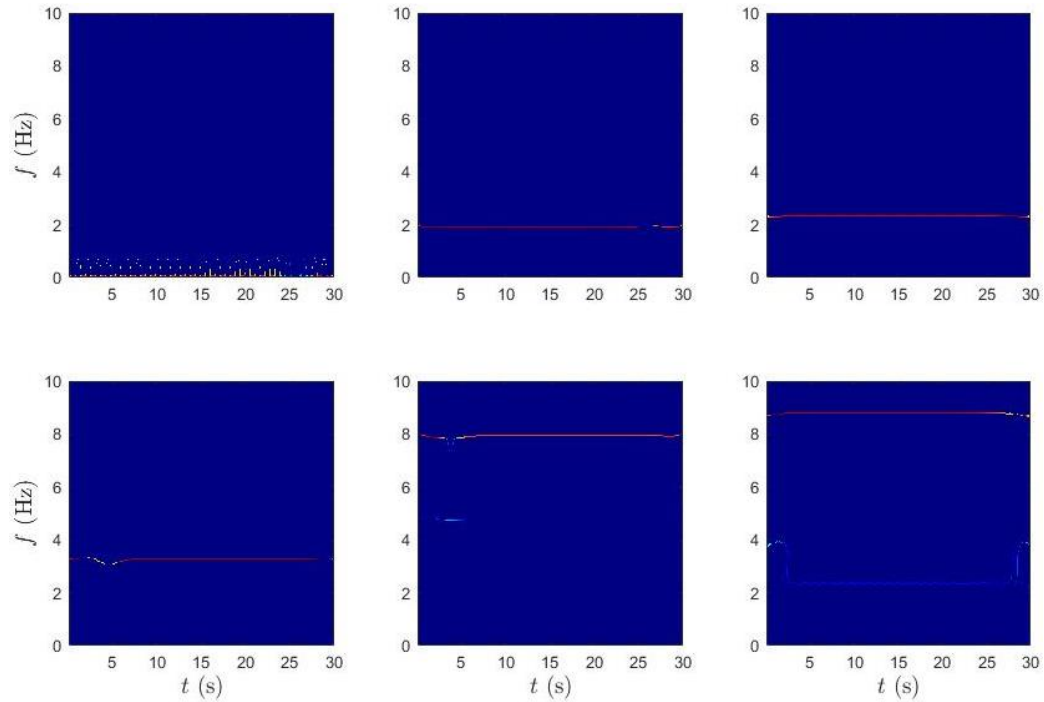


Figure 5.5: SET results of vehicle acceleration response for vehicle speed of 40 km/h.

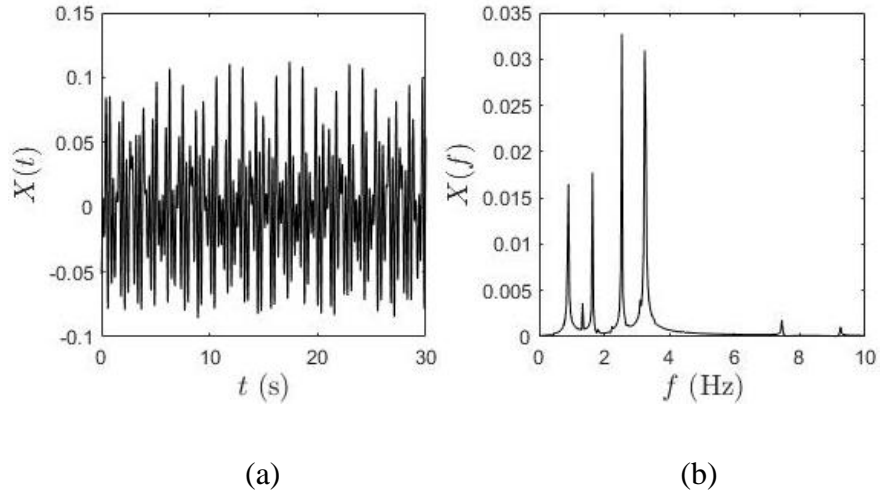


Figure 5.6: (a) Time history, and (b) Fourier spectra of vehicle acceleration response for vehicle speed of 80 km/h.

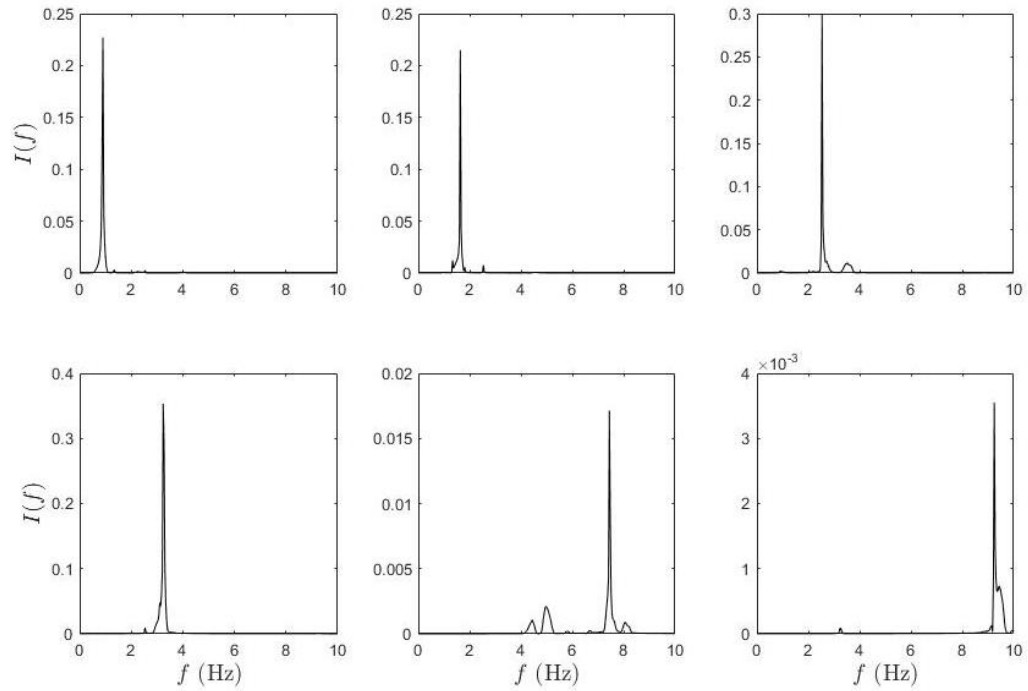


Figure 5.7: WPT coefficients of vehicle acceleration response for vehicle speed of 80 km/h.

Table 5.1: Frequency values identified with different values of vehicle speed.

		$v = 40$ km/h		$v = 80$ km/h	
Mode #	f_b (Hz)	\hat{f} from Fig. 5.5	\hat{f}_b	\hat{f} from Fig. 5.8	\hat{f}_b

		(Hz)	(Hz)	(Hz)	(Hz)
		$f_d = 0.43$ (0.44)		$f_d = 0.9$ (0.88)	
1	2.08	$f_{b1}^1 = 1.86$ (1.86), $f_{b1}^2 = 2.30$ (2.30)	2.08	$f_{b1}^1 = 1.63$ (1.64), $f_{b1}^2 = 2.53$ (2.52)	2.08
		$f_v = 3.2$		$f_v = 3.2$	
2	8.33	$f_{b2}^1 = 7.89$ (7.89), $f_{b2}^2 = 8.77$ (8.77)	8.33	$f_{b2}^1 = 7.44$ (7.45), $f_{b2}^2 = 9.24$ (9.21)	8.34

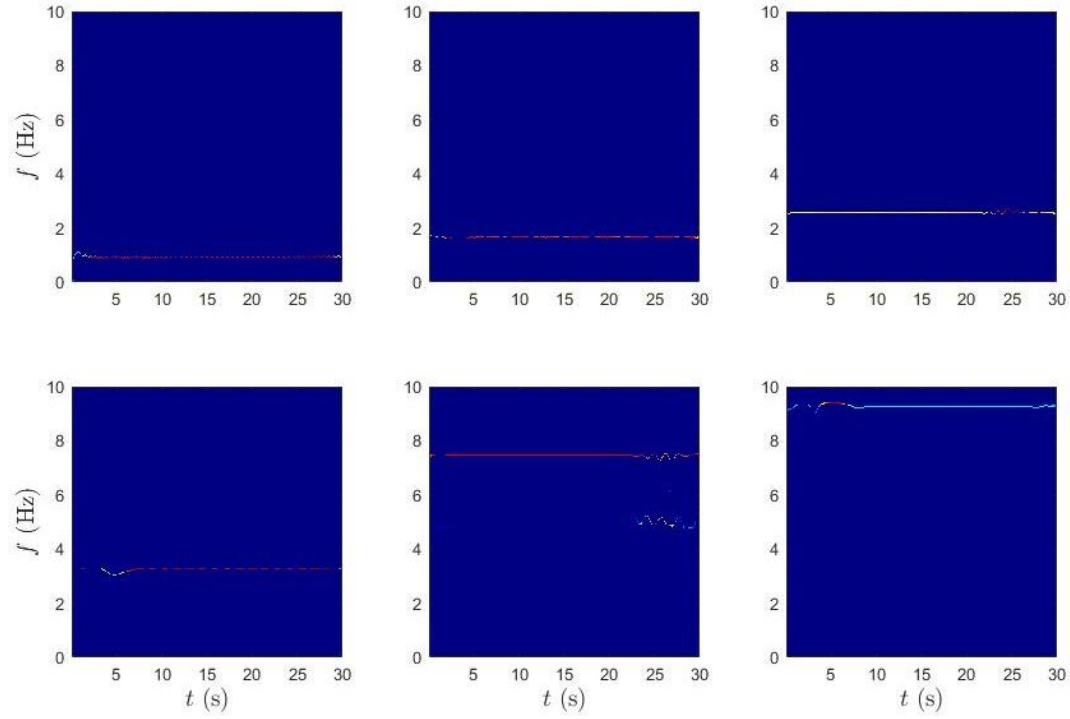


Figure 5.8: SET results of vehicle acceleration response for vehicle speed of 80 km/h.

5.4.3 Effect of structural damage

To study the performance of the proposed methodology on the effect of structural damage, two damage cases are simulated, namely 20% and 50% structural damage. The damage cases are simulated by reducing the bending rigidity of the beam. It affects the dynamic behavior of the beam, and this change in behavior manifests itself in the form of changes in structural frequency. Fig. 5.9 shows the Fourier spectra of the vehicle acceleration response for the vehicle traveling at a speed of 80 km/h over a beam with (a) 20%, and (b) 50% structural damage. The driving frequency and vehicle frequency can be seen unchanged concerning the values from Fig. 5.6 (b). The WPT results for the vehicle acceleration response at 20% structural damage are presented in Fig. 5.10, in

which the WPT coefficients can be seen as separated by the algorithm. Furthermore, the SET results are generated using the WPT coefficients and are shown in Fig. 5.11. The SET results for the 50% structural damage case are shown in Fig. 5.12, and the results from Figs. 5.11 and 5.12 are shown in Table 5.2, in which the bridge frequency pair values, as well as their average values, are shown. The theoretical values for the resonant peaks are shown in brackets in Table 5.2. The structural frequencies change due to structural damage, and the beam frequency pairs can also be seen to have changed in Figs. 5.11 and 5.12. This demonstrates that the proposed methodology is a robust way to successfully identify the bridge and vehicle frequencies in damage cases.

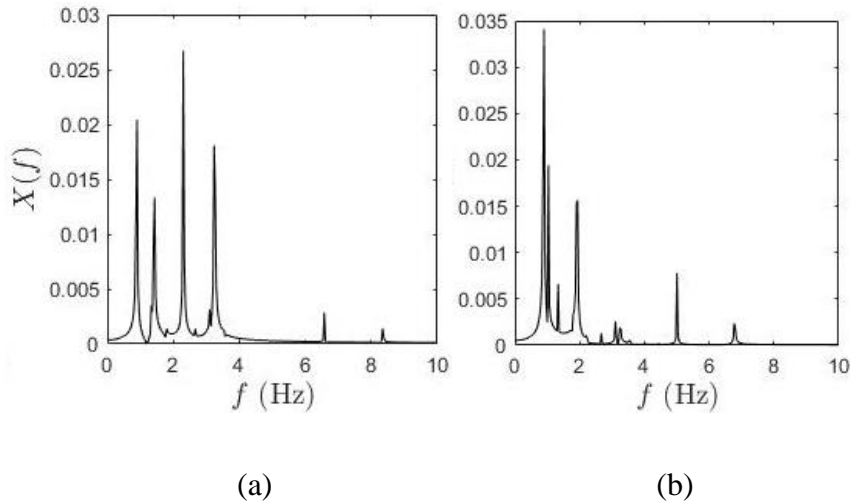


Figure 5.9: Fourier spectra of vehicle acceleration response for vehicle speed of 80 km/h with (a) 20%, and (b) 50% structural damage.

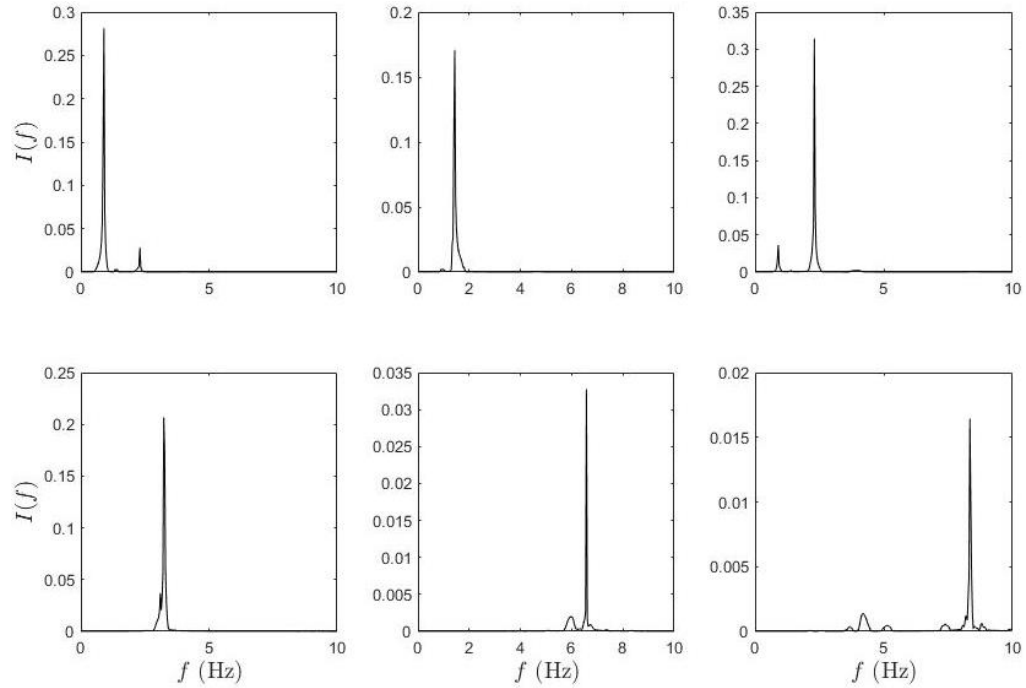


Figure 5.10: WPT coefficients of vehicle acceleration response for vehicle speed of 80 km/h with 20% structural damage.

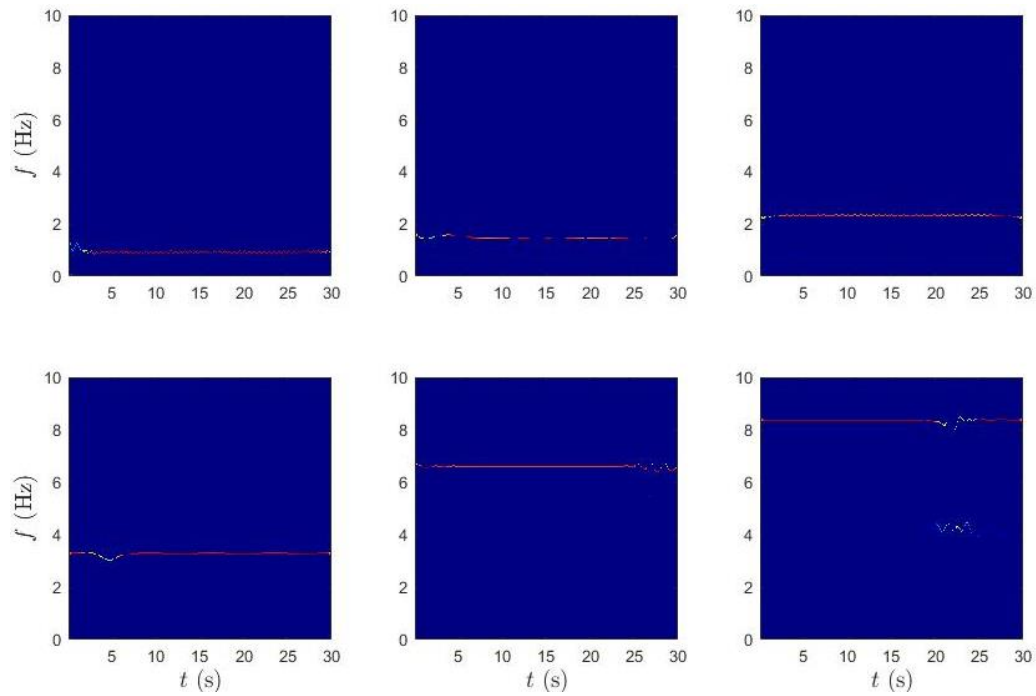


Figure 5.11: SET results of vehicle acceleration response for vehicle speed of 80 km/h with 20% structural damage.

Table 5.2: Frequency values identified for vehicle speed of 80 km/h with different levels of structural damage.

	No damage	20% damage			50% damage		
Mode #	f_b (Hz)	f_b (Hz)	\hat{f} from Fig. 5.11 (Hz)	\hat{f}_b (Hz)	f_b (Hz)	\hat{f} from Fig. 5.12 (Hz)	\hat{f}_b (Hz)
			$f_d = 0.90$ (0.88)			$f_d = 0.90$ (0.88)	
1	2.08	1.86	$f_{b1}^1 = 1.43$ (1.42), $f_{b1}^2 = 2.30$ (2.30)	1.86	1.47	$f_{b1}^1 = 1.03$ (1.03), $f_{b1}^2 = 1.93$ (1.91)	1.48
			$f_v = 3.2$			$f_v = 3.1$	
2	8.33	7.45	$f_{b2}^1 = 6.57$ (6.57), $f_{b2}^2 = 8.34$ (8.33)	7.45	5.89	$f_{b2}^1 = 5.01$ (5.01), $f_{b2}^2 = 6.77$ (6.77)	5.89

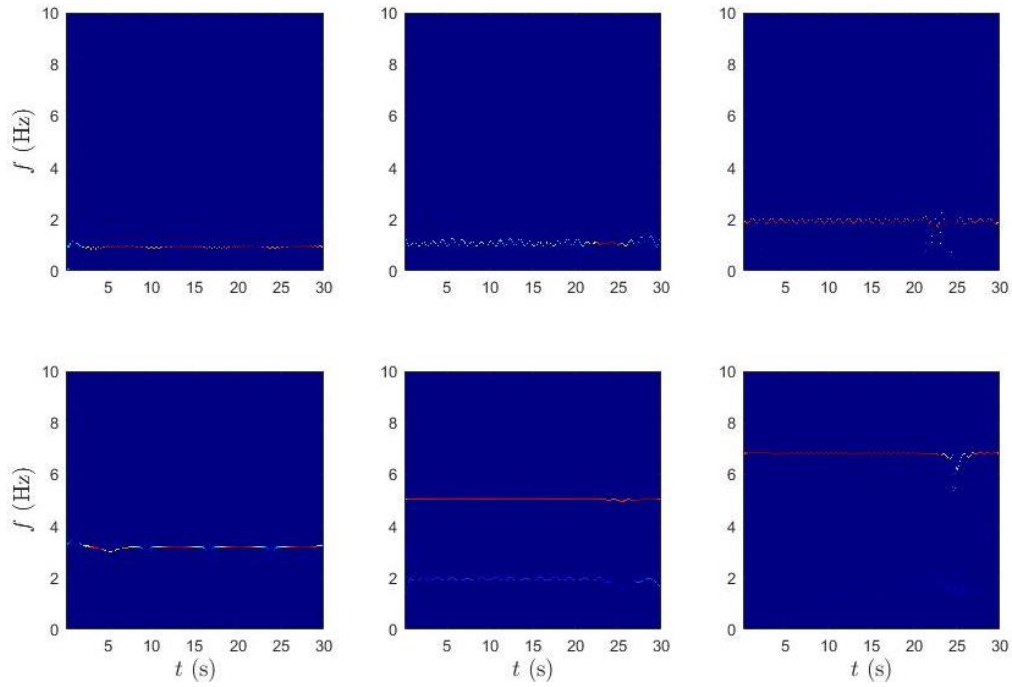


Figure 5.12: SET results of vehicle acceleration response for vehicle speed of 80 km/h with 50% structural damage.

Similarly, the effect of structural damage is shown using the vehicle speed of 40 km/h. Fig. 5.13 shows the Fourier spectra results for (a) 20%, and (b) 50% structural damage while the vehicle is traveling at a speed of 40 km/h. WPT and SET results for 20% structural damage are presented in Figs. 5.14 and 5.15, respectively, and SET results for 50% structural damage are shown in Fig. 5.16. The results for vehicle speed of 40 km/h

are summarized in Table 5.3. The average values of bridge frequencies, \hat{f}_b , calculated using the proposed method are identical with the theoretical values of bridge frequencies f_b . This shows that the proposed method can detect the bridge frequencies using a passing vehicle in the presence of structural damage to the model.

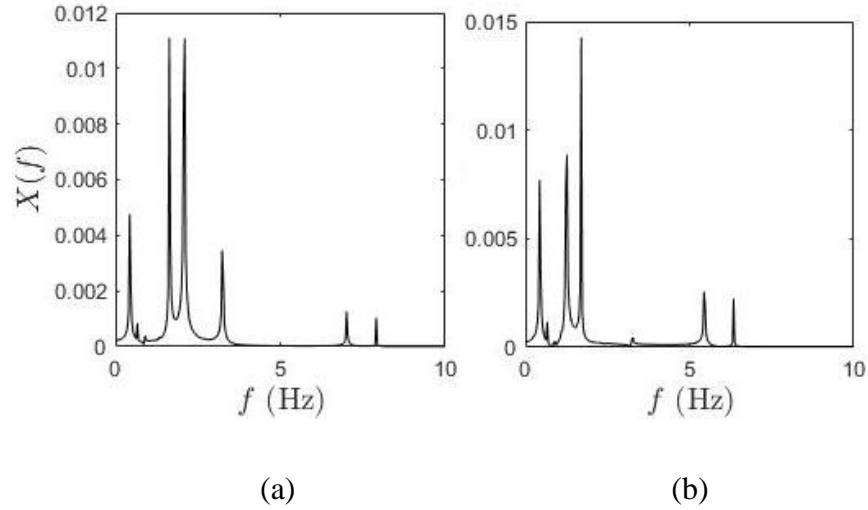


Figure 5.13: Fourier spectra of vehicle acceleration response for vehicle speed of 40 km/h with (a) 20%, and (b) 50% structural damage.

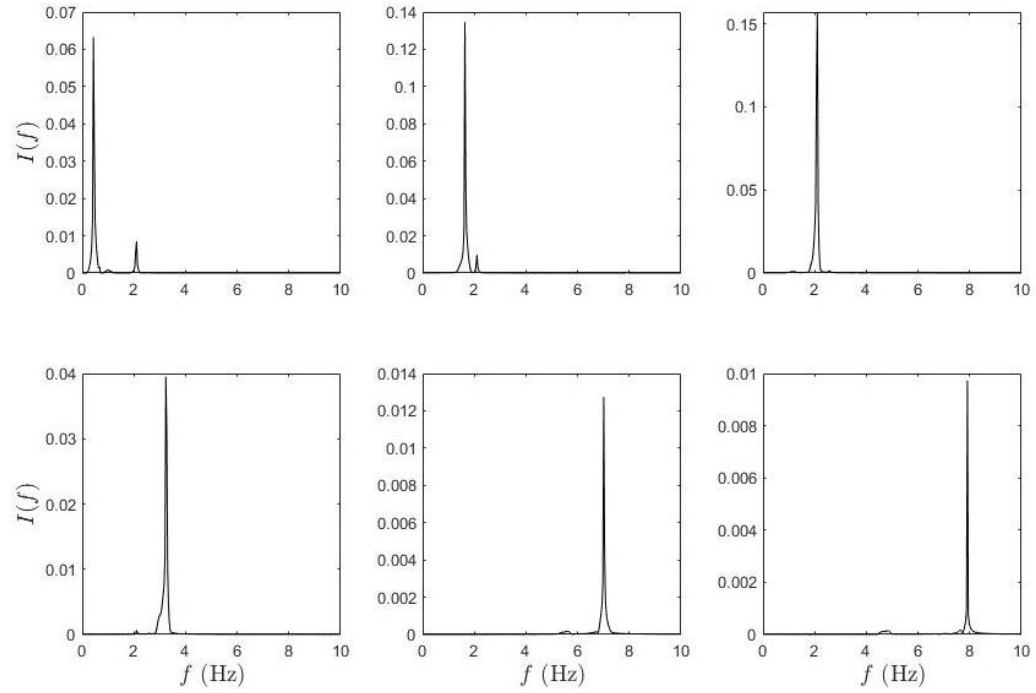


Figure 5.14: WPT coefficients of vehicle acceleration response for vehicle speed of 40 km/h with 20% structural damage.

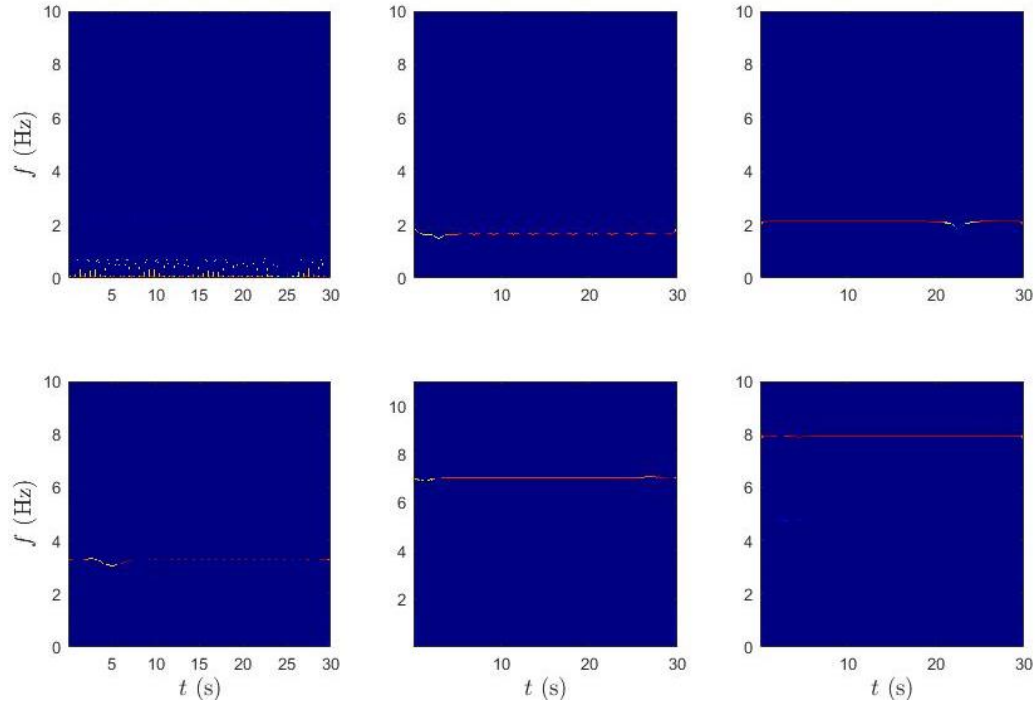


Figure 5.15: SET results of vehicle acceleration response for vehicle speed of 40 km/h with 20% structural damage.

Table 5.3: Frequency values identified for vehicle speed of 40 km/h with different levels of structural damage.

	No damage	20% damage			50% damage		
Mode #	f_b (Hz)	f_b (Hz)	\hat{f} from Fig. 5.15 (Hz)	\hat{f}_b (Hz)	f_b (Hz)	\hat{f} from Fig. 5.16 (Hz)	\hat{f}_b (Hz)
			$f_d = 0.43$ (0.44)			$f_d = 0.43$ (0.44)	
1	2.08	1.86	$f_{b1}^1 = 1.67$ (1.64), $f_{b1}^2 = 2.10$ (2.08)	1.86	1.47	$f_{b1}^1 = 1.27$ (1.25), $f_{b1}^2 = 1.70$ (1.69)	1.48
			$f_v = 3.2$			$f_v = 3.2$	
2	8.33	7.45	$f_{b2}^1 = 7.00$ (7.01), $f_{b2}^2 = 7.91$ (7.89)	7.46	5.89	$f_{b2}^1 = 5.44$ (5.45), $f_{b2}^2 = 6.34$ (6.33)	5.89

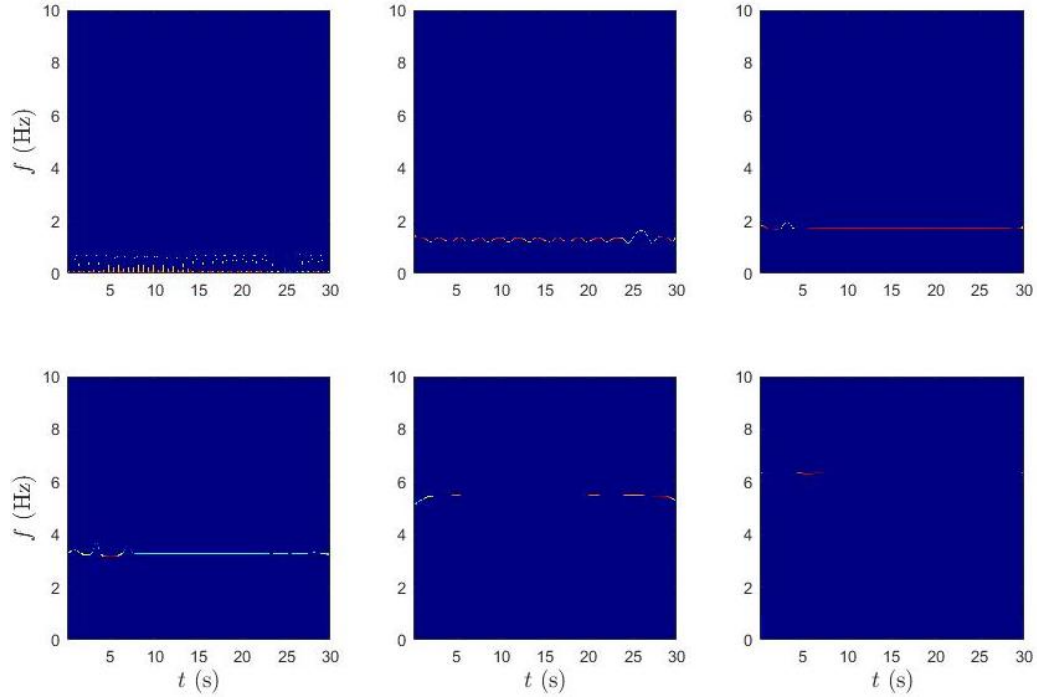


Figure 5.16: SET results of vehicle acceleration response for vehicle speed of 40 km/h with 50% structural damage.

5.4.4 Effect of measurement noise

In this section, the effect of background noise and road roughness is studied by introducing measurement noise in the simulated vehicle acceleration response. The vehicle speed is kept at 80 km/h, and measurement noise is added to the vehicle acceleration response. Figs. 5.17 and 5.18 show the SET results for 10% and 20% measurement noise, respectively, added to the vehicle acceleration response. SET results are generated using the WPT coefficients obtained from the simulated noisy vehicle response. SET results clearly show the profiles of the individual frequency components for the duration of the test. The identification results from Figs. 5.17 and 5.18 are summarized in Table 5.4. In addition, the effect of measurement noise on the performance of the proposed methodology is investigated using a lower vehicle speed of 40 km/h, and the results are summarized in Table 5.5. By comparing Table 5.1 with Tables 5.4 and 5.5, it may be observed that the frequency pairs have a slight deviation from initial values in the case of 20% measurement noise compared to 10% measurement noise, however, the averaged value of the frequency pairs remained unaffected in both

cases. This provides evidence that the proposed method can be used to identify the individual frequency components regardless of the background measurement noise in vehicle response due to the denoising capability of WPT.

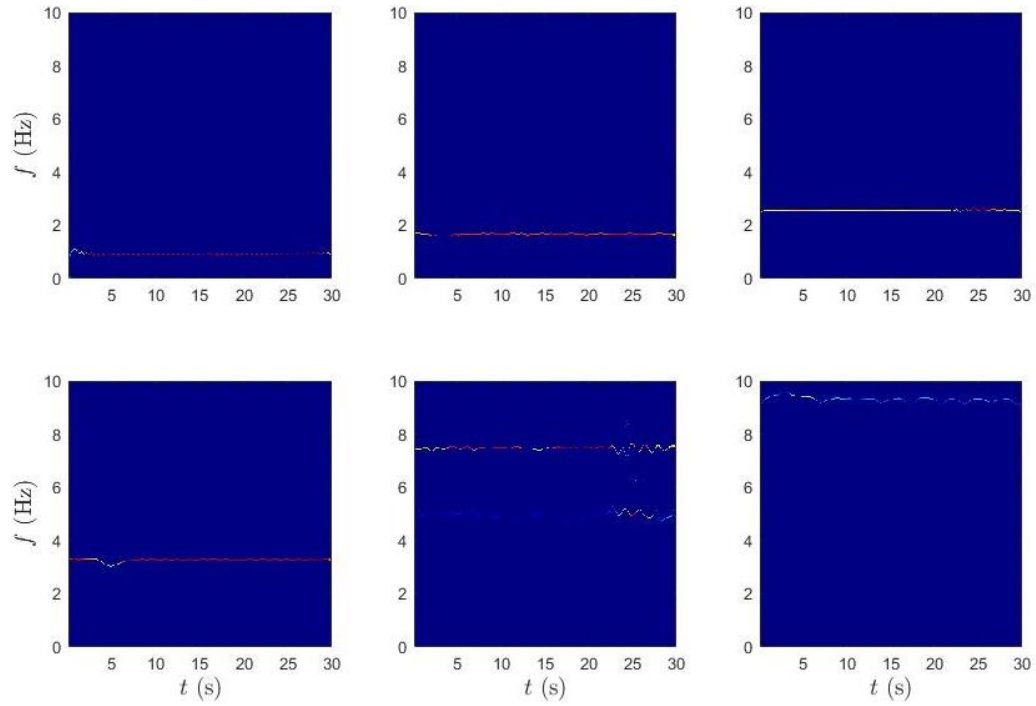


Figure 5.17: SET results of vehicle acceleration response with 10% measurement noise.

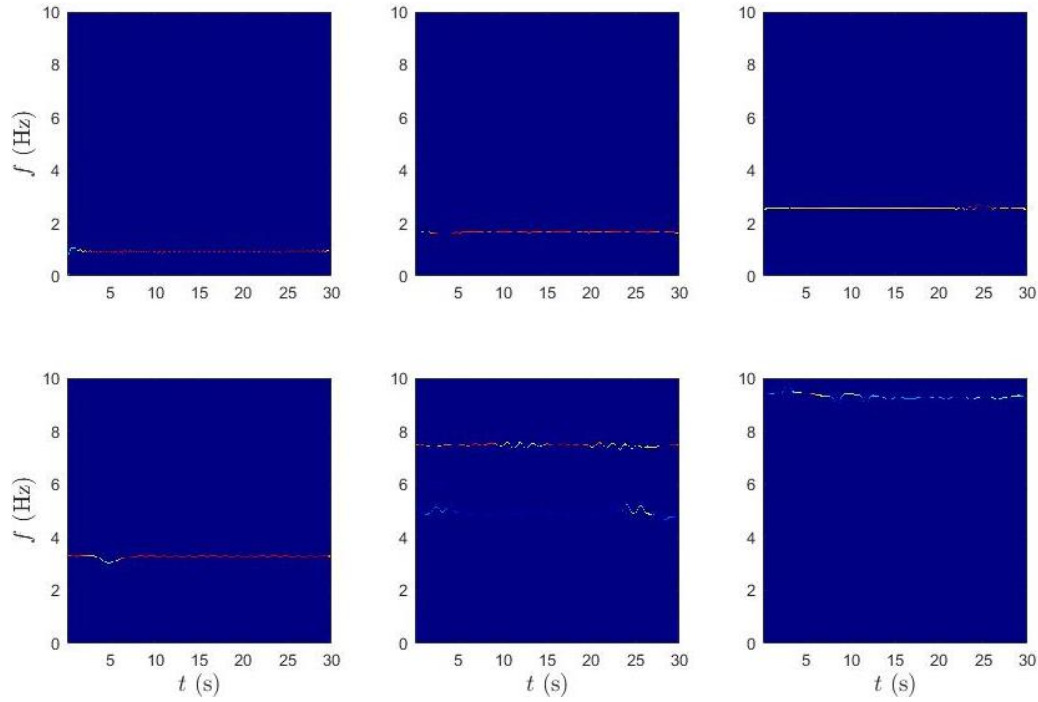


Figure 5.18: SET results of vehicle acceleration response with 20% measurement noise.

Table 5.4: Frequency values identified for vehicle speed of 80 km/h with different levels of measurement noise.

Mode #	f_b (Hz)	10% noise		20% noise	
		\hat{f} from Fig. 5.17 (Hz)	\hat{f}_b (Hz)	\hat{f} from Fig. 5.18 (Hz)	\hat{f}_b (Hz)
		$f_d = 0.90$ (0.88)		$f_d = 0.90$ (0.88)	
1	2.08	$f_{b1}^1 = 1.63$ (1.64), $f_{b1}^2 = 2.53$ (2.52)	2.08	$f_{b1}^1 = 1.62$ (1.64) $f_{b1}^2 = 2.54$ (2.52)	2.08
		$f_v = 3.2$		$f_v = 3.2$	
2	8.33	$f_{b2}^1 = 7.44$ (7.45), $f_{b2}^2 = 9.24$ (9.21)	8.34	$f_{b2}^1 = 7.42$ (7.45), $f_{b2}^2 = 9.26$ (9.21)	8.34

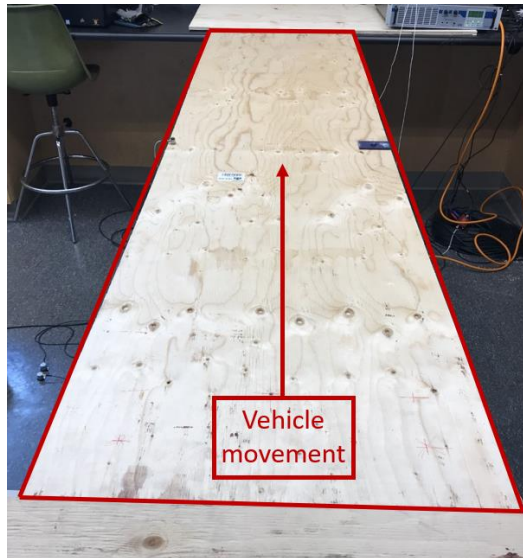
Table 5.5: Frequency values identified for vehicle speed of 40 km/h with different levels of measurement noise.

Mode #	f_b (Hz)	10% noise		20% noise	
		\hat{f} (Hz)	\hat{f}_b (Hz)	\hat{f} (Hz)	\hat{f}_b (Hz)
		$f_d = 0.43$ (0.44)		$f_d = 0.43$ (0.44)	
1	2.08	$f_{b1}^1 = 1.86$ (1.86), $f_{b1}^2 = 2.30$ (2.30)	2.08	$f_{b1}^1 = 1.86$ (1.86) $f_{b1}^2 = 2.30$ (2.30)	2.08
		$f_v = 3.2$		$f_v = 3.2$	

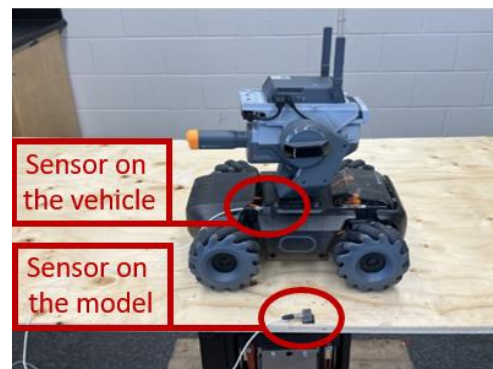
2	8.33	$f_{b2}^1 = 7.91 (7.89),$ $f_{b2}^2 = 8.77 (8.77)$	8.34	$f_{b2}^1 = 7.92 (7.89),$ $f_{b2}^2 = 8.76 (8.77)$	8.34
---	------	---	------	---	------

5.5 Experimental Validation

A scaled VBI model is built to investigate the viability of the proposed iBHM method. The bridge model used in the laboratory experiment is a 2.4 m simply supported wooden beam shown in Fig. 5.19 (a). The model is instrumented with an accelerometer at the mid-span to collect the bridge response. The parameters for the bridge model are shown in Table 5.6. A two-axle vehicle, shown in Fig. 5.19 (b), is selected to travel along the bridge at a speed of 2 m/s. The vehicle is remotely controlled using a smartphone during its multiple passages over the bridge model. The weight of the vehicle is approximately 3.3 kg, and the weight of the wooden beam is approximately 8 kg. The bridge model to vehicle weight ratio is 2.4. An accelerometer is mounted on the vehicle between the two axles to collect the vibration response of the vehicle, as presented in Fig. 5.19 (b). A sampling frequency of 200 Hz is used for both sensors (on bridge and vehicle) used in this experiment. The bridge is subjected to forced vibrations using a shake table shown in Fig. 5.20, where a zero-mean white Gaussian noise is used to mimic the ambient vibrations and traffic-induced vibration of a bridge.



(a)



(b)

Figure 5.19: (a) Simply supported wooden beam, and (b) two-axle vehicle model.

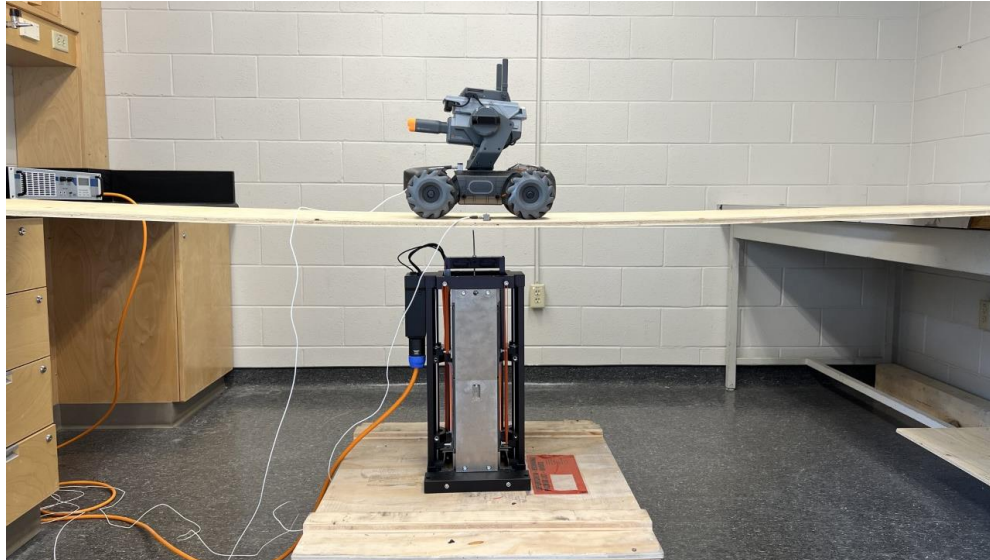


Figure 5.20: Simply supported wooden beam subjected to measurement noise excitation.

Table 5.6: Properties of the scaled bridge model.

Width (m)	Length (m)	Thickness (mm)	\bar{m} (kg/m)	f_{b1} (Hz)	f_{b2} (Hz)
0.6	2.4	12.7	3.34	4.78	9.74

Figs. 5.21 (a) and (b) show the time history and Fourier spectra of the vehicle acceleration response, respectively. In Fig. 5.21 (b), several resonant peaks can be seen, and the signal is analyzed using WPT. Figs. 5.22 and 5.23 show the WPT coefficients and SET results, respectively, resulting from the vehicle acceleration response. The individual frequency components are well-separated by the WPT algorithm and can be easily identified as the f_b pairs. The first two plots in Fig. 5.23 show the f_{b1} pair, and the last plot shows f_{b2} . The identification results are summarized in Table 5.7.

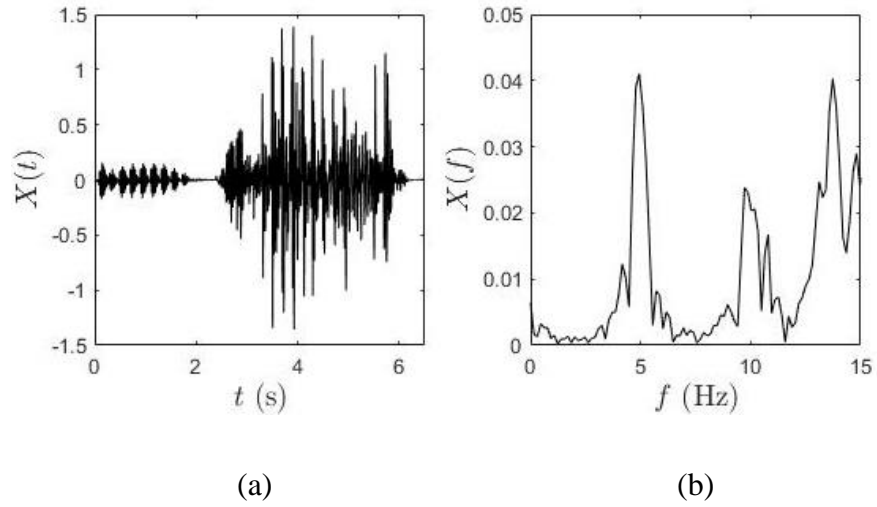


Figure 5.21: (a) Time history, and (b) Fourier spectra of vehicle acceleration response.

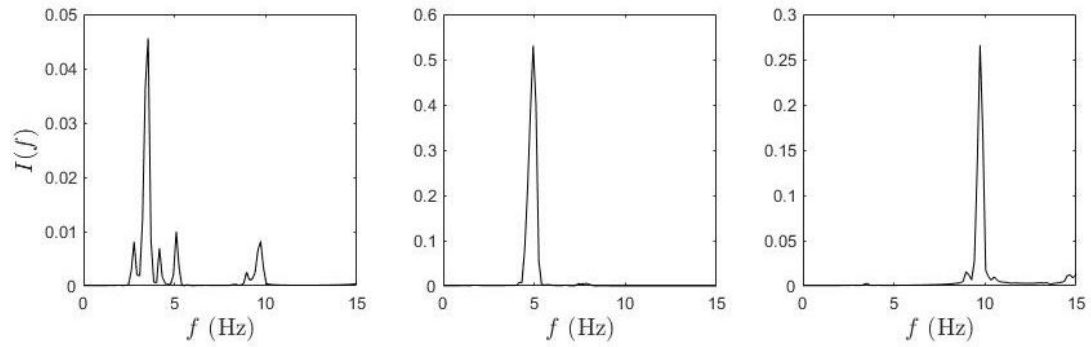


Figure 5.22: WPT coefficients of vehicle acceleration response.

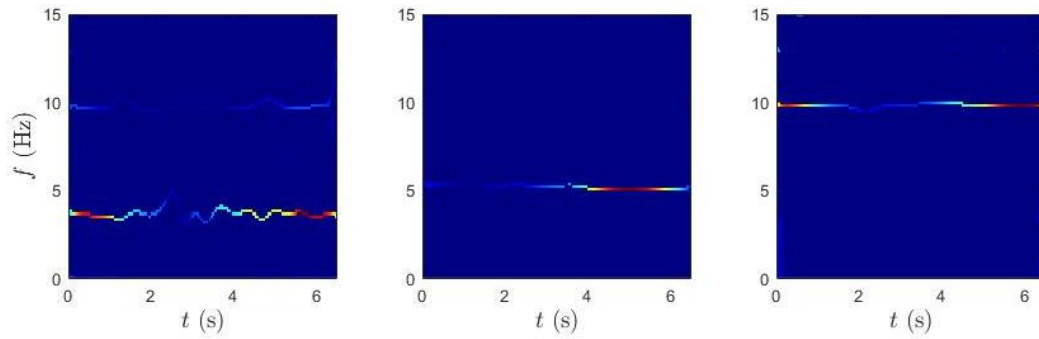


Figure 5.23: SET results of vehicle acceleration response.

Table 5.7: Frequency values identified from the scaled VBI model.

Mode #	f_b (Hz)	\hat{f} from Fig. 5.23 (Hz)	\hat{f}_b (Hz)
--------	------------	-------------------------------	------------------

1	4.78	4.03, 5.03	4.53
2	9.74	9.85	9.85

5.6 Full-Scale Validation

The proposed method is validated using a full-scale bridge and a passing vehicle in this section.

5.6.1 Details of full-scale study

The bridge used for the full-scale study is a five-span continuous box-girder bridge located in London, Ontario, Canada, as shown in Fig. 5.24. The bridge has a total length of 220 m, with outer spans of 36.5 m and three inner spans of 49 m. There are four lanes on this bridge, with two serving the traffic flow in each direction. In this study, the bridge is used for direct monitoring by installing the sensors directly onto the bridge deck, and indirect monitoring by using a vehicle scanning over it. The bridge remains operational for the duration of testing to enhance the amplitude of bridge vibrations and collect quality data. Direct monitoring of the bridge is carried out using the data acquisition (DAQ) system shown in Fig. 5.25 (a) and nine accelerometers, one of which can be seen in Fig. 5.25 (b).

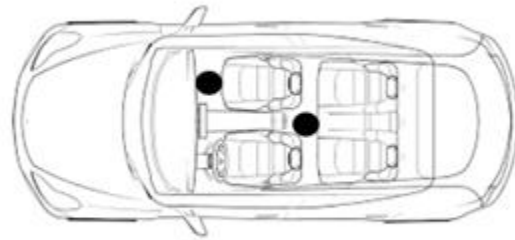


Figure 5.24: Five-span continuous box-girder bridge.



Figure 5.25: (a) Data acquisition system, and (b) contact sensor instrumented on the bridge.

The vibration testing of the bridge includes several data collection intervals ranging from several minutes under the impact of ongoing traffic, which included vehicles such as sedans, pick-up trucks, buses, heavy trucks, etc., traveling at an average speed of 60 km/h. A sampling frequency of 200 Hz was used to measure the bridge as well as vehicle response. While undertaking iBHM, a hatchback car (Hyundai Elantra), as shown in Fig. 5.26 (a) is considered. The plan view of the sensor arrangement used for the test vehicle is presented in Fig. 5.26 (b). The black dots in Fig. 5.26 (b) represent the sensors used to collect the vibration data, which are fixed to the floor of the vehicle. The accelerometers are instrumented on the front passenger side, as shown in Fig. 5.26 (c), and in the back of the test vehicle, as shown in Fig. 5.26 (d).



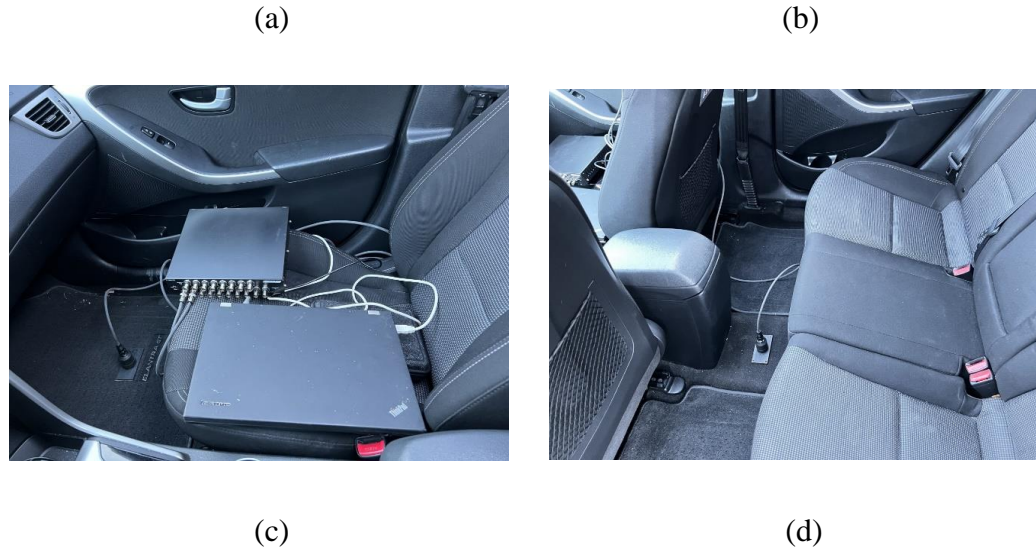


Figure 5.26: (a) Test vehicle, (b) plan view of sensor arrangement, sensor instrumentation in the (c) front, and (d) back of the test vehicle.

The data from direct BHM serves as a reference for the comparison of iBHM. Before conducting iBHM using the test vehicle, a few calibration tests are performed to acquire dynamic information about the engine noise and suspension system of the vehicle. Upon conducting a few tests of the stationary vehicle in ignition mode, the two modes of engine noise are recorded as 5.4 Hz and 10.9 Hz. The contribution of vehicle suspension is identified by performing several trial runs over a bump. The tests conclude that the frequency due to vehicle suspension is 1.65 Hz. After conducting these preliminary tests, the iBHM data is collected using the test vehicle traveling over the bridge at a speed of 60 km/h in the presence of regular traffic. To follow the traffic constraints and avoid the traffic impediment, only the vehicle speed of 60 km/h was followed. Moreover, the speed limit of 60 km/h is widely used on most arterial and collector roads.

5.6.2 Identification results

Data collected by one of the sensors instrumented on the midspan of the bridge is shown in Fig. 5.27. The time history of acceleration response and its Fourier spectra are shown in Figs. 5.27 (a) and (b), respectively. The outcome of the WPT analysis is shown in Fig. 5.28. All the resonant peaks from Fig. 5.27 (b) are well separated by the WPT algorithm. From Fig. 5.28, three bridge frequencies can be identified as 2.8 Hz, 6.4 Hz, and 13.0 Hz.

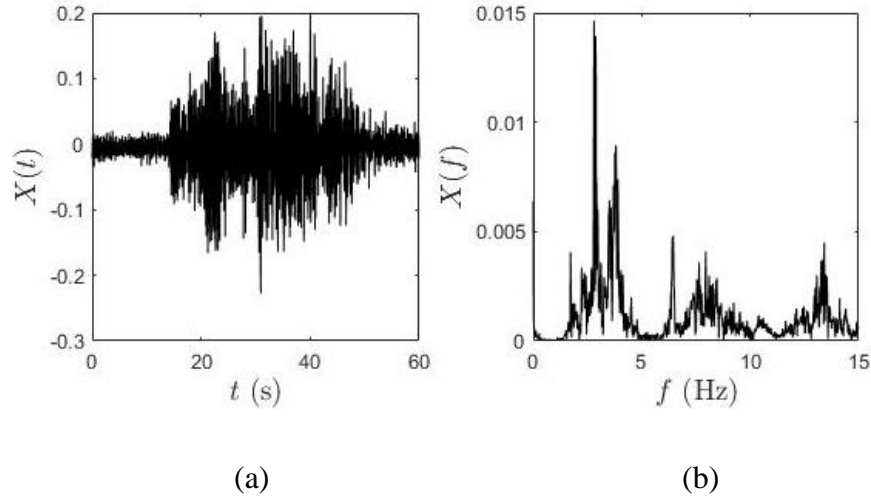


Figure 5.27: (a) Time history, and (b) Fourier spectra of bridge acceleration response.

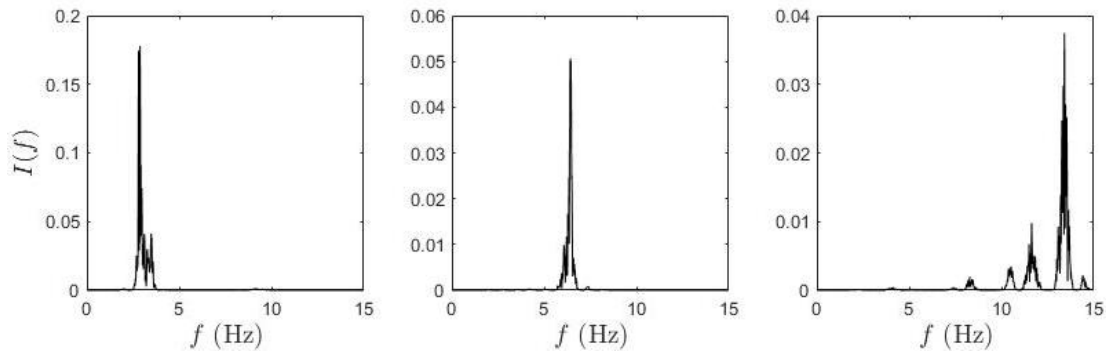


Figure 5.28: WPT coefficients of bridge acceleration response.

Figs. 5.29 shows the Fourier spectra of the data collected from (a) the front, and (b) the back of the test vehicle. Furthermore, the SET results for the front sensor vehicle data are provided in Fig. 5.30. The individual components are well separated and include the contributions of bridge frequencies, vehicle engine noise, vehicle suspension, etc. The first column of Fig. 5.30 shows three plots which include frequency components for vehicle suspension (1.65 Hz), the first mode of vehicle engine noise (5.1 Hz), and the second mode of vehicle engine noise (10.1 Hz), respectively. These values are confirmed by the prior results described in the previous paragraph, with a slight difference in frequency due to the ignition mode (i.e., the former one) and steady-state movement of the vehicle. The rest of the two plots in the first row show the first pair of natural bridge frequencies (2.5 Hz and 2.7 Hz), which average out to be 2.6 Hz. In the second row of

Fig. 5.30, the second and third plots show the pair (6.3 Hz and 7.1 Hz) of the second natural bridge frequency, and their mean value is 6.7 Hz. The last two plots in the third row of Fig. 5.30 show the pair (12.6 Hz and 13.0 Hz) of the third natural bridge frequency, which results in 12.8 Hz as the average value. A comparison of direct and iBHM data is provided in Table 5.8, and SET results for the sensor in the back of the test vehicle are shown in Fig. 5.31.

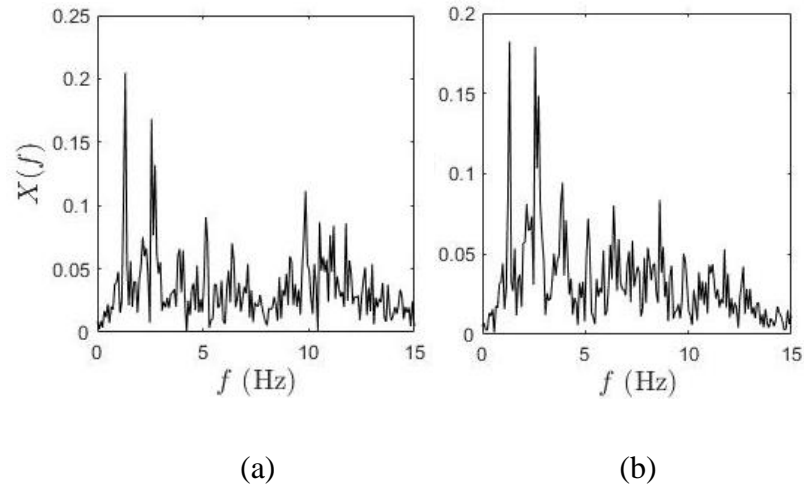


Figure 5.29: Fourier spectra of test vehicle acceleration response from (a) front sensor, and (b) back sensor.

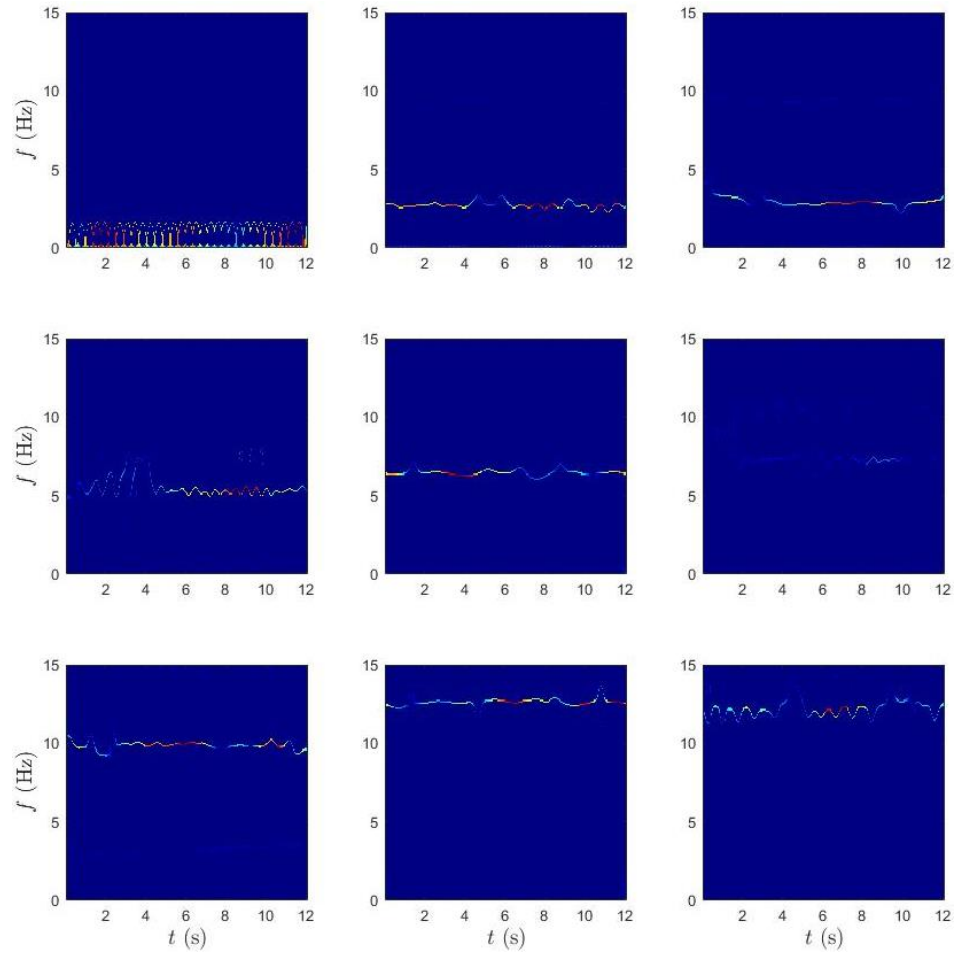


Figure 5.30: SET results of test vehicle acceleration response from the front sensor.

Table 5.8: Frequency values identified from direct and indirect BHM results.

Mode #	Direct BHM	iBHM	
	\hat{f}_b from Fig. 5.28 (Hz)	\hat{f}_b from Fig. 5.30 (Hz)	\hat{f}_b (Hz)
1	2.8	$f_v = 1.65$	2.6
		$f_{b1}^1 = 2.5,$	
		$f_{b1}^2 = 2.7$	
2	6.4	$f_v = 5.1$	6.7
		$f_{b2}^1 = 6.3,$	
		$f_{b2}^2 = 7.1$	
3	13.0	$f_v = 10.1$	12.8
		$f_{b3}^1 = 12.6,$	
		$f_{b3}^2 = 13.0$	

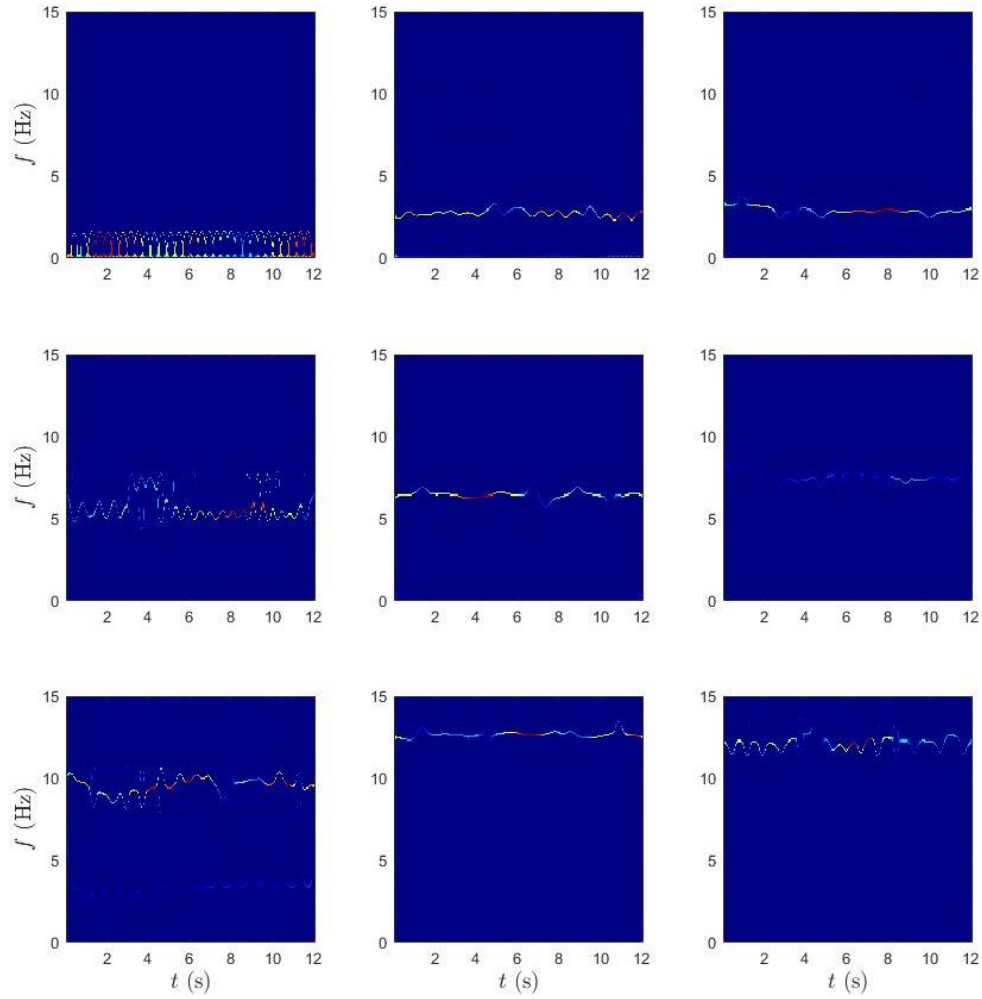


Figure 5.31: SET results of test vehicle acceleration response from the back sensor.

5.7 Summary

This chapter proposed a methodology to extract the modal frequencies of a bridge using iBHM. Apart from the numerical and experimental investigation, a real-life application of drive-by monitoring is used to demonstrate the proposed framework. The data originating from an instrumented vehicle traveling over the bridge contains dynamic vibrations of the bridge, vehicle suspension, engine vibration, and measurement noise due to ambient traffic. The proposed algorithm can accurately detect the modal parameters by using a single sensor instrumented on the test vehicle. This method has the potential to significantly reduce the economic footprint of bridge monitoring. The proposed method

can be enhanced with the application of smartphones to extract the bridge modal parameters.

Chapter 6

6 Vehicle Scanning Method Based on Contact Point Response

This chapter features a vehicle scanning method capable of extracting bridge modal parameters using the contact point (CP) response of a passing vehicle. In the numerical study, the feasibility of the application of Robust Empirical Mode Decomposition (REMD) to the CP response is verified using various parameters such as vehicle speed, measurement noise, and structural damage. The proposed method can detect the changes in bridge frequencies due to changes in the parameters of the numerical study. A comparison of the proposed approach is provided with the direct monitoring approach using data from a full-scale bridge.

6.1 Introduction

In general, indirect bridge health monitoring (iBHM) is the practice of using vibration data collected using the sensors placed in the moving test vehicle traveling over the bridge to detect structural damage. The collected data includes the dynamic response of the bridge accompanied by the vehicle suspension input and road roughness. Bridge frequencies estimated from vehicle acceleration data can be used as indicators for bridge health. This method aims to continuously monitor bridges in a more efficient, economical, and less labor-intensive way than conventional BHM methods.

To deal with high-speed vehicles and bridges with short characteristic lengths, Jin *et al.* (2022) established a subspace identification method. The feasibility of a multivariable output error state space model for bridge frequency estimation was tested using two traverses over the target bridge. The study employed the use of a single-value decomposition-based pseudo-inverse algorithm to account for the time-varying nature of the vehicle-bridge system. The results from numerical experiments demonstrated that the proposed approach successfully identified the bridge frequencies in the presence of high vehicle speed and high road surface roughness. Analysis of iBHM vibration data requires a powerful decoupling framework due to the presence of sensor-vehicle-bridge

interactions. Variabilities due to some operational and environmental factors need to be addressed to ensure the accuracy of iBHM. Operational and environmental parameters such as road roughness, vehicle speed, traffic, and temperature have been shown to shift the bridge frequencies such that accurate damage detection becomes very difficult (Yang *et al.* 2013). One challenge with the iBHM method is the presence of vehicle frequency that can render the estimation of bridge frequencies difficult especially when coupled with road surface roughness. To resolve this problem, the response of the vehicle's CP was proposed as a better method for scanning bridge dynamics.

Corbally and Malekjafrian (2021) derived an expression for CP response to be inferred directly from vehicle responses. The study examined the response at the point of contact between the tire and the bridge as a means of monitoring bridge frequency. The proposed approach could successfully identify the bridge frequencies and any changes caused by bridge damage without being affected by vehicle frequencies. The closed-form solutions for vehicle and CP responses were derived by Xu *et al.* (2021). Since the CP response was free from vehicle frequency, it enabled the extraction of more bridge frequencies. Numerical simulations and field tests confirmed that the performance of the CP response was better than that of the vehicle response. The study also confirmed that the adverse effect of surface roughness could be outbalanced by the positive effect of ongoing traffic. A data-driven approach based on Artificial Neural Network (ANN) was proposed by Corbally and Malekjafarian (2022). The proposed algorithm was trained to predict bridge behavior using vehicle responses. CP response calculated from vehicle response was fed into the ANN along with the vehicle speed. A structural damage indicator was also proposed by training the ANN to recognize the influence of temperature on the vehicle response.

The coupled problem of vehicle bridge interaction (VBI) in CP response, as the vehicle travels over the bridge and the signals are recorded from the passing vehicle, is non-stationary. In addition, the presence of measurement noise in the nonstationary CP response yields significant inaccuracy in iBHM subjected to various vehicle speeds and the extent of the structural damage. This current challenge of CP-based iBHM is resolved in this chapter using a novel time-frequency decomposition method. In this study, REMD

is used to analyze the CP response. REMD is powered by a soft sifting stopping criterion (SSSC) which can adaptively stop the sifting process for EMD. EMD and its variants such as Ensemble EMD (EEMD), REMD, and Time-Varying Filter-EMD (TVF-EMD), are analyzed to determine their suitability for signal decomposition of CP response in this study. However, by comparing the computational processing time required to use these variants (Barbosh *et al.* 2020), an optimized method, REMD, is selected due to its least computational processing time. A numerical study is used to validate the proposed method of using REMD to analyze the CP response. In the numerical study, the effect of parameters such as vehicle speed, measurement noise, and structural damage on the performance of the proposed method is studied. A full-scale study is also conducted to show the in-field application of the proposed method. The vehicle responses collected from the test vehicle are processed to obtain the CP response, and REMD is used to analyze the CP response.

After a brief introduction and literature review of iBHM, and CP response, governing equations of CP response and REMD are provided in section 6.2. Following the background section, the proposed methodology is explained in section 6.3. The details and results of the numerical simulation and full-scale experimental studies are summarized in sections 6.4, and 6.5, respectively, followed by a summary in section 6.6.

6.2 Background

In this section, a brief background of CP response and REMD is discussed.

6.2.1 Contact point response

In this section, the analytical formulation of the moving test vehicle and its CP with the bridge is illustrated. A simply supported beam is used in this analysis to obtain closed-form solutions. Fig. 6.1 shows the model used for this study as a simply supported bridge subjected to a test vehicle moving at speed v . The vehicle is modeled as a quarter car or single degree-of-freedom sprung mass m_v supported with a spring of stiffness k_v . The bridge is assumed to be a uniform Euler-Bernoulli beam of length L , flexural rigidity EI , and mass per unit length m . In this analytical formulation, there is a significant assumption that the vehicle mass is negligible compared with the bridge mass. Another

important point in the formulation is to keep the vehicle speed as constant as possible, which is also followed in numerical and full-scale studies.

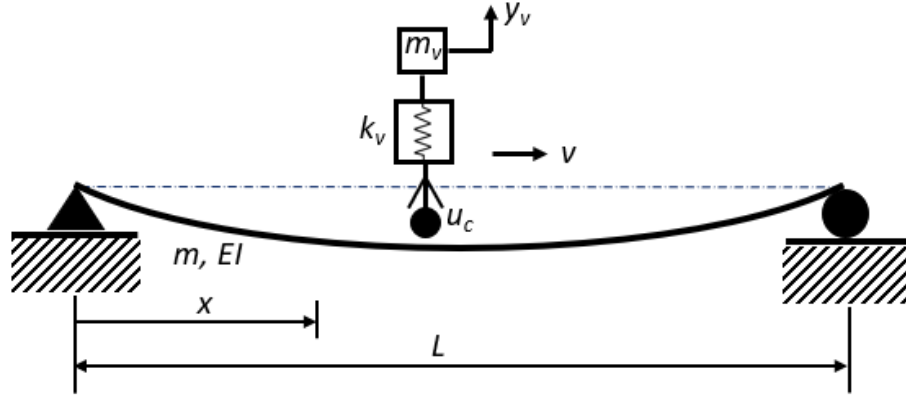


Figure 6.1: Schematic of the vehicle traveling along a simply supported beam.

The CP displacement can be written as (Xu *et al.* 2021):

$$u_c(t) = \sum_n \frac{\Delta_{stn}}{1 - S_n^2} \left(\sin \frac{n\pi vt}{L} - S_n \sin \omega_{b,n} t \right) \sin \frac{n\pi vt}{L} . \quad (6.1)$$

The CP acceleration $\ddot{u}_c(t)$ can be determined using twice differentiation:

$$\ddot{u}_c(t) = \sum_n \frac{\Delta_{stn}}{2(1 - S_n^2)} \left(\omega_{d,n}^2 \cos \omega_{d,n} t + S_n \omega_{bl,n}^2 \cos \omega_{bl,n} t - S_n \omega_{br,n}^2 \cos \omega_{br,n} t \right), \quad (6.2)$$

where $\Delta_{st,n}$ is the n -th modal static deflection, S_n the speed parameter, and $\omega_{b,n}$ is the n th bridge frequency:

$$\Delta_{st,n} = -\frac{2m_v g L^3}{EI n^4 \pi^4} , \quad (6.3)$$

$$S_n = -\frac{n\pi v}{L\omega_{b,n}} , \quad (6.4)$$

$$\omega_{b,n} = \frac{n^2 \pi^2}{L^2} \sqrt{\frac{EI}{m}} , \quad (6.5)$$

and $\omega_{d,n}$ is the driving frequency, $\omega_{bl,n}$ and $\omega_{br,n}$ are two shifted bridge frequencies:

$$\omega_{d,n} = \frac{2n\pi v}{L} , \quad (6.6)$$

$$\omega_{bl,n} = \omega_{b,n} - \frac{n\pi v}{L} , \quad (6.7)$$

$$\omega_{br,n} = \omega_{b,n} + \frac{n\pi v}{L} . \quad (6.8)$$

To analyze data from the full-scale study, the CP response is calculated using the vehicle response. The CP acceleration \ddot{u}_c can be related to vehicle acceleration \ddot{y}_v by (Yang *et al.* 2020b):

$$\ddot{u}_c = \ddot{y}_v + \frac{d^2 \ddot{y}_v}{\omega_v^2 dt^2} , \quad (6.9)$$

where ω_v is the vehicle frequency. The term $d^2 \ddot{y}_v / dt^2$ can be replaced with the central difference, as the accelerations recorded by the vehicle are discrete data:

$$\frac{d^2 \ddot{y}_v}{dt^2} = \frac{\ddot{y}_v|_{i+1} - 2\ddot{y}_v|_i + \ddot{y}_v|_{i-1}}{(\Delta t)^2} , \quad (6.10)$$

where i and Δt denote the i th sampling point and sampling interval, respectively.

6.2.2 Robust Empirical Mode Decomposition

A powerful signal processing technique is required to process a complex time-frequency signal that is nonlinear and nonstationary. EMD (Huang *et al.* 1998, Barbosh *et al.* 2020) has been used as a tool which is based on a sifting process that can be used to decompose any complicated dynamic signal into a set of intrinsic mode functions (IMFs) EMD can be applied to the recorded vehicle responses to generate the IMFs and Fast Fourier Transform (FT) can be applied to the IMFs to extract the bridge frequencies. EMD can be used to decompose a discrete-time signal into many mono-component signals. The sifting iteration number in EMD is directly decided by SSSC. This iteration number holds significant importance in the mode-mixing problem. If the iteration number is too small,

it may result in an under-sifting case wherein multiple mono-component signals may appear in a single IMF. If the iteration number is too large, it can result in over-sifting and a large number of computation time increments. The issue of mode mixing hampers the application of EMD (Gao *et al.* 2008, and Xu *et al.* 2019) to complex and coupled signals, such as a signal originating from VBI. Therefore, optimizing the iteration number is crucial to tackling the mode mixing problem. REMD incorporates the implementation of SSSC into the sifting process of EMD. SSSC can monitor the sifting process of separation in the EMD and select the optimal iteration number (Liu *et al.* 2022). The steps for implementation of REMD are as follows (Wu *et al.* 2022):

- (i) Initialize the algorithm: $j=1$, initialize residue $r_o(t) = x(n)$
- (ii) Identify all the local maxima and minima of $r_{j-1}(n)$
- (iii) Evaluate the upper $U_j(n)$ and lower $L_j(n)$ envelope by cubic spline interpolation of local maxima and minima, respectively.
- (iv) Calculate the mean of the envelope as $m_j(n) = \frac{(U_j(n)+L_j(n))}{2}$.
- (v) Take the difference between the data and the mean as the proto-IMF: compute the j th component $h_j(n) = r_{j-1}(n) - m_j(n)$.
- (vi) $h_j(n)$ is processed as $r_{j-1}(t)$. Assume $h_{j0} = h_j(n)$ and $m_{j,k}(n), k = 0, 1 \dots$ Compute $h_{jk}(n) = h_{jk-1}(n) - m_{jk-1}(n)$ until the soft stop criterion is satisfied. The stop criterion is described as:

$$f_{jk} = RMS_{jk} + |EK_{jk}| , \quad (6.11)$$

$$RMS_{jk} = \sqrt{\frac{1}{N_s} \sum_{n=1}^{N_s} (m_{jk}[n])^2} , \quad (6.12)$$

$$EK_{jk} = \frac{\frac{1}{N_s} \sum_{n=1}^{N_s} (m_{jk}[n] - \bar{m}_j)^4}{\left(\frac{1}{N_s} \sum_{n=1}^{N_s} (m_{jk}[n] - \bar{m}_j)^2\right)^2} - 3 , \quad (6.13)$$

where \bar{m}_j is the mean of $m_{jk}[n]$. If it meets: (1) the number of zero points (N_{zp}) and extremal points (N_{ep}) is equal, or the difference between them is less than one; and (2) $f_{k-2} < f_{k-1}$ and $f_{k-1} < f_k$ the sifting process stops and returns the $(k-2)th$ decomposition results. If not, the sifting process does not stop until the iteration number reaches the maximum iteration number.

- (vii) Compute the jth IMF as $IMF_j(t) = h_{j,k}(n)$.
- (viii) Update the residue $r_j(n) = r_{j-1}(n) - IMF_j(n)$.
- (ix) Increase the sifting index j and repeat steps (ii) to (viii). The signal reconstruction process $x(n)$, which involves combining the IMFs formed from the EMD and the residual:

$$x(n) = \sum_{j=1}^N IMF_j(n) + r_N(n) . \quad (6.14)$$

6.3 Proposed Methodology

Based on the Eqs. mentioned in the previous section, the procedural steps of iBHM using CP response from the test vehicle and REMD are shown in Fig. 6.2 (Singh and Sadhu 2023) and are as follows:

- (i) Record the vehicle CP response using the accelerometer sensor placed in the test vehicle, $\ddot{u}_c(t)$. For numerical investigation, the CP acceleration response is simulated using Eq. 6.2.
- (ii) After determining the CP acceleration response, REMD is used to decompose the discrete time signal into a suite of mono-component signals, which involves a sifting process, and an SSC is required to end the sifting process of EMD. The SSSC of REMD can monitor the sifting process of separation in the EMD and can select the optimal iteration number. Therefore, it can help suppress the mode-mixing problem of EMD and provide IMFs corresponding to a mono-component using steps outlined in section 6.2.2.

$$\ddot{u}_c(t) = \sum_{j=1}^N IMF_j(t) + r_N(t) . \quad (15)$$

- (iii) The individual IMFs can be further analyzed to determine the natural frequencies and damping ratio of the bridge.

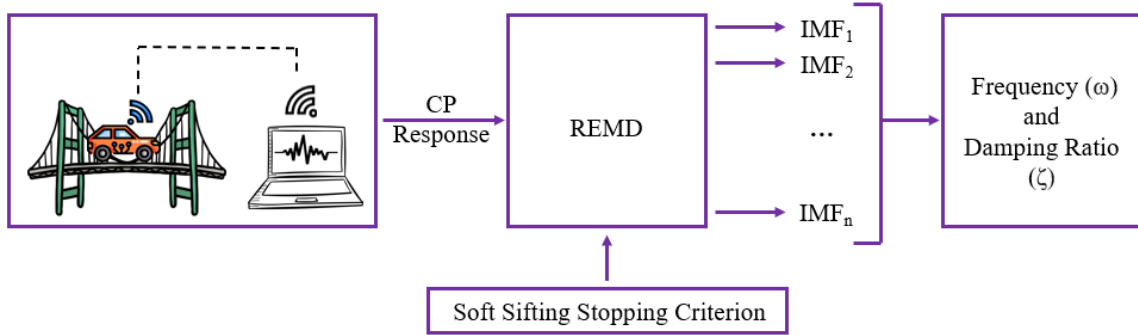


Figure 6.2: Framework of the proposed CP-based BHM method.

6.4 Numerical Validation

In this section, a parametric study is performed to examine the effect of driving velocity, measurement noise, and structural damage on the performance of the proposed methodology. A quarter-car VBI model is adopted, which is shown in Fig. 6.1. The road surface profile is not considered in this study, and the vehicle is assumed to travel at a constant speed. The dynamic interaction between the bridge and the vehicle is modeled

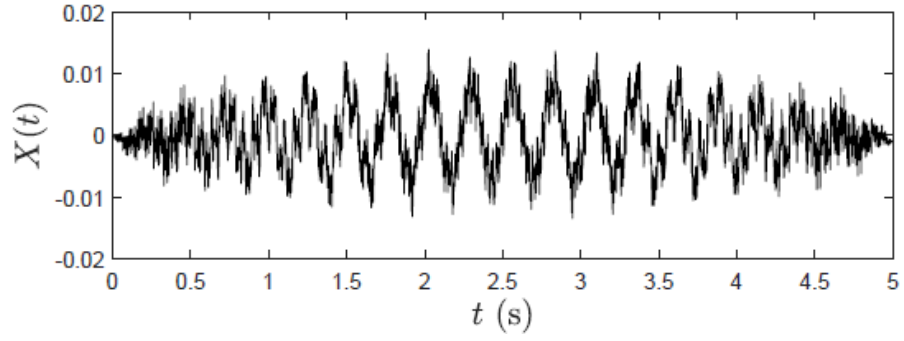
using MATLAB and the properties used are listed in Table 6.1. The bridge is modeled as a simply supported Euler-Bernoulli beam with uniform properties throughout its cross-section. The first three natural frequencies of the bridge are identified as 3.8, 15.22, and 34.24 Hz, respectively. The CP acceleration response is simulated using Eq. 6.2, and subsequently, REMD is applied to the CP response.

Table 6.1: Properties of test vehicle and bridge.

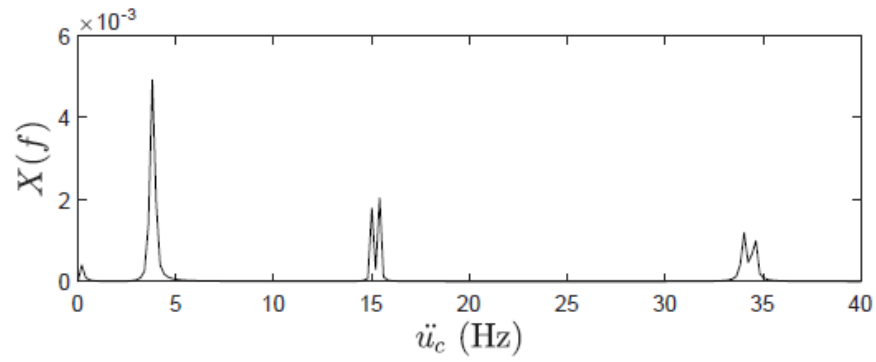
	Property	Value
Vehicle	Mass	$m_v = 900 \text{ kg}$
	Spring Coefficient	$k_v = 1780 \text{ kN/m}$
Bridge	Length	$L = 25 \text{ m}$
	Young's Modulus	$E = 27.5 \text{ GPa}$
	Moment of Inertia	$I = 0.2 \text{ m}^4$
	Mass per unit length	$m = 2400 \text{ kg/m}$

6.4.1 Effect of vehicle speed

Vehicle speed holds an important role in the excitation of the bridge. In this section, the test vehicle is allowed to cross the bridge at two speeds: 18 and 30 km/h. Considering the small length of the bridge model, a relatively low vehicle speed is considered for this study to achieve a significant travel time for the decomposed signal using REMD. All the other properties of the vehicle and bridge are kept, as mentioned in Table 6.1. Fig. 6.3 shows (a) the time history, and (b) the Fourier spectra of the CP response collected from the test vehicle traveling at a speed of 18 km/h. In Fig. 6.3 (b), the bridge natural frequencies can be observed in pairs except for the first natural frequency. This can be attributed to the low magnitude of vehicle speed that is responsible for the frequency pairs. Fig. 6.4 shows the Fourier spectra of the CP response for a vehicle speed of 30 km/h. By comparing Figs. 6.3 (b) and 6.4, it can be observed that the amplitude increases with the increase in vehicle speed as the energy input to the bridge increases with an increase in vehicle speed. Also, all three natural bridge frequencies can be observed in pairs.



(a)



(b)

Figure 6.3: (a) Time history, and (b) Fourier spectra of CP response for vehicle speed of 18 km/h.

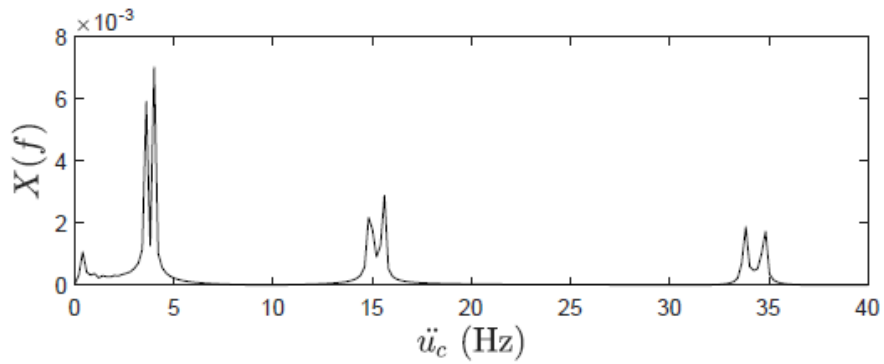


Figure 6.4: Fourier spectra of CP response for vehicle speed of 30 km/h.

The REMD results for the CP responses of two different speeds of 18 and 30 km/h are shown in Figs. 6.5, and 6.6, respectively. With the increase in speed, the shift becomes

clearer as bridge frequencies split into a pair of frequencies. The resonant peaks for three bridge frequencies are well separated using REMD. By observing Figs. 6.5 and 6.6, it is clear that the bridge frequencies can be easily identified because CP response is used in this study instead of vehicle response. Also, the proposed method is capable of separating the closely-spaced frequencies from the CP response, demonstrating the suitability of the proposed method in iBHM.

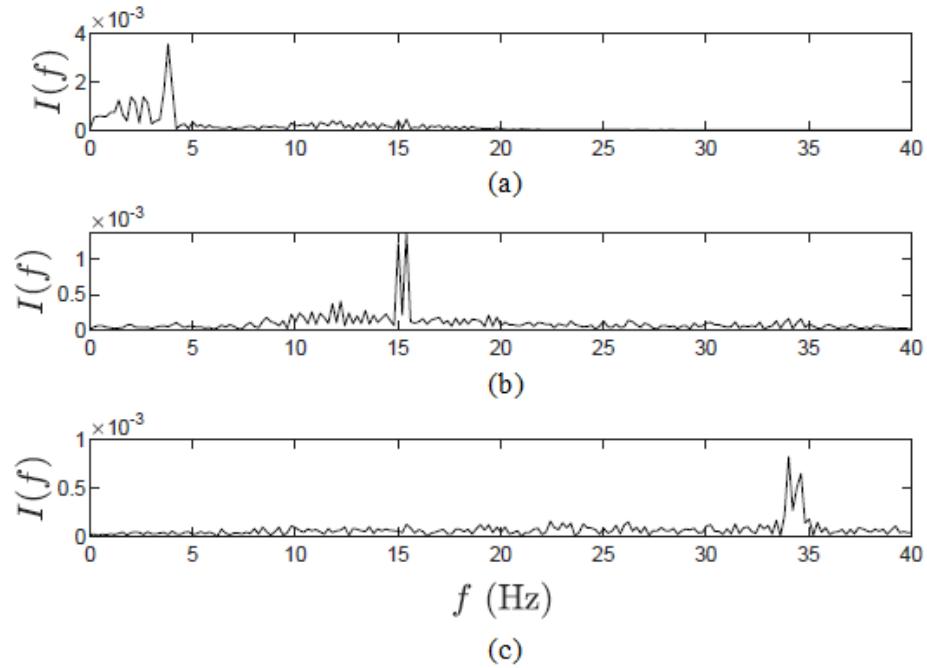


Figure 6.5: REMD results of (a-c) the first, second, and third modes of bridge model obtained from CP response for vehicle speed of 18 km/h.

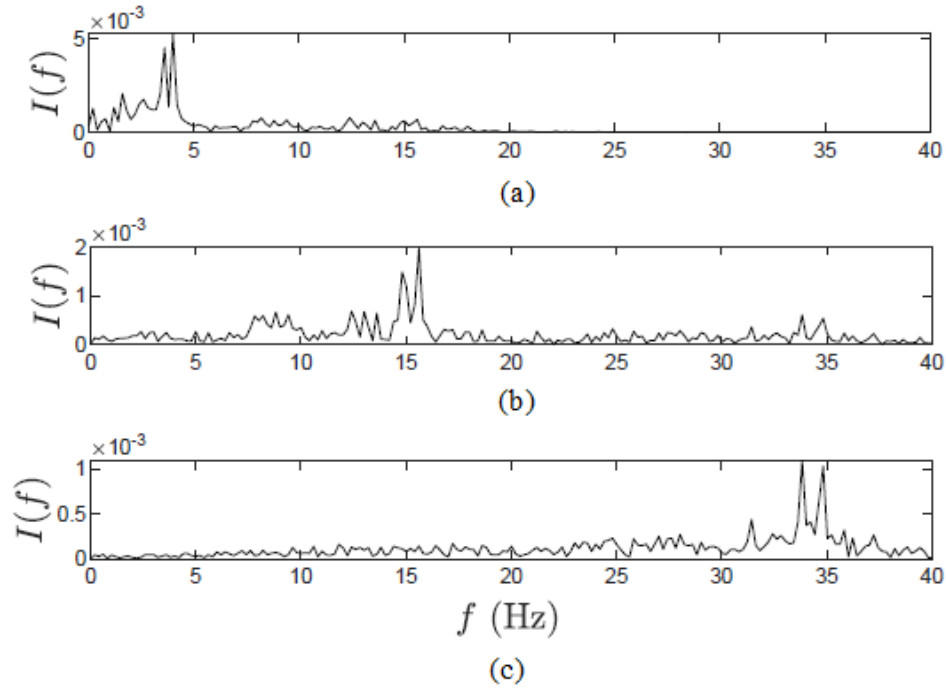


Figure 6.6: REMD results of (a-c) the first, second, and third modes of bridge model obtained from CP response for vehicle speed of 30 km/h.

6.4.2 Effect of measurement noise

In full-scale studies, vehicle responses collected using sensors in the test vehicle are contaminated by measurement noise. To examine the reliability of the proposed method against such interference, the measurement noise of various levels is added to the CP response while keeping the vehicle speed constant at 18 km/h. Figs. 6.7 shows the Fourier spectra of CP response with added 20% measurement noise collected from the test vehicle. The time history plot and Fourier spectra for CP response with an additional measurement noise of 50% are shown in Figs. 6.8 (a), and (b), respectively. The REMD results of CP response with additional measurement noise levels of 20% and 50% are shown in Figs. 6.9, and 6.10, respectively. From the REMD results in Figs. 6.9, and 6.10, in which the resonant peaks of bridge frequencies are separated, the performance of the proposed method under measurement noise is confirmed. The damping values are calculated for the IMFs generated from REMD and are summarized along with the frequency values in Table 6.2.

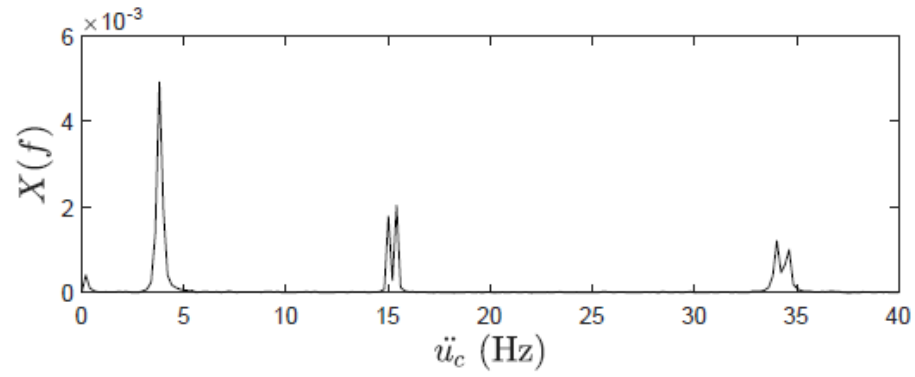
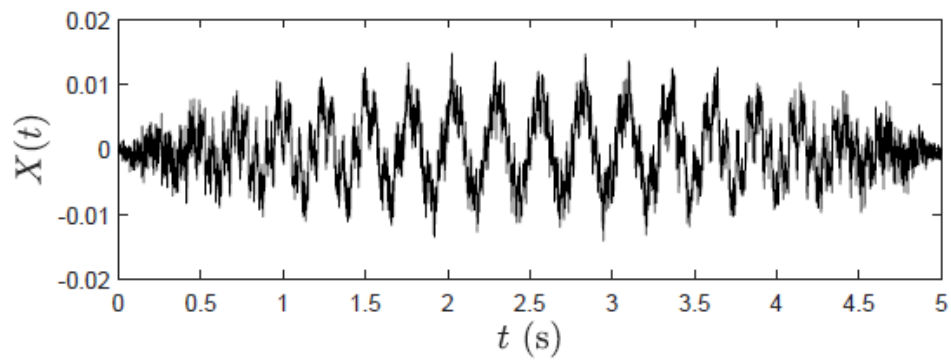
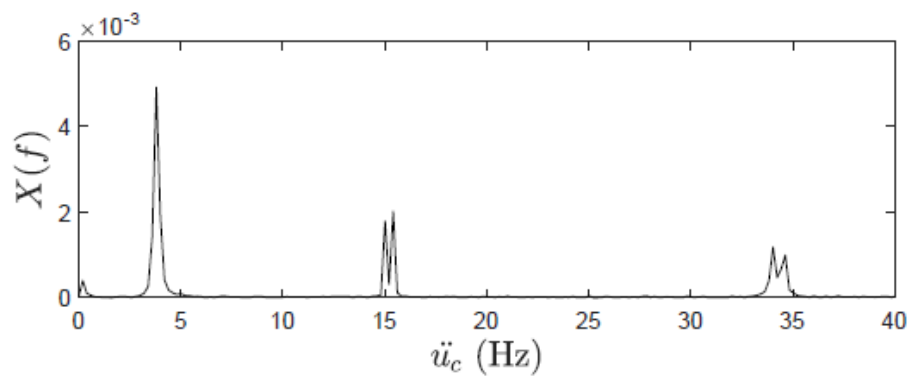


Figure 6.7: Fourier spectra of CP response with 20% measurement noise.



(a)



(b)

Figure 6.8: (a) Time history, and (b) Fourier spectra of CP response with 50% measurement noise.

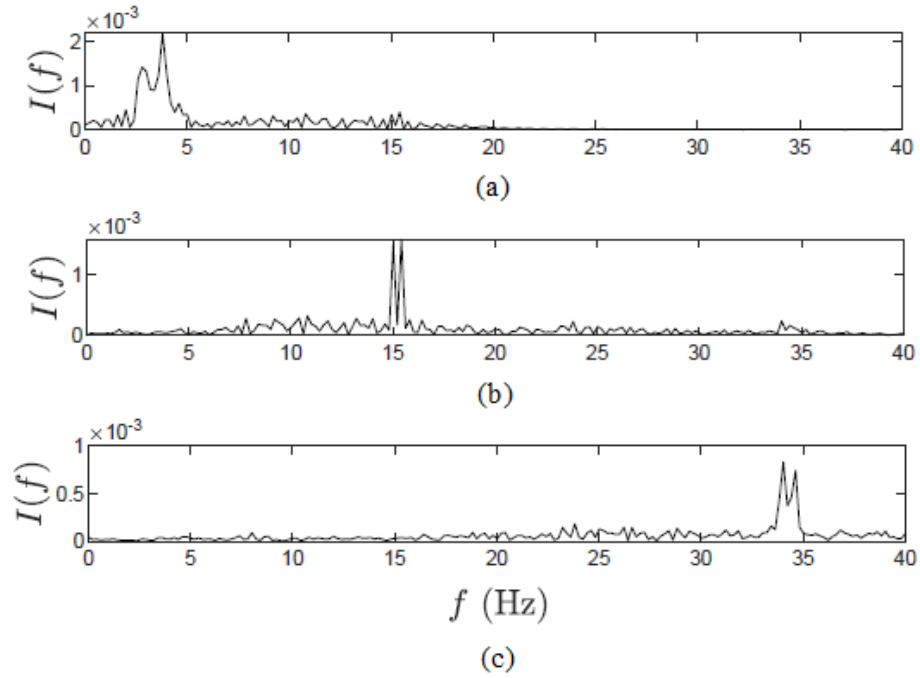


Figure 6.9: REMD results of (a-c) the first, second, and third modes of bridge model obtained from CP response with 20% measurement noise.

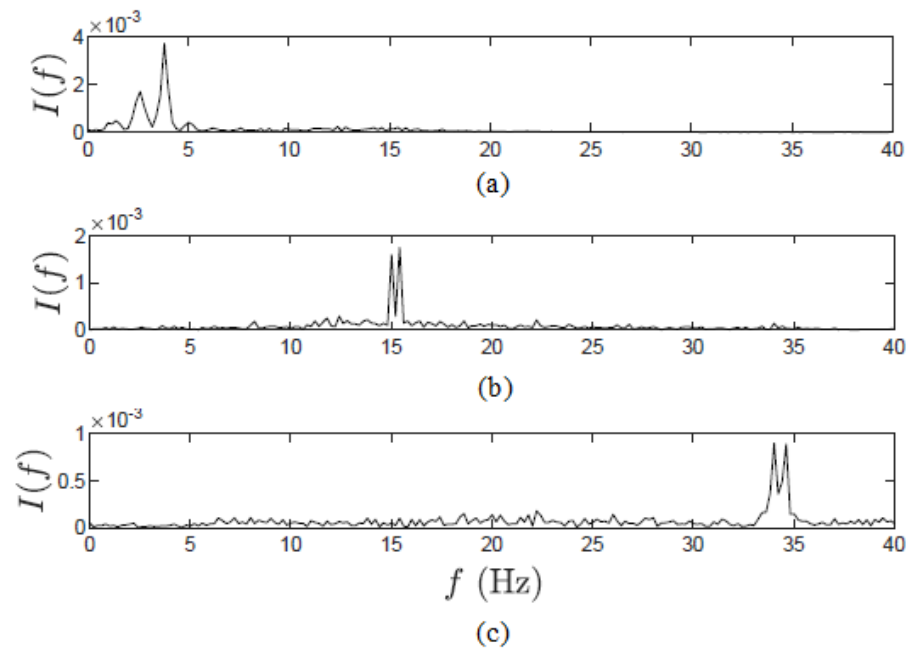


Figure 6.10: REMD results of (a-c) the first, second, and third modes of bridge model obtained from CP response with 50% measurement noise.

Table 6.2: Frequency and damping ratio values identified with different levels of measurement noise.

	No noise		20% noise		50% noise	
	ω (Hz)	ζ (%)	ω (Hz)	ζ (%)	ω (Hz)	ζ (%)
$\omega_{b,1}$	3.80	3.26	3.80	3.74	3.80	2.11
$\omega_{bl,2}$	15.01	-	15.01	-	15.01	-
$\omega_{br,2}$	15.41	-	15.41	-	15.41	-
$\omega_{b,2avg}$	15.21	1.18	15.21	1.01	15.21	1.63
$\omega_{bl,3}$	34.03	-	34.03	-	34.03	-
$\omega_{br,3}$	34.63	-	34.63	-	34.63	-
$\omega_{b,3avg}$	34.33	1.09	34.33	1.05	34.33	0.87

6.4.3 Effect of structural damage

With the use of the proposed framework, the changes in bridge frequencies for each mode of vibration can be studied. To simulate structural damage, the bending stiffness (EI) is reduced by 20% and 50%. Vehicle speed is kept at 18 km/h, and no measurement noise is added to the CP response. Figs. 6.11 and 6.12 show the Fourier spectra of CP response for structural damage cases of 20% and 50%, respectively. By comparing Figs. 6.11 and 6.12 with Fig. 6.3 (b), a reduction of bridge frequencies can be observed as the extent of damage increases. A similar trend can be observed in Figs. 6.13 and 6.14 when compared with Fig. 6.5. The frequency values from the undamaged bridge are compared with 20% and 50% structural damage cases in Table 6.3. For comparison, other structural damage cases are also added to Table 6.3, which include 1%, 5%, and 10% structural damage to the bridge. It is noted that the first natural bridge frequency remains unchanged until 10% structural damage, whereas the second and third natural average bridge frequencies show a change at 5% and 1% structural damage cases, respectively.

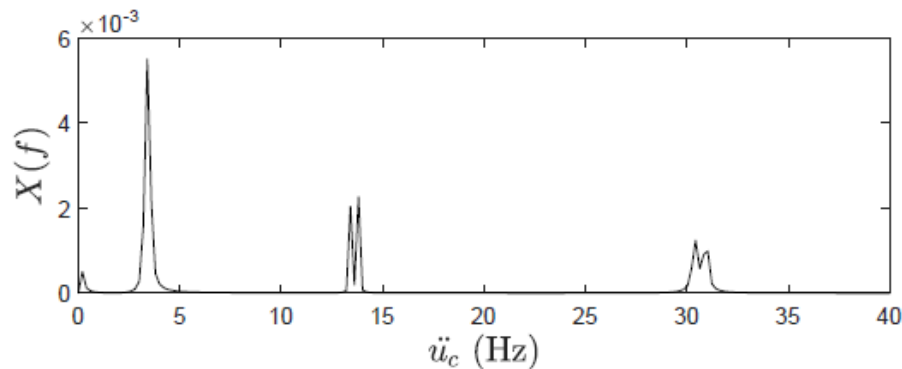


Figure 6.11: Fourier spectra of CP response with 20% structural damage.

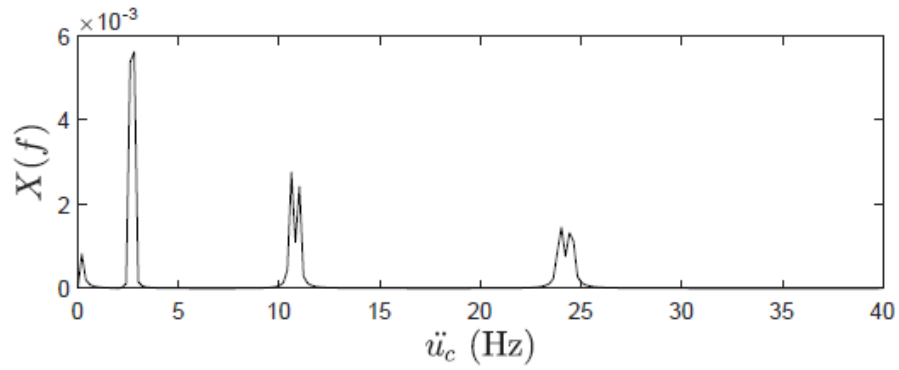


Figure 6.12: Fourier spectra of CP response with 50% structural damage.

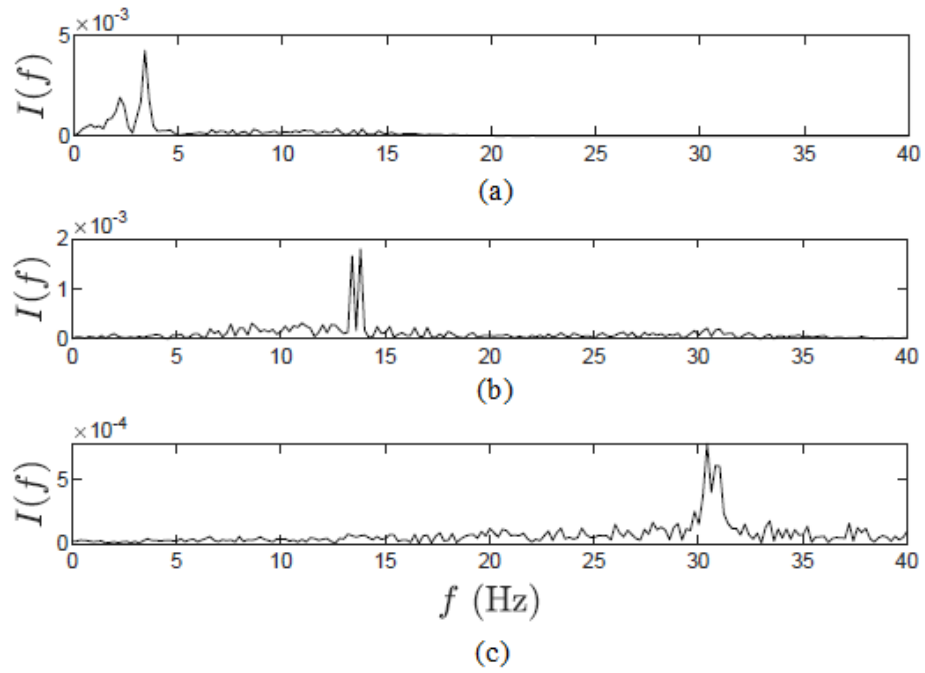


Figure 6.13: REMD results of (a-c) the first, second, and third mode of bridge model obtained from CP response with 20% structural damage.

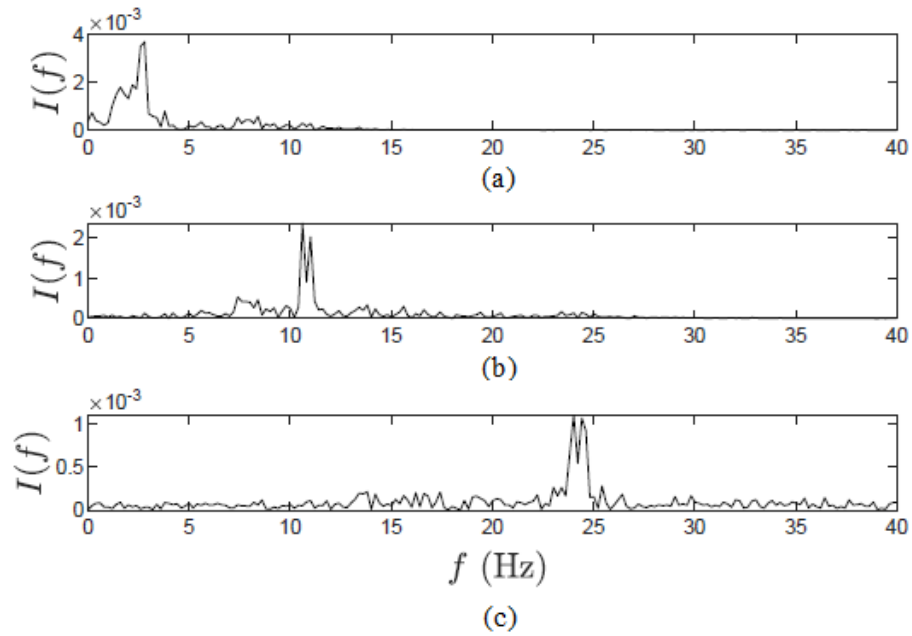


Figure 6.14: REMD results of (a-c) the first, second, and third mode of bridge model obtained from CP response with 50% structural damage.

Table 6.3: Frequency values identified with different levels of structural damage.

ω (Hz)	0% damage	1% damage	5% damage	10% damage	20% damage	50% damage
$\omega_{b,1}$	3.80	3.80	3.80	3.60	3.40	2.80
$\omega_{bl,2}$	15.01	15.01	14.61	14.21	13.41	10.61
$\omega_{br,2}$	15.41	15.41	15.01	14.61	13.81	11.01
$\omega_{b,2avg}$	15.21	15.21	14.81	14.41	13.61	10.81
$\omega_{bl,3}$	34.03	33.83	33.03	32.23	30.42	24.02
$\omega_{br,3}$	34.63	34.43	33.63	32.83	31.02	24.42
$\omega_{b,3avg}$	34.33	34.13	33.33	32.53	30.72	24.22

6.5 Full-Scale Validation

In this section, a full-scale experiment is conducted to demonstrate the proposed method. The test bridge is a five-span continuous box-girder bridge with a total length of 220m, outer spans of 36.5m, and three inner spans of 49m, as shown in Figs. 6.15 and 6.16. The bridge has four lanes, with two lanes serving the traffic flow in each direction. The bridge is the one to be used both in direct monitoring and vehicle scanning tests for comparison.

The bridge is subjected to moderate traffic, and while collecting direct and indirect data, the bridge remains in operational conditions.



Figure 6.15: Five-span continuous box-girder bridge.

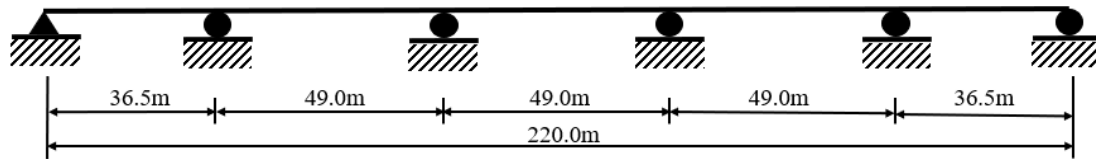


Figure 6.16: Schematics of the five-span test bridge.

6.5.1 Direct bridge health monitoring

In the direct monitoring test, the accelerometer sensors are placed throughout the length of the bridge. Various trials are performed to collect the vibration data under normal traffic conditions that include vehicles such as sedans, pick-up trucks, buses, heavy trucks, etc. traveling at a speed of 60 km/h. The sampling frequency is kept at 200 Hz for direct and indirect monitoring tests. Fourier spectra of data collected by one of the sensors located at the mid-span of the bridge is shown in Fig 6.17. REMD results for the direct data interval are shown in Fig. 6.18 from which three bridge frequencies can be identified as 2.8, 6.4, and 13.0 Hz. The damping ratios are estimated using the IMFs from

REMD results and the values for the first three vibration modes are 0.63%, 0.19%, and 0.29%. The challenge with direct monitoring is that it is generally expensive, labor-intensive, and time-consuming. For a test to be completed, numerous technological concerns must be handled flawlessly on the testing site. In contrast, the same results can be achieved using a vehicle scanning method outlined in the next subsection.

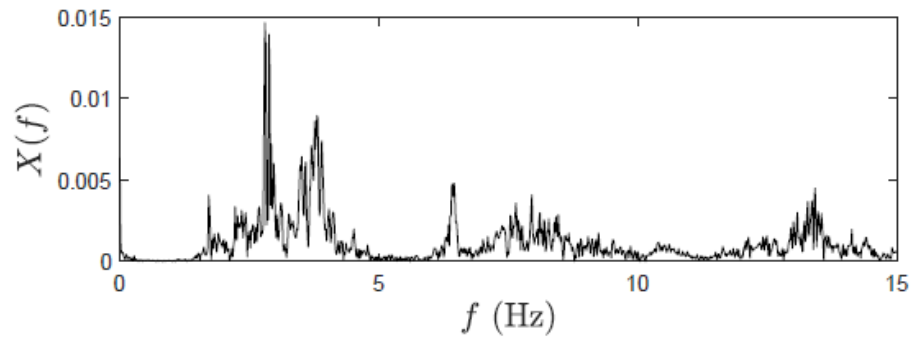


Figure 6.17: Fourier spectra of bridge acceleration response.

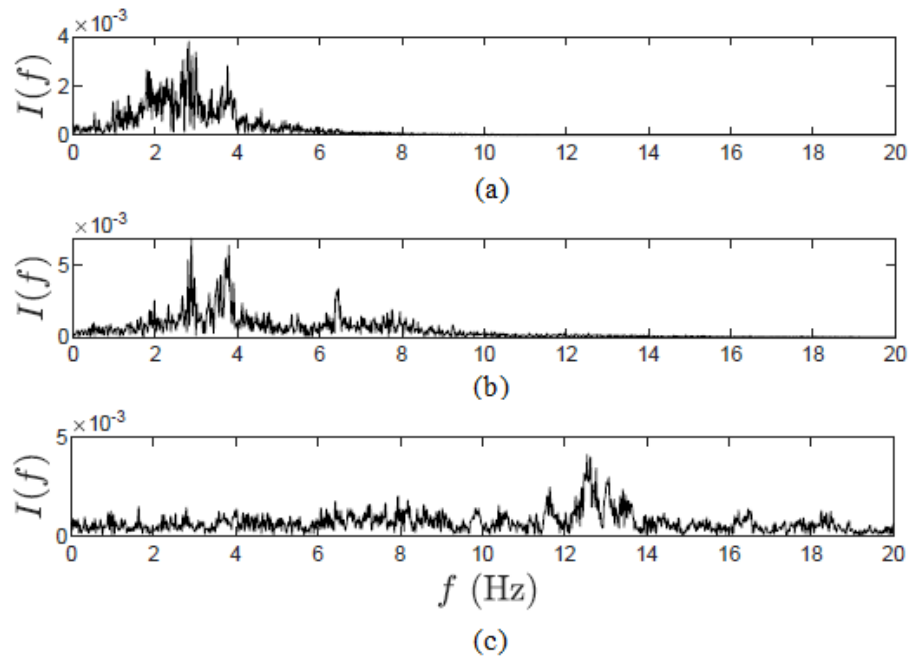


Figure 6.18: REMD results of (a-c) the first, second, and third modes of test bridge obtained from bridge acceleration response.

6.5.2 Indirect bridge health monitoring

In the iBHM test, the test vehicle used to collect the bridge response is shown in Fig. 6.19 (a). The test vehicle is a hatchback car that is instrumented with two accelerometer sensors. Sensors are placed on the passenger side floor, one in the front and the other in the back of the vehicle, as shown in Figs. 6.19 (b) and (c) respectively. In this study, Fourier spectra and REMD results are shown for the front sensor only. The dynamic properties of the test vehicle are investigated using flat road tests and bump tests before the bridge data collection. Upon conducting a few tests, the modes of the engine noise are found to be 5.4 and 10.9 Hz, and the contribution of suspension is found to be 1.65 Hz. The iBHM data is collected at a speed of 40 km/h. To avoid traffic impediments, data is collected at off-traffic timings.



(a)



(b)



(c)

Figure 6.19: (a) Test vehicle, sensor instrumentation in the (b) front, and (c) back of the test vehicle.

The response of the vehicle's CP with the bridge has been demonstrated to be a better parameter than the vehicle response for identifying bridge modal parameters since it is free of vehicle frequency. Using Eq. 6.9, the CP response is generated using the collected vehicle response. Fourier spectra of vehicle acceleration response is shown in Fig. 6.20. And Fourier spectra of CP response, determined using vehicle response, is shown in Fig. 6.21. REMD results for the CP response generated using vehicle acceleration response are shown in Fig. 6.22. From Fig. 6.22, the values for three bridge frequencies and damping ratio are identified and summarized in Table 6.4. The time duration of iBHM data is limited due to the limited length of the bridge and therefore, limited travel time for the test vehicle. This may result in inaccurate results as the data stream may be short depending on the length of the bridge. The resolution of the results depends on the time duration of the test.

Without an adequate period, the bridge dynamic features cannot be successfully captured. Since iBHM is performed using a sensor in the passing vehicle, the test can be repeated multiple times to increase the accuracy of the approach. Damping ratio values from column 5 of Table 6.4 represent only one trip made by the test vehicle. Multiple passes over the bridge can provide results that can be averaged out to provide accurate results. In this study, five round trips are made and therefore, ten test durations are used to average the acquired results. The distributions of bridge frequency and damping ratio values identified from these trials are summarized in Figs. 6.23 (a), and (b), respectively. For the first three modes of vibration, the average values for the frequencies are 2.45, 6.19, and 13.08 Hz, and damping ratios are 0.38, 0.19, and 0.15%.

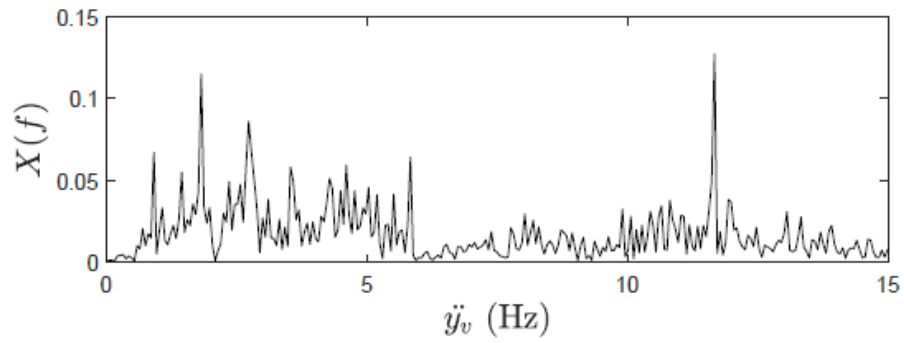


Figure 6.20: Fourier spectra of vehicle acceleration response.

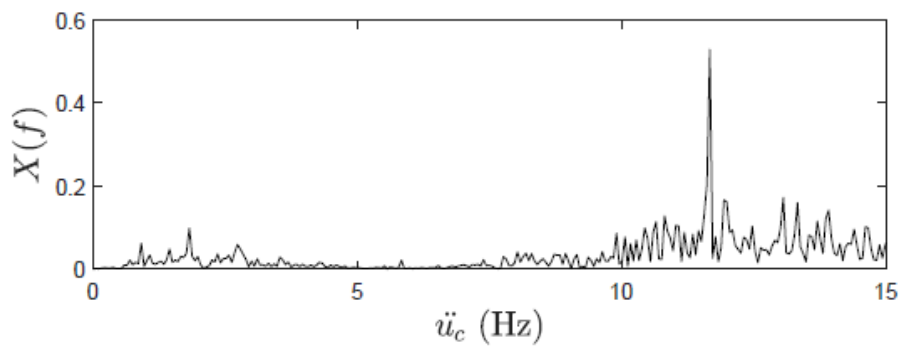


Figure 6.21: Fourier spectra of CP response generated using vehicle acceleration response.

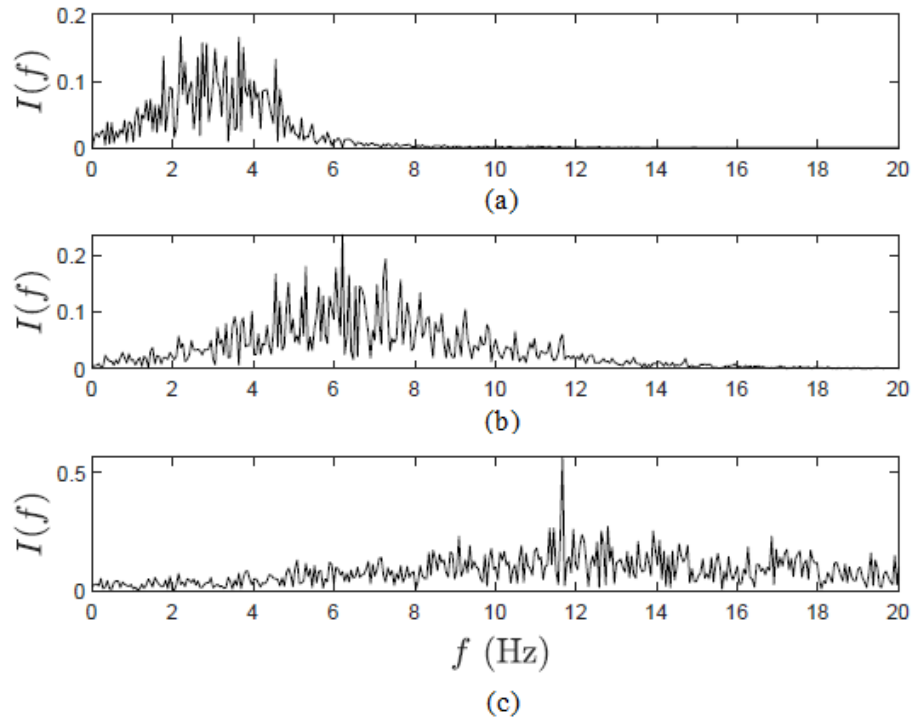
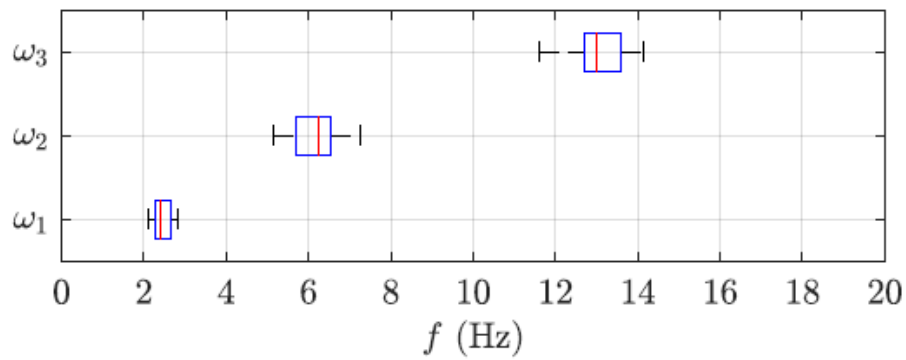


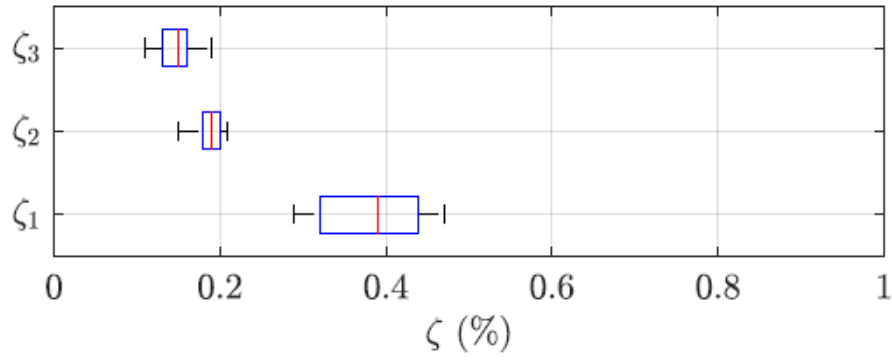
Figure 6.22: REMD results of (a-c) the first, second, and third modes of test bridge obtained from CP response generated using vehicle acceleration response.

Table 6.4: Frequency and damping ratio values identified from direct and indirect BHM results.

	Direct BHM		Indirect BHM	
	$\omega(\text{Hz})$	$\zeta(\%)$	$\omega(\text{Hz})$	$\zeta(\%)$
$\omega_{b,1}$	2.8	0.63	2.83	0.29
$\omega_{b,2}$	6.4	0.19	6.21	0.18
$\omega_{b,3}$	13.0	0.29	11.66	0.19



(a)



(b)

Figure 6.23: Distribution of (a) bridge natural frequencies, and (b) bridge damping ratio values.

6.6 Summary

This chapter proposes a vehicle scanning method that can extract the bridge's natural frequencies using the dynamic response of the vehicle. Since the vehicle response contains the contributions of vehicle and bridge vibrations, the CP response is calculated from the vehicle response using an analytical relationship between the vehicle response and the vehicle's CP response. Once the CP response is known, it is processed using a variant of EMD. REMD can decompose a vibration signal into its simpler components, and it is explored to provide IMFs from the original signal from which the bridge frequencies can be successfully identified. The proposed method is verified using numerical and full-scale studies.

Chapter 7

7 Visualization Tool for Bridge Infrastructure Monitoring and Maintenance

In this chapter, it is attempted to integrate system identification (SID) within the framework of Bridge Information Modeling (BrIM). A single-sensor-based modal identification technique is used, which enables visualization of the bridge frequencies at a given sensor location for different periods. By linking the real sensory data with the virtual sensor, this chapter extends the BrIM model from static to dynamic and provides an effective management and visualization tool for engineers and project owners at large by providing them with updated, monitored information.

7.1 Introduction

Vibration data originating from the structure, collected using direct bridge health monitoring (BHM) or indirect BHM (iBHM) methods, goes through a post-processing phase that includes sorting and de-noising of the data, and vital information about the structure is determined, including critical deflections and modal parameters such as frequency, damping ratio, and mode shapes, etc. Once such parameters are studied and documented from the measured structural response over a long period, automated alerts can be set up using the appropriate thresholds for safe and reliable use of the public infrastructure. However, the interpretation of long-term data collected from continuous monitoring can be overwhelming due to the processing of an enormous amount of data. Automated processing and visualization of data facilitate accurate decision-making promptly. Building Information Modeling (BIM) is a digital representation of the physical and functional characteristics of a structure (Ren *et al.* 2018), which is utilized here for structural monitoring and maintenance.

BIM is not only a computer-aided-design tool but also a three-dimensional (3D) modeling and information management tool that can aid stakeholders and infrastructure owners in monitoring projects remotely. Traditional BIM aims at the design and life-cycle analysis of a new building and its construction (Arayici and Aouad 2010, Grilo and

Goncalves 2010, Liu *et al.* 2014, Singh and Sadhu 2019). BIM is capable of integrating various engineering aspects through 3D spatial representation. The capabilities of BIM are not only limited to being a software environment, but it also serves as a visualization tool providing a better understanding of the project and helping designers to convey the design information and ideas to the project owners (Ivson *et al.* 2019). With all the information about each component being in one place in a single model, it enables end-users to access such information at any time during its lifecycle. Such capability of big data inventory is utilized in this study and explored how it can provide a real-time representation of BHM data to the end-users. During long-term monitoring of structure, raw and preprocessed data can add up to hundreds of gigabytes of data, which makes the process of data retrieval prone to errors (Alampalli *et al.* 2016, Cremona and Santos 2018, Almasri *et al.* 2019). Damage detection can be visualized in the model by assimilating the sensor data within the BIM model. BIM uses a static data source to assess the structure. Therefore, the sensor data collected from the bridge, while linked to BIM, can extend the application of BrIM model from a static to a dynamic model as it can feature real-time data retrieval and interpret the current performance of the bridge.

Recently, there have been several efforts to develop BIM-based structural health monitoring (SHM) strategies. For example, (Zhang and Bai 2015) created a low-cost structural condition assessment device that used BIM computing environment for automated health management of structures. (Chen *et al.* 2014) developed a dynamic BIM framework by developing a prototype to insert real-time data into the BIM model. The dynamic BIM model developed in the study represented real-time building information by connecting the sensor data with the BIM model. A geothermal bridge deck de-icing system monitored with embedded sensors was used as a case study. (Delgado *et al.* 2017) formulated a standard data model to include and visualize SHM data directly to BIM models. A case study was conducted in a pre-stressed concrete girder bridge featuring a fiber optic-based SHM system. The goal to accurately represent the SHM sensory system, including damage-sensitive features in the object properties, was achieved by (Grosso *et al.* 2017). The authors demonstrated the linking of data to sensor representations within the BIM model.

The viability of bridge information modeling with different modules of bridge management systems was explored by (Marzouk and Hisham 2011). (Huston *et al.* 2016) worked on the integration of BIM and decision-making systems with SHM involving collection, storage, transmission, and processing of information obtained from sensor data and design documents. The extended Industry Foundation Classes (IFC) schema, referred to as *IFC Monitor* was formulated by (Theiler *et al.* 2017) to facilitate the documentation of SHM systems since the current schema was unable to support the full description of modeling-related information. The automatic generation of parametric building models of SHM systems and efficient integration with other data sets was enabled by (Delgado *et al.* 2018). Recently, (Boddupalli *et al.* 2019) developed a data visualization tool for systematic decision-making using the computing environment of BIM as a primary platform.

The significant limitation of these studies is the lack of a single standardized neutral exchange format for sharing information among the various data software. The problem arises when attempting to extract data from sensors in many different protocols. The handling of large volumes of data requires high-performance hardware. Lack of interoperability is another challenge in the seamless integration of a BHM system with the BIM platform. There is a lot of software commercially available for the modeling and development of structures. However, the development of various computational tools, such as add-ins or plug-ins, is undertaken in a standalone fashion, which is also inefficient in addressing the complications arising from multiple data sources. The existing BIM-based SHM tools lack interoperability and information sharing with other software and technology (Grillo and Jardim-Goncalves 2010, Cemesova *et al.* 2015, Karan and Irizarry 2015, Tomasi *et al.* 2015). Moreover, the capability of SID and the evolution of structural parameters over time are not available in the existing visualization tools in the literature, which forms the focus of this chapter.

After a basic introduction of BIM and BHM techniques and identification of the limitations in the current literature, the proposed method is discussed in section 7.2. The proposed framework is finally illustrated using a case study consisting of visualization of the BHM data in section 7.3, followed by a summary in section 7.4.

7.2 Proposed Visualization Framework

This section provides an overview of the proposed methodology implemented to visualize BHM data within BrIM through Autodesk REVIT®. The proposed framework utilizes the relative merits of BHM and BrIM to develop a visualization tool for monitoring bridge infrastructure. This method uses REVIT and MATLAB (MathWorks 2018) online portal to integrate the sensor information with condition data and diagnostic results. Virtual sensors in this study are used to visualize the BHM information in the BrIM environment. Accelerometer sensors used for vibration data collection are modeled in the REVIT as a new class of family, as shown in Fig. 7.1. Sensor metadata is used to create a sensor family and can be accessed by highlighting any sensor from the BrIM model. The dynamic behavior of the structure is analyzed using the sensor data in MATLAB.

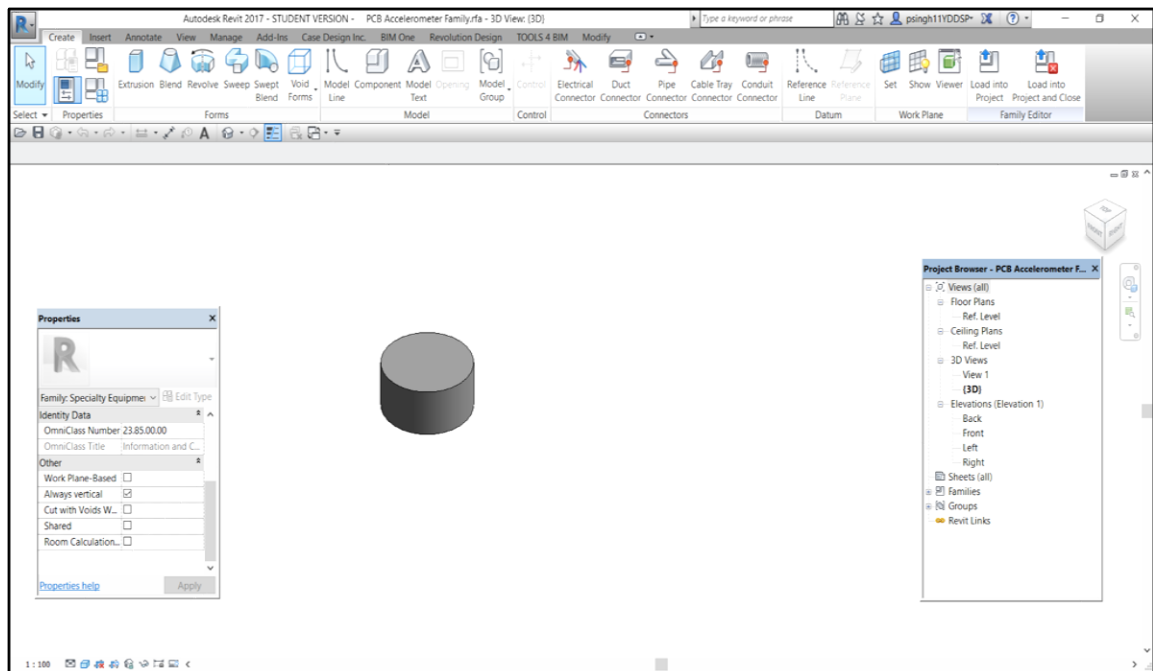
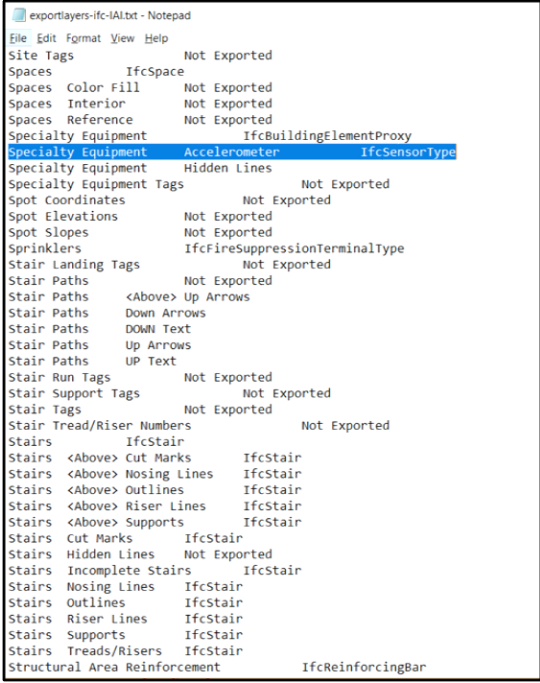


Figure 7.1: Virtual sensor modeled in Autodesk REVIT.



IFC Class	Export Status	IFC Class	Export Status
Site Tags	Not Exported		
Spaces	IfcSpace		
Spaces Color Fill	Not Exported		
Spaces Interior	Not Exported		
Spaces Reference	Not Exported		
Specialty Equipment	IfcBuildingElementProxy		
Specialty Equipment Accelerometer	IfcSensorType		
Specialty Equipment	Hidden Lines		
Specialty Equipment Tags	Not Exported		
Spot Coordinates	Not Exported		
Spot Elevations	Not Exported		
Spot Slopes	Not Exported		
Sprinklers	IfcFireSuppressionTerminalType		
Stair Landing Tags	Not Exported		
Stair Paths	Not Exported		
Stair Paths <Above> Up Arrows			
Stair Paths Down Arrows			
Stair Paths DOWN Text			
Stair Paths Up Arrows			
Stair Paths UP Text			
Stair Run Tags	Not Exported		
Stair Support Tags	Not Exported		
Stair Tags	Not Exported		
Stair Tread/Riser Numbers	Not Exported		
Stairs	IfcStair		
Stairs <Above> Cut Marks	IfcStair		
Stairs <Above> Nosing Lines	IfcStair		
Stairs <Above> Outlines	IfcStair		
Stairs <Above> Riser Lines	IfcStair		
Stairs <Above> Supports	IfcStair		
Stairs Cut Marks	IfcStair		
Stairs Hidden Lines	Not Exported		
Stairs Incomplete Stairs	IfcStair		
Stairs Nosing Lines	IfcStair		
Stairs Outlines	IfcStair		
Stairs Riser Lines	IfcStair		
Stairs Supports	IfcStair		
Stairs Treads/Risers	IfcStair		
Structural Area Reinforcement	IfcReinforcingBar		

Figure 7.2: IFC sensor data.

Virtual sensors used in this study to mimic the sensors installed on a real structure are created as a new REVIT family using the IFC standard of data exchange shown in Fig. 7.2. IFC is used by building-model-based applications to exchange data with each other, and it constitutes a specification that can describe model data related to all phases of the life-cycle of a project (Rio *et al.* 2013, Augenbroe *et al.* 2004). The IFC model represents tangible building elements such as doors, walls, ceilings, beams, etc., and even more abstract entities such as time, schedule, space, cost, organization, etc. There are different IFC classes for each element, while the sensors are included in the *IFCBuildingControls* domain module. There are two classes associated with sensors; *IFCSensor* and *IFCSensorType*. As the sensors are defined in the BIM environment, sensor information can be accessed using the properties box of each sensor. The link to MATLAB is also connected to the properties box. By clicking the MATLAB link, the user is taken to the MATLAB online portal, where SID scripts can be run. Subsequently, the SID results can be analyzed for decision-making.

Pre-processed and processed BHM data is embedded within the BrIM software such that long-term health monitoring information can be visualized. A wide range of SID methods (Dessi and Camerlengo 2015, Perez Ramirez *et al.* 2016, Pappalardo and Guida 2018, Barbosh *et al.* 2018, Mao *et al.* 2019) were developed by the researchers to estimate modal parameters from the measured vibration data. Most of these techniques are suitable where all critical locations of the structure are instrumented. For visualization purposes, each sensor installed in a real structure corresponds to a virtual sensor in the BIM model. Therefore, while visualizing a particular virtual sensor, each sensor creates a time history that requires a SID method that is capable of using only a single channel measurement. In this study, a newer time-frequency method, Time-Varying Filter-based Empirical Mode Decomposition (TVF-EMD) (Li *et al.* 2017, Lazhari and Sadhu 2019) is used to conduct SID using single-channel measurement.

The details of the TVF-EMD method can be found in section 3.2.2. TVF-EMD uses the root-mean-square (RMS) value of the resulting intrinsic mode functions (IMFs) to extract the modal responses. However, all the frequencies with energy higher than the average RMS value cannot be utilized to differentiate the actual structural frequencies from the background noise. To automate the identification step, it is proposed that when the difference between the respective Fourier peaks in an IMF is more than a specific percent (say, 70%) of the higher peak value, then the IMF represents a structural modal response rather than a mixed modal response.

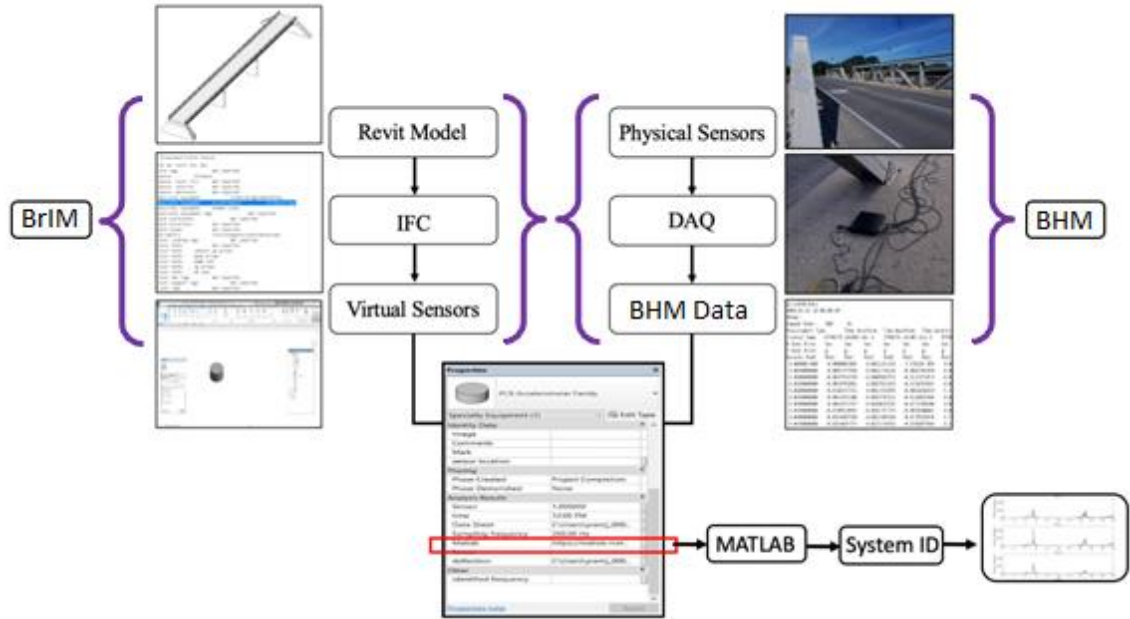


Figure 7.3: Proposed framework for the BrIM-based BHM method.

The proposed framework (Singh and Sadhu 2020) has three-fold advantages of online visualization of data, real-time SID, and decision-making by tracking the SID results obtained from the measured data. Fig. 7.3 shows the proposed framework that can automate SID and visualization of BHM data in the BIM environment. First, a parametric 3D model of the structure is developed in Autodesk REVIT. Since the virtual sensors are not predefined elements in the REVIT library, these are manually created using a new REVIT family and IFC attributes. On the other hand, physical sensors, which are connected to a data acquisition (DAQ) system, record the BHM data for structural condition assessment. Therefore, accelerometers are used to collect the BHM data, and virtual sensors are created in the BIM environment using IFC (as shown in Fig. 7.2) to mimic the physical sensors on site. Data file from each physical sensor is associated with the respective virtual sensor in REVIT. SID is performed using the TVF-EMD algorithm, which is integrated with REVIT through an online MATLAB portal linked via the “Properties” box of the virtual sensor in the BrIM model. Owing to its capability of analyzing single-sensor data associated with a virtual sensor, the TVF-EMD is adopted to undertake SID from single-channel data. It is automated and can be implemented in real-

time for condition assessment of structures within the BrIM platform. A case study is presented next to demonstrate the implementation of the developed framework.

7.3 Full-Scale Validation

The proposed framework is validated using a 90 m pony-truss bridge in London, Ontario, shown in Fig. 7.4 (a). This section demonstrates the application of the proposed visualization tool developed in this study. Bridge vibrations are monitored while different numbers of vehicles travel over the bridge. A virtual model for the bridge is developed in REVIT and sensor data is integrated with the virtual sensors. SID results from the BHM data are shown in a user-friendly format integrated with the visualization platform of REVIT.



(a)



(b)



(c)

Figure 7.4: (a) Direct sensor instrumentation of steel bridge, (b) DAQ system, and (c) sensor instrumented on bridge sidewalk.

7.3.1 Details of instrumentation

The bridge is instrumented with accelerometers to evaluate its modal parameters and analyze and predict the structural health of the bridge. Nine high-sensitive sensors are placed along the walkway of the bridge, and the sensors are set up to measure uniaxial vertical vibration. The sensors used for the testing have a sensitivity of 10V/g. A sampling frequency of 200 Hz is used. Sensors are placed at a distance of 3, 6, 15, and 30 m on both sides from the centerline of the bridge shown in Fig. 7.4 (a). The data collection is performed through (b) the DAQ system by connecting it with (c) sensors using BNC cables and a laptop using a USB cable shown in Fig. 7.4. Test details regarding the number and class of vehicles during each test run are tabulated in Table 7.1. The duration of each test is between 30 seconds to 5 minutes. Tests 4, 5, and 6 include the free vibration response recorded during the jumping of a single subject near the center of the bridge.

Table 7.1: Description of test data.

Test #	Bus	Car	Truck	Total
1	0	11	0	11
2	1	20	1	22
3	1	29	3	33
4	3 jumps of 2 subjects			
5	3 jumps of 3 subjects			
6	3 jumps of a single subject			

7.3.2 Bridge Information Modeling-based model

For the framework presented in this study, a structural model is developed that closely represents the real bridge. Data attributes define the physical, geometrical, and abstract properties of the structure. REVIT is used as a BrIM tool to visualize the bridge virtually. With the help of 2D drawings provided by the City engineers, a virtual model of the bridge is developed into a 3D model with the generic parameters and properties using REVIT as shown in Fig. 7.5.

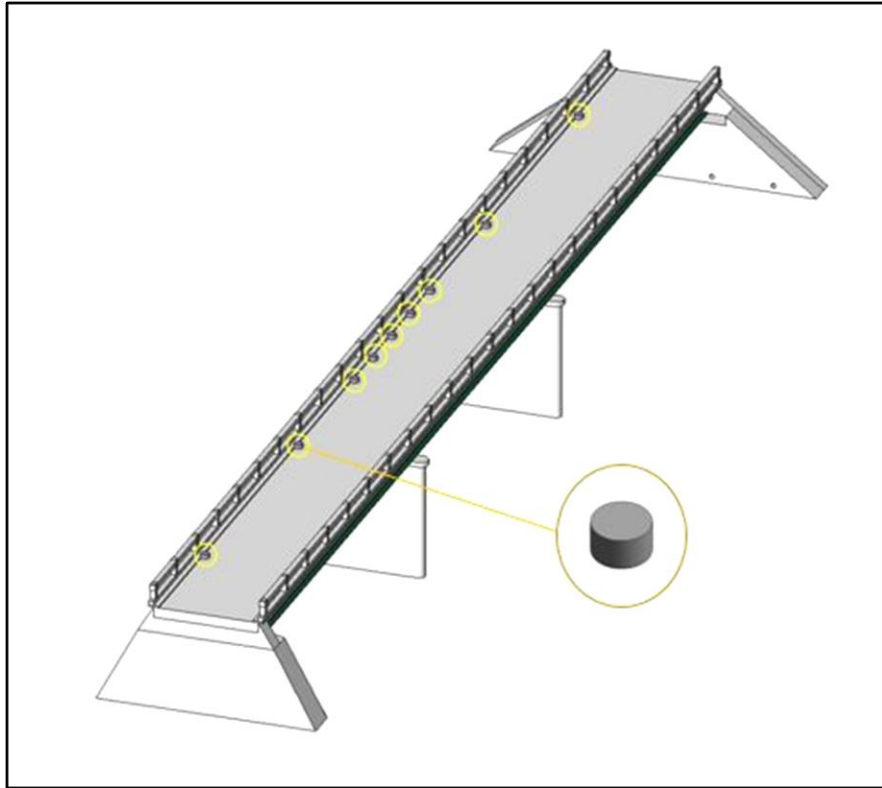


Figure 7.5: Virtual 3D model of bridge and sensor.

This model is used to define the real-time dynamic behavior of the bridge that can be used for visualization of long-term monitored BHM data. Sensors feed the vibration data to DAQ, which is connected to a computer. The raw data file generated by the DAQ system is used to perform SID and serves as a link to connect the BrIM model with the MATLAB online portal. Virtual sensors that are not pre-defined in Autodesk REVIT are manually created in the BrIM model. A new REVIT family is used to create the accelerometer sensor virtually and the IFC exchange format is used to define the virtual sensor attributes shown in Figs. 7.1 and 7.2, respectively. Fig. 7.5 shows the virtual sensors placed in the BrIM model of the bridge. Properties related to sensors used for this particular study are defined in REVIT shown in Fig. 7.6. Upon selecting a particular virtual sensor in the bridge, its properties box shows all the data associated with that specific sensor, including sampling frequency, raw datasheet location, sensor serial and location, MATLAB link for SID, etc.

The 'Type Properties' dialog box in Autodesk Revit displays the following information:

- Family:** PCB Accelerometer Family
- Type:** PCB Accelerometer Family
- Buttons:** Load..., Duplicate..., Rename...
- Type Parameters Table:**

Parameter	Value
Identity Data	
Type Image	
Keynote	
Model	393812
Manufacturer	PCB Piezotronics
Type Comments	
URL	http://www.pcb.com/products.
Description	Shear Accelerometer
Assembly Code	
Cost	
Assembly Description	
Type Mark	
OmniClass Number	23.85.00.00
OmniClass Title	Information and Communication
Code Name	
- Buttons:** << Preview, OK, Cancel, Apply

Figure 7.6: Sensor metadata defined in Autodesk REVIT.

7.3.3 Implementation of the proposed framework

The data collected from the building and MATLAB scripts (Mathworks, 2018) is linked with the virtual sensors which are modeled in REVIT shown in Figs. 7.1 and 7.6. By selecting a sensor, its related properties are shown in the properties box, including serial number, date, time, sensor location, sampling frequency, datasheet link, MATLAB link, etc. The properties box for a highlighted sensor is shown in Fig. 7.7. After clicking on the MATLAB link for a particular sensor, the user is taken to the MATLAB online portal, which performs the SID using the datasheet assigned to the specific sensor. The DAQ file, containing the raw and unprocessed data collected by the sensors, is saved as a text file and is shown in Fig. 7.7.

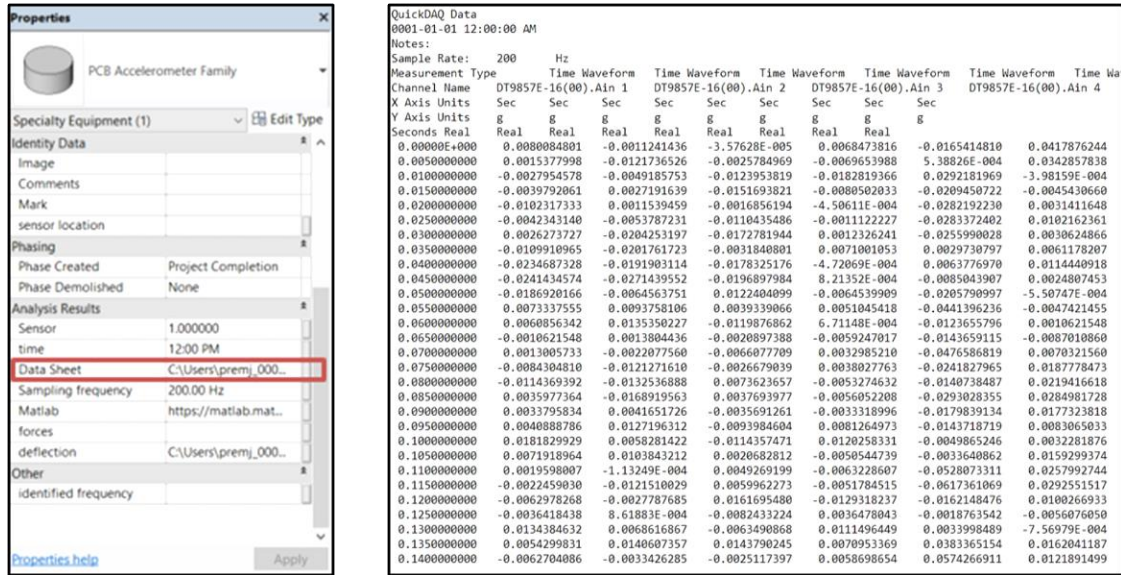


Figure 7.7: DAQ file containing raw and unprocessed data.

This file is linked with the virtual sensor of the BrIM model of the bridge and can be accessed by clicking on the datasheet link on the properties box of the virtual sensor. This text file is also uploaded on the MATLAB online compiler along with the scripts of the TVF-EMD method. By clicking on a sensor in the BrIM model, the respective sensor gets highlighted, and a “Properties box” shows up in the REVIT window, and all necessary sensor information is contained in this icon shown in Fig. 7.7. By clicking on the datasheet link in the properties box, the user is taken to the raw data file linked to that particular sensor containing unprocessed data. By clicking the MATLAB link, highlighted in Fig. 7.8, the user is taken to the MATLAB online portal. In the portal, by executing the MATLAB scripts, SID results can be generated using single-channel measurement through the TVF-EMD method.

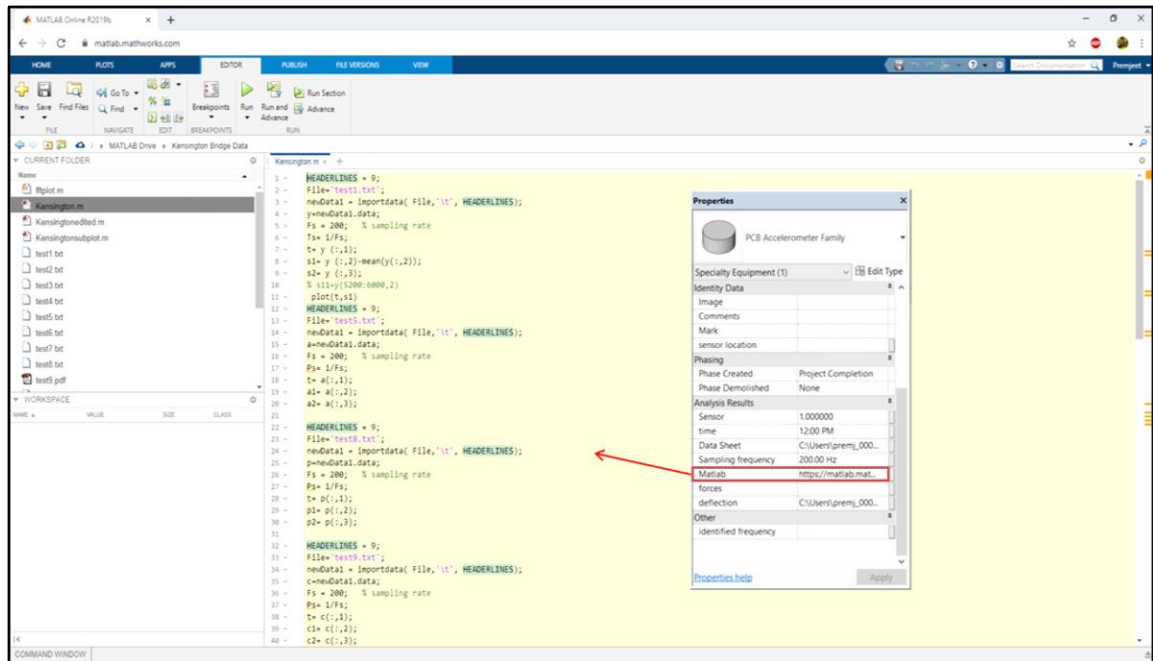


Figure 7.8: Execution of SID in Autodesk REVIT using MATLAB online portal.

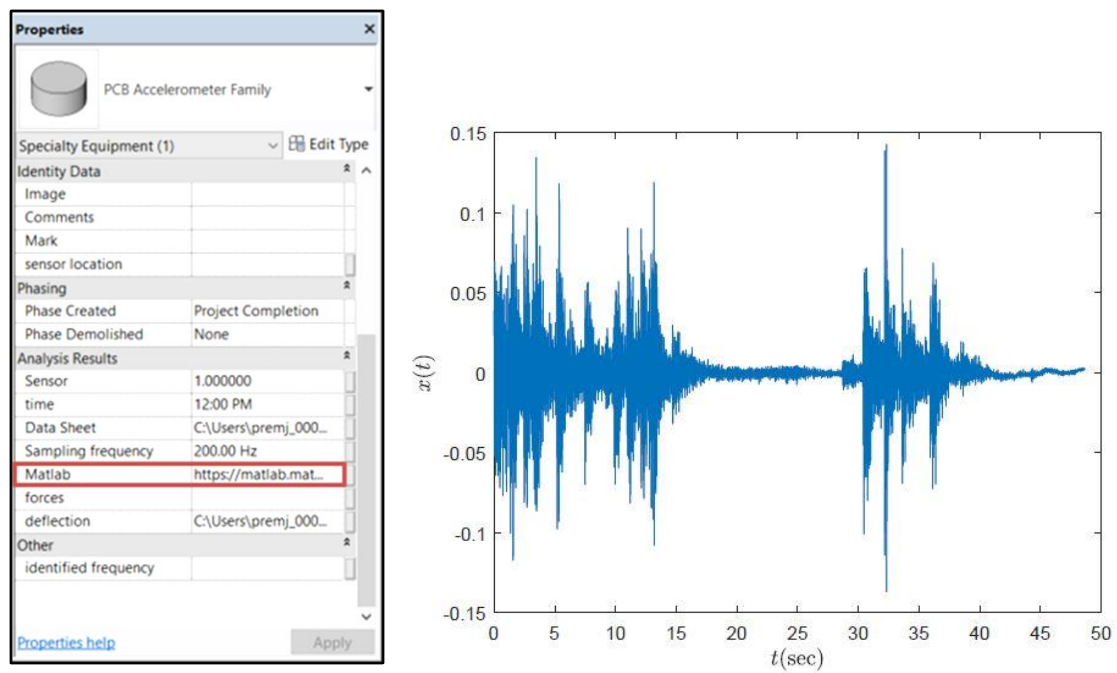


Figure 7.9: Time history of measured bridge response.

The framework presented in this study is used to perform modal identification using a single sensor measurement. The time history of the physical response of the bridge is shown in Fig. 7.9. The method used in this study successfully extracts the mono-component modal responses. The resulting IMFs (i.e., extracted modal responses) are separated by the TVF-EMD algorithm. The resulting mono-component responses and the identified structural frequencies are discussed below.

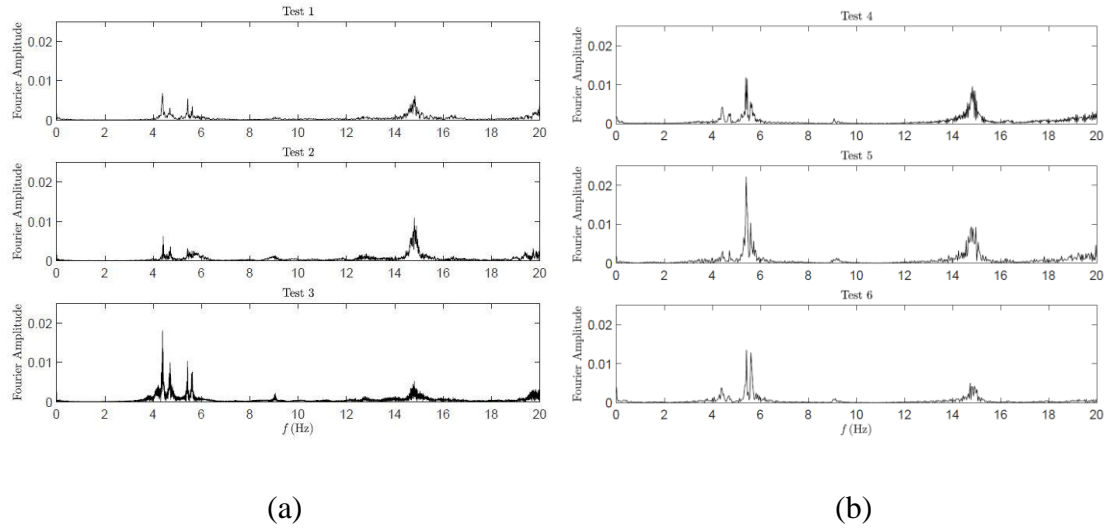


Figure 7.10: Fourier spectra of the measured (a) free vibration response, and (b) vehicle traffic-induced response of the bridge.

Test runs are selected for analysis in such a way that represents live traffic conditions. All the test runs except 4, 5, and 6 include the structural response generated by passing vehicles over the bridge. Tests 1, 2, and 3 are selected for further analysis as their vehicle count is 11, 22, and 31, respectively which represent a wide range of vehicles passing over the bridge. Fig. 7.10 (a) shows the processed data from the first three tests, which cover most of the range of vehicle count. As seen in Fig. 7.10 (a), Fourier amplitudes have higher values with an increasing number of vehicles in the bridge.

Free vibration tests are conducted to estimate the natural frequencies of the bridge. To achieve this, the bridge is excited by the jumping action of a subject at the center of the bridge. This test has another significance of mimicking the pedestrian activity (walking or running) on the bridge. As shown in Fig. 7.10 (b) and Table 7.2, around four resonant

peaks can be observed between 0-20 Hz, indicating four natural frequencies of the bridge in this range, which are consistent with traffic-induced vibration.

Table 7.2: Frequency values identified from free vibration response of bridge.

Test #	ω_1	ω_2	ω_3	ω_4
4	4.43	5.41	9.24	14.83
5	4.45	5.41	9.22	14.83
6	4.42	5.41	9.15	14.78

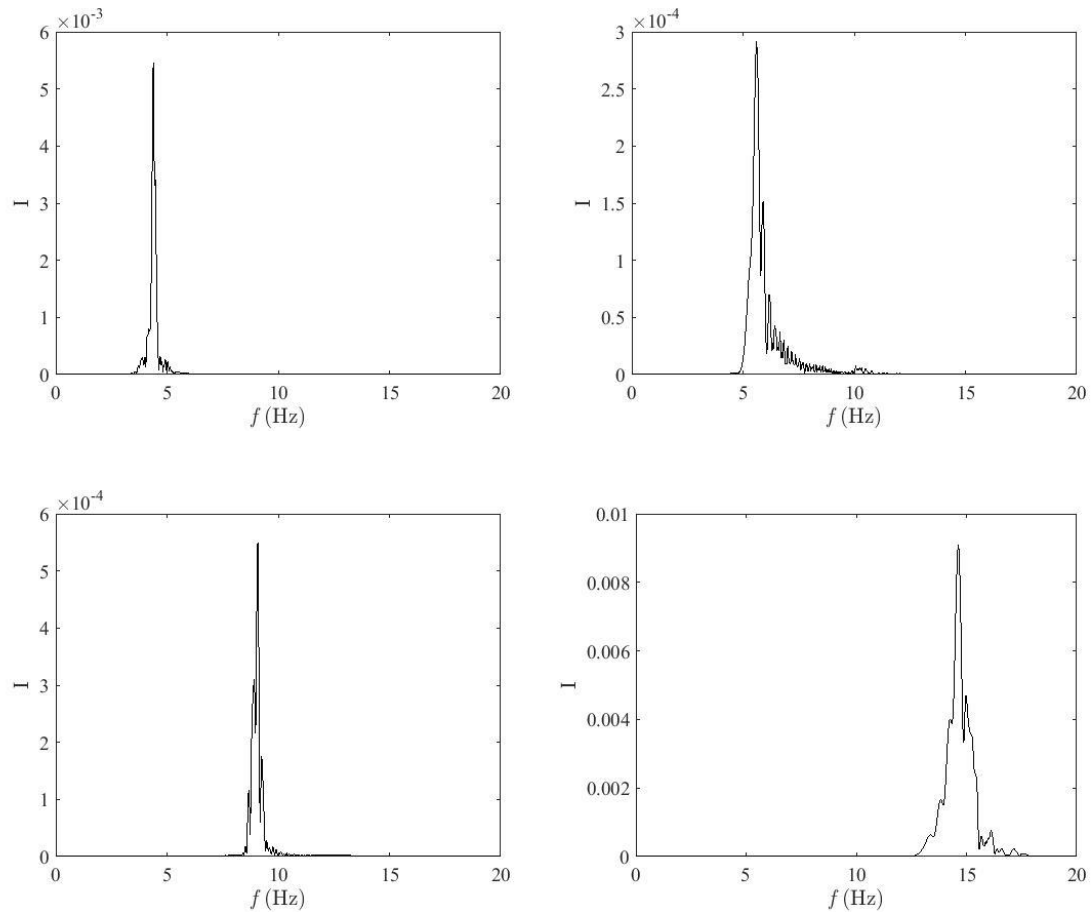


Figure 7.11: TVF-EMD results of vehicle traffic-induced response of the bridge.

TVF-EMD is used to acquire the bridge frequencies from the single-channel measurement or vibration response generated by a bus driving over the bridge, and the results are shown in Fig. 7.11. The resulting IMFs are separated by the TVF-EMD method. The mono-component responses and the identified structural frequencies are

shown in Fig. 7.11. Table 7.3 contains the modal frequencies obtained from different sensors generated using the proposed framework.

Table 7.3: Frequency values identified from bridge response originating from various sensors.

Test #	ω_1	ω_2	ω_3	ω_4
1	4.45	5.52	9.18	14.82
2	4.45	5.45	9.41	13.15
3	4.43	5.45	9.92	14.82
4	4.44	5.46	9.91	14.82
5	4.44	5.47	9.14	14.81
6	4.43	5.47	9.15	14.84

7.4 Summary

This chapter investigated the potential of BrIM in data management and maintenance of infrastructure using a web-based workflow. The use of different data formats can be omitted since the process is web-based and features real-time integration of sensor data with the BIM model. The proposed framework enhances software interoperability and frequent communication, which are required on civil infrastructure projects. The extension of the BrIM model from static to dynamic enables the real-time link between the data-driven SHM techniques and BrIM software. The web-based approach can be utilized to identify the modal frequencies from the sensor data using the TVF-EMD method used in this study. In this way, the SID of BHM data is integrated within the BrIM model, which can be beneficial for better interpretation of BHM data.

Chapter 8

8 Conclusion and Discussion

In this chapter, the key conclusions, thesis contributions, thesis limitations, and future work are summarized.

8.1 Key Conclusions

- A novel system identification (SID) technique is developed to solve the practical challenges associated with direct bridge health monitoring (BHM). The method employs a limited number of sensors for monitoring bridges when subjected to ambient and forced vibrations. A time-varying Empirical Mode Decomposition (EMD) variant is utilized to decompose the nonstationary bridge response, and a wavelet-based reallocation algorithm is used to provide the time-frequency representation of the response. The sparse SID capability of the proposed method is demonstrated using numerical and full-scale studies.
- A drive-by modal identification method is proposed that uses a single sensor instrumented on the test vehicle for the SID of the bridge. This method has the potential to significantly reduce the economic footprint of BHM. Vehicle response contains dynamic information about the bridge, vehicle suspension, engine noise, ambient traffic noise, road roughness, etc. Due to the presence of sensor-vehicle-bridge interactions in vehicle response, a decoupling framework featuring wavelet transforms is proposed to extract bridge modal parameters. The results from numerical, laboratory, and full-scale studies provide evidence that the proposed method can serve as a promising indirect BHM (iBHM) method.
- A vehicle scanning method is introduced to perform modal identification of bridges using the contact point (CP) response of the test vehicle. CP of the vehicle is independent of vehicle frequency and can enable a more accurate extraction of bridge modal parameters. The analysis of nonstationary CP response is challenged by the presence of measurement noise, varying vehicle speed, and extent of structural

damage, which yield significant inaccuracies. In this method, a variant of EMD is employed for computationally efficient modal identification by analyzing the CP response. The accuracy of the proposed method is illustrated using numerical and full-scale validation studies.

- The potential of Bridge Information Modeling (BrIM) in bridge infrastructure maintenance and BHM data management is investigated using a web-based workflow. The proposed framework enhances software interoperability and frequent communication and extends the BrIM model from static and dynamic by enabling a real-time link between the data-driven BHM techniques and BrIM software. The proposed method features visualization and processing of BHM data on a web-based platform to facilitate the end-users in identifying the changes in structural performance.

8.2 Thesis Contributions

The research conducted through this thesis is directed toward creating a bridge infrastructure management system with limited and mobile sensing technology. BrIM-based visualization and advanced basis-free time-frequency methods are explored to provide a framework capable of detecting structural damage in bridges. The broad contributions of this thesis are mentioned below:

- A sparse SID technique to track the dynamic behavior of bridges subjected to ambient and moving vehicle-induced nonstationary vibrations is developed.
- iBHM leverages a vehicle traveling over a bridge as a data acquisition device as well as a source of excitation. A robust drive-by modal identification is attempted in this thesis using vehicle response and CP response for damage identification in bridges.
- A step forward from static to dynamic BrIM is attempted to facilitate the representation and visualization of BHM data. The proposed BrIM-based visualization framework provides a tool for long-term monitoring and maintenance of bridge infrastructure.

The thesis results followed research articles in leading journals and conference papers.

8.2.1 Journal papers

1. **Singh, P.**, and Sadhu, A. (2023). Contact point response-based indirect bridge health monitoring using robust empirical mode decomposition. *Under review*.
2. **Singh, P.**, Mittal, S., and Sadhu, A. (2023). Recent advancements and future trends in indirect bridge health monitoring. *Practical on Structural Design and Construction*, ASCE, 28(1).
3. **Singh, P.**, and Sadhu, A. (2022). A hybrid time-frequency method for robust drive-by modal identification of bridges. *Engineering Structures*, Elsevier, 264, 114624.
4. **Singh, P.**, and Sadhu, A. (2021). Limited sensor-based bridge condition assessment using vehicle-induced nonstationary measurements. *Structures*, Elsevier, 32, 1207-1220.
5. **Singh, P.**, Keyvanlou, M., and Sadhu, A. (2021). An improved time-varying empirical mode decomposition for structural condition assessment using limited sensors. *Engineering Structures*, Elsevier, 232, 111882.
6. **Singh, P.**, and Sadhu, A. (2020). System identification enhanced automated visualization tool for infrastructure monitoring and maintenance. *Structural Sensing*, Frontiers in Built Environment, 6(76).
7. Barbosh, M., **Singh, P.**, and Sadhu, A. (2020). Empirical mode decomposition and its variants: A review with applications in structural health monitoring. *Smart Materials and Structures*, IOP, 29(9), 093001.
8. Yan, J., Laflamme, S., **Singh, P.**, Sadhu, A., and Dodson, J. (2020). A comparison of time-frequency methods for real-time application to high-rate dynamic systems. *Vibration*, MDPI, 3(3), 204-216.

9. **Singh, P.**, and Sadhu, A. (2019). Multicomponent energy assessment of buildings using building information modeling. *Sustainable Cities and Society*, Elsevier, 49, 101603.

8.2.2 Conference papers

1. **Singh, P.**, and Sadhu, A. (2023). An improved vehicle scanning method based on contact point response. *CSCE General Conference*, Moncton, Canada.
2. **Singh, P.**, and Sadhu, A. (2023). Modal identification framework for bridges using traffic smartphone data. *CSCE General Conference*, Moncton, Canada.
3. Peplinski, J., **Singh, P.**, and Sadhu, A. (2022). Real-time structural inspection using augmented reality. *CSCE Structural Specialty Conference*, Victoria, Canada.
4. **Singh, P.**, and Sadhu, A. (2022). Indirect bridge health monitoring using time-frequency analysis: Analytical and experimental analysis. *IMAC-XL*, Society for Experimental Mechanics, Orlando, USA.
5. **Singh, P.**, and Sadhu, A. (2020). Towards mobile sensing technique in bridge health monitoring. *CSCE General Conference*, Saskatoon, Canada.
6. Barbosh, M., **Singh, P.**, and Sadhu, A. (2020). Structural condition assessment using empirical mode decomposition and its variants. *CSCE General Conference*, Saskatoon, Canada.
7. **Singh, P.**, and Sadhu, A. (2019). Towards building information modeling-based automated structural health monitoring tool. *CSCE General Conference*, Montreal, Canada.

8.3 Limitations of the Proposed Thesis

After an extensive review of the BHM research, iBHM has enormous potential for future implications in bridge monitoring. This research field has garnered significant attention from BHM researchers worldwide since its inception in 2004. Despite the use of this

research for general applications, several challenges must be addressed that this research field faces.

- **Appropriate modeling of the test vehicle:** The vehicle model used in numerical simulations is simplified as a single degree of freedom (SDOF) system. If a vehicle is to be modeled as a multi-DOF (MDOF) system, the coupling effect of MDOFs needs to be considered in numerical studies. A limited number of full-scale studies have been identified in the literature, as very few test vehicles resemble the theoretical models presented in the respective studies. If MDOF systems are to be used, the mechanical coupling between the MDOFs of the vehicle should be considered.
- **Effect of road roughness:** The presence of road roughness excites the vehicle overwhelmingly more than the bridge does. This can result in the bridge acceleration spectrum being masked by the vehicle response. Road roughness analysis and road profile estimation are not commonly included in iBHM studies. One solution to the road roughness problem is to subtract the signal of two consecutive axles to remove the roughness effect.
- **Effect of optimal vehicle speed:** The traveling speed of the test vehicle dictates the amount of time the vehicle is present over the bridge and is collecting data related to the bridge acceleration spectrum. The duration of VBI could be rendered very short due to the vehicle speed. This problem can be dealt with by reducing the test vehicle speed; however, this might not be an ideal solution for in-service roads and bridges.
- **Effect of vehicle configuration:** The sensitivity of the test vehicle (i.e., damping and stiffness of the vehicle) is another challenging aspect of iBHM research. Each researcher has utilized a specific test vehicle which may only be suitable for the specific bridge used in that study. There is a lack of literature that focuses on generalizing the design and parameters of the test vehicle.
- **Sensor placement on test vehicle:** Sensor placement on the test vehicle can be considered another challenge for iBHM. Even though the CP response can provide more accurate bridge information, free from any kind of vehicle input, extracting the

CP response using a sensor placed on vehicle axles is a challenging task. Advanced sensing techniques, such as sensors based on the Internet of Things (IoT), can be employed to accomplish this task. Such sensors can streamline the sensor placement and data collection phases of iBHM

8.4 Potential Future Research

The research field of iBHM has grown exponentially since its introduction, and its role in making bridge monitoring economical is evident. After enumerating the challenges in the previous section, a couple of recommended steps for the future development of iBHM research field are provided in this section.

- **Test vehicle design:** Optimizing the design for a test vehicle can be beneficial for the iBHM research. A test vehicle designed for monitoring various types of bridges such as short bridges, long bridges, truss bridges, cable-stayed bridges, suspension bridges, etc. Such a test vehicle, which most likely can be simulated using an unmanned ground vehicle, may be highly customizable in terms of different vehicle mass and vehicle stiffness values and different sensitivity characteristics depending upon the boundary conditions and type of the bridge.
- **Sensor communication:** Vehicles traveling on the roads nowadays are undergoing distinct evolution in design and technology. Autonomous driving vehicles are expected to revolutionize the transportation system. These vehicles are equipped with sophisticated sensors such as cameras, light detection and ranging (LIDAR), and ultrasonic sensors. It is essential to direct the future development of such vehicles toward integration with smart bridge monitoring. A monitoring system built based on the constant communication between the smart vehicles, and smart infrastructure can result in higher reliability and self-sufficiency and provide enhanced decision-making capabilities to the stakeholders by fusion of various sensor data.
- **Sensor sustainability:** In the realm of wireless sensor networks, the development of self-powered sensors has gathered a great deal of research interest. These sensors are capable of harvesting energy from the sensed vibrations and can potentially transform

the data acquisition by enhancing energy efficiency. The implementation of self-powered sensors attached to the test vehicle will significantly reduce the maintenance cost and increase the efficiency of data collection.

- **IoT-based applications:** Wireless data transmission and cloud-based computation have given rise to IoT-based sensors. The tasks of data collection, transmission, and processing can be facilitated using IoT sensors. Smart and sustainable infrastructure, cities, and communities have been the prime directive for the concept of IoT. Future studies can focus on extracting information from a large amount of data by deploying IoT sensors on a large scale and expanding the boundaries of iBHM.
- **Mode shape identification:** Most of the studies worked on the identification of the bridge frequencies and the effects of vehicle damping, bridge damping, and road roughness for the identification of the CP response. However, limited studies have explored ways to identify the mode shapes from the CP response. The moving public transportation system, such as buses and taxis, could be used as test vehicles to record the mode shapes or any other modal parameters.
- **Vision-based monitoring:** With the advancements in the video camera, computer vision using video could be a viable alternative for iBHM, which has not been appropriately explored. With the use of a computer vision algorithm, a pixel in the image could be modified and tracked to detect the vibration response at any point. This new field of study may open the doors to access the inaccessible structural parts of the bridge for its timely maintenance.

Bibliography

- Adhikari, S. (2007). On the quantification of damping model uncertainty. *Journal of Sound and Vibration*. 306, 153-171.
- Aied, H., González, A., and Cantero, D. (2016). Identification of sudden stiffness changes in the acceleration response of a bridge to moving loads using Ensemble Empirical Mode Decomposition. *Mechanical Systems and Signal Processing*. 66–67, 314–338.
- Alamdari, M. M., Chang, K. C., Kim, C. W., Kildashti, K., and Kalhori, H. (2021). Transmissibility performance assessment for drive-by bridge inspection. *Engineering Structures*. 242, 112485.
- Alampalli, S., Alampalli, S., and Ettouney, M. (2016). Big-data and high-performance analytics in structural health monitoring for bridge management. *Sensors and Smart Structures Technologies for Civil, Mechanical, and Aerospace Systems*. In *Proceedings of the SPIE Smart Structures /NDE Conference*. Las Vegas, NV.
- Allemang, R., and Brown, D. (1998). A unified matrix polynomial approach to modal identification. *Journal of Sound and Vibration*. 211(3), 301-322.
- Almasri, N., Sadhu, A., and Chaudhuri, S. R. (2019). Towards compressed sensing of structural monitoring data using Building Information Modeling. *ASCE Journal of Computing in Civil Engineering*. 34(1), 04019041.
- An, Y., Chatzi, E., Sim, S. H., Laflamme, S., Blachowski, B., and Ou, J. (2019). Recent progress and future trends on damage identification methods for bridge structures. *Structural Control and Health Monitoring*. 26(10), e2416.
- Antoni, J., and Chauhan, S. (2011). An alternating least squares (ALS) based blind source separation algorithm for operational modal analysis. In: *Proceedings of the 29th IMAC*. Jacksonville, FL, USA, 2011.
- Arayici, Y., and Aouad, G. (2010). Building Information Modelling (BIM) for construction lifecycle management. *Construction and Building: Design, Materials and Construction*. Nova Science Publishers. NY, USA. 1, 99-118.

Arjomandi, K., and Araki, Y. (2019). Monitoring time in operational modal tests with broad and narrow band excitations. *Structures*. 22, 245-251.

ASCE Infrastructure Report Card (2021). <https://infrastructurereportcard.org/>.

Augenbroe, G. P., Wilde, D., Moon, H. J., and Malkawi, A. (2004). An interoperability workbench for design analysis integration. *Energy and Buildings*. 36(8), 737-748.

Bagheri, A., Alipour, M., Ozbulut, O. E., and Harris, D. K. (2018). A non-destructive method for load rating of bridges without structural properties and plans. *Engineering Structures*. 171, 545–556.

Bahar, O., and Ramezani, S. (2012). Enhanced Hilbert-Huang transform and its applications to modal identification. *Structural Design of Tall and Special Buildings*. 23(4): 239-253.

Barbosh, M., Sadhu, A., and Vogrig, M. (2018). Multisensor-based hybrid empirical mode decomposition method towards system identification of structures. *Structural Control and Health Monitoring*. 25(5), e2147.

Barbosh, M., Singh, P., and Sadhu, A. (2020). Empirical Mode Decomposition and its variants: A review with applications in structural health monitoring. *Smart Materials and Structures*. 29(9): 093001.

Bodupalli, C., Sadhu, A., Azar, E., and Pattyson, S. (2019). Improved visualization of infrastructure monitoring data using Building Information Modeling. *Structures and Infrastructure Engineering*. 15(9), 1247–1263.

Brincker, R., Andersen, P., and Cantieni, R. (2001b). Identification and level I damage detection of the Z24 highway bridge. *Experimental Techniques*, 25: 51-57.

Brincker, R., Zhang, L., and Anderson, P. (2001a). Modal identification of output-only systems using frequency domain decomposition. *Smart Materials and Structures*. 10, 441-445.

Cantero, D., and González, A. (2015). Bridge damage detection using weigh-in-motion technology. *Journal of Bridge Engineering*. 20(5), 04014078.

- Celik, O., Dong, C., and Catbas, F. N. (2020). Investigation of structural response under human induced excitations using noise-assisted and adaptively transformed multivariate empirical mode decomposition. *Journal of Structural Engineering*. 146(4), 04020019.
- Cemesova, A., Hopfe, C. J., and Mcleod, R. S. (2015). PassiveBIM: Enhancing interoperability between BIM and low energy design software. *Automation in Construction*. 57, 17-32.
- Chang, S. J., and Kim, N. S. (2011). Estimation of displacement response from FBG strain sensors using empirical mode decomposition technique. *Experimental Mechanics*. 52(6), 573–589.
- Chen, J., Bulbul, T., Taylor, J., and Olgun, J. (2014). A case study of embedding real-time infrastructure Sensor Data to BIM. *Construction Research Congress, ASCE*. Atlanta, GA, USA.1, 269-278.
- CIRC Canadian Infrastructure Report Card (2019),
<http://canadianinfrastructure.ca/downloads/canadian-infrastructure-report-card-2019.pdf>
- Corbally, R., and Malekjafarian, A. (2021). Examining changes in bridge frequency due to damage using the contact-point response of a passing vehicle. *Journal of Structural Integrity and Maintenance*. 6(3), 148-158.
- Corbally, R., and Malekjafarian, A. (2022). A data-driven approach for drive-by damage detection in bridges considering the influence of temperature change. *Engineering Structures*. 253, 113783.
- Cremona, C., and Santos, J. P. (2018). Structural health monitoring as a big-data problem. *Structural Engineering International*. 28(3), 243-254.
- Cronin, L. M., Eshkevari, S. S., Sen, D., and Pakzad, S. N. (2021). Transfer learning for input estimation of vehicle systems. *IEEE International Conference on Acoustics. Speech and Signal Processing*. 7953-7957.
- Dang, N. S., and Shim, C. S. (2020). BIM-based innovative bridge maintenance system using augmented reality technology. *Innovation for Sustainable Infrastructure*. 54, 1217–1222.

- Daubechies, I., Lu, J., and Wu, H. T. (2010). Synchrosqueezed wavelet transforms: An empirical mode decomposition-like tool. *Applied and Computational Harmonic Analysis*. 30(2): 243-261.
- Delgado, J. M. D., Butler, L. J., Brilakis, I., Elshafie, M. Z. E. B., and Middleton, C. R. (2018). Structural performance monitoring using a dynamic data-driven BIM environment. *Journal of Computing in Civil Engineering*. 32(3), 04018009.
- Delgado, J. M. D., Butler, L. J., Gibbons, N., Brilakis, I., Elshafie, M. Z. E. B., and Middleton, C. (2017). Management of structural monitoring data of bridges using BIM. *Institution of Civil Engineers- Bridge Engineering*. 170(3), 204-218.
- Deng, L., Lai, S., Ma, J., Lei, L., Zhong, M., Liao, L., and Zhou, Z. (2021). Visualization and monitoring information management of bridge structure health and safety early warning based on BIM. *Journal of Asian Architecture and Building Engineering*. 21 (2): 427–438.
- Dertimanis, V., and Chatzi, E. (2020). Sensor networks in structural health monitoring: From theory to practice. *Journal of Sensor and Actuator Networks*. 9(4), 47.
- Dessi, D., and Camerlengo, G. (2015). Damage identification techniques via modal curvature analysis: Overview and comparison. *Mechanical Systems and Signal Processing*. 52-53, 181-205.
- Ditommaso, R., Mucciarelli, M., Parolai, S., and Picozzi, M. (2012). Monitoring the structural dynamic response of a masonry tower: Comparing classical and time-frequency analyses. *Bulletin of Earthquake Engineering*. 10(4), 1221–1235.
- Douka, E., Loutridis, S., and Trochidis, A. (2003). A crack identification in beams using wavelet analysis. *International Journal of Solids and Structures*. 40(13-14), 3557-3569.
- Elhatab, A., and Uddin, N. (2017). Drive-by bridge damage monitoring: Concise review. *Civil Engineering Research Journal*. 1(1), 6.
- Elhatab, A., Uddin, N., and OBrien, E. (2018). Drive-by bridge frequency identification under operational roadway speeds employing frequency independent underdamped pinning stochastic resonance (FI-UPSR). *Sensors*. 18(12), 4207.

- Entezami, A., and Shariatmadar, H. (2019). Damage localization under ambient excitations and nonstationary vibration signals by a new hybrid algorithm for feature extraction and multivariate distance correlation methods. *Structural Health Monitoring*. 18(2), 347–375.
- Eshkevari, S. S., Matarazzo, T. J., and Pakzad, S. N. (2020a). Bridge modal identification using acceleration measurements within moving vehicles. *Mechanical Systems and Signal Processing*. 141, 106733.
- Eshkevari, S. S., Matarazzo, T. J., and Pakzad, S. N. (2020b). Simplified vehicle-bridge interaction for medium to long-span bridges subject to random traffic load. *Journal of Civil Structural Health Monitoring*. 10, 693-707.
- Eshkevari, S. S., Pakzad, S. N., Takac, M., and Matarazzo, T. J. (2020c). Modal identification of bridges using mobile sensors with sparse vibration data. *Journal of Engineering Mechanics*. 146(4), 04020011.
- Fitzgerald, P. C., Malekjafarian, A., Cantero, D., OBrien, E. J., and Prendergast, L. J. (2019). Drive-by scour monitoring of railway bridges using a wavelet-based approach. *Engineering Structures*. 191, 1-11.
- Gao, Y., Ge, G., Sheng, Z., and Sang, E. (2008). Analysis and solution to the mode mixing phenomena in EMD. *Congress on Image and Signal Processing IEEE*. 5, 223-227.
- Gonzalez, A., OBrien, E. J., and McGetrick, P. J. (2012). Identification of damping in a bridge using a moving instrumented vehicle. *Journal of Sound and Vibration*. 331, 4115-4131.
- Goyal, D., and Pabla, B. S. (2015). The vibration monitoring methods and signal processing techniques for structural health monitoring: a review. *Archives of Computational Methods in Engineering*. 23(4), 585-594.
- Grilo, A., and Jardim-Goncalves, R. (2010). Value proposition on interoperability of BIM and collaborative working environments. *Automation in Construction*. 19(5), 522-530.
- Grosso, A. D., Basso, P., Ruffini, L., Figini, F., and Cademartori, M. (2017). Infrastructure management integrating SHM and BIM procedures. *4th Conference on*

Smart Monitoring, Assessment and Rehabilitation of Civil Structures. Zurich, Switzerland, September 13, 2017.

Hashlamon, I., Nikbakht, E., Topa, A., and Elhattab, A. (2021). Numerical parametric study on the effectiveness of the contact-point response of a stationary vehicle for bridge health monitoring. *Applied Sciences*. 11(15), 7028.

Hazra, B., Sadhu, A., Roffel, A. J., Paquet, P. E., and Narasimhan, S. (2012). Underdetermined blind identification of structure by using the modified cross-correlation method. *Journal of Engineering Mechanics*. 138(4): 327-337.

He, W. Y., Ren, W. X., and Zhu, S. (2017). Damage detection of beam structures using quasi-static moving load-induced displacement response. *Engineering Structures*. 145: 70-82.

He, X. H., Hua, X. G., Chen, Z. Q., and Huang, F. L. (2011). EMD-based random decrement technique for modal parameter identification of an existing railway bridge. *Engineering Structures*. 33(4), 1348–1356.

Hong, J. C., Kim, Y. Y., Lee, H. C., and Lee, Y. W. (2002). Damage detection using the Lipschitz exponent estimated by the wavelet transform: Applications to vibration modes of a beam. *International Journal of Solids and Structures*. 39(7), 1803-1816.

Hou, Z., Noori, M., and Amand, R. S. (2000). Wavelet-based approach for structural damage detection. *Journal of Engineering Mechanics*. 126(7), 677-683.

Huang, N. E., Shen, Z., Long, S. R., Wu, M. C., Shih, H. H., Zheng, Q., Yen, N. C., Tung, C. C., and Liu, H. H. (1998). The Empirical Mode Decomposition and the Hilbert Spectrum for nonlinear and non-stationary time series analysis. *Proceedings: Mathematical, Physical, and Engineering Sciences*. 454(1971), 903-995.

Huang, S., Wang, X., Li, C., and Kang, C. (2019). Data decomposition method combining permutation entropy and spectral substitution with Ensemble Empirical Mode Decomposition. *Measurement*. 139, 438–453.

Huston, D., Burns, D., and Razingar, J. (2016). Structural health monitoring and maintenance aided by Building Information Modelling and repair information tools. *11th*

International Conference on Urban Regeneration and Sustainability. Alicante, Spain, June 12, 2016.

Ibrahim, S., and Mikulcik, E. (1973). A time-domain modal vibration test technique. *Shock Vibration Bulletin*. 43, 21-37.

Ivson, P., Moreira, A., Queiroz, F., Santos, W., and Celes, W. (2019). A systematic review of visualization in Building Information Modeling. *IEEE Transactions on Visualization and Computer Graphics*. X(X), 1–20.

Jeong, S., Hou, R., Lynch, J. P., Sohn, H., and Law, K.H. (2017). An information modeling framework for bridge monitoring. *Advances in Engineering Software*. 114, 11–31.

Jin, N., Dertimanis, V. K., Chatzi, E. N., Dimitrakopoulos, E. G., and Katafygiotis, L. S. (2022). Subspace identification of bridge dynamics via traversing vehicle measurements. *Journal of Sound and Vibration*. 523, 116690.

Juang, J., and Pappa, R. (1985). An eigensystem realization algorithm for modal parameter identification and model reduction. *Journal of Guidance Control and Dynamics*. 8, 620-627.

Kaloop, M., Kim, K. H., Elbeltagi, E., Jin, X., and Hu, J. W. (2020). Service-life evaluation of existing bridges subjected to static and moving trucks using structural health monitoring system: Case study. *KSCE Journal of Civil Engineering*. 1976-2808.

Kankanamge, Y., Hu, Y., and Shao, X. (2020). Application of wavelet transform in structural health monitoring. *Earthquake Engineering and Engineering Vibration*. 19(2), 515-532.

Karan, E. P., and Irizarry, J. (2015). Extending BIM interoperability to preconstruction operations using geospatial analyses and semantic web services. *Automation in Construction*. 53, 1-12.

Khorram, A., Bakhtiari, F., and Rezaeian, M. (2012). Comparison studies between two wavelet-based crack detection methods of a beam subjected to a moving load. *International Journal of Engineering Science*. 51: 204–215.

- Kildashti, K., Alamdari, M. M., Kim, C. W., Gao, W., and Samali, B. (2020). Drive-by bridge inspection for damage identification in a cable-stayed bridge: Numerical investigations. *Engineering Structures*. 223, 110891.
- Kilic, G., and Caner, A. (2020). Augmented reality for bridge condition assessment using advanced non-destructive techniques. *Structure and Infrastructure Engineering*. 17 (7), 977–989.
- Kim, B., Kim, C., and Kim, H. (2012). Interactive modeler for construction equipment operation using augmented reality. *Journal of Computing in Civil Engineering*. 26 (3): 331–341.
- Kodestani, H., Xiang, Y. Q., Ye, X. W., and Jia, Y. K. (2018). Application of the random decrement technique in damage detection under moving load. *Applied Sciences*. 8(5): 753.
- Kong, X., Cai, C. S., Deng, L., and Zhang, W. (2017). Using dynamic responses of moving vehicles to extract bridge modal properties of a field bridge. *Journal of Bridge Engineering*. 22(6), 04017018.
- Kramer, C., De Smet, C.A.M., and De Roeck, G. (1999). Z24 Bridge damage tests. *Proceedings of the 17th International Modal Analysis Conference (IMAC)*. Kissimmee, Florida.
- Kullaa, J. (2003). Damage detection of the Z24 bridge using control charts. *Mechanical Systems and Signal Processing*. 17(1): 163-170.
- Kumar, R., Sumathi, P., Member, S., and Kumar, A. (2017). Synchrosqueezing transform-based frequency shifting detection for earthquake-damaged structures. *IEEE Geoscience and Remote Sensing Letters*. 1–5.
- Lazhari, M., and Sadhu, A. (2019). Decentralized modal identification of structures using an adaptive empirical mode decomposition. *Journal of Sound and Vibration*. 447, 20-41.
- Li, H., Li, Z., and Mo, W. (2017). A time varying filter approach for empirical mode decomposition. *Signal Processing*. 138, 146-158.

- Li, J., Zhu, X., and Guo, J. (2022). Enhanced drive-by bridge modal identification via dual Kalman filter and singular spectrum analysis. *Structural Control and Health Monitoring*. e2927.
- Li, J., Zhu, X., Law, S. S., and Samali, B. (2019a). Indirect bridge modal parameters identification with one stationary and one moving sensors and stochastic subspace identification. *Journal of Sound and Vibration*. 446, 1-21.
- Li, J., Zhu, X., Law, S. S., and Samali, B. (2019b). Drive-by blind modal identification with singular spectrum analysis. *Journal of Aerospace Engineering*. 32(4), 04019050.
- Li, Y., Ma, X., and Zhang, W. (2018). Dynamic performance of a concrete-filled steel tube high-pier curved continuous truss girder bridge due to moving vehicles. *Advances in Structural Engineering*. 22(6), 1297-1311.
- Li, Z., Gao, J., Li, H., Zhang, Z., Liu, N., and Zhu, X. (2020). Synchroextracting transform: The theory analysis and comparisons with the Synchrosqueezing transform. *Signal Processing*. 166, 107243.
- Li, Z., and Park, H. S. (2017). New method for modal identification of super high-rise building structures using discretized Synchrosqueezed Wavelet and Hilbert transforms. *The Structural Design of Tall and Special Buildings*. 26(3), e1312.
- Liu, W., Guo, H., Li, H., and Li, Y. (2014). Using BIM to improve the design and construction of bridge projects: A case study of a long span steel-box arc bridge project. *International Journal of Advanced Robotic Systems*. 11(125).
- Liu, Z., Peng, D., Zuo, M.J., Xia, J., and Qin, Y. (2022). Improved Hilbert-Huang transform with soft sifting stopping criterion and its application to fault diagnosis of wheelset bearings. *ISA Transactions*. 125, 426-444.
- Locke, W., Sybrandt, J., Redmond, L., Safro, I., and Atamturktur, S. (2020). Using drive-by health monitoring to detect bridge damage considering environmental and operational effects *Journal of Sound and Vibration*. 468, 115088.
- Lofrano, E., Romeo, F., and Paolone, A. (2019). A pseudo-modal structural damage index based on orthogonal Empirical Mode Decomposition. *Proceedings of the*

Institution of Mechanical Engineers. Part C: Journal of Mechanical Engineering Science, 233 (23-24), 7545-7564.

Loutridis, S., Douka, E., and Trochidis, A. (2004). A crack identification in double-cracked beams using wavelet analysis. *Journal of Sound and Vibration*. 277(4-5), 1025-1039.

Ma, T., Yang, H., and Chang, C. (2005). Structural damage diagnosis and assessment under seismic excitation. *Journal of Engineering Mechanics*. 131(10), 1036-1045.

Maeck, J., Peeters, B., and De Roeck, G. (2001). Damage identification on the Z24 bridge using vibration monitoring. *Smart Materials and Structures*. 10, 512-517.

Mahato, S., and Chakraborty, A. (2019). Sequential clustering of synchrosqueezed wavelet transform coefficients for efficient modal identification. *Journal of Civil Structural Health Monitoring*. 9(2), 271-291.

Malekjafarian, A., Golpayegani, F., Moloney, C., and Clarke, S. (2019). A machine learning approach to bridge-damage detection using responses measured on a passing vehicle. *Sensors*. 19, 4035.

Malekjafarian, A., McGetrick, P. J., and O'Brien, E. J. (2015) A review of indirect bridge monitoring using passing vehicles. *Shock and Vibration*. 286139.

Malekjafarian, A., and O'Brien, E. J. (2014). Identification of bridge mode shapes using Short Time Frequency Domain Decomposition of the responses measured in a passing vehicle. *Engineering Structures*. 81, 386-397.

Mallat, S. (2009). A wavelet tour of signal processing: The sparse way. *Academic Press*.

Mao, Q., Mazzotti, M., DeVitis, J., Braley, J., Young, C., Sjoblom, K., Aktan, E., Moon, F., and Bartoli, I. (2019). Structural condition assessment of a bridge pier: A case study using experimental modal analysis and Finite Element Model updating. *Structural Control and Health Monitoring*. 26(1).

Marzouk, M. M., and Hisham, M. (2011). Bridge Information Modeling in sustainable bridge management. *ICSDC 2011*. Kansas City, Missouri.

- Masciotta, M. G., Ramos, L. F., Lourenco, P. B., Vasta, M., and De Roeck, G. (2016). A spectrum-driven damage identification technique: Application and validation through the numerical simulation of the Z24 bridge. *Mechanical Systems and Signal Processing*. 70-71, 578-660.
- Mata, J., Tavares de Castro, A., and Sá da Costa, J. (2013). Time-frequency analysis for concrete dam safety control: Correlation between the daily variation of structural response and air temperature. *Engineering Structures*. 48, 658-665.
- Matarazzo, T. J., Kondor, D., Milardo, S., Eshkevari, S. S., Santi, P., Pakzad, S. N., Buehler, M. J., and Ratti, C. (2022). Crowdsourcing bridge vital signs with smartphone vehicle trips. *Computers and Society*. Preprint.
- MathWorks. 2018. *Signal processing toolbox: User's guide (R2018b)*. Retrieved January 04, 2023 from https://www.mathworks.com/help/pdf_doc/signal/signal_tb.pdf.
- Matsuoka, K., Tanaka, H., Kawasaki, K., Somaschini, C., and Collina, A. (2021). Drive-by methodology to identify resonant bridges using track irregularity measured by high-speed trains. *Mechanical Systems and Signal Processing*. 158, 107667.
- McGuire, B., Atadeo, R., Clevenger, C., and Ozbek, M. (2016). Bridge information modeling for inspection and evaluation. *Journal of Bridge Engineering*. 21 (4), 04015076.
- McNeill, S. I. (2013). A modal identification algorithm combining blind source separation and state space realization. *Journal of Signal and Information Processing*. 14, 173–185.
- Meng, D., Xiao, F., Zhang, L., Xu, X., Chen, G. S., Zatar, W., and Hulsey, J. L. (2018). Nonlinear vibration analysis of vehicle–bridge interaction for condition monitoring. *Journal of Low Frequency Noise, Vibration and Active Control*. 38(3-4), 1422-1432.
- Micu, E. A., O'Brien, E. J., Bowe, C., Fitzgerald, P., and Pakrashi, V. (2022). Bridge damage and repair detection using an instrumented train. *Journal of Bridge Engineering*. 27(3), 05021018.

- Moreu, F., Bleck, B., Vemuganti, S., Rogers, D., and Mascarenas, D. (2017). Augmented reality tools for enhanced structural inspection. *Structural Health Monitoring*.
- Na, W. S., and Baek, J. (2017). Impedance-based non-destructive testing method combined with unmanned aerial vehicle for structural health monitoring of civil infrastructures. *Applied Sciences*. 7(15).
- Nagamaya, T., Reksowardojo, A. P., Su, D., and Mizutani, T. (2017). Bridge natural frequency estimation by extracting the common vibration component from the responses of two vehicles. *Engineering Structures*. 150, 821-829.
- Nagarajaiah, S. (2009). Adaptive passive, semiactive, smart tuned mass dampers: Identification and control using Empirical Mode Decomposition, Hilbert Transform, and Short-Term Fourier Transform. *Structural Control and Health Monitoring*. 16(7-8), 800–841.
- Nagarajaiah, S., and Basu, B. (2009). Output-only modal identification and structural damage detection using time-frequency and wavelet techniques. *Earthquake Engineering and Engineering Vibration*. 8(4), 583-605.
- Napolitano, R., Blyth, A., and Glisic, B. (2017). Virtual environments for structural health monitoring. *Structural Health Monitoring*.
- Napolitano, R., Blyth, A., and Glisic, B. (2018). Virtual environments for visualizing structural health monitoring sensor networks, data, and metadata. *Sensors*. 18 (1), 243.
- Napolitano, R., Liu, Z., Sun, C., and Glisic, B. (2019). Combination of image-based documentation and augmented reality for structural health monitoring and building pathology. *Frontiers in Built Environment*. 5, 50.
- Nguyen, K. V. (2013). Comparison studies of open and breathing crack detections of a beam-like bridge subjected to a moving vehicle. *Engineering Structure*. 51, 306–314.
- Ni, P., Li, J., Hao, H., Xia, Y., Wang, X., Lee, J., and Jung, K. (2018). Time-varying system identification using variational mode decomposition, *Structural Control and Health Monitoring*. 25(6), e2175.

- Nie, Z., Lin, J., Li, J., Hao, H., and Ma, H. (2019). Bridge condition monitoring under moving loads using two sensor measurements. *Structural Health Monitoring*. 147592171986893.
- O'Brien, E., Khan, M. A., McCrum, D. P., and Znidaric, A. (2020). Using statistical analysis of an acceleration-based bridge weigh-in-motion system for damage detection. *Applied Sciences*. 10(63).
- O'Brien, E. J., Carey, C., and Keenahan, J. (2015). Bridge damage detection using ambient traffic and moving force identification: Bridge damage detection and moving force identification. *Structural Control and Health Monitoring*. 22(12), 1396-1407.
- O'Brien, E. J., Malekjafarian, A., and Gonzalez, A. (2017). Application of empirical mode decomposition to drive-by bridge damage inspection. *European Journal of Mechanics A/Solids*. 61, 151-163.
- O'Brien, E. J., McGetrick, P. J., and Gonzalez, A. (2014). A drive-by inspection system via vehicle moving force identification. *Smart Structures and Systems*. 13(5), 821-848.
- Pagnoncelli, A. P., and Miguel, L. F. (2019). Methodology to obtain dynamic response of road bridges considering bridge-vehicle interactions. *Practice Periodical on Structural Design and Construction*. 24(3), 04019010.
- Pappalardo, C. M., and Guida, D. (2018). System identification and experimental modal analysis of a frame structure. *Engineering Letters*. 26(1).
- Perez-Ramirez, C. A., Amezcua-Sanchez, J. P., Adeli, H., Valtierra-Rodriguez, M., Romero-Troncoso, R. D. J., Dominguez-Gonzalez, A., and Osornio-Rios, R. A. (2016). Time-frequency techniques for modal parameters identification of civil structures from acquired dynamic signals. *Journal of Vibroengineering*. 18(5), 3164-3185.
- Perry, M. J., and Koh, C. G. (2000). Output-only structural identification in time domain: numerical and experimental studies. *Earthquake Engineering and Structural Dynamics*. 37, 517-533.
- Plaza, E. G., and Lopez, P. J. N. (2018). Application of the wavelet packet transform to vibration signals for surface roughness monitoring in CNC turning operations. *Mechanical Systems and Signal Processing*. 98, 902-919.

- Qin, S., Wang, Q., and Kang, J. (2015). Output-only modal analysis based on improved empirical mode decomposition method, *Advances in Materials Science and Engineering*, 1-12.
- Reddy, D. M., Krishna, P., and Sathesa. (2014). Innovative method of empirical mode decomposition as a spatial tool for structural damage identification, *Structural Control and Health Monitoring*, 22(2), 365–373.
- Ren, X., Fan, W., Li, J., and Chen, J. (2018). Building Information Model-based Finite Element Analysis of high-rise building community subjected to extreme earthquakes. *Advances in Structural Engineering*. 22(4), 971-981.
- Rio, J., Ferreira, B., and Pocas-Martins, J. (2013). Expansion of IFC model with structural sensors. *Informes de la Construcción*. Portugal, 530(65), 219-228.
- Sadhu, A. (2013). Decentralized ambient system identification of structures. *PhD Thesis*. Department of Civil and Environmental Engineering, University of Waterloo.
- Sadhu, A., Goldack, A., and Narasimhan, S. (2014). Ambient modal identification using multi-rank parallel factor decomposition. *Structural Control Health Monitoring*. 22(4), 595-614.
- Sadhu, A., Narasimhan, S., and Antoni., J. (2017). A review of output-only structural mode identification literature employing blind source separation methods. *Mechanical Systems and Signal Processing*. 94, 415–431.
- Sadhu, A., Narasimhan, S., and Goldack, A. (2013). Decentralized modal identification of pony truss bridge using wireless sensors. *Journal of Bridge Engineering*. 19(6).
- Sadhu, A., Sony, S., and Friesen, P. (2019). Evaluation of progressive damage in structures using tensor decomposition-based wavelet analysis. *Journal of Vibration and Control*. 25(19-20), 2595-2610.
- Shao, Y., Miao, C., Li, B., and Wu, Q. (2019). Simultaneous de-noising and enhancement method for long-span bridge health monitoring data based on Empirical Mode Decomposition and fractal conservation law. *Measurement Science and Technology*, 30(6), 065103.

- Shi, Z., and Uddin, N. (2021). Extracting multiple bridge frequencies from test vehicle-a theoretical study. *Journal of Sound and Vibration*. 490, 115735.
- Shirzad-Ghaleoudkhani, N., and Gul, M. (2020). Inverse filtering for frequency identification of bridges using smartphones in passing vehicles: Fundamental developments and laboratory verifications. *Sensors*. 20(4), 1190.
- Shirzad-Ghaleoudkhani, N., and Gul, M. (2021). An enhanced inverse filtering methodology for drive-by frequency identification of bridges using smartphones in real-life conditions. *Smart Cities*. 4, 499-513.
- Shirzad-Ghaleoudkhani, N., Mei, Q., and Gul, M. (2020). Frequency identification of bridges using smartphones on vehicles with variable features. *Journal of Bridge Engineering*. 25(7), 04020041.
- Shokravi, H., Shokravi, H., Bakhary, N., Heidarrazaei, M., Kaloore, S. S. R., and Petru, M. (2020). Vehicle-assisted techniques for health monitoring of bridges. *Sensors*. 20, 3460.
- Singh, P., Keyvanlou, M., and Sadhu, A. (2021). An improved time-varying empirical mode decomposition for structural condition assessment using limited sensors. *Engineering Structures*. 232, 111882.
- Singh, P., Mittal, S., and Sadhu, A. (2022). Recent advancements and future trends in indirect bridge health monitoring. *Practice Periodical on Structural Design and Construction*. 28(1).
- Singh, P., and Sadhu, A. (2019). Multicomponent energy assessment of buildings using Building Information Modeling. *Sustainable Cities and Society*. 49, 101603.
- Singh, P and Sadhu, A. (2020). System identification-enhanced visualization tool for infrastructure monitoring and maintenance. *Structural Sensing*. 6(76).
- Singh, P., and Sadhu, A. (2021). Limited sensor-based bridge condition assessment using vehicle induced nonstationary measurements. *Structures*. 32, 1207-1220.
- Singh, P., and Sadhu, A. (2022). A hybrid time-frequency method for robust drive-by modal identification of bridges. *Engineering Structures*. 266, 114624.

- Singh, P., and Sadhu, A. (2023). Contact point response-based indirect bridge health monitoring using Robust Empirical Mode Decomposition. *Journal of Sound and Vibration*. (in revision).
- Siringoringo, D. M., and Fujino, Y. (2012). Estimating bridge fundamental frequency from vibration responses of instrumental passing vehicle: Analytical and experimental study. *Advances in Structural Engineering*. 15(3), 417-433.
- Siringoringo, D. M., and Fujino, Y. (2012). “Estimating bridge fundamental frequency from vibration responses of instrumental passing vehicle: Analytical and experimental study”, *Advances in Structural Engineering*, 15(3), 417-433.
- Sitton, J. D., Rajan, D., and Story, B. A. (2020). Bridge frequency estimation strategies using smartphones. *Journal of Civil Structural Health Monitoring*. 10, 513-526.
- Song, X., Ma, H., and Wang, K. (2017). A new developed modal parameter identification method based on empirical mode decomposition and natural excitation technique, *Procedia Engineering*, 199, 1020–1025.
- Sony, S., Dunphy, K., Sadhu, A., and Capretz, M. (2021). A systematic review of convolutional neural network-based structural condition assessment techniques. *Engineering Structures*. 226, 111347.
- Sony, S., Gamage, S., Sadhu, A., and Samarabandu, J. (2022). Mutliclass damage identification in a full-scale bridge using optimally tuned one-dimensional convolutional neural network. *ASCE Journal of Computing in Civil Engineering*. 36(2), 04021035.
- Sony, S., Laventure, S., and Sadhu, A. (2019). A literature review of next-generation smart sensing technology in structural health monitoring. *Structural Control and Health Monitoring*. 26(3), e2321.
- Sony, S., and Sadhu, A. (2020). Synchro-squeezing transform-based identification of time-varying structural systems using multi-sensor data. *Journal of Sound and Vibration*. 486, 115576.
- Sun, G., Gao, Y., Lin, K., and Hu, Y. (2019). Fine-grained fault diagnosis method of rolling bearing combining multisynchrosqueezing transform and sparse feature coding based on dictionary learning. *Shock and Vibration*. 1531079.

- Sun, L., Shang, Z., Xia, Y., Bhowmick, S., and Nagarajaiah, S. (2020). Review of bridge structural health monitoring aided by big data and artificial intelligence: From condition assessment to damage detection. *Journal of Structural Engineering*. 146(5).
- Tan, C., Elhattab, A., and Uddin, N. (2017). Drive-by bridge frequency-based monitoring utilizing wavelet transform. *Journal of Civil Structural Health Monitoring*. 7, 615-625.
- Tan, C., Elhattab, A., and Uddin, N. (2020b). Wavelet-energy approach for detection of bridge damages using direct and indirect bridge records. *Journal of Infrastructure Systems*. 26(4), 04020037.
- Tan, C., Uddin, N., O'Brien, E. J., McGetrick, P., and Kim, C. W. (2019). Extraction of bridge modal parameters using passing vehicle response. *Journal of Bridge Engineering*. 24(9), 04019087.
- Tan, C., Zhao, H., O'Brien, E. J., Uddin, N., Fitzgerald, P. C., McGetrick, P. J., and Kim, C. W. (2020a). Extracting mode shapes from drive-by measurements to detect global and local damage in bridges. *Structure and Infrastructure Engineering*. 1-15.
- Tang, B., Liu, W., & Song, T. (2010). Wind turbine fault diagnosis based on Morlet wavelet transformation and Wigner-Ville distribution. *Renewable Energy*. 35(12), 2862-2866.
- Tang, J., Zhao, L. J., Yeu, H., Yu, W., and Chai, T. (2011). Vibration analysis based on Empirical Mode Decomposition and partial least square. *Procedia Engineering*. 16, 646-652.
- Thakur, G. (2015). The synchrosqueezing transform for instantaneous spectral analysis. *Applied and Numerical Harmonic Analysis*. 4(1), 397-406.
- Theiler, M., Dragos, K., and Smarly, K. (2017). BIM-based design of structural health monitoring systems. *11th International Workshop on Structural Health Monitoring*. Stanford, CA, USA, September 12, 2017.
- Tian, Y., and Zhang, J. (2020). Structural flexibility identification via moving-vehicle-induced time-varying modal parameters. *Journal of Sound and Vibration*. 474, 115264.

- Trung, N. T. (2018). Application of Hilbert-huang transform to identify the dynamic characteristics of a caisson foundation during liquefaction, *Structural Control and Health Monitoring*, e2427.
- Tomasi, R., Sottile, F., Pastrone, C., Mozumdar, M. M. R., Osello, A., and Lavagno, L. (2015). Leveraging BIM interoperability for UWB-based WSN planning. *IEEE Sensors Journal*. 15(10), 5988-5996.
- Wang, H., Nagamaya, T., Nakasuka, J., Zhao, B., and Su, Di. (2018). Extraction of bridge fundamental frequency from estimated vehicle excitation through a particle filter approach. *Journal of Sound and Vibration*. 428, 44-58.
- Wang, H., Nagayama, T., and Su, D. (2019). Estimation of dynamic tire force by measurement of vehicle body responses with numerical and experimental validation. *Mechanical Systems and Signal Processing*. 123, 369-385.
- Wang, Q., and Deng, X. (1999). Damage detection with spatial wavelets. *International Journal of Solids and Structures*. 36(23), 3443-3468.
- Wu, B., Wu, G., Yang, C., and He, Y. (2016). Damage identification and bearing capacity evaluation of bridges based on distributed long-gauge strain envelope line under moving vehicle loads, *Journal of Intelligent Material Systems and Structures*, 27(17), 2344–2358.
- Wu, J. D., and Liu, C. H. (2009). An expert system for fault diagnosis in internal combustion engines using wavelet packet transform and neural network. *Expert Systems with Applications*. 36(3), 4278-4286.
- Wu, Q., Han, B., Yu, J., Yan, W., Zhang, J., and Xie, H. (2022). A theoretical model to identify the fundamental frequency of simply supported girders from a passing heavy vehicle. *Applied Sciences*. 12, 2422.
- Wu, R. T., and Jahanshahi, M. R. (2018). Data fusion approaches for structural health monitoring and system identification: Past, present, and future. *Structural Health Monitoring*. 1-35.
- Xu, B., Sheng, Y., Li, P., Cheng, Q., and Wu, J. (2019). Causes and classification of EMD mode mixing. *Vibroengineering Procedia*. 22, 158-164.

- Xu, H., Huang, C. C., Wang, Z. L., Shi, K., Wu, Y. T., and Yang, Y. B. (2021). Damped test vehicle for scanning bridge frequencies: Theory, simulation and experiment. *Journal of Sound and Vibration*. 506, 116155.
- Xu, Y. L., Chen, S. W., and Zhang, R. C. (2003). Modal identification of Di Wang building under Typhoon York using Hilbert Huang transform method. *Structural Design of Tall Buildings*. 12(1), 21-47.
- Xue, K., Nagayama, T., and Zhao, B. (2020). Road profile estimation and half-car model identification through the automated processing of smartphone data. *Mechanical Systems and Signal Processing*. 142, 106722.
- Yan, J., Laflamme, S., Singh, P., Sadhu, A., and Dodson, J. (2020). A comparison of time-frequency methods for real-time application to high-rate dynamic systems. *Vibration*. 3(3), 204-216.
- Yang, D. S., and Wang, C. M. (2022a). Modal properties identification of damped bridge using improved vehicle scanning method. *Engineering Structures*. 256, 114060.
- Yang, D. S., and Wang, C. M. (2022b). Bridge damage detection using reconstructed mode shape by improved vehicle scanning method. *Engineering Structures*. 263, 114373.
- Yang, J. N., Lei, Y., Lin, S., and Huang, N. (2004b). Hilbert-Huang based approach for structural damage detection. *Journal of Engineering Mechanics*. 130(1), 85-95.
- Yang, Y., Chen, W., Yu, H., and Chan, C. (2013). Experimental study of a hand-drawn cart for measuring the bridge frequencies. *Engineering Structures*. 57, 222-231.
- Yang, Y., Zhu, Y., Wang, L. L., Jia, B. Y., and Jin, R. (2018b). Structural damage identification of bridges from passing test vehicles. *Sensors*. 18, 4035.
- Yang, Y. B., and Chang, K. C. (2009). Extraction of bridge frequencies from the dynamic response of a passing vehicle enhanced by the EMD technique. *Journal of Sound and Vibration*. 322, 718-739.
- Yang, Y. B., Li, Y. C., and Chang, K. C. (2012). Effect of road roughness on the response of a moving vehicle for identification of bridge frequencies. *Interaction and Multiscale Mechanics*. 5(4), 347-368.

- Yang, Y. B., Li, Z., Wang, Z. L., Shi, K., Xu, H., Qiu, F. Q., and Zhu, J. F. (2022b). A novel frequency-free movable test vehicle for retrieving modal parameters of bridges: Theory and experiment. *Mechanical Systems and Signal Processing*. 170, 108854.
- Yang, Y. B., and Lin, C. W. (2005a). Vehicle-bridge interaction dynamics and potential applications. *Journal of Sound and Vibration*. 284, 205-226.
- Yang, Y. B., and Lin, C. W. (2005b). Use of a passing vehicle to scan the fundamental bridge frequencies: an experimental verification. *Engineering Structures*. 27, 1865-1878.
- Yang, Y. B., Lin, C. W., and Yan, J. D. (2004a). Extracting bridge frequencies from the dynamic response of a passing vehicle. *Journal of Sound and Vibration*. 272, 471-493.
- Yang, Y. B., Lu, H., Tan, X., Chai, H. K., Wang, R., and Zhang, Y. (2022a). Fundamental mode shape estimation and element stiffness evaluation of girder bridges by using passing tractor-trailers. *Mechanical Systems and Signal Processing*. 169, 108746.
- Yang, Y. B., Shi, K., Wang, Z. L., Xu, H., and Wu, Y. T. (2021a). Theoretical study on a dual-beam model for detection of track/bridge frequencies and track modulus by a moving vehicle. *Engineering Structures*. 244, 112726.
- Yang, Y. B., Wang, B. Q., Wang, Z. L., Shi, K., Xu, H., Zhang, B., and Wu, Y. T. (2020a). Bridge surface roughness identified from the displacement influence lines of the contact points by two connected vehicles. *International Journal of Structural Stability and Dynamics*. 20(14), 2043003.
- Yang, Y. B., Xu, H., Mo, X. Q., Wang, Z. L., and Wu, Y. T. (2021c). An effective procedure for extracting the first few bridge frequencies from a test vehicle. *Acta Mechanica*. 232(3), 1227-1251.
- Yang, Y. B., Xu, H., Wang, Z. L., and Shi, K. (2022c). Using vehicle-bridge contact spectra and residue to scan bridge's modal properties with vehicle frequencies and road roughness eliminated. *Structural Control and Health Monitoring*. E2968.
- Yang, Y. B., Xu, H., Wang, Z. L., Shi, K., and Wu, Y. T. (2022d). Refined detection technique for bridge frequencies using rocking motion of single axle moving vehicle. *Mechanical Systems and Signal Processing*. 162, 107992.

- Yang, Y. B., Xu, H., Zhang, B., Xiong, F., and Wang, Z. L. (2020b). “Measuring bridge frequencies by a test vehicle in non-moving and moving states. *Engineering Structures*. 203, 109859.
- Yang, Y. B., and Yang, J. P. (2017). State-of-the-art review on modal identification and damage detection of bridges by moving test vehicles. *International Journal of Structural Stability and Dynamics*. 18(2), 1850025.
- Yang, Y. B., Zhang, B., Qian, Y., and Wu, Y. (2018a). Contact-point response for modal identification of bridges by a moving test vehicle. *International Journal of Structural Stability and Dynamics*. 18(5), 1850073.
- Yi, T. H., Li, H. N., and Zhang, X. D. (2012). A modified monkey algorithm for optimal sensor placement in structural health monitoring. *Smart Materials and Structures*. 21(10), 105033.
- Yu, G., and Lin, T. R. (2020). Second-order transient-extracting transform for the analysis of impulsive-like signals. *Mechanical Systems and Signal Processing*. 147(1).
- Yu, G., Wang, Z., and Zhao, P. (2019). Multisynchrosqueezing transform. *IEEE Transactions on Industrial Electronics*. 66(7), 5441–5455.
- Yu, G., Yu, M., and Xu, C. (2017). Synchroextracting Transform. *IEEE Transactions on Industrial Electronics*. 64(10), 8042–8054.
- Yuan, M., Sadhu, A., and Liu, K. (2017). Condition assessment of structure with tuned mass damper using empirical wavelet transform. *Journal of Vibration and Control*. 24(20), 4850-4867.
- Zhan, Y., Au, F. T., and Zhang, J. (2021). Bridge identification and damage detection using contact point response difference of moving vehicle. *Structural Control and Health Monitoring*. 28(12), e2837.
- Zhang, J., Yang, D., Ren, W. X., and Yuan, Y. (2021). Time-varying characteristics analysis of vehicle-bridge interaction system based on modified S-transform reassignment technique. *Mechanical Systems and Signal Processing*. 160, 107807.

- Zhang, L., Kanda, H., Brown, D. L., and Allemang, R. J. (1985). Frequency-domain poly-reference method for modal analysis. *Journal of Applied Mechanics*. 106.
- Zhang, L., Wu, G., Li, H., and Chen, S. (2020). Synchronous identification of damage and vehicle load on simply supported bridges based on long-gauge fiber bragg grating sensors. *Journal of Performance of Constructed Facilities*. 34(1), 04019097.
- Zhang, Y., and Bai, L. (2015). Rapid structural condition assessment using radio frequency identification (RFID)-based wireless strain sensor. *Automation in Construction*. 54, 1-11.
- Zhang, Y., and Song, H. W. (2016). Non-overlapped random decrement technique for parameter identification in operational modal analysis. *Journal of Sound and Vibration*. 366, 528-543.
- Zhang, Y., Wu, L. J., and Song, H. W. (2015). Triggering expectation and residual excitation of distributed random decrement technique. *Journal of Sound and Vibration*. 340, 368-382.
- Zhu, X., Cao, M., Ostachowicz, W., and Xu, W. (2019). Damage identification in bridges by processing dynamic responses to moving loads: Features and evaluation. *Sensors*. 19, 463.
- Zoubi, A. B., Adams, D. O., and Mathews, V. J. (2019). Lamb Wave Mode Decomposition based on Cross-Wigner Ville Distribution and its application to anomaly imaging for structural health monitoring. *IEEE Transactions on Ultrasonics, Ferroelectrics and Frequency Control*. 66(5), 984-997.

Curriculum Vitae

Name:	Premjeet Singh
Post-secondary Education and Degrees:	<p>Seneca College Toronto, Ontario, Canada 2010-2012 Technologist Diploma.</p> <p>Lakehead University Thunder Bay, Ontario, Canada 2015-2017 M.ESc.</p> <p>The University of Western Ontario London, Ontario, Canada 2018-2023 Ph.D. (Current)</p>
Honours and Awards:	<p>Post Graduate Scholarship-Doctoral (NSERC) 2021-2024</p> <p>L G Soderman Award, Geotechnical Research Centre The University of Western Ontario 2023</p> <p>+5 undergraduate awards</p>
Related Work Experience	<p>Teaching Assistant The University of Western Ontario 2018-2023</p> <p>Research Assistant The University of Western Ontario 2018-2023</p> <p>Teaching Assistant Lakehead University 2017-2018</p> <p>Research Assistant Lakehead University 2017-2018</p>
Publications:	<p>Singh, P., and Sadhu, A. (2023). Contact Point Response-Based Indirect Bridge Health Monitoring Using Robust Empirical Mode Decomposition. <i>Under Review</i>.</p>

Singh, P., Mittal, S., and Sadhu, A. (2023). Recent Advancements and Future Trends in Indirect Bridge Health Monitoring. *Practice Periodical on Structural Design and Construction*, 28(1).

Singh, P., and Sadhu, A. (2023). An Improved Vehicle Scanning Method Based on Contact Point Response. *CSCE General Conference*, Moncton, Canada.

Singh, P., and Sadhu, A. (2023). Modal Identification Framework for Bridges Using Traffic Smartphone Data. *CSCE General Conference*, Moncton, Canada.

Singh, P., and Sadhu, A. (2022). A Hybrid Time-Frequency Method for Robust Drive-By Modal Identification of Bridges. *Engineering Structures*, 266, 114624.

Peplinski, J., Singh, P., and Sadhu, A. (2022). Real-Time Structural Inspection Using Augmented Reality. *CSCE Structural Specialty Conference*, Victoria, Canada.

Singh, P., and Sadhu, A. (2022). Indirect Bridge Health Monitoring Using Time-Frequency Analysis: Analytical and Experimental Analysis. *IMAC-XL, Society for Experimental Mechanics*, Orlando, USA.

Singh, P., and Sadhu, A. (2021). Limited Sensor-Based Bridge Condition Assessment Using Vehicle-Induced Nonstationary Measurements. *Structures*, 32, 1207-1220.

Sing, P., Keyvanlou, M., and Sadhu, A. (2021). An Improved Time-Varying Empirical Mode Decomposition for Structural Condition Assessment Using Limited Sensors. *Engineering Structures*, 232, 111882.

Singh, P., and Sadhu, A. (2020). System Identification Enhanced Automated Visualization Tool For Infrastructure Monitoring and Maintenance. *Structural Sensing*, 6(76).

Barbosh, M., Singh, P., and Sadhu, A. (2020). Empirical Mode Decomposition and Its Variants: A Review With Applications in Structural Health Monitoring. *Smart Materials and Structures*, 29(9), 093001.

Yan, J., Lalamme, S., Singh, P., Sadhu, A., and Dodson, J. (2020). A Comparison of Time-Frequency Methods for Real-Time Application to High-Rate Dynamic Systems. *Vibration*, 3(3), 204-216.

Singh, P., and Sadhu, A. (2020). Towards Mobile Sensing Technique in Bridge Health Monitoring. *CSCE General Conference*, Saskatoon, Canada.

Barbosh, M., Singh, P., and Sadhu, A. (2020). Structural Condition Assessment Using Empirical Mode Decomposition and Its Variants. *CSCE General Conference*, Saskatoon, Canada.

Singh, P., and Sadhu, A. (2019). Multicomponent Energy Assessment of Buildings Using Building Information Modeling. *Sustainable Cities and Society*, 49, 101603.

Singh, P., and Sadhu, A. (2019). Towards Building Information Modeling-Based Automated Structural Health Monitoring Tool. *CSCE General Conference*, Montreal, Canada.